



**HAL**  
open science

# Investigation of FEM numerical simulation for the process of metal additive manufacturing in macro scale

Shuai Chen

► **To cite this version:**

Shuai Chen. Investigation of FEM numerical simulation for the process of metal additive manufacturing in macro scale. Mechanical engineering [physics.class-ph]. Université de Lyon, 2019. English. NNT : 2019LYSEI048 . tel-02402859

**HAL Id: tel-02402859**

**<https://theses.hal.science/tel-02402859v1>**

Submitted on 10 Dec 2019

**HAL** is a multi-disciplinary open access archive for the deposit and dissemination of scientific research documents, whether they are published or not. The documents may come from teaching and research institutions in France or abroad, or from public or private research centers.

L'archive ouverte pluridisciplinaire **HAL**, est destinée au dépôt et à la diffusion de documents scientifiques de niveau recherche, publiés ou non, émanant des établissements d'enseignement et de recherche français ou étrangers, des laboratoires publics ou privés.



N° d'ordre NNT: 2019LYSEI048

# THÈSE de DOCTORAT DE L'UNIVERSITÉ DE LYON

préparée au sein de  
l'Institut National des Sciences Appliquées de Lyon

École Doctorale 162  
Mécanique, Énergétique, Génie civil, Acoustique

Spécialité/ discipline de doctorat  
**GÉNIE MÉCANIQUE**

Soutenue publiquement le 5 juillet, 2019, par:

**Shuai CHEN**

---

## Investigation of FEM Numerical Simulation for the Process of Metal Additive Manufacturing in Macro Scale

---

Devant le jury composé de:

Jean-Michel BERGHEAU  
Michel CORET  
Fabrice MORESTIN  
Pierre VACHER  
Laurent VAN BELLE  
Hélène WALTER-LE BERRE

Professeur (ENISE Saint-Etienne)  
Professeur (École Centrale de Nantes)  
Professeur (INSA Lyon)  
Professeur (Université Savoie Mont Blanc)  
Docteur (Centre Technique IPC)  
Maître de conférences (INSA Lyon)

Examinateur  
Rapporteur  
Directeur de thèse  
Rapporteur  
Examinateur  
Examinateur

LaMCoS - UMR CNRS 5514 - INSA de Lyon  
20, avenue Albert Einstein, 69621 Villeurbanne Cedex (FRANCE)



**Département FEDORA – INSA Lyon - Ecoles Doctorales – Quinquennal 2016-2020**

<b>SIGLE</b>	<b>ECOLE DOCTORALE</b>	<b>NOM ET COORDONNEES DU RESPONSABLE</b>
<b>CHIMIE</b>	<b>CHIMIE DE LYON</b> <a href="http://www.edchimie-lyon.fr">http://www.edchimie-lyon.fr</a> Sec. : Renée EL MELHEM Bât. Blaise PASCAL, 3e étage <a href="mailto:secretariat@edchimie-lyon.fr">secretariat@edchimie-lyon.fr</a> INSA : R. GOURDON	<b>M. Stéphane DANIELE</b> Institut de recherches sur la catalyse et l'environnement de Lyon IRCELYON-UMR 5256 Équipe CDFA 2 Avenue Albert EINSTEIN 69 626 Villeurbanne CEDEX <a href="mailto:directeur@edchimie-lyon.fr">directeur@edchimie-lyon.fr</a>
<b>E.E.A.</b>	<b>ÉLECTRONIQUE, ÉLECTROTECHNIQUE, AUTOMATIQUE</b> <a href="http://edeea.ec-lyon.fr">http://edeea.ec-lyon.fr</a> Sec. : M.C. HAVGOUDOUKIAN <a href="mailto:ecole-doctorale.eea@ec-lyon.fr">ecole-doctorale.eea@ec-lyon.fr</a>	<b>M. Gérard SCORLETTI</b> École Centrale de Lyon 36 Avenue Guy DE COLLONGUE 69 134 Écully Tél : 04.72.18.60.97 Fax 04.78.43.37.17 <a href="mailto:gerard.scorletti@ec-lyon.fr">gerard.scorletti@ec-lyon.fr</a>
<b>E2M2</b>	<b>ÉVOLUTION, ÉCOSYSTÈME, MICROBIOLOGIE, MODÉLISATION</b> <a href="http://e2m2.universite-lyon.fr">http://e2m2.universite-lyon.fr</a> Sec. : Sylvie ROBERJOT Bât. Atrium, UCB Lyon 1 Tél : 04.72.44.83.62 INSA : H. CHARLES <a href="mailto:secretariat.e2m2@univ-lyon1.fr">secretariat.e2m2@univ-lyon1.fr</a>	<b>M. Philippe NORMAND</b> UMR 5557 Lab. d'Ecologie Microbienne Université Claude Bernard Lyon 1 Bâtiment Mendel 43, boulevard du 11 Novembre 1918 69 622 Villeurbanne CEDEX <a href="mailto:philippe.normand@univ-lyon1.fr">philippe.normand@univ-lyon1.fr</a>
<b>EDISS</b>	<b>INTERDISCIPLINAIRE SCIENCES-SANTÉ</b> <a href="http://www.ediss-lyon.fr">http://www.ediss-lyon.fr</a> Sec. : Sylvie ROBERJOT Bât. Atrium, UCB Lyon 1 Tél : 04.72.44.83.62 INSA : M. LAGARDE <a href="mailto:secretariat.ediss@univ-lyon1.fr">secretariat.ediss@univ-lyon1.fr</a>	<b>Mme Emmanuelle CANET-SOULAS</b> INSERM U1060, CarMeN lab, Univ. Lyon 1 Bâtiment IMBL 11 Avenue Jean CAPELLE INSA de Lyon 69 621 Villeurbanne Tél : 04.72.68.49.09 Fax : 04.72.68.49.16 <a href="mailto:emmanuelle.canet@univ-lyon1.fr">emmanuelle.canet@univ-lyon1.fr</a>
<b>INFOMATHS</b>	<b>INFORMATIQUE ET MATHÉMATIQUES</b> <a href="http://edinfomaths.universite-lyon.fr">http://edinfomaths.universite-lyon.fr</a> Sec. : Renée EL MELHEM Bât. Blaise PASCAL, 3e étage Tél : 04.72.43.80.46 Fax : 04.72.43.16.87 <a href="mailto:infomaths@univ-lyon1.fr">infomaths@univ-lyon1.fr</a>	<b>M. Luca ZAMBONI</b> Bât. Braconnier 43 Boulevard du 11 novembre 1918 69 622 Villeurbanne CEDEX Tél : 04.26.23.45.52 <a href="mailto:zamboni@maths.univ-lyon1.fr">zamboni@maths.univ-lyon1.fr</a>
<b>Matériaux</b>	<b>MATÉRIAUX DE LYON</b> <a href="http://ed34.universite-lyon.fr">http://ed34.universite-lyon.fr</a> Sec. : Marion COMBE Tél : 04.72.43.71.70 Fax : 04.72.43.87.12 Bât. Direction <a href="mailto:ed.materiaux@insa-lyon.fr">ed.materiaux@insa-lyon.fr</a>	<b>M. Jean-Yves BUFFIÈRE</b> INSA de Lyon MATEIS - Bât. Saint-Exupéry 7 Avenue Jean CAPELLE 69 621 Villeurbanne CEDEX Tél : 04.72.43.71.70 Fax : 04.72.43.85.28 <a href="mailto:jean-yves.buffiere@insa-lyon.fr">jean-yves.buffiere@insa-lyon.fr</a>
<b>MEGA</b>	<b>MÉCANIQUE, ÉNERGÉTIQUE, GÉNIE CIVIL, ACOUSTIQUE</b> <a href="http://edmega.universite-lyon.fr">http://edmega.universite-lyon.fr</a> Sec. : Marion COMBE Tél : 04.72.43.71.70 Fax : 04.72.43.87.12 Bât. Direction <a href="mailto:mega@insa-lyon.fr">mega@insa-lyon.fr</a>	<b>M. Jocelyn BONJOUR</b> INSA de Lyon Laboratoire CETHIL Bâtiment Sadi-Carnot 9, rue de la Physique 69 621 Villeurbanne CEDEX <a href="mailto:jocelyn.bonjour@insa-lyon.fr">jocelyn.bonjour@insa-lyon.fr</a>
<b>ScSo</b>	<b>ScSo*</b> <a href="http://ed483.univ-lyon2.fr">http://ed483.univ-lyon2.fr</a> Sec. : Viviane POLSINELLI Brigitte DUBOIS INSA : J. Y. TOUSSAINT Tél : 04.78.69.72.76 <a href="mailto:viviane.polsinelli@univ-lyon2.fr">viviane.polsinelli@univ-lyon2.fr</a>	<b>M. Christian MONTES</b> Université Lyon 2 86 Rue Pasteur 69 365 Lyon CEDEX 07 <a href="mailto:christian.montes@univ-lyon2.fr">christian.montes@univ-lyon2.fr</a>

\*ScSo : Histoire, Géographie, Aménagement, Urbanisme, Archéologie, Science politique, Sociologie, Anthropologie



# Acknowledges

This thesis is the result of a research work I have carried out between 2015 and 2018 at the Laboratory of Mechanic of Contacts and Structures (LaMCoS), funded by the China Scholarship Council.

I would like to express my gratitude to all those whole helped me during the completion of the thesis. Without their support and encouragement, this thesis could not have reached its present form.

First and foremost, I want to extend my sincere gratitude to Ms. H  l  ne WALTER-LE BERRE, whose patient guidance, valuable suggestion and constant encouragement make me successfully complete this thesis. She has instructed me through all the stages of the accomplishment of this thesis. Her conscientious academic spirit and modest, open-minded personality inspire me both in academic study and daily life. She gives me much help and advice during the whole process of my research. Our frequent discussions make it possible for me to promote my study in the rapid development of additive manufacturing.

Second, I would like to express my heartfelt gratitude to Mr. Fabrice MORESTIN, who do me a great favour in the work of my thesis. He has many innovative ideas about additive manufacturing, and we have exchanged some interesting discussions in this work. His academic insight helped me to discover the value of my research. When I was confused during this work, his sagacious advice led me to return to the correct research direction.

The reviews and critics from my jury are also of importance for me to improve my thesis' quality. I'd like also deliver my thanks for their review work on my thesis manuscript.

This thesis was one part of a large project of LaMCoS aiming at metal additive manufacturing, which involved multi-disciplinary aspects (macroscopic simulations, microscopic melt pool model, and automation, etc.). Mr. Daniel N  LIAS has also helped me with the proposal of this thesis's topic at the beginning. Here I'd like to express my thanks to him, too.

Moreover, I would like to express my gratitude to Mr. Ning DANG, a doctor in the laboratory MATEIS. We discussed a lot about the knowledge of metallurgical transformation, which is of great significance for me to complete the multi-physics simulation.

Special thanks for all of my friends that are present in our laboratory: Alexis BONETTO, Chao ZHANG, Deqi LIU, Efoe WALLACE, Lv ZHAO, Meng WANG, Quanshangze DU, Thomas JAILIN, Tristan DJOURACHKOVITCH, Wenfeng YE, Wenjun GAO, Wenqi ZHU, Ye LU, Zikang LOW. During these four years, we enjoyed coffee breaks, lunches and so many other pleasant moments in LaMCoS. They helped me in many different manners, and I hope to continue to see them regularly.

I wish to appreciate all professors who have taught me in INSA de Lyon. Their instructions have helped broaden my horizon and their enlightening teaching has provided me with a solid foundation to accomplish this thesis and will always be of great value for my future career and academic research.

---

I would also like to thank the China Scholarship Council for supporting my study and life in France. I'm grateful to Shanxi Duoyuan Technology, a plastic 3D printing company, who also sponsored me to complete this thesis.

Last but not least, I would like to deliver my special thanks to my parents, whose supports from more than 8000 kilometres have motivated me to overcome difficulties in study and life during these years.

# Abstract

Additive manufacturing (AM) has become a new option for the fabrication of metallic parts in industry. However, there are still some limitations for this application, especially the unfavourable final shape and undesired macroscopic properties of metallic parts built in AM systems. The distortion or crack due to the residual stress of these parts leads usually to severe problems for some kinds of metal AM technology. In an AM system, the final quality of a metallic part depends on many process parameters, which are normally optimized by a series of experiments on AM machines. In order to reduce the considerable time consumption and financial expense of AM experiments, the numerical simulation dedicated to AM process is a prospective alternative for metallic part fabricated by additive manufacturing. Because of the multi-scale character in AM process and the complex geometrical structures of parts, most of the academic researches in AM simulation concentrated on the microscopic melting pool. Consequently, the macroscopic simulation for the AM process of a metallic part becomes a current focus in this domain.

In this thesis, we first study the pre-processing of AM simulation on Finite Element Method (FEM). The process of additive manufacturing is a multi-physics problem of coupled fields (thermal, mechanical, and metallurgical fields). The macroscopic simulation is conducted in two different levels with some special pre-processing work. For the layer level, the reconstruction of 3D model is conducted from the scan path file of AM machine, based on the inverse manipulation of offsetting-clipping algorithm. For the part level, the 3D model from CAD is reconstructed into a voxel-based mesh, which is convenient for a part with complex geometry. The residual stress of a part is analysed under different preheat temperatures and different process parameters. These simulations imply the potential technique of reducing residual stress by the optimisation of process parameters, instead of the traditional way by increasing preheat temperature.

Based on the FEM simulation platform above, two simulations at line level are also studied in this thesis, aiming at the relation between the AM process and part's final quality. These examples demonstrate the feasibility of using macroscopic simulations to improve the quality control during the AM process. In the first task, dataset of heating parameters and residual stress are generated by AM simulation. The correlation between them is studied by using some regression algorithm, such as artificial neural network. In the second task, a PID controller for power-temperature feedback loop is integrated into AM process simulation and the PID auto-tuning is numerically investigated instead of using AM machine. Both of the two tasks show the important role of AM macroscopic process simulation, which may replace or combine with the numerous trial and error of experiments in metal additive manufacturing.

**KEYWORDS:** Additive manufacturing, Numerical simulation, Finite element method, Multiphysics, Residual stress, Voxelization, PID controller, Regression, Artificial neural network





# Résumé

La fabrication additive (FA) est devenue une nouvelle alternative pour la fabrication des pièces dans l'industrie. Cependant, il existe encore des limites pour ce procédé, en particulier la forme finale défavorable et les propriétés macroscopiques indésirables des pièces métalliques construites dans les systèmes de FA. La distorsion ou la fissure due à la contrainte résiduelle de ces pièces pose généralement de graves problèmes pour certains types de technologie de la FA métallique. Dans un système de FA, la qualité finale d'une pièce métallique dépend de nombreux paramètres de procédé, qui sont normalement optimisés par une série d'expériences sur des machines de FA. Afin de réduire la consommation de temps et le coût financier qui sont considérables dans des expériences de FA, la simulation numérique dédiée au procédé de FA est une alternative potentielle pour les pièces métalliques fabriquées par la fabrication additive. En raison du caractère multi-échelle des procédés de FA et des structures géométriquement complexes, la plupart des recherches académiques qui travaillent sur la simulation de FA se sont concentrées sur le bain de fusion microscopique. Par conséquent, la simulation macroscopique pour le procédé de FA d'une pièce métallique devient actuellement une priorité dans ce domaine.

Dans cette thèse, nous étudions d'abord le pré-processing de la simulation de FA par la méthode des éléments finis (FEM). Le procédé de fabrication additive est un phénomène multi-physique des champs couplés (champs thermique, mécanique et métallurgique). La simulation macroscopique est réalisée à deux niveaux différents. Au niveau de la couche, la reconstruction du modèle 3D est effectuée à partir du fichier de chemin de balayage de la machine de FA, basée sur la manipulation inverse de l'algorithme d'offsetting-clipping. Au niveau de la pièce, le modèle 3D de CAO est reconstruit dans un maillage des voxels, ce qui est pratique pour une pièce avec une géométrie complexe. Avec les températures de préchauffage différentes et les paramètres du procédé différents, la contrainte résiduelle d'une pièce est analysée. Ces simulations impliquent la technique potentielle pour réduire la contrainte résiduelle par l'optimisation des paramètres du procédé, au lieu de moyens traditionnels par augmenter la température de préchauffage.

Basées sur la plateforme de simulation de FEM ci-dessus, deux simulations au niveau de ligne sont également étudiées dans cette thèse, visant à la relation entre le procédé de FA et la qualité finale de la pièce. Ces exemples démontrent la possibilité d'utiliser des simulations macroscopiques pour améliorer le contrôle de la qualité pendant le procédé de FA. Dans la première tâche, l'ensemble de données des paramètres de chauffage et la contrainte résiduelle sont générés par la simulation de FA. La corrélation entre eux est étudiée en utilisant des algorithmes de régression, tel que le réseau neuronal artificiel. Dans la deuxième tâche, un contrôleur de PID pour la boucle de rétroaction puissance-température est intégré dans la simulation de procédé de FA et l'auto-réglage de PID est numériquement étudié au lieu d'utiliser la machine de FA. Les deux tâches montrent le rôle important de la simulation de procédé macroscopique de FA, qui peut remplacer ou combiner les nombreuses expériences essai-erreur dans la fabrication additive métallique.

---

**MOTS CLÉS:** Fabrication additive, simulation numérique, méthode des éléments finis, Multiphysique, Contrainte résiduelle, Voxélisation, Régulateur PID, Régression, Réseau neuronal artificiel

# Contents

<b>Contents</b>	<b>i</b>
<b>List of Figures</b>	<b>v</b>
<b>List of Tables</b>	<b>ix</b>
<b>General introduction</b>	<b>1</b>
<b>1 Basic knowledge on additive manufacturing</b>	<b>5</b>
1.1 Fundamentals of additive manufacturing . . . . .	7
1.1.1 Advantages . . . . .	7
1.1.2 Limitations . . . . .	8
1.2 Typical metal additive manufacturing technologies . . . . .	9
1.2.1 Extrusion-based or sheet-based additive manufacturing . . . . .	10
1.2.2 Powder-based additive manufacturing . . . . .	12
1.3 Some problems in metal additive manufacturing . . . . .	15
1.3.1 Problems for designers before AM manufacturing . . . . .	15
1.3.2 Problems during AM process . . . . .	17
1.3.3 Problems after the printing of an AM object . . . . .	23
1.4 Some typical techniques for the AM simulation . . . . .	24
1.4.1 Numerical Methods for dynamic AM process . . . . .	24
1.4.2 Numerical methods for irregular and free boundary condition . . . . .	27
1.5 Novelty of this work . . . . .	31
1.5.1 Pre-processing for macroscopic simulation . . . . .	32
1.5.2 Dynamic simulation at different levels . . . . .	32
1.5.3 Reduction of residual stress at lower preheat temperature . . . . .	33
1.5.4 Process parameters study and control loop platform . . . . .	35
<b>2 Theoretical basis for additive manufacturing simulation</b>	<b>37</b>
2.1 Thermal equation for temperature . . . . .	39
2.1.1 Basic heat equation for additive manufacturing . . . . .	39
2.2 Mechanical equation for residual stress . . . . .	43
2.3 Metallurgical phase models in macroscopic scale . . . . .	45
2.3.1 Martensitic transformation . . . . .	46

2.3.2	Diffusional transformation . . . . .	48
2.4	Conclusion . . . . .	52
<b>3</b>	<b>Macroscopic AM simulation for multiphysics fields</b>	<b>55</b>
3.1	Workflow of file formats for additive manufacturing process . . . . .	57
3.2	Pre-processing for 3D model with complex geometry . . . . .	60
3.2.1	Analysis G-code file and extraction of scan path information . . . . .	60
3.2.2	Reconstruction of 3D model at layer size: offsetting and clipping . . . . .	62
3.2.3	Map of sets in orphan FEM mesh and in CAD geometry . . . . .	67
3.2.4	Reconstruction of 3D model at part size: voxelization . . . . .	70
3.3	FEM simulation for multi-physics fields . . . . .	73
3.3.1	Thermal simulation at layer-level . . . . .	75
3.3.2	Thermal-mechanical-metallurgical simulation at part-level . . . . .	84
3.4	Study on AM process parameters for a part's residual stress . . . . .	98
3.4.1	Influence of preheat temperature . . . . .	99
3.4.2	Influence of AM process parameters ( $P_i, t_i$ ) . . . . .	101
3.5	Conclusion . . . . .	108
<b>4</b>	<b>Regression between process parameters and residual stress</b>	<b>111</b>
4.1	Influence of multi-parameters on residual stress . . . . .	113
4.2	A basic thermal-mechanical AM simulation of a zigzag line . . . . .	115
4.3	Post-processing of AM simulation with regression . . . . .	120
4.4	Regression implementations . . . . .	122
4.5	Artificial neural network for regression . . . . .	123
4.5.1	Fundamentals of back-propagation algorithm . . . . .	124
4.5.2	Construction of artificial neural network . . . . .	125
4.5.3	Regression after AM simulations . . . . .	126
4.6	Conclusion . . . . .	128
<b>5</b>	<b>Simulation for the control of the process in additive manufacturing</b>	<b>131</b>
5.1	Preparation for the study of AM thermal system's control . . . . .	133
5.2	PID controller in feedback loop . . . . .	139
5.3	AM simulation with PID power controller for temperature . . . . .	142
5.4	PID parameters tuning . . . . .	143
5.4.1	Manual PID tuning . . . . .	143
5.4.2	Auto-tuning . . . . .	143
5.5	Conclusion . . . . .	149
	<b>General conclusions and perspectives</b>	<b>151</b>
<b>A</b>	<b>Additive manufacturing's workflow in industry</b>	<b>155</b>
<b>B</b>	<b>Python codes for mesh incompatibility problem</b>	<b>157</b>

<b>C</b>	<b>Reconstruction of tracks in one layer from G-code</b>	<b>161</b>
<b>D</b>	<b>Script for simulating a feedback loop</b>	<b>167</b>
<b>E</b>	<b>Subroutines for simulating Ti6Al4V phase transformation</b>	<b>169</b>
<b>F</b>	<b>Abaqus post-process program to extract von Mises stress</b>	<b>175</b>
	<b>Bibliography</b>	<b>179</b>



# List of Figures

1	Overall structure of this thesis . . . . .	4
1.1	Bound Metal Deposition[MET 17] . . . . .	11
1.2	Laminated Object Manufacturing[MEK 16] . . . . .	12
1.3	Selective Laser Melting(SLM)[YAS 18] . . . . .	13
1.4	Interaction of laser-material in Selective Laser Sintering (SLS)[KOL 17] .	13
1.5	Electron Beam Melting (EBM)[QUR 18] . . . . .	14
1.6	Laser deposition device (DMD)[THO 15] . . . . .	15
1.7	Design of a part's support structure in additive manufacturing[WRI 15] .	16
1.8	Different printing qualities varying with part's orientation[WAR 16] . . .	17
1.9	Variation of the residual stress of different types along a line[WIT 01] . .	18
1.10	Crack caused by residual stress[COM 17] . . . . .	19
1.11	Two mechanisms of residual stress [WIT 07] . . . . .	19
1.12	A beam's wrapage induced by residual stress [FRU 15] . . . . .	20
1.13	Recoater tolerance[AUT 18] . . . . .	20
1.14	Blade crash of a part's shape in additive manufacturing[MCG 17] . . . . .	21
1.15	A part with optimal orientation suffers less from recoater blade interfer- ence effect[ZEL 15] . . . . .	22
1.16	Incompleted parts induced by lack of fusion[MCG 17] . . . . .	22
1.17	Balling effect on part's surface in EBM, caused by overheating[ZÄH 10] .	23
1.18	Wrapping of substrate after AM fabrication[ZEL 15] . . . . .	24
1.19	Difficulty in the removal of support structure without damage[STA 17] . .	24
1.20	Thermal simulation with DEM for powder-bed AM system. [STE 16a] . .	26
1.21	Computational domain with different mesh densities[STA 18] . . . . .	27
1.22	Dynamic mesh refinement preparing for heat affected zone[PAT 15] . . .	27
1.23	A scoliosis-brace-model reconstructed by voxelization[FRA 17] . . . . .	28
1.24	Interfaces tracked by the level set method[ZHA 18] . . . . .	29
1.25	Simulation results for keyhole and melt pool formation by volume of fluid[OTT 10] . . . . .	30
1.26	Concept of finite cell method [TAG 18] . . . . .	30
1.27	Difficulty of connecting AM machine data with FEM simulation . . . . .	31
1.28	Material deposition at line level[FAL 11] . . . . .	33
1.29	Different levels for birth and death method . . . . .	33
1.30	Preheating hardware for powder-bed based techniques[CAP 18] . . . . .	34



## List of Figures

---

1.31	Preheating hardware for powder-injection based techniques[BRA 16]	35
1.32	Hardware for the temperature closed-loop of an AM machine[FAR 16]	36
2.1	Interactions between multiphysics processes in additive manufacturing	39
2.2	Moving free boundary during material deposition	41
2.3	Laser profiles of different TEM[MOR 17]	42
2.4	Goldak heat source model[GOL 84]	42
2.5	Volumetric heat source model	43
2.6	Temperature-induced martensitic transformation[VAN 13]	46
2.7	Basic algorithm for calculating $f_{\alpha'}$	47
2.8	Kinetic parameters $k(T)$ at $n = 2.5$ for diffusional transformation[AHN 16]	48
2.9	Generalization of the Johnson-Mehl-Avrami equation for non-isothermal transformations [CRE 11]	49
2.10	Algorithm flow chart for diffusional transformation with modified JMA model	52
3.1	Basic workflow in additive manufacturing[TAU 13]	57
3.2	File format conversion from CAD to FEM analysis	58
3.3	A part with complex geometry in slicer software(CuraEngine)	59
3.4	G-code generated by CuraEngine	61
3.5	Reconstruction of a 3D thin-wall structure	63
3.6	Inner offsetting of a polygon[CHE 05]	63
3.7	Clipping for a rectangle[HSI 95]	63
3.8	Generation scan path in one layer, (a) is the background paths before clipping (b) is the final path [DIN 15a]	65
3.9	Flowchart for partitions in one layer, opposite to slicer's manipulation	65
3.10	Generation of the partition for FEM simulation from gcode scan paths	66
3.11	Detailed view of one layer in a thin wall during the pre-process	67
3.12	Loss of ElementSet definition during assembly between different coordinates	68
3.13	Flowchart of the algorithm to map ElementSet between two coordinates	69
3.14	File format conversion in voxelization	71
3.15	3D model of a turbine blade with a twist in vertical direction	72
3.16	Approximation of a blade by voxelization (length of voxel is 1.333mm)	72
3.17	Geometrical approximation of voxelization	73
3.18	Basic steps of AM simulation using birth and death technique	75
3.19	The first 4 layers of a wall structure (red, yellow, blue, green)	75
3.20	The scan path partition for the 4th layer	76
3.21	The mesh of 4 layers and their substrate.	76
3.22	Mechanical property of Maraging steel at different temperatures[VAN 13]	77
3.23	Screenshots of the AM deposition process (546 lines in total, 4 layers), the temperature unit is $^{\circ}C$	82
3.24	Position of 4 sensor points (yellow circles) in the centre of each layer	83

3.25	Temperature evolution at 4 sensor points . . . . .	84
3.26	Mesh of the turbine blade (partition of 30 layers) and its substrate . . . . .	85
3.27	Ti6Al4V's material properties which depend on temperature . . . . .	87
3.28	Mechanical boundary condition at the substrate's bottom face . . . . .	88
3.29	Position of 30 sensor points in each layers of the blade . . . . .	88
3.30	Screenshots of thermal simulation ( $^{\circ}C$ ) in part-level for a blade . . . . .	90
3.31	Temperature evolution at 30 sensor points . . . . .	90
3.32	Simple example of substrate effect . . . . .	91
3.33	Fraction of each layer's volume $V_i$ in whole part $V_{all}$ . . . . .	92
3.34	Decoupling of three multi-physics field in this thesis. . . . .	92
3.35	Screenshots of the simulation for $\alpha$ phase during AM process . . . . .	93
3.36	Screenshots of the simulation for $\beta$ phase during AM process . . . . .	94
3.37	Screenshots of the simulation for martensite $\alpha'$ during AM process . . . . .	94
3.38	$\alpha$ phase's evaluation at 30 sensor points . . . . .	95
3.39	$\beta$ phase evaluation's at 30 sensor points . . . . .	95
3.40	Evolution of temperature rate $dT/dt$ at 30 sensor points . . . . .	96
3.41	Final displacement ( $mm$ ) at environment temperature . . . . .	97
3.42	Final von Mises residual stress ( $MPa$ ) at environment temperature with different views . . . . .	98
3.43	Temperature evaluation of the case in which the preheat temperature $T_{pre}$ is $500^{\circ}C$ . . . . .	99
3.44	Final residual stress ( $MPa$ ) with different preheat temperature $T_{pre} = 500^{\circ}C$ and $T_{pre} = 240^{\circ}C$ (Reference case)(Other AM process parameters are the same) . . . . .	100
3.45	The input power and heating time for different AM simulation cases. . . . .	102
3.46	The coefficient $C_i$ for the input power of the case D. . . . .	102
3.47	Temperature evolution at 30 sensor points for different simulation cases (Each different colour represents one layer.) . . . . .	103
3.48	The AM thermal process of Case Ref and Case D. . . . .	104
3.49	Residual stress $\sigma_{vonMises}$ ( $MPa$ ) distribution for different simulation cases	104
3.50	Histogram of $\sigma_{vonMises}$ throughout the blade for different simulation cases	105
3.51	PDF of AM case with different preheat temperature $T_{pre} = 500^{\circ}C$ and $T_{pre} = 240^{\circ}C$ (Reference case). . . . .	106
3.52	PDF of AM cases (Case D and Reference Case). . . . .	107
3.53	PDF of AM cases (Case A, Case B, Case C and Reference Case). . . . .	107
4.1	Quality control in powder bed fusion[SAM 16] . . . . .	113
4.2	Influence of process parameters on the final quality of a part in additive manufacturing . . . . .	114
4.3	Detailed view of the zigzag track's mesh . . . . .	115
4.4	A zigzag track and its substrate . . . . .	116
4.5	Mesh and mechanical boundary condition . . . . .	116
4.6	Screenshots of thermal simulation ( $^{\circ}C$ ) for a zigzag track in AM process .	118

4.7	Residual stress ( $Pa$ ) as tensor components . . . . .	119
4.8	Residual stress $\sigma_{vonMises}$ ( $Pa$ ) for a zigzag track line . . . . .	120
4.9	PDF of the uniform distribution $U[0.1, 10.0]$ . . . . .	121
4.10	Basic structure of an artificial neuron . . . . .	123
4.11	Artificial neural network with multiple neurons and layers . . . . .	125
4.12	Regression using artificial neural network in Tensorflow . . . . .	127
4.13	Regression using different algorithms in Scikit-learn . . . . .	128
5.1	Powder-injection based AM system (LENS)[GU 15] . . . . .	133
5.2	Influence of process parameters (Heat source control) on the quality of component made by AM[VAN 13] . . . . .	134
5.3	Whole field (multiple points)'s control depends on scan path for an AM system . . . . .	135
5.4	Difference in temporal respond between LTI system and non-LTI system . . . . .	136
5.5	Block diagram of an open-loop AM system . . . . .	136
5.6	5 simulations for the open-loop AM system . . . . .	137
5.7	The difference of crowdedness for two deposits . . . . .	138
5.8	Block diagram of PID controller's internal structure . . . . .	140
5.9	Block diagram of a close-loop AM system with a PID controller . . . . .	140
5.10	Flow chart of PID controller's algorithm . . . . .	141
5.11	Relay method for auto-tuning [WIL 05] . . . . .	144
5.12	Flow chart of relay method for a PID controller's auto-tuning . . . . .	145
5.13	Block diagram of a close-loop with relay method for PID auto-tuning . . . . .	146
5.14	Relay method, $P_{preset} = 6.0 \times 10^{11} W/m^3$ , $T_{preset} = 1600^\circ C$ . . . . .	147
5.15	PID control in AM simulation with different controllers . . . . .	148
A.1	Additive manufacturing's workflow in industry[THO 18] . . . . .	155

# List of Tables

- 1.1 Catalogue of some AM technologies . . . . . 9
- 1.2 Some commercial AM machines and their preheat temperature . . . . . 34
  
- 3.1 Some G-code keywords in CuraEngine . . . . . 61
- 3.2 Material property and process parameters in simulation . . . . . 78
- 3.3 Ti6Al4V's material parameters and AM process parameters . . . . . 86
- 3.4 Johnson-Cook plastic properties for Ti6Al4V[ZHA 15] . . . . . 86
- 3.5 Some cases for AM process parameters adjustment . . . . . 101
- 3.6 Statistic results and Burr XII coefficients . . . . . 106
  
- 4.1 Steel parameters and some process parameters . . . . . 117
- 4.2 The input parameters and output criteria in 1 time of AM simulation . . . 121
  
- 5.1 Ziegler-Nichols auto-tuning method for PID controller . . . . . 144
- 5.2 Different kinds of PID controllers . . . . . 148

## List of Tables

---

# General introduction

Additive manufacturing (AM) is becoming more and more important in the fabrication of parts in industry [MIL 17] and it has become a multi-disciplinary hot spot for academic researchers during the last decade. For these metallic part built by additive manufacturing, their qualities aren't always satisfactory[THO 15]. In metal additive manufacturing, both the shape and property of a part are impacted by AM process, and some problems may limit the application of metallic part made by AM[MOY 13][YAN 17b], such as residual stress, dimensional accuracy, surface quality, mechanical properties, porosity/density, and fatigue, etc. These problems are generally studied by experiments and numerical simulations. The simulation of AM process provides an important mean to "virtually" run experiments. It is more cost-effective and less time-consuming relative to trial-and-error experimentation with difficult measurement techniques. Now researchers need AM macroscopic simulation as a more convenient tool to discover new techniques for some typical problems in additive manufacturing, such as reduction of residual stress (The older technique by increasing preheat temperature has physics limit). Although numerical simulation has many advantages in AM research, there are still some challenges to solve:

- Multi-scale modelling for AM process

The process of additive manufacturing is a multi-physics problem from micro-scale (melting pool) to macro-scale (track, layer, part). The separation of these scales makes it quite difficult to describe the complex phenomena in the AM process as a unique model[KIN 15][GHO 18]. In AM macroscopic simulation, the free surface boundary conditions is an unavoidable problem for the material addition and multi-track deposition effects of 3D objects.

- Geometric irregularity

The pre-processing is often a challenge for AM simulation in macro scale. This is one of the reasons why the majority of AM simulation focused on the thin wall or single line building process [MUK 17] [MIC 14][MAR 14][LIO 15]. The workflow of additive manufacturing from CAD to CAM, is established on knowledge of computer graphics [LIV 17]. Currently, most CAD software is based on parametric NURBS system. They are well suited to modelling geometries associated with conventional manufacturing processes (extrusions, revolves,lofts, etc.) but often inadequate for the more complex geometrical shapes. Moreover, it isn't easy to acquire multi-scale geometrical models (melting pool, track line, layer, part, etc.) from a 3D

object in traditional CAD software[THO 16]. Additionally, the scan path generated by slicer algorithms [STE 16b] can't be directly imported into FEM analysis. Because of the geometric irregularity of an object built by AM, it is necessary to apply special algorithms to reconstruct the 3D model in additive manufacturing[BAD 18].

- Control loop

In an open-loop AM system, fluctuations in the process parameters (e.g., laser power, scanning speed, and powder flow rate) often deflect the process from the pre-optimized condition, resulting in defects in the finished components. Some researchers have developed sensing and control system for the robotically controlled AM systems[MAN 15][SHA 15]. The process monitoring offers a way to ensure part quality and process efficiency. Nevertheless, these real-time systems are still in their infancy[DIN 16d][EVE 16], because they rely on not only hardware but also the understanding of the responsive behaviours of AM systems to process parameters.

- Process parameter optimization

The quality of an AM-fabricated component exhibit high dependence on input process parameters. By appropriately selecting the optimum parameter values, the quality of a part fabricated by AM machine can be improved. It is generally hard to obtain the explicit formulation between process parameters and quality criteria, due to the complexity of AM process. However, the real-time feedback control loop in an AM system relies strongly on the rapid calculation of correlation between input parameters and output parameters. Thus this correlation should be acquired before the start of AM process. The method to reveal phenomenological correlation from datasets of experiments or simulations will be helpful for the quality control in additive manufacturing.

- Ecosystem of AM simulation tools

The additive manufacturing is a rapidly developing area. Many companies adopt the sale strategy of machine-material-software, which makes metal additive manufacturing's ecosystem quite complex [GAO 15]. It isn't always easy to convert different file formats in the workflow of AM simulation. The majority of in-house or commercial software are close-source. Academic researchers often need more flexible tool to study the detail of simulation detail. Thus it is essential to construct numerical platforms based on general-purpose FEM software and explore the methodology of AM simulation.

In this thesis, we investigate the macroscopic AM process of a metallic part by FEM simulation, mainly around the problems above. Here is the structure of this thesis:

In Chapter 1, the current situation of additive manufacturing is introduced, as well as its problems in the application of metallic part fabrication. Some trends in numerical simulation for additive manufacturing are also briefly introduced. The classification of

additive manufacturing is various according to different aspects. The mainstream of metal additive manufacture is generally powder-bed based or powder-injection based. For a metallic part fabricated on AM systems, its shape and properties may not be satisfactory as designed. Some numerical methods are applied for the macroscopic simulation of additive manufacturing by academic researchers and proprietary software. The novelty of this thesis is also summarized at the end of this chapter

In Chapter 2, additive manufacturing is mathematically described as a multi-physics coupling problem. The macroscopic behaviours of a building part and its substrate are decoupled into three aspects: thermal field, mechanical field, and metallurgical field. Heat source models are introduced in thermal analysis besides basic governing equation. Elasto-plastic equations are combined with Johnson-Cook hardening model so as to calculate residual stress. For the evolution of metallurgical phases, we take titanium alloy Ti6Al4V as an example and two-phase transformation models, Koistinen-Marburger (KM) model and modified Johnson-Mehl-Avrami (JMA) model, are briefly introduced.

In Chapter 3, the special problems on pre-processing are investigated for the AM simulation on different levels: layer level and part level. We construct the platform for macroscopic FEM simulation by using polygon offsetting/clipping algorithm and voxelization method. Because of numerous repeated operations in AM FEM simulation, these pre-processing work are completed by programming instead of manual manipulation. In layer level simulation, text-processing on G-code file and coordinates transformation on database are accomplished, which overcome some obstacles of simulating an object with complex geometry. Then the thermal field of 4 thin layers is simulated during their dynamic AM process. Additionally, we use voxelization representation as an approximation of the object created by boundary representation (B-Rep), then voxelization is proved to be a convenient method for part level's simulation of additive manufacturing. Multi-physics fields are simulated for a twisted turbine blade's printing process. Its residual stress is analysed with different preheat temperature or with different process parameters. This implies a new potential technique to reduce residual stress at lower preheat temperature.

In Chapter 4, some regression analysis is conducted to reveal the statistic relation between AM process parameters and the final quality of the product made by additive manufacturing. Artificial neural network and other algorithms are compared as post-processing for data acquired from AM macroscopic simulation. The maximum residual stress of part is chosen as the criterion of the product's final quality while three parameters (deposition order, heat source power and heating time) represents the intricate process in additive manufacturing. With some regression tools, we attempt to obtain the phenomenological relation which estimates quantitatively the influence of these three process parameters on residual stress.

In Chapter 5, the evolution of temperature in an AM thermal field is simulated to demonstrate the feasibility of simulating the feedback control loop in additive manufacturing. The one-point temperature control is the fundamental framework for AM process control-loop. PID controller and its parameter auto-tuning are investigated by iterations of calculating and post-processing. Regulation of heat source power is conducted so as



to control part's maximum temperature. A PID controller is integrated into AM simulation in which the temperature's sampling is employed by post-processing work. Ziegler-Nichols method and relay method are adopted, aiming to improving the efficiency of PID controller's auto-tuning.

General conclusions and perspectives of this work will be given at the end of this manuscript.

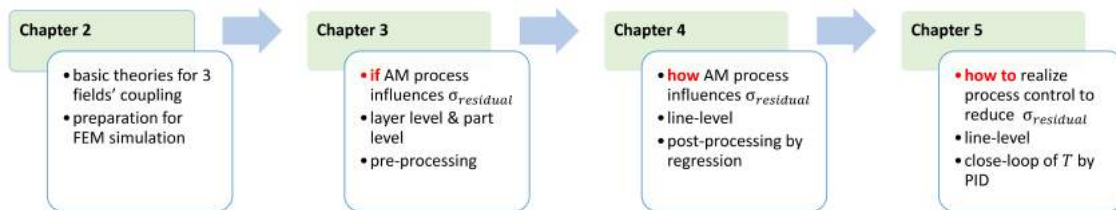


**Figure 1:** Overall structure of this thesis

# Chapter 1

## Basic knowledge on additive manufacturing

*This chapter presents the current situation of additive manufacturing, and its problems in the application of metallic part fabrication. Some trends in numerical simulation for additive manufacturing are also briefly introduced. The novelty of this thesis is listed at the end of this chapter.*

## Contents

---

<b>1.1</b>	<b>Fundamentals of additive manufacturing</b>	<b>7</b>
1.1.1	Advantages	7
1.1.2	Limitations	8
<b>1.2</b>	<b>Typical metal additive manufacturing technologies</b>	<b>9</b>
1.2.1	Extrusion-based or sheet-based additive manufacturing	10
1.2.2	Powder-based additive manufacturing	12
<b>1.3</b>	<b>Some problems in metal additive manufacturing</b>	<b>15</b>
1.3.1	Problems for designers before AM manufacturing	15
1.3.2	Problems during AM process	17
1.3.3	Problems after the printing of an AM object	23
<b>1.4</b>	<b>Some typical techniques for the AM simulation</b>	<b>24</b>
1.4.1	Numerical Methods for dynamic AM process	24
1.4.2	Numerical methods for irregular and free boundary condition	27
<b>1.5</b>	<b>Novelty of this work</b>	<b>31</b>
1.5.1	Pre-processing for macroscopic simulation	32
1.5.2	Dynamic simulation at different levels	32
1.5.3	Reduction of residual stress at lower preheat temperature	33
1.5.4	Process parameters study and control loop platform	35

---

## 1.1 Fundamentals of additive manufacturing

Additive manufacturing (AM), also known as 3D printing, is the general term for those technologies that create digitally 3D physical objects by successive addition of material. In additive manufacturing, a 3D object is usually built from a digital model into its designed shape using layer by layer process. In comparison with formative (eg. casting, forging, mould or dies, plastic injection) or subtractive (e.g. carving, milling, drilling, grinding) manufacturing, additive manufacturing is fundamentally different in methodologies and it can significantly simplify the process of producing complex 3D objects. Nowadays, Additive manufacturing technologies have already been used for various applications in the engineering industry as well as other areas of society, such as medicine, education, architecture, entertainment, jewellery, and so on[TOF 18].

All AM machines presently use a layer-based approach, in which each layer is a thin cross-section of the part derived from the original Computer Aided Design (CAD) data[ONS 18]. The final part made by AM technology can be considered as a geometrical approximation of the originally designed data. The additive manufacturing is broadly applicable in different material categories, including metals, ceramics, polymers, composites and biological materials. Correspondingly, additive manufacturing applies different technologies for the material joining process. Hence, the categories of additive manufacturing technologies are still increasing with the rapid development of AM in both industrial and academic research.

### 1.1.1 Advantages

Additive manufacturing provides many opportunities to design and improve products. Since the first stereolithography fabrication system in the 1980s, additive manufacturing has been revolutionizing the way things are made for more than 30 years. The product portfolio and product life-cycle, such as design (CAD), engineering (CAE), manufacturing (CAM) and manufacturing operations management (MOM), will benefit from the advantages of AM technologies including:

#### 1. Geometrical complexity

Weight is an important parameter in automotive industry and aeronautic industry, correlating to fuel consumption. Additive manufacturing's flexibility in highly complex geometries gives the designer more freedom during the design process to optimize the product. The lightweight design of parts can be developed with less manufacturing constraints after topology optimization.

#### 2. Less assembly

In additive manufacturing, detailing screw holes and assembly drawing is greatly reduced by combining features into single-piece part [CUE 18]. Therefore, AM technology is an alternative option for solving geometric dimensioning and tolerancing (GD&T) issues in assembly.

#### 3. Less waste of material

in comparison with subtractive manufacturing the required material can be significantly reduced in additive manufacturing. The use of material can be minimised while part's strength/weight ratio is still retained after optimization.

### **4. Highly customizable On-demand production**

With the help of AM, manufacturers can increase the diversity of product offerings which are currently too small to specialize due to costs of mould, die or tooling. With a more affordable price, the consumer can buy built-to-order products more closely suitable for individual needs and wants. Without the need for moulds and dies, AM enables the engineers or designer to try multiple iterations simultaneously with less costs. It is also the reason why AM is also sometimes named as Rapid Prototyping.

### **1.1.2 Limitations**

Additive manufacturing has distinct advantages and disadvantages. Thus AM is not always the best choice for all kinds of products. Before the application of additive manufacturing, designers and engineers should take the trade-off into consideration between its benefits and its limitations. Some limitations restrict the application of AM technology and overcoming these problems is still challenging for scientists and researchers. These limitations are partially summarized as follow:

#### **1. Poor mechanical property and excessive distortion**

Due to the layer-by-layer fabrication process, usually some properties of a part is non-isotropic. Therefore, parts made by some AM technologies, especially metallic parts, are often weaker in strength and endurance than their traditionally manufacturing counterparts. Distortion may occur in the AM process and this may lead to the bad quality of shape, even to the cease of fabricating process.

#### **2. Hardware expense**

As opposed to conventional manufacturing machine, additive manufacturing is relatively more expensive for large production runs. Specialized equipment, such as devices of high-voltage power supply, are essential for some AM machines. Some auxiliary modules should be installed as well. For example, large numbers of ultra-fine powder or some hazardous volatile organic compounds may be emitted during printing. The devices treating harmful emission are indispensable in these AM systems. The integration of sophisticated devices makes the price of AM machines still expensive for industrial application.

#### **3. Limited component size and slow build rate**

Many AM machines lay down material in small building chambers and it assures printing resolution with nozzles or other delicate deposition devices. The limited volume of AM system and the speed of material deposition often makes additive manufacturing less competitive in part size and building rate than conventional manufacturing.

#### **4. Difficult process configuration and control**

AM machine works digitally from CAD file to its final part. It involves many process parameters impacting the final quality of product. The configuration and control is usually empirical on AM machines. If one factor is changed in AM, the other parameter should be

re-determined after a series of trial. This is one reason why some AM machine companies often sell their machine bundled with their special raw material. The configuration and control of these parameters during process relies on a better understanding of AM systems and improvement of hardware.

## 1.2 Typical metal additive manufacturing technologies

The range of materials usable for AM technologies is very wide. Parts can be printed from different plastics like Nylon, polystyrene to metals (steel, titanium, aluminium or other alloys). Today there are so many kinds of materials in AM systems, and even the same kinds of material can be treated by different forming methods in additive manufacturing [CHU 14]. It is quite hard to categorize AM technologies into logical groups. Here is only a brief summary of current additive manufacturing, based on three aspects: material chemical composition, material initial state, and technological method. Since the development of AM technologies is fast in recent decades and inventions of new systems are still continued in industrial and academic domain, the categorization of AM technologies only includes here some relatively mature technologies.

**Table 1.1:** Catalogue of some AM technologies

Technology	Material	Phase	Heat
Selective Laser Melting(SLM)	metal	powder	laser
Selective Laser Sintering(SLS)	plastics, ceramics	powder	laser
Electron Beam Melting(EBM)	metal	powder	electron
Laser Engineered Net Shaping /Directed Light Fabrication /Laser solid Forming /Laser Metal Deposition(LENS/DLF/LSF/LMD)	metal	powder	laser
Wire Arc Additive Manufacture(WAAM)[DIN 15b]	metal	wire	arc welding
Electromagnetic-Compressed Plasma Deposition Manufacturing(EPDM)	metal	powder	plasma
Shaped Metal Deposition(SMD)	metal	wire	TIG welding
Direct Metal Deposition(DMD)	metal	powder	laser
Uniform Droplet Spray/Net Droplet-Based Manufacturing(UDS/NDM)	metal	droplet	induction coil
Electron Beam Freeform Fabrication (EBF3)	metal	wire	electron
Laminated Object Manufacturing(LOM)	metal,non-metal	laminate	heated roller
Laser Cladding(LC)	metal,non-metal	powder/wire	laser

Different AM technologies can be distinguished by the material chemical composition including paper, polymers, wax, resins, metals, ceramics and the mixture of them [IAN 15]. Extensive knowledge of material is necessary for an appropriate choice of forming methods.

Metal is one of the essential materials widely used in current AM systems. Metals have generally higher yield strength among conventional structural materials. Their

applications for AM systems are widely researched as its important role in industry, architecture, jewellery and bio-medicine, etc. Nevertheless, for some metal AM systems based on melting or sintering, heat process such as sintering during manufacturing will cause rapid temperature gradients and residual stress or cracking occurs. Nowadays, metal AM technologies have still some severe problems in comparison to conventional subtractive metal manufacturing. Laser and electron beam are usually be used as heat source in metal AM system.

A final workpiece fabricated by additive manufacturing is usually a solidified object. However, the joining process of material depends on the different initial states of raw material in different AM systems [MEL 14]. Powder materials are usually used for metal printing. Powder material can be processed by partially or fully melting and fusing together, creating a solid part with "powder bed fusion" or "directed energy deposition" technologies. Laser or electron beam can be used to melt the powder. Also, the powder can be glued by a special substance called binder. The physics properties of discrete metal powder and a solidified metal sample are generally different because of their difference in scales.

In the development of AM technologies, patents have significant influence on the technical solution. During the validity of one patent, relevant companies often work on similar basic AM systems with certain specific improvement. which makes the nomenclature of AM technologies quite ambiguous and confusing. Different companies often name their AM system with different names to apply for patents, however, the fundamentals of their approaches often have certain similarities. Here we need to review briefly commercialized AM technologies neglecting details in differences between AM companies and trademarks. Different metal additive manufacturing technologies are introduced following.

### 1.2.1 Extrusion-based or sheet-based additive manufacturing

Some metal additive manufacturing technologies use the metal material whose initial state is semi-liquid or solid sheet. These materials at macro scale are often adopted by some low-cost AM metal systems. In comparison with these powder-based AM technologies (vacuum or inert gas are needed for active micro powder), these macroscopic material require less in terms of working environment.

#### **Bound Metal Deposition**

Bound Metal Deposition is an extrusion-based metal additive manufacture technology[NIC 18][BOS 18]. In this AM technology (see Figure 1.1), metal components are constructed by extrusion of a powder-filled thermoplastic media. Bound metal rods (metal powder held together by wax and polymer binder) are heated and extruded onto the build plate, shaping a part layer-by-layer. The printer of Bound Metal Deposition is similar to a printer of FDM (Fused Deposition Modelling [MEL 14]) with two extruders. Two different materials are deposited by extrusion, called bound metal rods and ceramic interface media rods. These two materials are fed from the cartridges into the extruder, heated to soften the binder, then dispensed through the nozzle. The part and its

supports are printed using bound metal rods, however, the interface layers between them are printed using ceramic interface media rods. The printed part is placed in the debinder where most of binder can be removed by chemical dissolution. Since the bound metal rod is a mixture of metal and binder. After the process of debinder, An open-pore structure is created in the printed part. Then the part will be sent into sintering furnace like the process of the metal injection moulding (MIM) technology. The part is heated at sintering temperature. Remaining binder is vaporized and metal particles fuse together. During the densification of metal, the interface layer printed between the part and its supports doesn't bond to metal since this interface is printed of ceramic. This design of separation makes it easy to remove parts from their supports after sintering. In this FDM-like technology, the controlling of shrinkage due to sintering is critical to guarantee the geometrical accuracy of metal part.



**Figure 1.1:** Bound Metal Deposition[MET 17]

## Laminated Object Manufacturing

Laminated Object Manufacturing (LOM) is an AM technology where the part cross-section is laminated sequentially. In this technology[MEK 16], the metal sheet with thin thickness is precisely cut to the shape of one layer by laser cutting tool, then this layer is bonded to the previous layer. Combining subtractive/additive manufacturing, this layer stacking and bonding process enables the relative quick and cheap printing of part. In LOM technology, the bonding between layers can be activated by solid-state diffusion (see Figure 1.2) at high temperature or by ultrasonic welding.



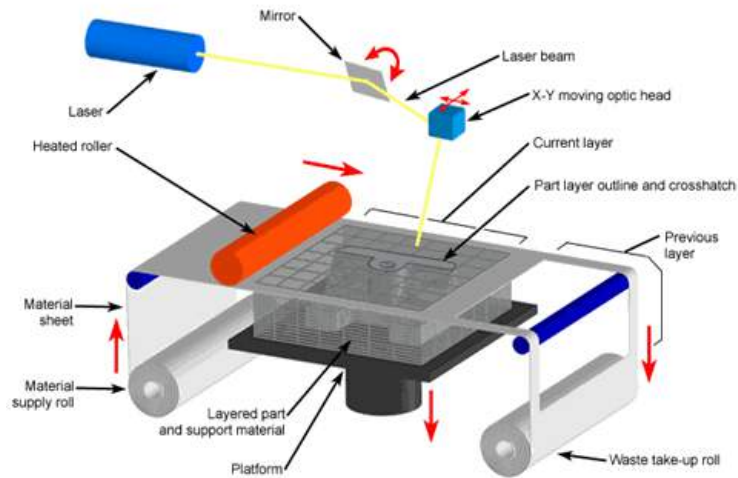


**Figure 1.2:** Laminated Object Manufacturing[MEK 16]

### 1.2.2 Powder-based additive manufacturing

In this thesis, we concentrate mainly on the AM technologies dedicating to the fabrication of metallic part. Special attention is paid here to metal additive manufacturing technologies. Currently, most of popular metal AM systems in industry are based on powder-bed or powder-injection.

#### **Powder-bed based technologies**

Selective Laser Sintering (SLS) and Selective Laser Melting(SLM) are two kinds of powder-based AM technology[SON 15][WAH 16]. The equipment of SLM and SLS are similar, while the normal materials used in these two systems are different [HEJ 17]: SLM works generally with metal, such as stainless steel, aluminium and titanium alloys. SLS works usually with plastics, glass, ceramics and so on. In these kinds of systems, a thin layer of heat-fusible powder is deposited onto the part-building chamber. Laser device and optics scanning mirror are installed above powder bed in the vacuum or inert-gas filled chamber. The powder is held in a cartridge which might be pre-heated by infrared. The build platform moves downwards by one layer thickness after one layer of a part is built. Then the new powder layer will be spread uniformly and precisely onto the previous powder bed by a levelling roller or a blade. After the deposition of new powder layer, the zone of cross-section of layers is melted or is sintered selectively by the heat of laser. In SLS/SLM system, the support of part is not necessary since the powder bed can support newly built cross-section layer. The post-process is quite important for these technologies, the whole part must be cool down slowly to avoid warping and curling.

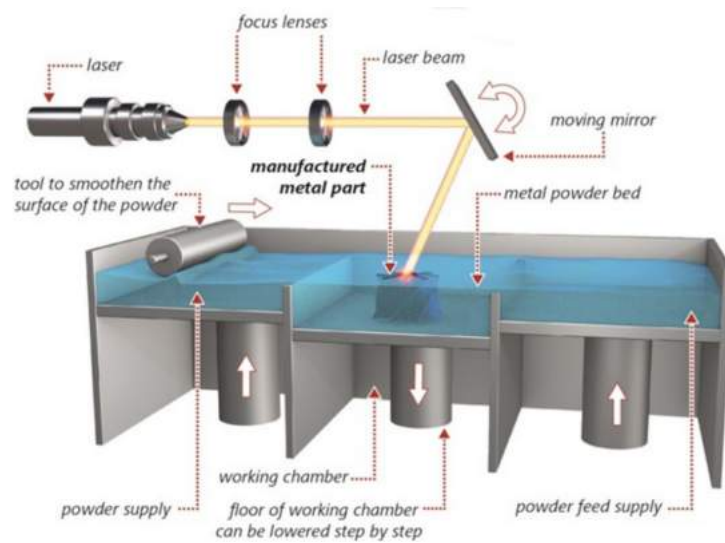


**Figure 1.3:** Selective Laser Melting(SLM)[YAS 18]

In SLM, powder is melted and the material consolidates in a welding pool. This different feature makes the final part made by SLM has less porosity than that made by SLS, as the powder is heated below its melting point in SLS. In SLS, solid is formed by the fusion between material particles (sintering). For both systems of SLM and SLS, the control of laser energy input is of significance for the quality of part[VAI 15]. The parts made by SLM/SLS often require stress relieving and annealing to reduce internal residual stress.

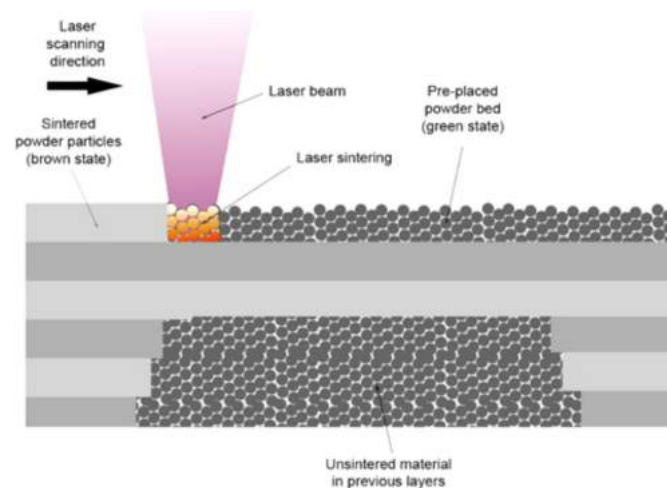


**Figure 1.4:** Interaction of laser-material in Selective Laser Sintering (SLS)[KOL 17]

The electron beam melting (EBM) is an AM technology similar to SLS/SLM [ZÄH 10]. The EBM (see Figure 1.5) uses electron beam as heat source instead of laser in

## 1. Basic knowledge on additive manufacturing

---

SLS/SLM. Only materials with high electrical conductivity can be used in EBM technology. In EBM system, electron beam is focused by deflection coil surrounding the beam. The movement of electron beam's focus is driven magnetically instead of the mirror galvanometers in SLS/SLM. Because of the different mechanisms between the interaction of material/electron beam and that of material/laser, usually EBM is much more efficient in terms of energy absorptivity.

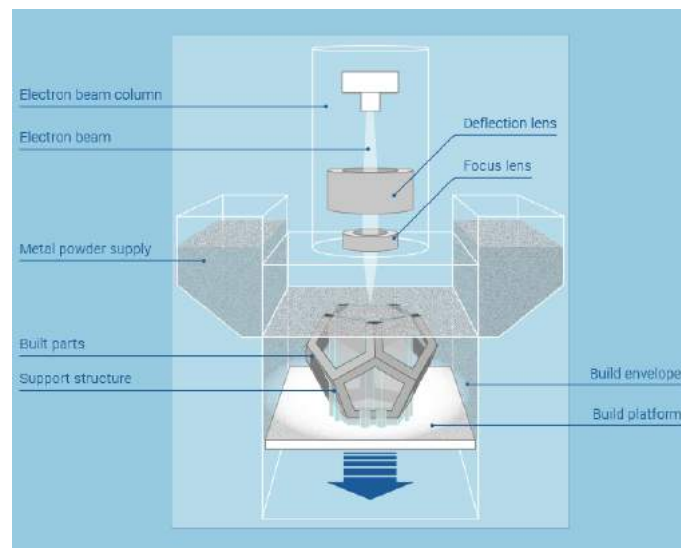


**Figure 1.5:** Electron Beam Melting (EBM)[QUR 18]

Compared to SLS/SLM system, parts made by EBM technology generally have less precision, worse surface resolution and bigger grain sizes. However, EBM has advantages in less cost and faster scan speed. This makes EBM an important technology in metal additive manufacturing.

### **Powder-injection based technologies**

Direct Metal Deposition (DMD) is a typical powder-jet based AM technology [LAB 17]. This technology can be used not only to manufacture new parts, but also to repair/ rebuild worn or damaged components and to apply wear- and corrosion-resistant coatings [AHS 11]. In DMD system (see Figure 5.1), the metal powder is injected from the coaxial nozzle (see Figure 1.6) into a molten pool, which is created by heat source (usually laser). The powder nozzle moves with the laser beam back and forth, then leaves a track of solidified material. Shield inert gas is also fed with the sprayed metal powder stream. The DMD printer head (nozzles of powder/inert gas, laser beam) is usually integrated into CNC/robotic system. With some feedback sensors for melt pool, DMD can be controlled by a closed loop to maintain the quality of a part.

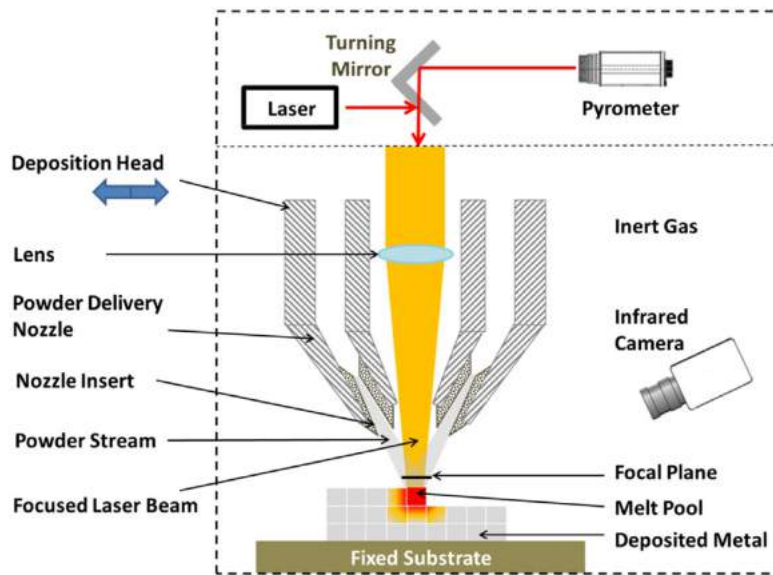


**Figure 1.6:** Laser deposition device (DMD)[THO 15]

The DMD involves complicated interactions between the laser beam, metal powders, the substrate, and processing gases. The physical phenomena in DMD include laser-powder-melt pool interactions, heat transfer, fusion, fluid flow, and solidification. Compared with powder bed based AM technologies, the printing speed of DMD is faster with higher roughness and DMD allows building or repairing larger parts.

DMD technology isn't only applied in additive manufacturing of new parts, but also in refurbishing-repairing of damaged parts.

Laser Engineered Net Shaping (LENS) and laser cladding are powder-injection based AM technology similar to DMD technology[MAH 14], because they are different patents issued to companies or individuals.

## 1.3 Some problems in metal additive manufacturing

In industrial application of metal additive manufacturing, the quality of a metallic part isn't always satisfactory as its design, in terms of both geometrical shape and properties. Some severe problems in macro scale may even lead to the cease of fabrication. Here are some typical macroscopic problems in metal additive manufacturing. Solutions for these issues are still being studied by researchers with experiments or simulations

### 1.3.1 Problems for designers before AM manufacturing

Before the printing process of additive manufacturing, designers and engineer should consider some problems as follow:

#### 1. Support design

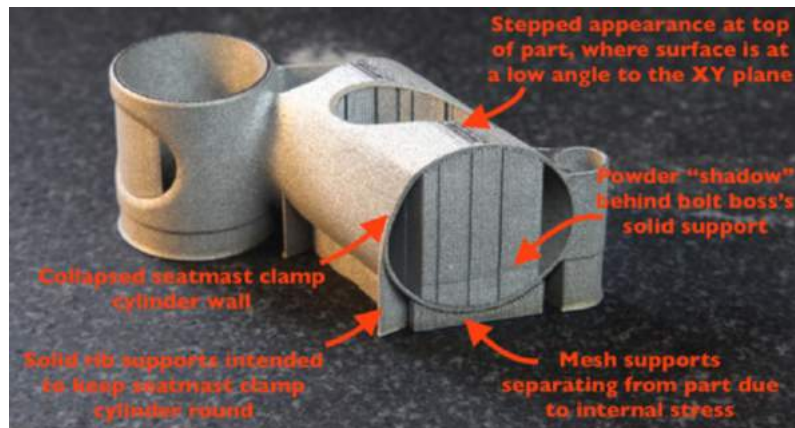


**Figure 1.7:** Design of a part's support structure in additive manufacturing[WRI 15]

In the stage of AM design, not only the workpiece's 3D geometry should be designed in CAD software, but also its support structure should be generated and optimized manually or automatically in some special AM software. The support structure (see Figure 1.7) plays a significant role in the quality of final part[HU 15][JÄR 14]. Generally, two functions of support structure should be considered in AM modelling of 3D geometry. Mechanical supports help prevent overhangs from deformation from gravity or growth stress. Thermal supports allow applied energy a conductive path away from the melt surface, so as to optimize the temperature field distribution [COO 18]. In practice, the maximum overhang angle is an important parameter before the generation of support structure, including internal support, external support. In support design, the minimization of contact surface between workpiece and its support should also be considered, aiming to reduce the difficulty of support removal in post-processing [DAS 17].

## 2. Part orientation optimization

Optimization of part's orientation is an important task in file preparation stage of the AM process chain to achieve better quality product[DAS 15]. In AM pre-process software, the part's geometry can be rotated around the axes of AM machine's coordinate system. The determination of the final orientation in the AM build space depends on several trade-off actors, thus this is a multi-objective optimization where the designer has to decide the priority among different objectives.

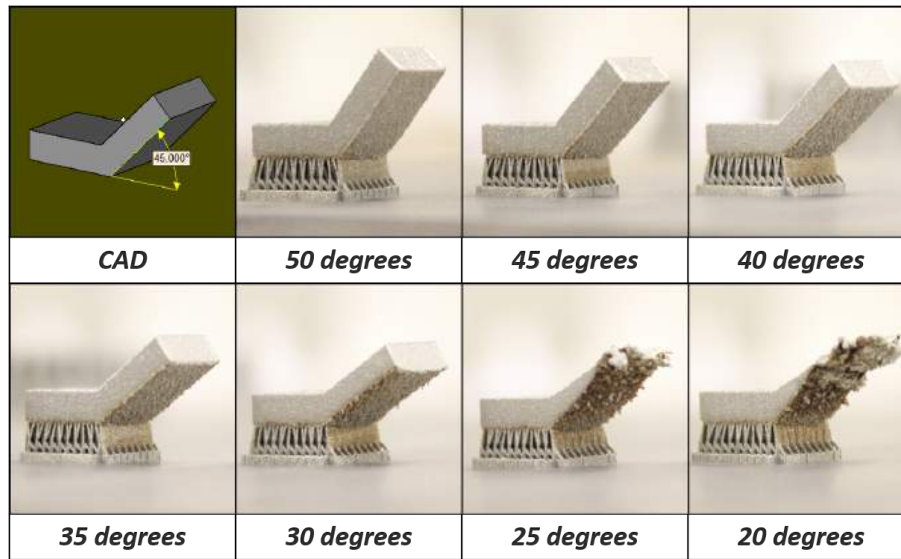


**Figure 1.8:** Different printing qualities varying with part's orientation[WAR 16]

Common objective functions to optimize the part orientation selection are to improve surface finish (reduce roughness and the risk of warping), increase part strength in a specific direction, reduce support volume, minimize build time and maximizing part geometric accuracy[TAU 13].

In AM systems, the orthogonal shape is produced almost continuous while the part production in build direction is discontinuous in discrete steps of one layer thickness. Most of parts built by AM technologies have inherently anisotropic properties, usually their strengths are much weaker in Z direction (building direction ) than the XY direction [CAR 15]. Due to the staircase effect caused by adjacent layers, an appropriate orientation of part will eliminate dimensional inaccuracy and is helpful to attain the desired surface finish of workpiece.

### 1.3.2 Problems during AM process

In the stage of producing a part by AM technology, we should always monitor the property and shape of this part, since the AM part's quality isn't always satisfactory.

#### 1. Distortion and crack caused by residual stress

Residual stress is the stress that remains inside a material, when it has reached equilibrium with its environment. Residual stress is generally classified according to the scale (see Figure 1.9) at which they occur[EVE 18]. The type I residual stress (macroscopic homogeneous residual stress) vary over several crystal grains. The type I residual stress can lead to part's large deformations. The type II residual stress (microscopic homogeneous residual stress) are introduced by different phases in the material. The type III residual stress (microscopic heterogeneous residual stress) occurs due to dislocations at atomic scale. The measurement resolution of most test methods is not precise enough to measure



## 1. Basic knowledge on additive manufacturing

---

type II and type III residual stress. Moreover, they are of less importance for the macroscopic quality of part. Thus most of investigation for part's scale consider principally the type I residual stress.

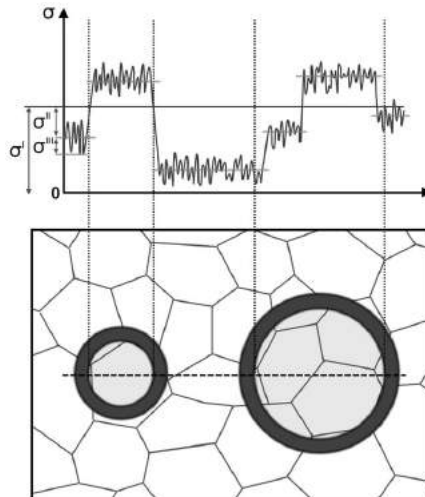


**Figure 1.9:** Variation of the residual stress of different types along a line[WIT 01]

Residual stress is not always disadvantageous, for example, in the produce of tempered glass, annealed glass plates are rapidly cooled by forced air. This procedure can introduce compressive stress in the surface area of the plate, thus increasing the overall loading resistance and preventing crack growth at the surface. However, in most cases, residual stress is harmful to the quality of workpiece, since they result in deformations from the intended shape [RAD 92]. Moreover, tensile pre-stress will be added to the stress caused by external loads, thus reducing the strength of the parts and favouring propagation of cracks from the surface.

The metal part's AM processes, especially these powder-based AM systems, can introduce large amounts of residual stress, due to the large thermal gradients which are present inherently in the frequent heating-cooling cycles. It is one of the major issues for the additive manufacturing of metallic parts and it will negatively impact the mechanical properties of the final part [YAD 15] [VAN 16]. The residual stress leads to part's distortion (see Figure 1.12) or crack (see Figure 1.10) during building process and the premature failure during use.



**Figure 1.10:** Crack caused by residual stress[COM 17]

When molten metal is deposited on a cold underlying layer, the thermal contraction of the solidified material occurring during solidification creates tensile stress in the deposit and compression stress in the underlying layer. Since this deposition is repeated frequently in AM process, the residual stress of final part can reach a remarkable level.

Two mechanisms can be distinguished which cause residual stress (see Figure 1.11). The first mechanism introducing residual stress is the temperature gradient mechanism. The second mechanism is the cooling of molten top layers mechanism[WIT 07][VOR 17].

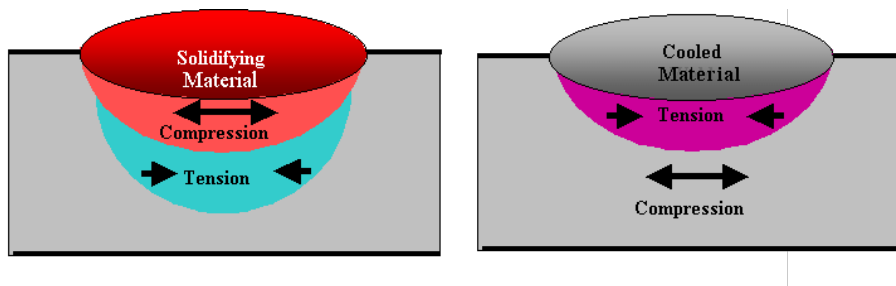


**Figure 1.11:** Two mechanisms of residual stress [WIT 07]

The temperature gradient mechanism explains the generation of residual stress in heating step [MER 06]. It results from the large thermal gradients that happen around the spot of laser or electron beam. Because of the rapid heating of the upper deposit in AM process and the rather slow heat conduction, a steep temperature gradient develops. When material is deposited on a cold underlying layer, this newly deposited heated layer's expansion is restricted by its underlying layer, then elastic compressive strains are induced[CAS 11]. When the material's yield strength is reached, the top layer will be plastically compressed[VOR 17]. In the absence of mechanical constraints, a counter bending away from the heat source would be perceived. During the cooling, the plastically compressed upper layers start shrinking and a bending angle towards the laser beam develops. In fact, even the material isn't molten yet in heat step, the residual stress can occur just because of the different behaviours of thermal expansion between layers.

The cooling of molten top layers mechanism can explain the residual stress induced in the cooling step. In the cooling step, The molten top tends to shrink due to the thermal



contraction[CAS 11]. This deformation is inhibited again by the underlying solidified layers, thus introducing tensile stress in the added top layer and compressive stress in the underlying layers[VOR 17].



**Figure 1.12:** A beam's warpage induced by residual stress [FRU 15]

In additive manufacturing of metallic part, the local temperature at the spot of heat source is very high and the material bears rapid heating and cooling cycle. These features make it complex to foresee the residual stress in parts made by AM systems. Controlling of detrimental residual stress and reducing its magnitude to a manageable level are inevitable tasks for most of AM technologies dedicating to metallic part. In practice, some heat treatments are executed as post-process of stress relief for the fabricated workpiece. When excessive distortion or shrinkage due to residual stress can be predicted, the initial geometry file of workpiece can be modified and some compensation design can be added before the AM building process so as to improve part's final quality

### 2. Recoater interference (blade crash)

For the AM technologies based on powder bed system, one of the factors that impacts quality is the recoater. Recoater is a device in powder delivery system of powder-bed based AM machine, which is able to spread the powder in a homogeneous way. Before the construction of one layer, it spreads the powder from one side of the build platform to the other, then the new powder layer is prepared with accurate thickness. According to the material of blade, two kinds of recoaters are used in powder-bed based AM machines[AUT 18]. The soft recoater's blade is made from silicon, rubber or soft carbon fibre (for instance a brush recoater). The hard recoater's blade is made of steel or ceramic.

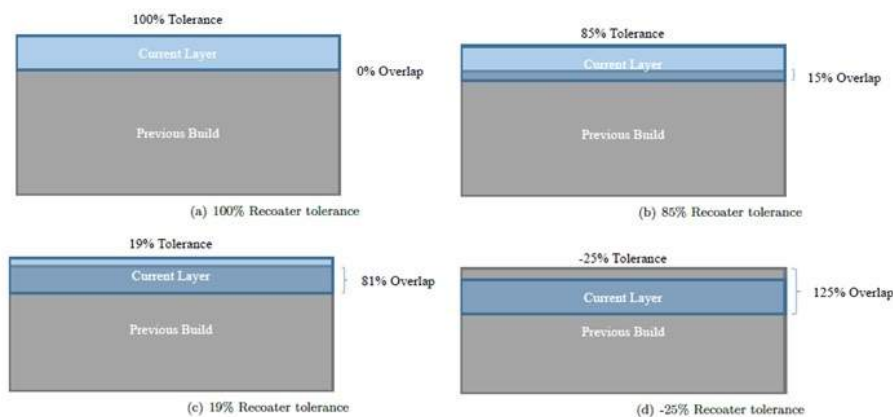


**Figure 1.13:** Recoater tolerance[AUT 18]

Because of its flexibility, the soft recoater can give way slightly in case of a collision with any metal parts being built[MCG 17]. The hard recoater, in comparison with the soft recoaters, exerts pressure on the powder and doesn't allow much part deformation. This also means that when the hard recoater collides with a part, the build stops or some of your models are dragged across the powder bed [MOY 13][LIO 14]. In order to measure the interference of recoater blade on the powder layer previously deposited, recoater clearance is configured in powder-bed based AM system. Recoater clearance is the percentage of the next powder layer that is not impinged upon by the upward deflection of the component[AUT 18], as is shown in Figure 1.13. A low recoater clearance leads potentially to the damage of newly built layers (see Figure 1.14)or the recoater blade itself.

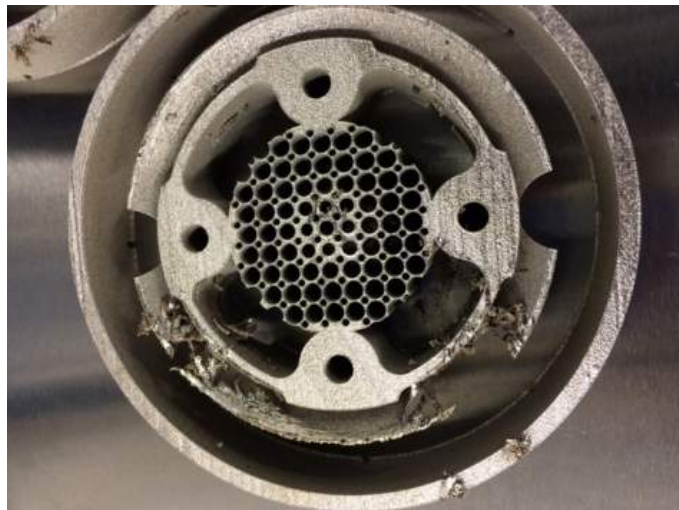


**Figure 1.14:** Blade crash of a part's shape in additive manufacturing[MCG 17]

In practice, designers need to optimise the part's orientation (see Figure 1.15) before the fabrication using additive manufacturing, depending on experience from trial-and-error.

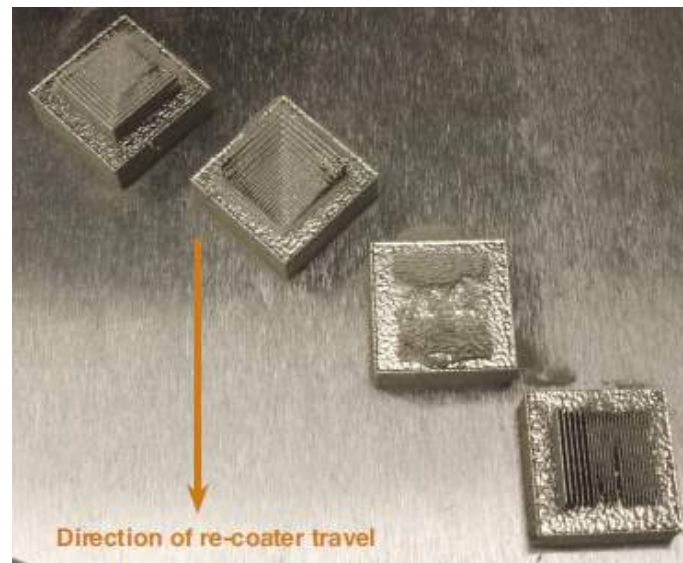


**Figure 1.15:** A part with optimal orientation suffers less from recoater blade interference effect[ZEL 15]

### 3. Lack of fusion or overheating

The quality of workpiece depends on the temperature control in AM process. Delamination, swelling and excess porosity are the unfavourable phenomena caused by inaccurate energy input control [TAN 17].

Due to incomplete melting of powder or insufficient re-melting of the underlying solid, delamination may occur and it may lead to interlayer cracking. A lack of layer adherence may also induce delamination when the temperature of the material isn't high enough to reach its melt temperature.



**Figure 1.16:** Incompleted parts induced by lack of fusion[MCG 17]

If the material is overheated, the melted material may solidify into spheres instead of solid layers. In macroscopic scale, the materials humps above the underlying layer and the swelling happens. In fact, these are caused by the surface tension effect in the melt pool at excessive temperature.

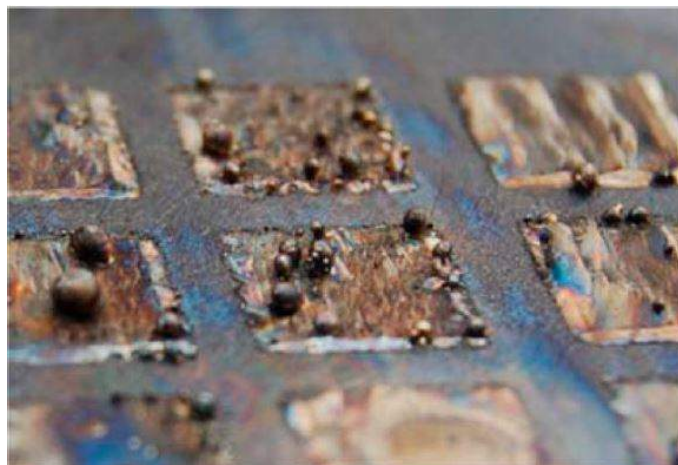


**Figure 1.17:** Balling effect on part's surface in EBM, caused by overheating[ZÄH 10]

It is still hard to control precisely the input power in AM building process as the reaction between the material and heat source is quite complex. For parts with excessive porosity, isostatic pressing (HIP) is often used as densification post-processing of AM systems, especially those based on sintering.

### 1.3.3 Problems after the printing of an AM object

After the end of AM process, there are still some problems should be taken into consideration.

#### **Removal/cutting of the part from substrate**

In an AM machine, metal workpieces are usually built on a substrate with which the first layer forms ductile interface. As a consequence, the part's removal from its substrate is necessary during post-processing. Additionally, the substrate, a plate usually made of metal, is also affected by the heating process in additive manufacturing (see Figure 1.18). It may warp and cause the distortion of workpiece's geometry. This warping may result in permanent plastic deformation [PRA 15]. The distortion will be more severe when the materials of workpiece and its substrate have different thermal expansion coefficient. In practice, the substrate is often pre-heated before the deposition of the first layer. Moreover, skilful operations are often needed for a part with complex support structure like the object in Figure 1.19.

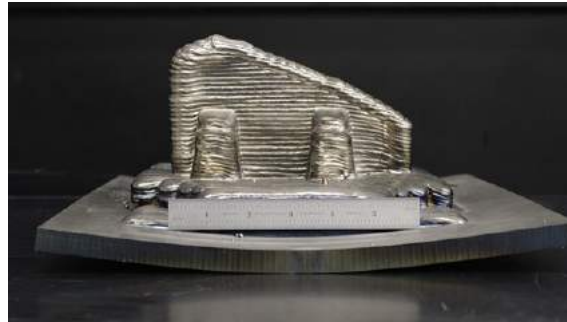


**Figure 1.18:** Wrapping of substrate after AM fabrication[ZEL 15]



**Figure 1.19:** Difficulty in the removal of support structure without damage[STA 17]

## 1.4 Some typical techniques for the AM simulation

Investigations of the problems in metal additive manufacturing usually depend on lots of expensive/extensive experiments. Additionally, measuring the evolution of multi-physics fields during AM process is often restricted by hardware limitation. Numerical simulations, especially these macroscopic simulations for the AM process, provide an important alternative of for engineers and researchers[MIN 15]. Because of the complexity of AM process, this simulation often apply some special method to resolve the multi-scale and multi-physics problem. Here are some brief introductions for the trends of AM simulations.

### 1.4.1 Numerical Methods for dynamic AM process

In the dynamic process in additive manufacturing, the metal material is deposited on its substrate or its previous layer one chunk by one chunk. All of these complex phenomenon (stacking of material, moving heat source, interaction of new melt powder/solidified metal, etc.), require some special numerical method for AM process simulation.

#### 1. Birth and death technique in FEM

Element birth and death technique is widely used in FEM software such as ANSYS, ABAQUS, COMSOL, etc. For the simulation of a system where material is added or removed, the element birth and death technique can be used to deactivate or reactivate selected elements. This technique is useful in analysing excavation (as in mining and tunnelling), staged construction (as in shored bridge erection), sequential assembly (as in fabrication of layered computer chips). For AM simulation, this technique makes it possible to describe the process of material deposition. Most of AM simulations based on FEM, including academic research or industrial design, have applied element birth and death technique in order to treat the geometrical deformation process in additive manufacturing [HU 09][ROB 12][COZ 10]. This procedure can be useful for modelling effects due to phase changes (as in welding processes, when structurally inactive molten material solidifies and becomes structurally active), failure-surface propagation, and other analysis-dependent element changes.

Before using this technique, first we should identify the locations of selected elements to activate or to deactivate, which means the change of material status in these elements (for example, melting, solidification, rupture, etc.)

In element death step, this technique doesn't actually remove elements. In fact, the stiffness (or conductivity, or other analogous quantity) of these elements will be multiplied by a severe reduction factor (In ANSYS, this factor is set to  $1.0 \times 10^{-6}$  as default[ANS]).

Element loads associated with deactivated elements are zeroed out of the load vector, however, they still appear in element-load lists. Similarly, mass, specific heat, damping, and other such effects are set to zero for deactivated elements. The energy and mass of deactivated elements are not included in the summations over the model[RAJ 12]. As soon as that element is killed An element's strain is also set to zero .

The element birth step is manipulated in a reverse manner. When an element is reactivated, its mass, stiffness, element loads and other values return to their full original values. In the reactivated elements, strain history (or heat storage, etc.) isn't recorded while the initial strain defined as a constant will not be affected by this birth and death method. The element types will be also reactivated in their originally specified geometric configuration. The activation of element type should be specially treated when large-deformation effects happen in order to obtain meaningful results[RAJ 12]. During the AM process, the stress-free option can be applied to simulate newborn elements and previously-deposit elements. Especially in powder-bed based AM simulation, the influence of powder surrounding the workpiece can be treated by this option.

## **2. Discrete Element Method**

Discrete element method(DEM) is a numerical method that is capable of simulating the motion of a large number of individual particles including contact interactions between particles/particles and particles/walls [LEE 15][BIC 07]. In powder-bed based AM technologies or powder-injection based technologies, DEM model is applied for micro-scale simulation, especially the simulation of melting pool. DEM method has also been expanded to simulate the macro-scale AM process, such as the deposition process by recoater blade/roller. The powder particles in AM simulation are simplified as spheres. The DEM is a numerical approximation method which is based on an interacting system of



particles.

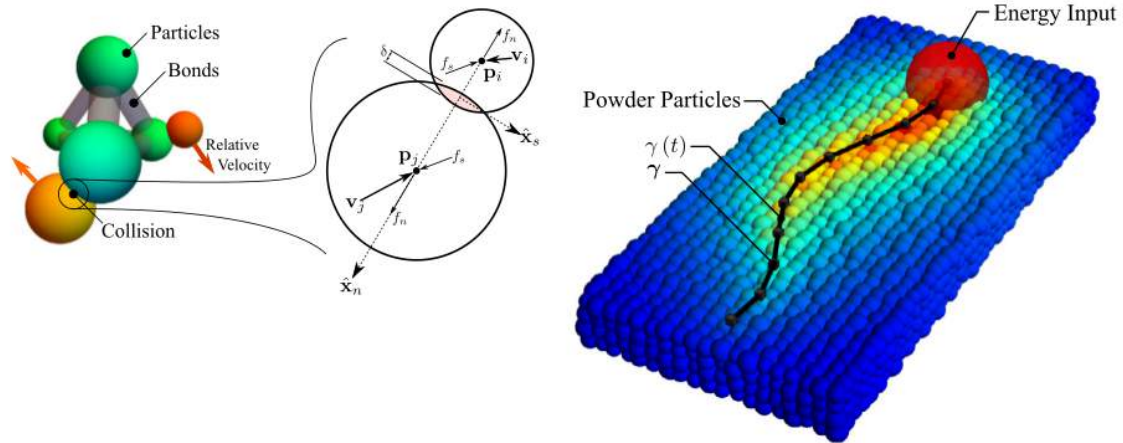


**Figure 1.20:** Thermal simulation with DEM for powder-bed AM system. [STE 16a]

A sufficiently large number of particles are tracked to enable reliable statistical analysis of granular dynamics[MEG 16]. A subset of particles contact each other while the others are unbonded. These unattached particles participate in collisions which produce reaction forces, then reaction forces propagate, changing the velocity and the position of particles. Particles in DEM conduct heat transfer, respond to external fields, and may form or break inter-particle bonds. Before using DEM, we should first define Inter-particle contact laws, and boundary condition contact laws. For simulation of consolidation or melting, the conditions when bond formation, deformation, and breakage should also be defined. Since it is not practicable to exhaustively check every particle in the DEM simulation for contact with all other particles, some collision detection techniques can be used so that collision searching is reduced to local neighbourhoods.

### 3. Mesh adaptation

The mesh in Finite Element Method is often the bottleneck of calculation time. The simulation time is proportional to the quantity of elements and expected to increase enormously. AM simulation is executed for multi-scale models of melt pool, hatch pass, layer and the whole part. This makes the mesh adaptation a powerful tool to satisfy the different accuracy of detail.

In FEM simulation of additive manufacturing, the mesh density should be adjusted spatially according to the need of detail instead of mapping a uniform mesh to the entire calculation domain. The whole mesh can be divided into two or three areas. For a simulation of part level, the elements are concentrated in the vicinity of the workpiece in order to obtain more reliable results. Taking most of the mesh of AM substrate as an example, different mesh densities are applied to working area, transition area and far field area.

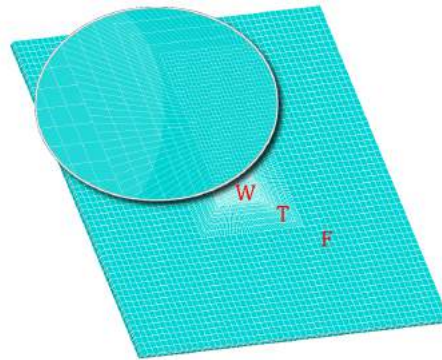


**Figure 1.21:** Computational domain with different mesh densities[STA 18]

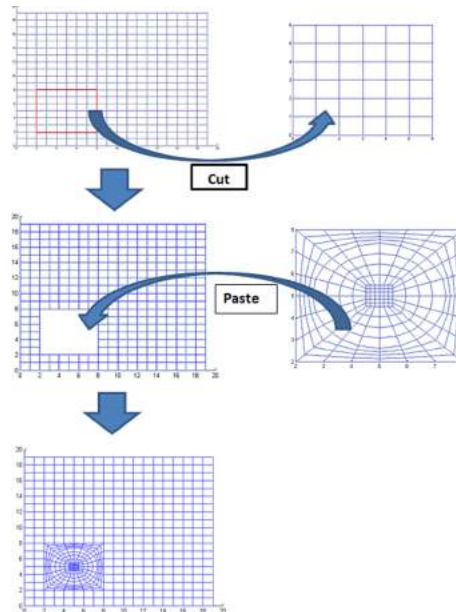


**Figure 1.22:** Dynamic mesh refinement preparing for heat affected zone[PAT 15]

Temporally, the geometry of workpiece evolves while the material is deposited. The mesh should also be dynamically adapted so as to adjust the local mesh refinement to the position of the laser spot or the current printed layer. In each analysis step, dynamic mesh refinement (DMR) approach updates the mesh of the heat affected zone (HAZ) after calculating the mesh metric matrix, which depends on the minimum curvature radius of workpiece's free surface and the mesh node's distance from the interface [GEO 07].

### 1.4.2 Numerical methods for irregular and free boundary condition

Before its arrival to the designed geometry, the form of a 3D part changes with the process of additive manufacturing. AM machines are able to print parts with complex and irregular geometry. How to simulate the moving free surface is still very difficult for additive



manufacturing. Most of numerical methods for these problems are based on microscopic and multi-phase fluid dynamics.

### 1. Voxelization for complex geometries in pre-processing

Voxel is a straightforward generalization of pixel graphics as known from computer graphics. 3D space is split into a regular cubic grid consisting of voxels. The easiest way to represent an object with voxels is to assign to each voxel a Boolean value, deciding if the volume described by the voxel is part of the object or not. In voxel-based approach, voxels do not necessarily need to be cubes, but can be cuboids with different side lengths.

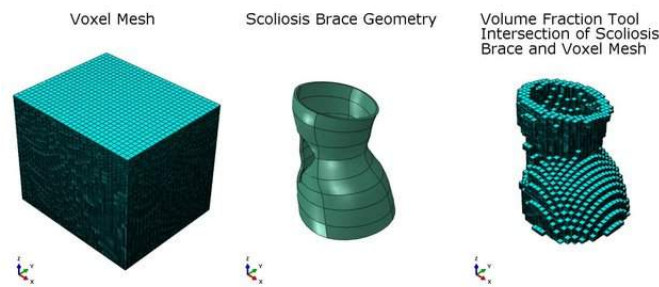


**Figure 1.23:** A scoliosis-brace-model reconstructed by voxelization[FRA 17]

In AM simulation, voxels can be considered as structured elements in FEM. If the resolution is high enough in this voxel based method, the approximation of a 3D object with voxels can be considered as an alternative of 3D model created by conventional CAD software [UEN 18]. Conventional CAD tools are not efficient at representing complex geometry in additive manufacturing, such as lattice structures, due to the underlying methods by which they handle and manipulate geometry. In conventional CAD, the main geometry representation schemes are boundary representation (B-rep), constructive solid geometry (CSG), spatial subdivision, medial surface representation and procedural representation [GEO 07][SUR 16]. In AM simulation, the form of workpiece's geometry varies with the material deposition process. This feature makes the description of external surface's change difficult with conventional CAD. Nowadays, a problem of voxel-based representation is its huge memory consumption at high resolution. This problem still needs to be solved through some algorithms such as octrees [HAU 02][BEN 14] are used to reach a compromise between memory consumption and geometrical accuracy of representation. In voxel-based representation, the concept of feature edges or feature surfaces is no more necessary as boundary representation.

### 2. Level-Set Method for 3D geometry

The level set method has become popular in many disciplines, such as computer graphics, topology optimization, and multiphase fluid dynamics, etc. It is commonly used to identify and track an interface inside a continuum. The advantage of the level-set method is that one can simulate a time-varying interface between two different kinds of materials. In AM simulation, level set method is generally used in micro-scale modelling (melting pool)[QI 06][CHE 18]. However, this method can be expanded to the macro-

scale simulations. By using level set method in AM simulation, the shape evolution of workpiece's or melt pool's free surface can be described mathematically as the evolution of level set function  $\psi$ .

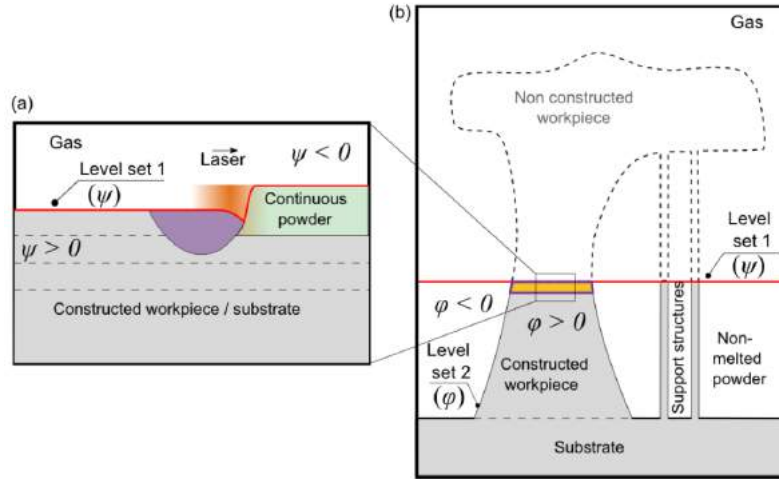


**Figure 1.24:** Interfaces tracked by the level set method[ZHA 18]

The interface is defined by the isovalue  $\psi = 0$ , where  $\psi = \psi(\mathbf{x}, t)$  is the signed distance function to the interface at any location  $\mathbf{x}$  in the continuum, and at any instant  $t$ . The discontinuity between inert gas and the consolidated workpiece will be treated with Heaviside function[WEN 10]. Then the field value of the whole domain will be calculated by mixture law. After one step of deposition, the level set function  $\psi$  should be updated as the interface has moved.

### 3. Volume of fluid method for free boundary

Volume of fluid (VOF) is a kind of techniques which enables the tracking of free surface. In micro-scale simulation of additive manufacturing, the VOF method is often used to track the position and shape of the molten pool surface [DUB 17]. It solves a scalar transportation equation for the volume fraction of fluid  $F$  which takes the values in the range from 0 to 1. The volume fraction represents the intrinsic materials (powder, consolidated workpiece, inert gas). The interface between different materials is captured artificially by a threshold volume fraction.

$$\frac{\partial F}{\partial t} + \mathbf{v} \cdot \nabla F = 0 \quad (1.1)$$

In fact, both level-set method and VOF method are approaches for the interface capturing problems of two phases. In comparison with VOF method, level set method permits us to define more exactly the location and curvature of the interface, but it does not guarantee the conservatism of mass.

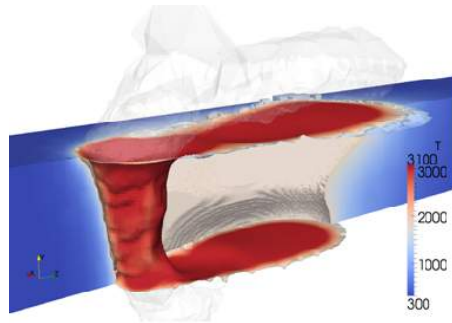


**Figure 1.25:** Simulation results for keyhole and melt pool formation by volume of fluid[OTT 10]

#### 4. Finite Cell Method

The finite cell method (FCM) is a fictitious domain approach using high order finite elements. It relies on an explicit description of the volume of the physical domain and is able to deliver high accuracy. The original idea of the finite cell method is to extend the physical domain  $\Omega_{phy}$  by a fictitious domain  $\Omega_{fict}$ . The union of physical domain  $\Omega_{phy}$  and its corresponding fictitious domain  $\Omega_{fict}$  has a simple shape, which can be meshed easily. As the procedures in traditional FEM, the problem solved by finite cell method should be first described mathematically by the weak formulation. The weak formulation is modified by extending integrals over the union  $\Omega_{\cup}$  domain of physical domain  $\Omega_{phy}$  and fictitious domain  $\Omega_{fict}$ .

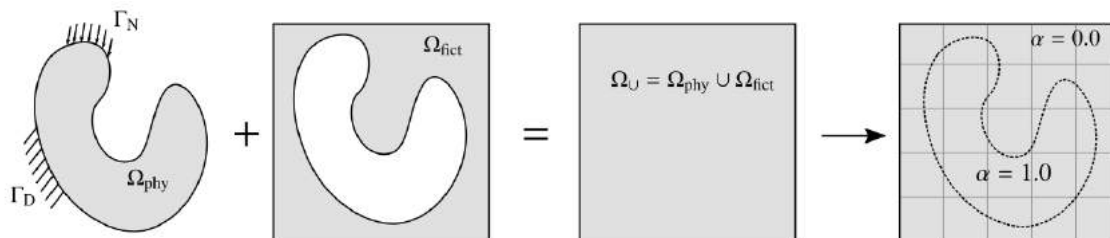


**Figure 1.26:** Concept of finite cell method [TAG 18]

Nevertheless, some terms in weak formulation of FCM, such as virtual work terms, are multiplied by a scalar field  $\alpha$ . This scalar field  $\alpha$  is defined as a discontinuous indicator function, representing the geometric description of the physical domain  $\Omega_{phy}$  and fictitious domain  $\Omega_{fict}$  [PAR 07]. With the help of adaptive mesh technique, it is possible to simulate the complex geometry of workpiece constructed by additive manufacturing. Regardless, the boundary conditions in FCM, both Neumann  $\Gamma_N$  or Dirichlet  $\Gamma_D$  condition, are difficult to treat and they are handled in special manners [WAS 17], because the boundaries of the physical domain  $\partial\Omega_{phy}$  typically do not coincide with that of the extended union domain  $\Omega_{cup}$ .

## 1.5 Novelty of this work

Aiming to solve different problems in the whole AM process chain, the development of software concerning AM includes different directions, such as generation of lattice filling structure, optimization of support structure, etc. However, the simulation of additive manufacturing, especially the macroscopic process simulation, has still many problems to resolve. These difficulties make the AM simulation develop generally much slower than the improvement of AM hardware.

Some commercial software are dedicated to simulating additive manufacturing process, for example, Virfac Additive Manufacturing of GeonX, Amphyon of Additive-Works, Simufact Additive of MSC[P.K 16] and Pan computing of Autodesk[DEN 15]. The commercial solvers of additive manufacturing simulation of multi-scale are often based on Cloud Computing, such as 3DSim of ANSYS [PAL 15]. The part's geometry file and AM processing information (material property/ AM machine configuration) are submitted to remote cluster, then the result of thermo-mechanical field is directly delivered to customers. Nevertheless, the algorithm of simulation is closed source and it can't be modified by customers (see the Figure 1.27).

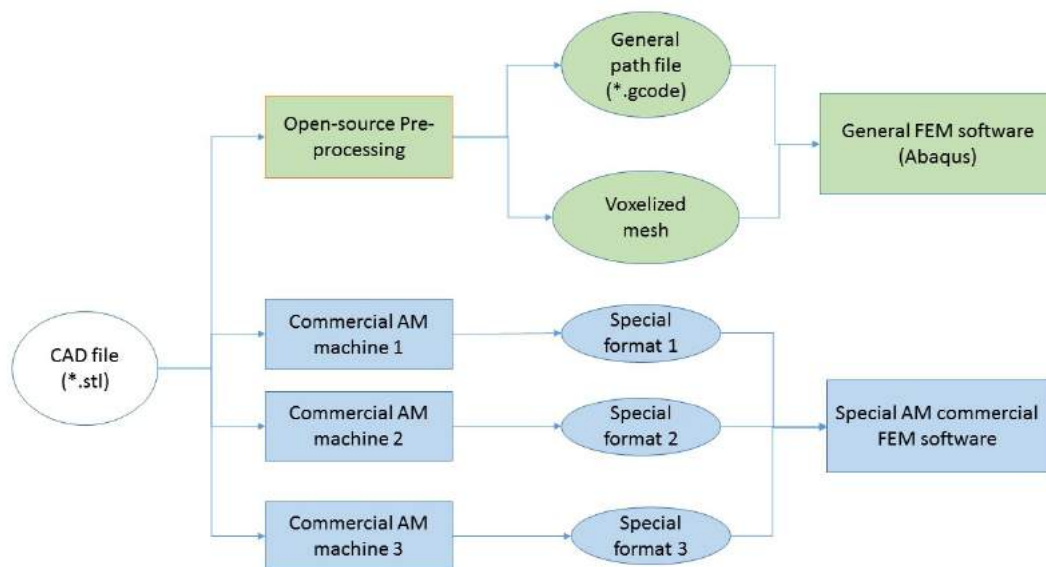


**Figure 1.27:** Difficulty of connecting AM machine data with FEM simulation

In this thesis, we study some problems in AM simulation in order to make progress for the academic researchers and industrial engineers in their domains. In this thesis, some digital processes for AM systems, such as conversion of model data, slicer algorithm, generation of deposition trajectory, are studied by taking the example of FDM technology

[JON 13][KLE 15], since we can develop basic pre-process code based on open-source software for FDM technology instead of the expensive commercial software. The main novelties in this thesis include mainly these aspects below:

### 1.5.1 Pre-processing for macroscopic simulation

The pre-processing work is often an obstacle for academic researchers to study AM macroscopic simulation because of the tedious and delicate programming work. In our work, some of the methodologies are implemented for pre-processing.

First, the connection between real scan path and FEM simulation in additive manufacturing is often separated. Most of scan path in AM simulation is subjectively defined to avoid the difficulty of reading real scan path in an AM machine. In this thesis, we apply the inversed algorithm of slicer to treat the G-code path file, then reconstruct the 3D model with path partitions. This work is important for AM simulation at layer level.

Second, the meshes of layers are usually incompatible with each other in CAD software before the assembly, which makes the reconstruct of the whole part's 3D model difficult when the partition information is lost during the assembly. We apply a data-based method to resolve this mesh compatibility problem. This method, in fact, can be expanded to many similar problems in FEM.

Third, almost all academic research efforts focused on very simple geometries in AM simulation, such as thin walls structure. In fact, the real AM machine has the ability to print complex geometries that cannot be easily built by traditional technology. We need some methodologies to treat the macroscopic 3D model with complex geometry. In this thesis, we adopt voxel-based mesh generation technique for a twisted turbine blade. The feasibility of this method is demonstrated by multi-physics simulation.

### 1.5.2 Dynamic simulation at different levels

The FEM simulation for AM process applies usually the birth and death technique, since it can simulate the dynamic material deposition process in additive manufacturing. However, most of researches focused on microscopic simulation (see Figure 1.28). It will cause an enormous quantity of calculation if we directly use this method for a larger size object without changing its resolution. Because of the multi-scale effect in additive manufacturing (shown in Figure 1.29), a unique model and method for AM simulation of all levels are impossible if the computational resource and calculating time are limited. We need to achieve a compromise between the precision and the calculating efficiency.

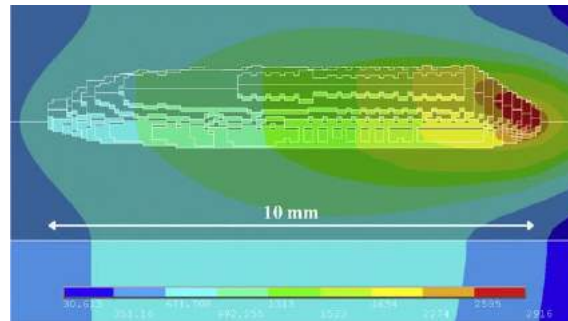


**Figure 1.28:** Material deposition at line level[FAL 11]

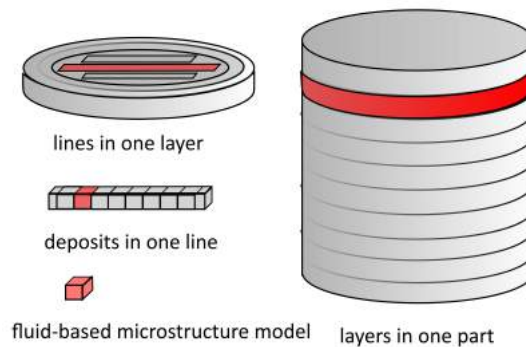


**Figure 1.29:** Different levels for birth and death method

In this simulation, we simulate the AM process at different levels using different resolutions: line-level (in Chapter 4, Chapter 5), layer-level (in Chapter 3), part-level (in Chapter 3). In the range of macroscopic simulation, the AM processes at different levels are all demonstrated in this thesis. When the birth and death technique is applied in AM process simulation, our methodology with different resolutions is helpful to reach a balance between the precision and acceptable calculation efficiency.

### 1.5.3 Reduction of residual stress at lower preheat temperature

For many commercial AM metal machine manufacturer, increasing the preheat temperature is one of techniques to improve efficaciously the quality of a part, especially to reduce the residual stress. Without special modification at the laboratory, only a few of sophisticated AM metal machines (e.g. Renishaw RenAM 500Q, TRUMPF TruPrint 5000, etc.), can reach a preheat temperature at 500 °C till the year 2019 (see Table 1.5.3). For most commercial AM machines, increasing preheat temperature is still a difficult task and this technique direction becomes harder and harder because of its inherent limits.

## 1. Basic knowledge on additive manufacturing

**Table 1.2:** Some commercial AM machines and their preheat temperature

Ref	Technique	Material	Machine	Preheat Temperature
[ALI 17]	SLM	Ti6Al4V	(modified)Renishaw SLM 125	370°C, 470°C, 570°C, 670°C, 770°C
[THO 17]	SLM	304L steel	Renishaw AM250	80°C
[KEM 14]	SLM	M2 High speed steel	Concept Laser M3	90°C, 150°C, 200°C
[AVE 17]	SLM	A357 aluminum alloy	EOS M270 Dual Mode	100°C, 140°C, 170°C, 190°C
[CAS 18]	SLM	AlSi10Mg	EOS M290	160°C
[BUC 14]	SLM	AlSi10Mg	EOSINT M 270	100°C, 150°C, 200°C, 250°C
[LI 16]	SLM	Ti-45Al-2Cr-5Nb	HRPM-II	150°C, 250°C, 350°C
[RAM 18]	LMD	42CrMoS4 steel	IBARMIA ZVH45/1600 Add+process	257°C
[BAE 17]	DED	D2 tool steel	Insstek DMT MX3	100°C, 200°C, 300°C, 400°C, 500°C
[SHI 17]	DED	M4 high speed steel	Insstek DMT MX3	resistance heating 200°C, induction heating 600°C
[COR 17]	DED	Inconel718	Optomec LENS MR-7	350°C
[COR 18]	DED	Ti6Al4V	Optomec LENS MR-7	400°C
[COR 16]	DED	Ti6Al4V	Optomec LENS MR-7	400°C
[KIS 17]	DED	Inconel718	Optomec LENS MR-7	350°C
[ZUM 17]	SLM	M2 High Speed Steel	Renishaw AM 250	160°C, 240°C, 320°C, 400°C
[DEM 17]	SLM	maraging steel 18Ni300	Renishaw AM250	170°C
[ABH 18]	LMD	Aluminum 7075	Synergy AM3018	260°C
[BUR 15]	SLM	Marage 300 steel	Realizer SLM100	100°C, 150°C, 200°C, 250°C, 300°C

First, the preheating device installed under substrate or powder container is often a resistance heater (for many powder-bed AM system). This heater itself has a temperature limit to sustain the preheating process (see the Figure 1.30).

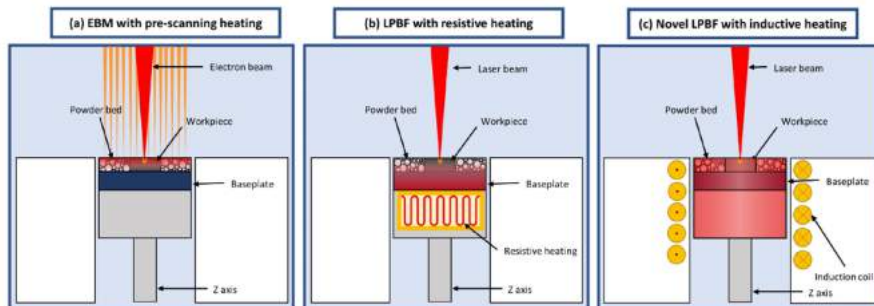


**Figure 1.30:** Preheating hardware for powder-bed based techniques[CAP 18]

Besides the hardware limit of the heater, there is also metal material's limit. For power-injection AM system, an induction coil is often installed near the nozzle to preheat the substrate or deposited surfaces (see Figure 1.31). Induction heating depends on the ferro-magnetism metal. This preheat device is suitable for some ferromagnetic metal such as steel. However, some non-ferromagnetic metals, like titanium, aluminium, are also widely used in additive manufacturing. The choice of metal material will restraint this kind of preheating device as well.



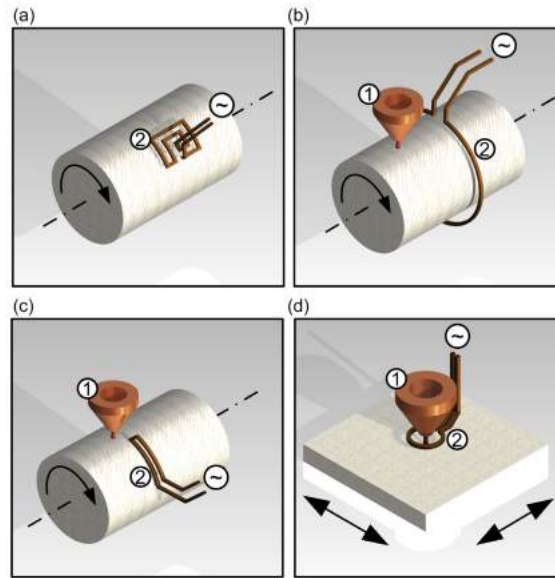


**Figure 1.31:** Preheating hardware for powder-injection based techniques[BRA 16]

Additionally, the energy efficiency is also a problem for the traditional preheat technique. Before the fabrication of a small metal part, the whole substrate and powder container should be preheated by this technique. The consumption of energy is also considerable during preheating step.

Finding a more efficient method will become helpful for an AM system's improvement instead of continuing the increment of preheat temperature. Among these potential methods, we study the metal AM process by macroscopic simulation, expecting to improve the AM part's quality by controlling AM process parameters during its fabrication.

#### 1.5.4 Process parameters study and control loop platform

It is not an easy task to analyse the relation between different process parameters and a part's final quality. However, a better understanding of this relation will play an important role in residual stress reduction. We try to apply some regression-based methods for discovering this relation. In this thesis, we realize the basic frame for combining regression method with AM macroscopic simulation. We hope the problems in our study can inspire other researchers when they use these kinds of methods. In fact, the regression-based method is developing very fast today. New software framework tool for technique, such as machine learning, is updated rapidly and these techniques are recently tried to integrated into different areas [AHN 18]. In terms of the traditional mechanical research, the application of this regression-based method is relatively rare because of its difficulties of programming. Our study may be an interesting entry for researchers who are trying to apply the regression-based technique into residual stress reduction.



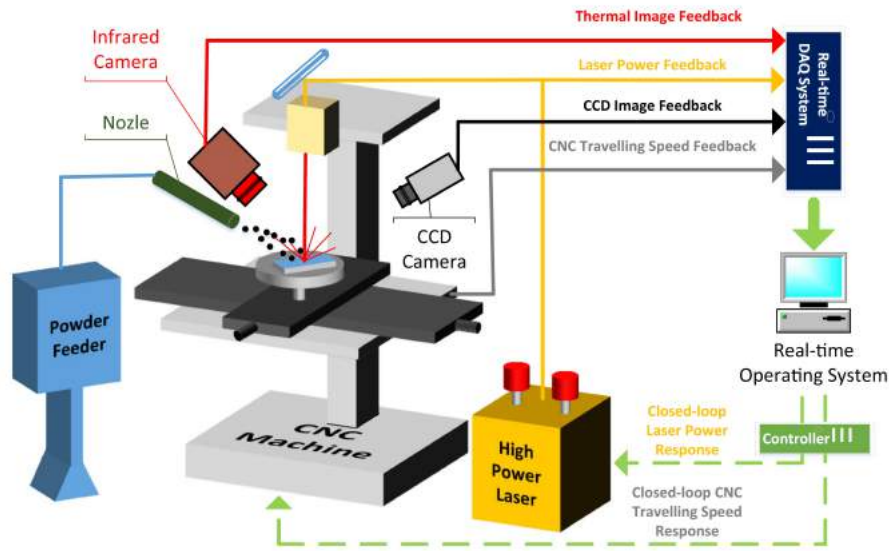


**Figure 1.32:** Hardware for the temperature closed-loop of an AM machine[FAR 16]

The temperature control is one of the fundamental technique directions for improving AM systems. We must first study the AM system's intrinsic non-LTI behaviour. For realizing the process parameters control in AM system, a closed-loop of temperature at one point is unavoidable and it plays the fundamental role for the other more complex control-loop. In this thesis, we take the PID controller and its auto-tuning as examples, in order to demonstrate how to combine the control-loop with AM macroscopic simulation. The closed-loop control systems (see Figure 1.32) are normally installed only on some advanced AM machines. For researchers without access to this kind of advanced AM machine, the limit of hardware prevents them from investigating this problem. Hence, the tool of AM macroscopic is a necessity for most of the researchers in this area. As an alternative to expensive experiment on AM machines, our AM simulation provides the possibility for researchers to configure the controller more easily and more securely. Our basic platform in this thesis may inspire other researchers to do further study on this problem. The methodology in our work can be expanded to more complex controllers and other input parameters in additive manufacturing. In comparison with AM simulation, the study of automation loop on an AM machine is probably much more expensive and riskier or even impossible due to hardware's limitation.

## Chapter 2

# Theoretical basis for additive manufacturing simulation

*In this chapter, the additive manufacturing is mathematically described as a multi-physics coupling problem. The macroscopic behaviours of a building part and its substrate are decoupled into three aspects: thermal field, mechanical field, and metallurgical field. The theoretical basis behind the simulations in this thesis is mathematically introduced in this chapter.*

## Contents

---

<b>2.1</b>	<b>Thermal equation for temperature . . . . .</b>	<b>39</b>
2.1.1	Basic heat equation for additive manufacturing . . . . .	39
<b>2.2</b>	<b>Mechanical equation for residual stress . . . . .</b>	<b>43</b>
<b>2.3</b>	<b>Metallurgical phase models in macroscopic scale . . . . .</b>	<b>45</b>
2.3.1	Martensitic transformation . . . . .	46
2.3.2	Diffusional transformation . . . . .	48
<b>2.4</b>	<b>Conclusion . . . . .</b>	<b>52</b>

---

Additive manufacturing is a multi-fields coupling problem involving the complex interactions among the three fields: thermal field, mechanical field, and metallurgical field. As the Figure 2.1 shows, it is difficult to solve directly this coupling problem. Mathematically, we need first to decouple the phenomena in the AM process before the numerical simulation. Additionally, the description of additive manufacturing is different for different scales. For example, most of the simulations apply the fluid-structure interaction model for the microscopic behaviour of melting pool in AM process, instead of pure solid model [DAL 16]. In our study, we concentrate on the numerical simulation at macro-scale. For a metal workpiece fabricated by AM technologies, its essential manufacturing process can be decoupled sequentially into three relatively independent aspects. The Finite Elements Method (FEM) is adopted in our simulation by using the software ABAQUS, a commercial solver for solid mechanics. In the explications of decoupling of equations, we will also indicate some INP keywords or FORTRAN subroutines of ABAQUS for certain functions. The AM simulations can be also classified into three different levels: hatch chunk level, layer level and part level.

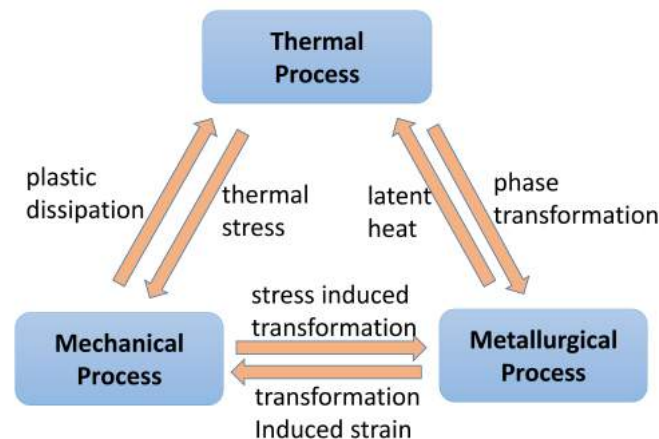


**Figure 2.1:** Interactions between multiphysics processes in additive manufacturing

## 2.1 Thermal equation for temperature

### 2.1.1 Basic heat equation for additive manufacturing

The evolution of temperature distribution in additive manufacturing can be briefly resumed as a heat equation [LIU 15] with free boundary conditions and moving heat flux load. Because of the resolution incompatibility of scales and the different properties of material states, the dynamic solidification of material at powder/liquid/ solid states is often neglected in the microscopic AM simulation. We consider the AM process as a heat transfer problem.

In the heat equation

$$\rho(T)C_p(T)\frac{\partial T}{\partial t} - k(T)\Delta T = \dot{Q}_v \quad (2.1)$$

$T$  is the temperature field.  $k(T)$  is the thermal conductivity.  $\rho(T)$  is the mass density of solid.  $C_p(T)$  is the specific heat capacity.  $\Omega$  is the free boundary of the workpiece. The volumetric heat flux is  $\dot{Q}_v$ , including the convection  $\dot{Q}_{conv}$ , radiation  $\dot{Q}_{rad}$ , and heat source  $\dot{Q}_{source}$ .

The metallic workpiece is usually surrounded by shield gas in additive manufacturing to avoid oxidation. In this case, the convective heat flux between the workpiece and shield gas should be taken into account as following

$$\dot{Q}_{conv} = h(T - T_0) \quad (2.2)$$

where  $h$  is the convective coefficient,  $T$  is the workpiece's surface temperature,  $T_0$  is the shield gas' temperature. The ABAQUS INP keyword for convection is \*FILM.

The thermal radiation of a workpiece occurs in the fabricating chamber of AM machine no matter whether it is a vacuum chamber or filled with shield gas [SAM 16]. The heat flux of radiation can be described as following

$$\dot{Q}_{rad} = \varepsilon\sigma(T^4 - T_0^4) \quad (2.3)$$

where  $\varepsilon$  is the emissivity,  $\sigma$  is the Stefan-Boltzmann constant,  $T$  and  $T_0$  are respectively the absolute temperatures (in Kelvins) of workpiece and the shield gas. For a vacuum chamber, the heat flux of radiation can be simplified as

$$\dot{Q}_{rad} = \varepsilon\sigma T^4 \quad (2.4)$$

The ABAQUS INP keyword for radiation heat flux is \*RADIATE.

The moving free boundary condition  $\partial\Omega$  is the mathematical description of material deposition process in additive manufacturing. At the instant,  $\Omega(t = 0)$  is the 3D volumetric geometry of substrate. When the material deposition begins,  $\omega_1$  is the geometrical volume of the first deposit. After the first deposition during the period  $\Delta t$ , the volume total of the substrate and the workpiece being fabricated changes to  $\Omega(\Delta t)$ . In fact, this is a union Boolean operation of the two volumes

$$\Omega(\Delta t) = \Omega(t = 0) \cup \omega_1 \quad (2.5)$$

By repeating this union Boolean operation

$$\Omega(k\Delta t) = \Omega((k - 1)\Delta t) \cup \omega_k \quad (2.6)$$

during the AM process and updating the volume  $\Omega(t)$  and its surface  $\partial\Omega(t)$ , the material deposition can be described quantitatively.

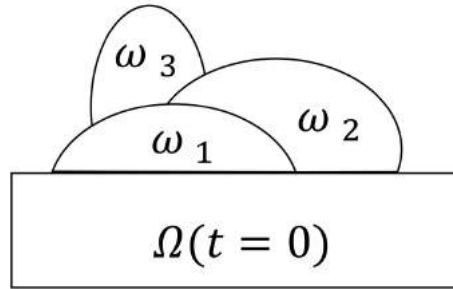


**Figure 2.2:** Moving free boundary during material deposition

The macroscopic AM simulation at higher level often depends on the numerous sub-volumes at lower level, as the AM part consists of multiple layers. In practice, the deposition isn't treated by the time-consuming series of Boolean operation in numerical simulation. This particularity of additive manufacturing can be simulated in FEM by the birth and death technique, and the corresponding ABAQUS INP keyword is \* MODEL CHANGE. The capture of free surface is one of the most important and difficult problems in AM simulation, since the previous free surface will be covered by a new deposit. ABAQUS in 2017 version offers FFS and RFS options for automatic updating the free surface definition of convection and radiation heat flux.

Here we introduce two models of heat source, which are widely used in current researches of additive manufacturing [VAS 16]. In these formulae of the two models above, we assume that the origin of coordinates locates at the focus of heat source.

### Laser heat source model

For AM systems using laser, the heat source profile corresponds to laser transverse mode. The irradiation profile at the fundamental transverse mode  $TEM_{00}$  is Gaussian beam[HUA 16]. In fact, the beam profile in cylindrical coordinates is described as a combination of a Gaussian beam with a Laguerre polynomial for the laser mode  $TEM_{pl}$  [ROB 09]. Though the profiles of laser are complex, as is shown in three examples in Figure 2.3,  $TEM_{00}$  is still used as a simplification of heat source in some researches.

$$\dot{Q}_{TEM00} = \frac{2AP}{\pi r_{laser}^2} \exp\left(-\frac{2(x^2 + y^2)}{r_{laser}^2}\right) \quad (2.7)$$

where  $P$  is the input laser power,  $A$  is the reflection coefficient, and  $r_{laser}$  is the laser beam's radius.

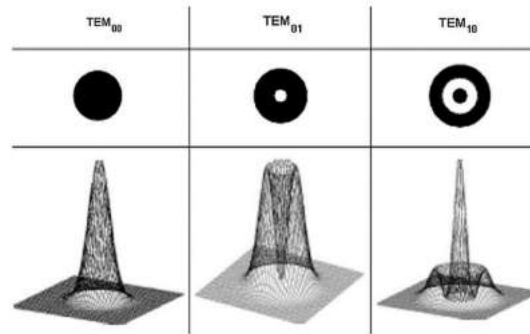


**Figure 2.3:** Laser profiles of different TEM[MOR 17]

### Goldak heat source model

In practice, researchers often adopt the Goldak double-ellipsoid model to calculate volumetric heat flux distributions. This model describes the power density around the moving heat source's focus. Many welding simulations have applied the Goldak model to predict their fusion zone (FZ) and heat affected zone (HAZ). By analogy to welding, the AM simulation at macro-scale can also use this model as the input heat flux model. For ABAQUS users, the moving heat source model and the laser/electron beam's trajectory are defined using FORTRAN subroutine DFLUX.

$$\dot{Q}_f = \frac{6\sqrt{3}f_f\eta_{abs}P}{a_fbc\pi\sqrt{\pi}} \exp\left(-3\left(\frac{x^2}{a_f^2} + \frac{y^2}{b^2} + \frac{z^2}{c^2}\right)\right) \quad (2.8)$$

$$\dot{Q}_r = \frac{6\sqrt{3}f_r\eta_{abs}P}{a_rbc\pi\sqrt{\pi}} \exp\left(-3\left(\frac{x^2}{a_r^2} + \frac{y^2}{b^2} + \frac{z^2}{c^2}\right)\right) \quad (2.9)$$

where  $f_f$  and  $f_r$  are the fractional factors of the heat deposited in the front and rear quadrant, as determined by  $f_f + f_r = 2$ .  $\eta_{abs}$  is the powder absorption coefficient.  $a_f$ ,  $a_r$ ,  $b$ ,  $c$  are shape parameters of heat source, shown in Figure 2.4.

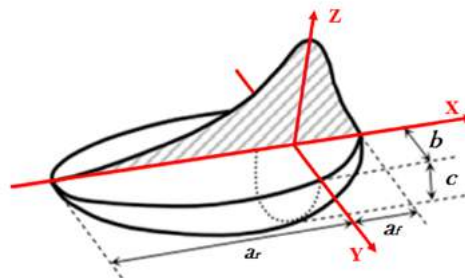


**Figure 2.4:** Goldak heat source model[GOL 84]

### Volumetric heat source model

In AM simulation with birth and death method, the heat source can be simplified using a volumetric heat source model. For a laser device with the power  $P_{laser}$ , the laser-material interaction leads to a loss of power. This energy conversion efficiency is defined as  $\eta$ , and the detail of  $\eta$  depends on the complexity of the melting pool's microscopic model. The influenced zone of heat source is defined by some basic geometry parameters (shown in Figure 2.5).  $v$  is the scan speed of the AM system.  $d$  is the width of a hatch, which is often the same value of one layer's thickness.

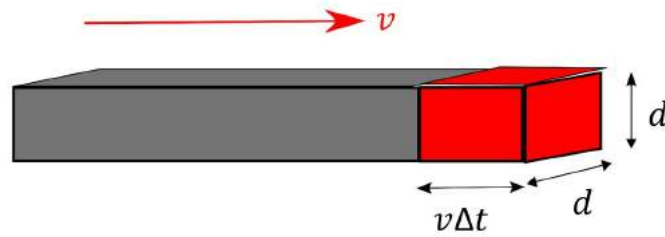


**Figure 2.5:** Volumetric heat source model

The volumetric heat power  $P_{volumetric}$  is then calculated as:

$$P_{volumetric} = \frac{\eta P_{laser}}{vd^2} \quad (2.10)$$

When the microscopic material-laser interaction is unknown, this volumetric heat model is simple enough for a FEM macroscopic simulation, since we can use directly  $P_{volumetric}$  in simulation. Additionally, this model requires less strictly the FEM mesh quality in practice than Laser heat source model and Goldak heat source model. In this thesis, we mainly apply the volumetric heat source model for FEM simulations.

## 2.2 Mechanical equation for residual stress

The mechanical behaviours of a metallic part built in AM systems are usually described by elasto-plastic model at macro-scale with some modifications[HUS 13a]. The basic conservation of momentum equation and angular momentum equation are

$$\frac{\partial \sigma_{ij}}{\partial x_j} = 0 \quad (2.11)$$

$$\sigma_{ij} = \sigma_{ji} \quad (2.12)$$

where  $\sigma_{ij}$  is the stress tensor. The Dirichlet boundary condition is defined for AM simulations. The displacement of the substrate's inferior surface is zero in Z direction and the corners of this surface are fixed as fully built-in points.

The total strain tensor  $\epsilon_{ij}$  consists of three parts: elastic strain  $\epsilon_{ij}^e$ , plastic strain  $\epsilon_{ij}^p$ , thermal expansion strain  $\epsilon_{ij}^{th}$  as follow



$$\boldsymbol{\varepsilon}_{ij} = \boldsymbol{\varepsilon}_{ij}^e + \boldsymbol{\varepsilon}_{ij}^p + \boldsymbol{\varepsilon}_{ij}^{th} \quad (2.13)$$

The thermal expansion strain  $\boldsymbol{\varepsilon}_{ij}^{th}$  at temperature  $T$  is calculated by

$$\boldsymbol{\varepsilon}_{ij}^{th} = \alpha(T - T_{ref})\boldsymbol{\delta}_{ij} \quad (2.14)$$

where  $\alpha$  is the dilatation coefficient,  $T_{ref}$  is the reference temperature,  $\boldsymbol{\delta}_{ij}$  is the Kronecker tensor.

The constitutive model of total stress  $\boldsymbol{\sigma}_{ij}$  and elastic strain  $\boldsymbol{\varepsilon}_{hk}^e$  is

$$\boldsymbol{\sigma}_{ij} = C_{ijkl}\boldsymbol{\varepsilon}_{hk}^e \quad (2.15)$$

where  $C_{ijkl}$  is the fourth-order elasticity tensor as a function of the elastic modulus  $E$  and the Poisson's ratio  $\nu$ . For isotropic material, this constitutive model can be simplified as

$$\boldsymbol{\varepsilon}_{ij}^e = \frac{1 + \nu}{E}\boldsymbol{\sigma}_{ij} - \frac{\nu}{E}\boldsymbol{\sigma}_{kk}\boldsymbol{\delta}_{ij} \quad (2.16)$$

Because of the high frequent heating and cooling cycles in additive manufacturing, the yield function criterion of metallic part is relatively complex. For sake of simplicity, A von Mises type criterion  $F$  is applied for metallic part:

$$F = \sqrt{\frac{3}{2}S_{ij}S_{ij}} - \sigma_y(\bar{\boldsymbol{\varepsilon}}^p, T) \quad (2.17)$$

where  $S_{ij}$  is the deviatoric stress

$$S_{ij} = \boldsymbol{\sigma}_{ij} - \frac{1}{3}\boldsymbol{\delta}_{ij}\boldsymbol{\sigma}_{kk} \quad (2.18)$$

and  $\sigma_y(\bar{\boldsymbol{\varepsilon}}^p, T)$  is the yield stress which depends on equivalent plastic strain  $\bar{\boldsymbol{\varepsilon}}^p$  and temperature  $T$ .

The equivalent plastic strain is a value to estimate quantitatively the accumulative effect of plastic deformation.

$$\bar{\boldsymbol{\varepsilon}}^p = \int_0^t \dot{\bar{\boldsymbol{\varepsilon}}}^p dt \quad (2.19)$$

where  $\dot{\bar{\boldsymbol{\varepsilon}}}^p$  is the equivalent plastic strain rate, defined as

$$\dot{\bar{\boldsymbol{\varepsilon}}}^p = \sqrt{\frac{2}{3}\dot{\boldsymbol{\varepsilon}}_{ij}^p\dot{\boldsymbol{\varepsilon}}_{ij}^p} \quad (2.20)$$

Here we should notice that the equivalent plastic strain  $\bar{\boldsymbol{\varepsilon}}^p$  isn't the plastic strain magnitude  $\sqrt{\frac{2}{3}\boldsymbol{\varepsilon}_{ij}^p\boldsymbol{\varepsilon}_{ij}^p}$ , and the latter doesn't take any accumulation effect into account.

For the hardening of metallic parts, the Johnson-Cook model [LEE 98] [WU 14] can be integrated into AM simulation. The yield stress  $\sigma_y$  in Johnson-Cook model is

$$\sigma_y(\bar{\epsilon}^p, \dot{\epsilon}^p, T) = [A + B(\bar{\epsilon}^p)^n] \left[ 1 + C \ln\left(\frac{\dot{\epsilon}^p}{\dot{\epsilon}_0^p}\right) \right] [1 - (T^*)^m] \quad (2.21)$$

where  $\dot{\epsilon}^p$  is the equivalent plastic strain rate.  $\bar{\epsilon}^p$  is the equivalent plastic strain,  $T^*$  is the normalized temperature, and  $A, B, C, n, m, \dot{\epsilon}_0^p$  are empirical parameters.

The normalized temperature  $T^*$  is a dimensionless number defined as

$$T^* = \begin{cases} 0, & T < T_{trans} \\ \frac{T - T_{trans}}{T_{melt} - T_{trans}}, & T_{trans} < T < T_{melt} \\ 1, & T > T_{melt} \end{cases} \quad (2.22)$$

where  $T_{trans}$  is the transition temperature and  $T_{melt}$  is the melting temperature.

The Johnson-Cook model is written as a product of three terms: power law term  $A + B(\bar{\epsilon}^p)^n$ , logarithmic term  $1 + C \ln\left(\frac{\dot{\epsilon}^p}{\dot{\epsilon}_0^p}\right)$ , and exponential term  $1 - (T^*)^m$ . They represent respectively the accumulative virtual work effect due to plastic strain over long time, the instantaneous effect of plastic strain rate, and the thermo-mechanical effect of material such as recrystallization annealing. In software ABAQUS, Johnson-Cook hardening model is an option of INP keyword \*PLASTIC. This empirical model is useful for the study of metal mechanical behaviour when the material's high-temperature plastic properties can't be directly obtained by experiments. In this thesis, we use Johnson-Cook model for the mechanical simulation of Ti6Al4V at part-level.

## 2.3 Metallurgical phase models in macroscopic scale

In additive manufacturing of a metallic part, the residual stress and distortion could be affected by the solid phase transformation during the high frequency heating and cooling cycles. The metallurgical properties of different metal solid phases impact the mechanical or thermal behaviour during additive manufacturing [SAM 16]. For a mixture of multiple phases, the overall material property is often simplified as a weighted sum of the property of each pure phase [CRE 09]. In this sum, the volume fraction is the weight which changes with the temperature evolution during AM process.

The field of a material's volume fraction is a macroscopic scalar field. This field can't be used to describe the metallurgical micro-structure of metal crystals, but it is of importance for the forecast or the measure of solid phase transformation. Most of AM machines for metallic part usually use the powder of steel [HUY 15] and titanium alloy (Ti6Al4V) [KIR 17] as their raw materials [FRA 14]. The solid phase transformation of steel or titanium alloy depends kinetically on the cooling rate of AM process. According to different mechanisms, the solid phase transformation can be classified into two kinds: the martensitic transformation [LI 15] and diffusional transformation. Without given the detail of material parameters, two models of transformation will be briefly introduced here. Titanium alloy (Ti6Al4V) will be used as an example, and the two-phase transformation models can be also applied for steel with appropriate modification. The transformation

model's implementation in ABAQUS involves the FORTRAN subroutine USDFLD, in which the volume fractions are defined as solution-dependent state variables (SDV) of temperature field [JIA 17]. In AM thermo-metallurgical simulation procedures, the temperature evolution history of thermal field is the input data for metallurgical simulation.

### 2.3.1 Martensitic transformation

When its temperature is less than  $M_s = 650.0^\circ\text{C}$  and its cooling rates faster than  $m_{cool} = -410^\circ\text{C}/\text{s}$ , the martensitic transformation happens in the metal Ti6Al4V during its cooling process. Instead of the long-range diffusion of atoms during a very short time, a lattice-distortive displacement occurs (see Figure 2.6), resulting in the phase change from body-centred cubic austenite  $\beta$  to martensite  $\alpha'$  [ELM 04]. The movement of an atom is usually less than the interatomic distances. The martensitic transformation  $\beta \rightarrow \alpha'$  occurs if the solid cools below the martensitic start temperature ( $M_s = 650^\circ\text{C}$ ). The volume fraction of phase  $\alpha'$  can be described by the Koistinen-Marburger (KM) model

$$f_{\alpha'}(T) = f_{\alpha'}(T_0) + (f_{\beta}(T_0) - f_{\beta,r})[1 - \exp(-\gamma(M_s - T))] \quad (2.23)$$

where  $f_{\alpha'}(T)$  and  $f_{\beta}(T)$  are respectively volume fractions of phase  $\alpha'$  and phase  $\beta$ ,  $T_0$  is the initial temperature at the beginning of the transformation,  $\gamma = 0.015^\circ\text{C}^{-1}$  is the coefficient of transformation.  $f_{\beta,r}$  is the retained phase  $\beta$  which can be calculated using the empirical formula [FAN 93].

$$f_{\beta,r} = \begin{cases} f_{\beta}(T_0), & f_{\beta}(T_0) < 0.25 \\ 0.25(1.0 - f_{\beta}(T_0)) & f_{\beta}(T_0) \geq 0.25 \end{cases} \quad (2.24)$$

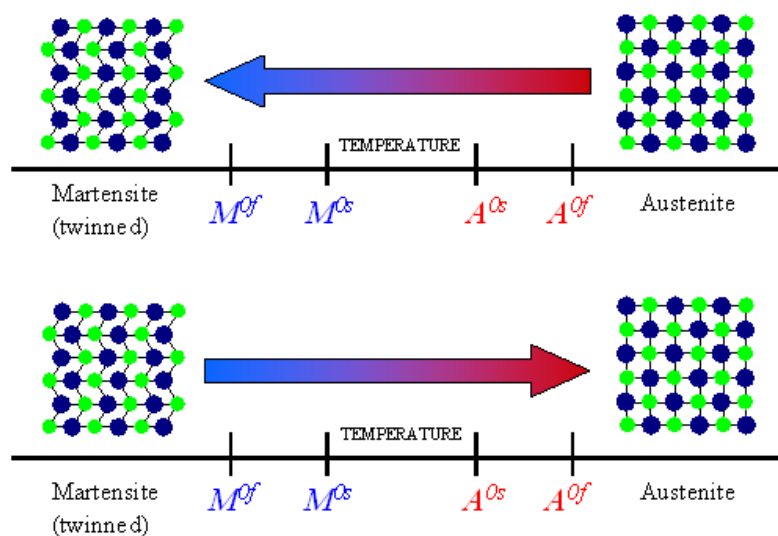
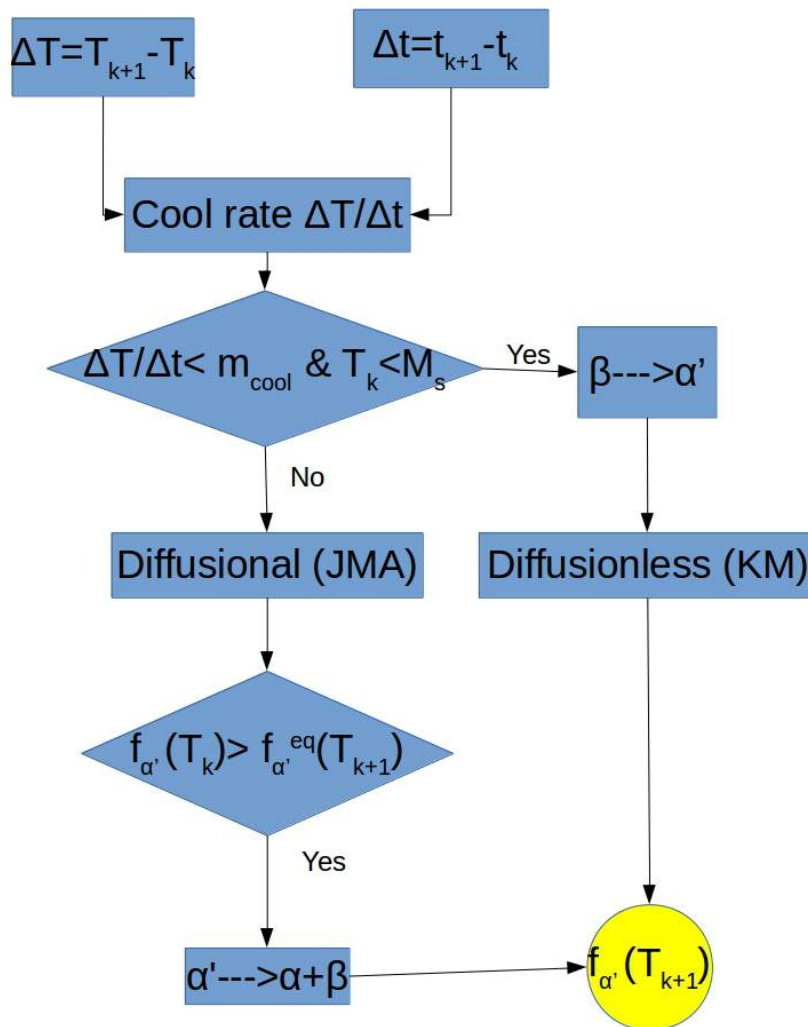


Figure 2.6: Temperature-induced martensitic transformation[VAN 13]

In the subroutine of USDFLD (see the Appendix E), the temperature  $T_{k+1}$ ,  $T_k$  and temperature change rate  $\Delta T/\Delta t$  can be automatically read from the result of thermal simulation after each time step  $\Delta t$ . The basic algorithm for calculating the evolution of martensite phase  $\alpha'$  fraction  $f_{\alpha'}(T_{k+1})$  is simply shown in Figure 2.7, in which the detail of diffusional transformation will be introduced later.



**Figure 2.7:** Basic algorithm for calculating  $f_{\alpha'}$

### 2.3.2 Diffusional transformation

When Ti6Al4V is heated, the phase  $\alpha'$  decomposes into a mixture of phase  $\beta$  and the hexagonal close-packed  $\alpha$ . During heating and slow cooling at a cooling rate lower than  $410^\circ\text{C}/\text{s}$ , crystal grain growth and nucleation are dominant, and transformations between phase  $\alpha$  and phase  $\beta$  occur. Both the transformation  $\alpha' \rightarrow \alpha + \beta$  and  $\alpha \leftrightarrow \beta$  are dominated by diffusion mechanism, which can be described by Johnson-Mehl-Avrami(JMA) model.

Johnson-Mehl-Avrami(JMA) model is the solution of Avrami equation [FAR 06] which describes how solids transform from one phase to another at constant temperature  $T_0$ . The volume fraction of the new phase is calculated using

$$\left\{ \begin{array}{l} \alpha' \rightarrow \alpha + \beta : \\ f_{\alpha'} = (1 - \exp(-k_1 t_1^n)) f_{\alpha'}^{eq}(T_0) \quad \text{if } f_{\alpha'} > f_{\alpha'}^{eq}(T_0) \\ \beta \rightarrow \alpha : \\ f_{\beta} = 1 - f_{\alpha'} - (1 - \exp(-k_2 t_2^n))(1 - f_{\alpha'} - f_{\beta}^{eq}(T_0)) \quad \text{if } f_{\beta} > f_{\beta}^{eq}(T_0) \\ \alpha \rightarrow \beta : \\ f_{\beta} = (1 - \exp(-k_2 t_2^n)) f_{\beta}^{eq} \quad \text{if } f_{\beta} < f_{\beta}^{eq}(T_0) \end{array} \right. \quad (2.25)$$

where  $f_{\alpha'}^{eq}(T_0)$  and  $f_{\beta}^{eq}$  are respectively the temperature-dependent equilibrium volume fractions of phases  $\alpha'$  and  $\beta$ ,  $k_1$ ,  $k_2$ ,  $n_1$ ,  $n_2$  are the coefficients depending on temperature  $T_0$ . These four coefficients ( $k_1$ ,  $k_2$ ,  $n_1$ ,  $n_2$ ) can be obtained from time-temperature-transformation (TTT) diagram or continuous cooling transformation (CCT) diagram [DOM 11].  $f_{\alpha'}^{eq}(T_0)$  and  $f_{\beta}^{eq}(T_0)$  can be read from Phase diagrams in equilibrium.

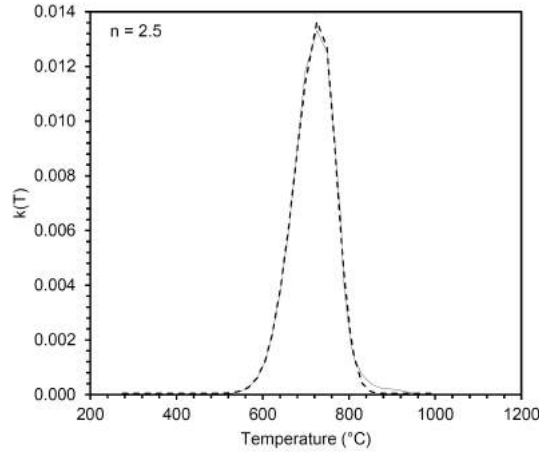


**Figure 2.8:** Kinetic parameters  $k(T)$  at  $n = 2.5$  for diffusional transformation [AHN 16]

The coefficient  $k$  depends on temperature  $T$  and its curve 2.8 is mathematically fitted as [AHN 16]:

$$k(T) = \begin{cases} k_0 + K \exp\left(-\frac{(T-T_c)^2}{2\sigma_1^2}\right) & T < T_c, \\ k_0 + K \exp\left(-\frac{(T-T_c)^2}{2\sigma_2^2}\right) & T \geq T_c \end{cases} \quad (2.26)$$

where  $k_0 = 3.84 \times 10^{-5} s^{-2.5}$ ,  $K = 0.01375$ ,  $T_c = 734.59204^\circ C$ ,  $\sigma_1 = 58.38677^\circ C$ ,  $\sigma_2 = 35.81163^\circ C$ . Referring to the Fortran subroutine in [AHN 16], the parameters are defined as  $k_1 = k_2 = k(T)$ ,  $n_1 = n_2 = 2.5$

It should be noticed that JMA model is ideally based on the isothermal process. The Johnson-Mehl-Avrami model can't directly calculate the transformed proportion in non-isothermal cooling or heating. Nevertheless, some researchers proposed special methods [MAL 01] to generalize the JMA model for the kinetics of non-isothermal transformations. In this additivity rule method, continuous cooling is replaced by a series of small consecutive isothermal steps where the Johnson-Mehl-Avrami equation can be applied (see Figure 2.9).

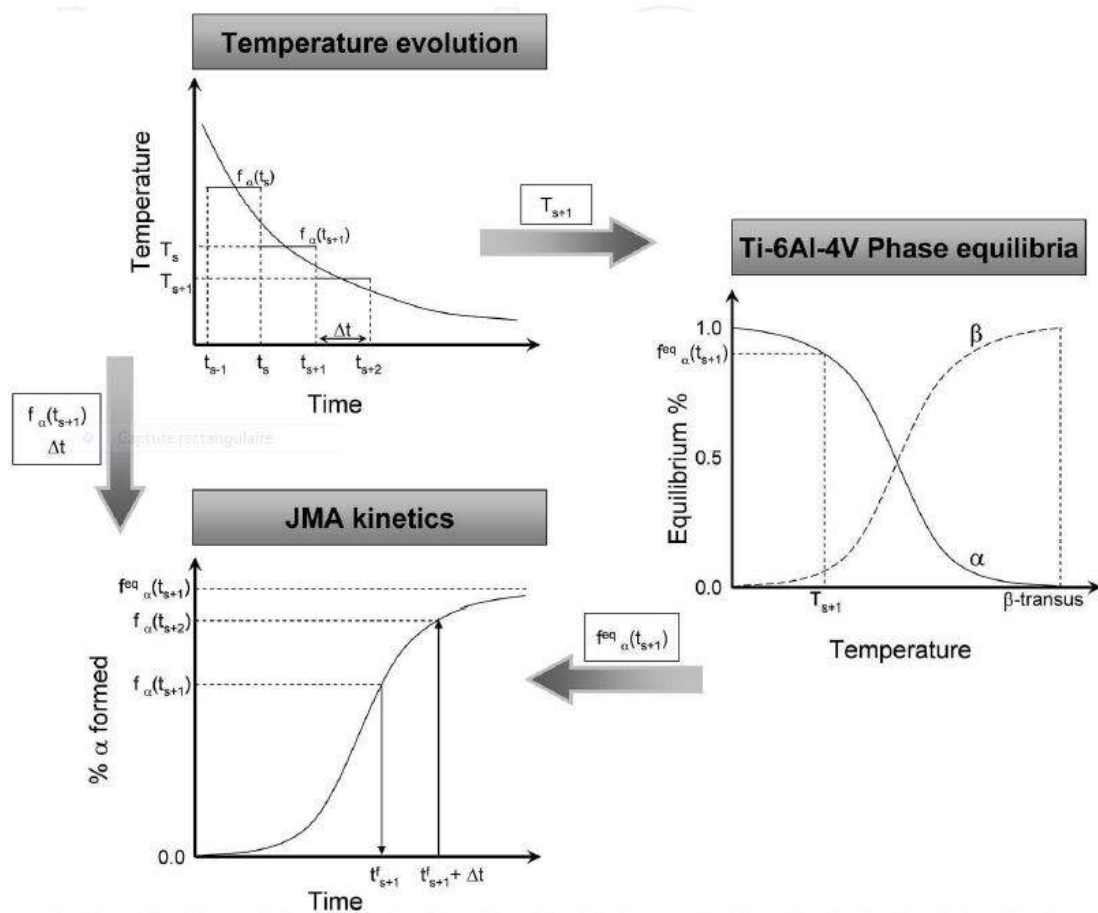


**Figure 2.9:** Generalization of the Johnson-Mehl-Avrami equation for non-isothermal transformations [CRE 11]

The metallurgical simulation is sequentially based on the result of thermal simulation, where the temperature changes from  $T_k$  to  $T_{k+1}$  during a time step  $\Delta t$ . At the beginning of phase calculation,  $T_k$  and  $T_{k+1}$  are already known, and the fractions of each phase  $f_{\alpha'}(T_k)$ ,  $f_{\beta}(T_k)$ ,  $f_{\alpha}(T_k)$  are also recorded.

### Phase equilibria at new temperature $T_{k+1}$

In JMA model's correction algorithm, the equilibrium volume fractions at the temperature  $T_{k+1}$  will be calculated. First, we calculate the equilibrium volume fraction  $f_{\alpha'}^{eq}(T_{k+1})$  of martensite phase  $\alpha'$ . There is an experimental expression for this equilibrium fraction[MAR 14]:

$$f_{\alpha'}^{eq}(T) = \frac{1}{2} \left( 1 + \tanh\left(\frac{c_1 - T}{c_2}\right) \right) \quad (2.27)$$

where  $c_1 = 450.0^\circ\text{C}$ ,  $c_2 = 80.0^\circ\text{C}$ .

Then we calculate the equilibrium volume fractions  $f_{\alpha}^{eq}(T_{k+1})$ ,  $f_{\beta}^{eq}(T_{k+1})$ . If we concentrate only on the mixture of two phases  $\alpha$  and  $\beta$ , we can define their respective fractions as

$$f_{\beta,0}(T_{k+1}) = 1.0 - f_{\alpha,0}(T_{k+1}) \quad (2.28)$$

In the mixture of  $\alpha$  and  $\beta$ , the equilibrium fraction  $f_{\alpha,0}^{eq}(T_{k+1})$  at the temperature  $T$  can be experimentally expressed as[CAS 66]:

$$f_{\alpha,0}^{eq}(T_{k+1}) = \begin{cases} c_3(1.0 - \exp(-c_4(T_{\beta\text{-transus}} - T_{k+1}))), & T \geq T_{\beta\text{-transus}} \\ 0, & T > T_{\beta\text{-transus}} \end{cases} \quad (2.29)$$

where  $T_{\beta\text{-transus}} = 980.0^\circ\text{C}$ ,  $c_3 = 0.925$ ,  $c_4 = 0.0085^\circ\text{C}^{-1}$ .

The  $f_{\beta,0}^{eq}(T)$  is indirectly calculated as

$$f_{\beta,0}^{eq}(T_{k+1}) = 1.0 - f_{\alpha,0}^{eq}(T_{k+1}) \quad (2.30)$$

In fact, the fractions  $f_{\beta}(T_{k+1})$  and  $f_{\alpha}(T_{k+1})$  can be calculated from the total three phases' mixture ( $\alpha - \beta - \alpha'$ ):

$$f_{\alpha}^{eq}(T_{k+1}) = f_{\alpha,0}(T_{k+1})^{eq}(1.0 - f_{\alpha'}) \quad (2.31)$$

$$f_{\beta}^{eq}(T_{k+1}) = f_{\beta,0}(T_{k+1})^{eq}(1.0 - f_{\alpha'}) \quad (2.32)$$

Now the equilibrium fractions at the temperature  $T_{k+1}$   $f_{\beta}^{eq}(T_{k+1})$ ,  $f_{\alpha}^{eq}(T_{k+1})$ , and  $f_{\alpha'}^{eq}(T_{k+1})$  are known from equations (Equation2.27, Equation2.31, Equation2.32) above.

### correction $\xi$ for JMA model

During the time step  $\Delta t$ , the temperature changes from  $T_k$  to  $T_{k+1}$ . This process is exactly non-isothermal. However, we can modify the basic JMA equations 2.25 with a special term  $\xi$  to calculate this diffusional transformation process for real cases [XIE 17].

First, we compare the fraction  $f_{\alpha}(T_k)$  with  $f_{\alpha}^{eq}(T_{k+1})$ . When  $f_{\alpha}(T_k) > f_{\alpha}^{eq}(T_{k+1})$ , the process  $\alpha' \rightarrow \alpha + \beta$  will happen and the correction term  $\xi_{\alpha'}$  for this process is

$$\xi_{\alpha'} = \left( -\frac{1}{k_1} \ln \left( \frac{f_{\alpha'}(T_k) - f_{\alpha'}^{eq}(T_{k+1})}{1.0 - f_{\alpha'}^{eq}(T_{k+1})} \right) \right)^{\frac{1}{n_1}} \quad (2.33)$$

We add this correction term to the ideal JMA equation 2.25 to obtain  $\alpha'$  phase's new fraction  $f_{\alpha'}(T_{k+1})$  during  $\Delta t$ :

$$f_{\alpha'}(T_{k+1}) = 1.0 - (1.0 - \exp(-k_1(\xi_{\alpha'} + \Delta t)^{n_1}))(1.0 - f_{\alpha'}^{eq}(T_{k+1})) \quad (2.34)$$

Then the phase transformation between  $\alpha$  and  $\beta$  is taken into our consideration. An intermediate fraction is calculated for the phase  $\beta$  as

$$f_{\beta}^* = f_{\beta}(T_k) \left( \frac{1.0 - f_{\alpha'}(T_{k+1})}{1.0 - f_{\alpha'}(T_k)} \right) \quad (2.35)$$

This fraction  $f_{\beta}^*$  will be used to determinate the phase transformation direction by comparing  $f_{\beta}^*$  with the equilibrium fraction  $f_{\beta}^{eq}(T_{k+1})$  at new temperature  $T_{k+1}$ .  $f_{\beta}^{eq}(T_{k+1})$  is already calculated using the Equation 2.32.

When  $f_{\beta}^*$  exceeds  $f_{\beta}^{eq}(T_{k+1})$ , some of the phase  $\beta$  will change into the phase  $\alpha$  during the time step  $\Delta t$ . For the process  $\beta \rightarrow \alpha$ , its correction term is:

$$\xi_{\beta} = \left( -\frac{1}{k_2} \ln \left( \frac{f_{\beta}(T_k) - f_{\beta}^{eq}(T_{k+1})}{1.0 - f_{\alpha'}(T_k) - f_{\beta}^{eq}(T_{k+1})} \right) \right)^{\frac{1}{n_2}} \quad (2.36)$$

We add  $\xi_{\beta}$  to the ideal JMA equation 2.25 for  $\beta \rightarrow \alpha$ :

$$f_{\beta}(T_{k+1}) = 1.0 - f_{\alpha'}(T_k) - (1.0 - f_{\alpha'}(T_k) - f_{\beta}^{eq}(T_{k+1}))(1.0 - \exp(-k_2(\xi_{\beta} + \Delta t)^{n_2})) \quad (2.37)$$

When  $f_{\beta}^* < f_{\beta}^{eq}(T_{k+1})$ , some of the phase  $\alpha$  will change into the phase  $\beta$  during the time step  $\Delta t$ . Similarly, the correction term is

$$\xi_{\beta} = \left( -\frac{1}{k_2} \ln \left( \frac{f_{\beta}^{eq}(T_{k+1}) - f_{\beta}(T_k)}{f_{\beta}^{eq}(T_{k+1})} \right) \right)^{\frac{1}{n_2}} . \quad (2.38)$$

The fraction of  $\beta$  is

$$f_{\beta}(T_{k+1}) = f_{\beta}^{eq}(T_{k+1})(1.0 - \exp(-k_2(\xi_{\beta} + \Delta t)^{n_2})) \quad (2.39)$$

If  $f_{\beta}^*$  equals to  $f_{\beta}^{eq}(T_{k+1})$ , no transformation occurs between  $\alpha$  and  $\beta$

$$f_{\beta}(T_{k+1}) = f_{\beta}^* \quad (2.40)$$

For the fraction of phase  $\alpha$ , it can be easily obtained after calculating  $f_{\beta}(T_{k+1})$  and  $f_{\alpha'}(T_{k+1})$ :

$$f_{\alpha}(T_{k+1}) = 1.0 - f_{\beta}(T_{k+1}) - f_{\alpha'}(T_{k+1}). \quad (2.41)$$

The global flow chart of this JMA algorithm for the non-isothermal process is shown below:



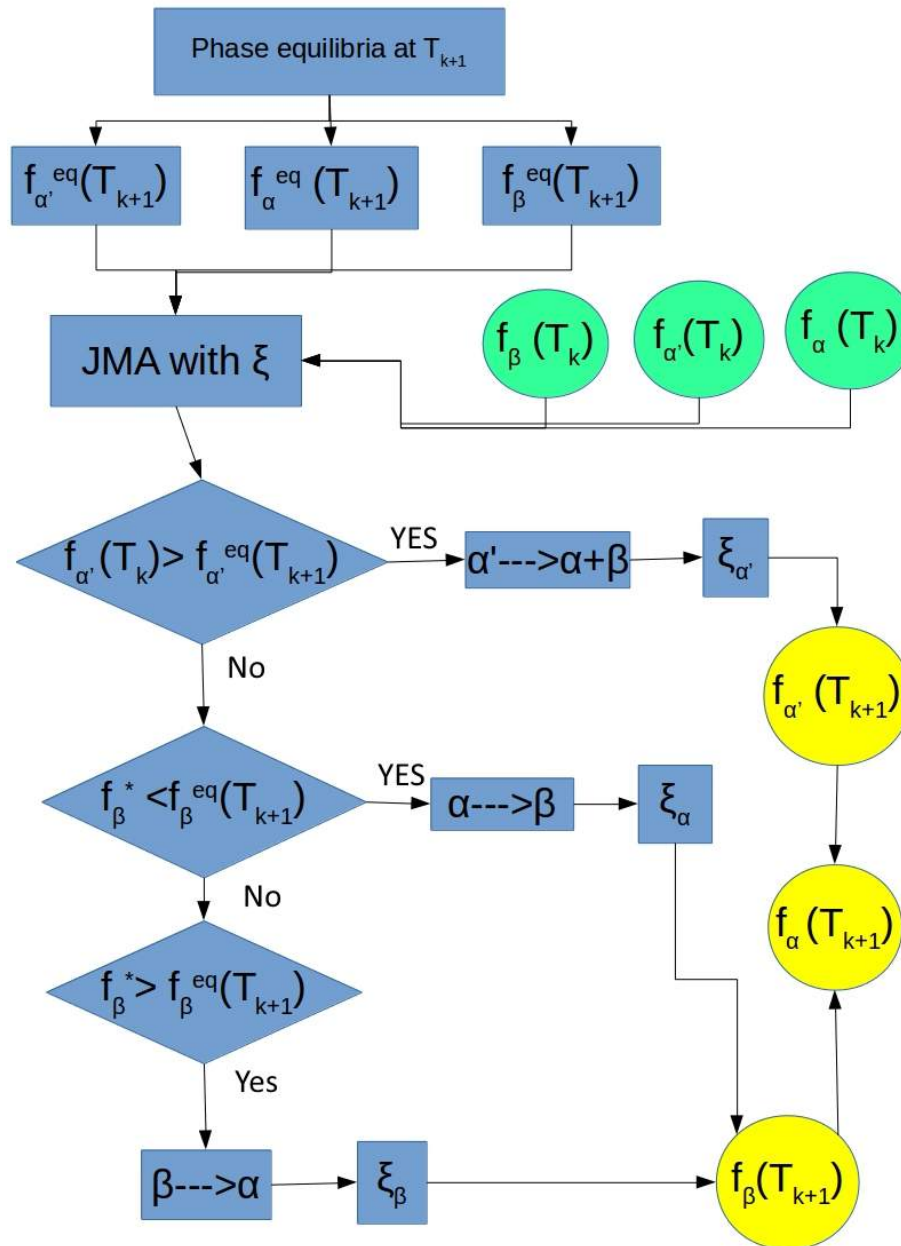


**Figure 2.10:** Algorithm flow chart for diffusional transformation with modified JMA model

## 2.4 Conclusion

Before simulating the process of additive manufacturing, we need first to analyse mathematically the complex coupled fields in metal AM systems. This multi-physics problem is usually divided into three fields: thermal field, mechanical field and metallurgical field.

In practice, the temperature distribution obtained from thermal field simulation is the basic input data for the other fields. The free surface that changes with material deposition is always a challenging problem in AM numerical simulation, as it serves as the moving free boundary condition for partial differential equations.

The decoupling of multi-physical fields is fundamental for FEM simulation. By solving the basic heat equation using FEM, temperature distribution's evolution can be understood and serve as the input data for the other two fields. Some heat source models are introduced for thermal analysis. In residual stress analysis, elasto-plastic equations are often combined with Johnson-Cook hardening model at high temperature. In terms of metallurgical phases' transformation, Koistinen-Marburger (KM) model and modified Johnson-Mehl-Avrami (JMA) model are usually integrated with the FEM method. We take Ti6Al4V as an example to explain the algorithm of phase transformation (martensitic and diffusional), which will be implemented in AM simulations for the next chapters.

## 2. Theoretical basis for additive manufacturing simulation

---

## Chapter 3

# Macroscopic AM simulation for multiphysics fields

*In this chapter, the special problems on pre-processing are investigated for the AM simulation at layer-level and at part-level. We construct the platform for macroscopic FEM simulation, using an example of a turbine blade part's thermal-mechanical-metallurgical fields. Then the influences of preheat temperature and AM process parameters are studied in order to reduce the residual stress of an AM part.*

## Contents

---

<b>3.1</b>	<b>Workflow of file formats for additive manufacturing process . . . . .</b>	<b>57</b>
<b>3.2</b>	<b>Pre-processing for 3D model with complex geometry . . . . .</b>	<b>60</b>
3.2.1	Analysis G-code file and extraction of scan path information . . . . .	60
3.2.2	Reconstruction of 3D model at layer size: offsetting and clipping . . . . .	62
3.2.3	Map of sets in orphan FEM mesh and in CAD geometry . . . . .	67
3.2.4	Reconstruction of 3D model at part size: voxelization . . . . .	70
<b>3.3</b>	<b>FEM simulation for multi-physics fields . . . . .</b>	<b>73</b>
3.3.1	Thermal simulation at layer-level . . . . .	75
3.3.2	Thermal-mechanical-metallurgical simulation at part-level . . . . .	84
<b>3.4</b>	<b>Study on AM process parameters for a part's residual stress . . . . .</b>	<b>98</b>
3.4.1	Influence of preheat temperature . . . . .	99
3.4.2	Influence of AM process parameters ( $P_i, t_i$ ) . . . . .	101
<b>3.5</b>	<b>Conclusion . . . . .</b>	<b>108</b>

---

In this chapter, we first study the pre-processing problems of AM simulation since they are particular constraints for the application of finite element method in this area. Using the framework from layer level to part level, we can then simulate the dynamic macroscopic process in additive manufacture for an object with complex geometry. Second, we use a turbine blade as an example to study the evolution of thermal-mechanical-metallurgical fields during its AM process. Third, we study the influences of preheat temperature and AM process parameters on residual stress. This methodology will be helpful for us to reduce residual stress of a part built by a AM system.

### 3.1 Workflow of file formats for additive manufacturing process

The basic procedures of different AM technologies have some similarities in common (see Figure 3.1), especially the manipulation CAD/CAM during the preparation of 3D model. However, the software is often dedicated to certain AM machines and most of them are commercial software with lots of limits in licenses and data formats.

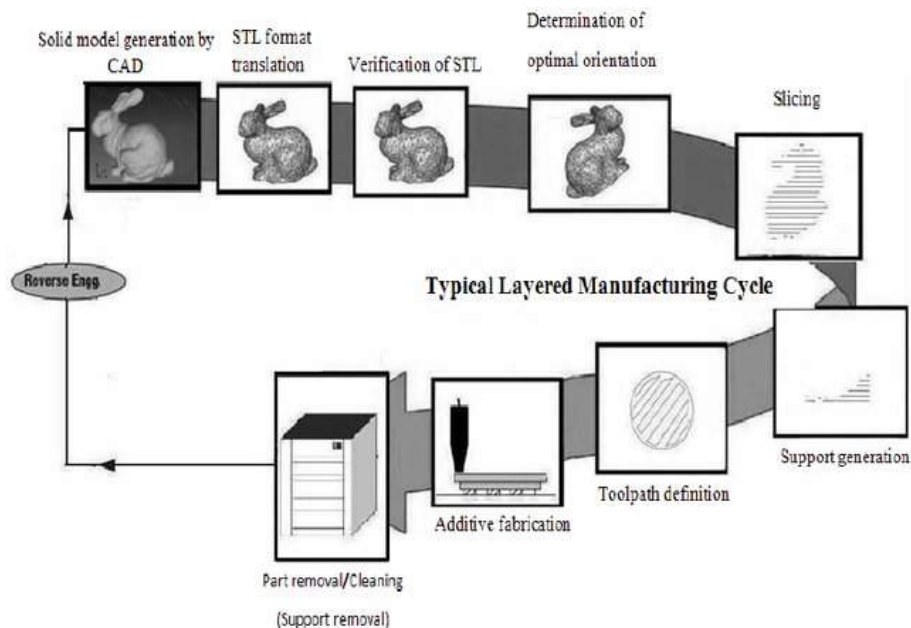


**Figure 3.1:** Basic workflow in additive manufacturing[TAU 13]

In AM simulation, it is quite normal to convert file formats in different procedures. The simulation of AM process makes this work more difficult since details at different levels (line-level, layer-level, part-level) should be considered. The 3D model of a part with complex geometry is indirectly imported into FEM simulation software, one schematic of this pre-processing work is shown in Figure 3.2.

### 3. Macroscopic AM simulation for multiphysics fields

---

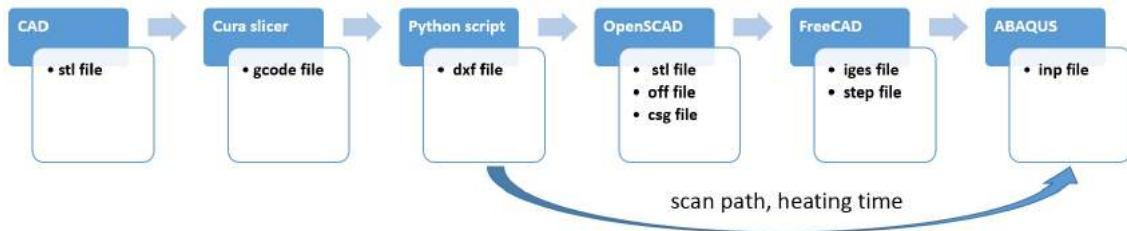
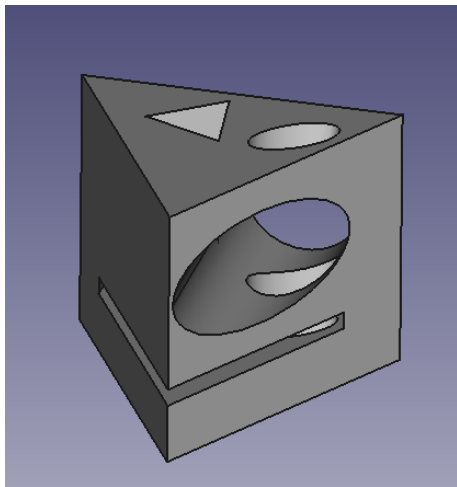


**Figure 3.2:** File format conversion from CAD to FEM analysis

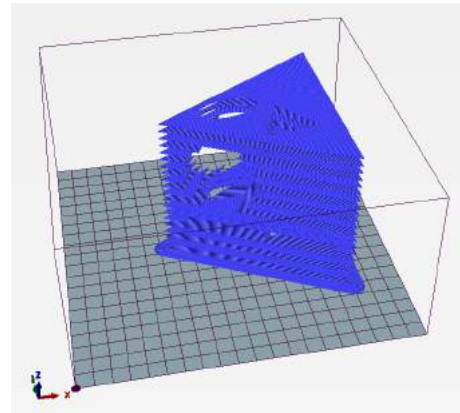
One of the difficulties in AM simulation is the connection between scan path and FEM software. Most of the academic researchers have to simulate objects with simpler geometry to avoid using the real scan path, since these objects usually use only back and forwards straight line scan strategy. For a more complex object, especially simulation at layer level, this simplification might lose the chance to observe the detail in the multiphysics field. In this thesis, we will study first how the slicer software works and then import scan path information into FEM simulation. We use some open source software rather than the commercial software of a particular AM machine, in order to obtain a generalizable workflow for AM simulation research.

There is some open source software for the preprocessing of additive manufacturing, mainly based on Skeinforge engine and CuraEngine. These codes generally provide slicers and G-code generators for additive manufacturing. Here CuraEngine is used to explain the procedures of pre-processing in AM simulation through it is mainly applied for FDM (Fused deposition modelling) printers now.

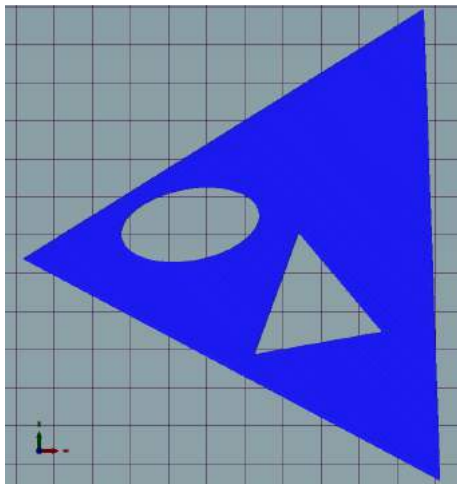
When a 3D CAD model is imported in CuraEngine in the file format STL or AMF [HIL 09], the volumes of this 3D geometry will be separated into different layers, each of whom contains closed 2D polygons. The STL file uses tessellated triangles to represent the surface of 3D geometry [MA 01a] [WAN 06]. In CuraEngine, all triangles are cut into lines per layer, for each layer these intersection line segments are added to that layer. Then all these line-segments are connected to each other to make closed polygons [BRO 13]. After these operations above, the slicer separates one 3D part into many layerparts. One layerpart contains parts inside only one single layer. For example, in the slicer operation of a 3D object with complex geometry in Figure 3.1 with 20 layers, its 9th layer may include 2 layerparts which represent 2 separated area. Hence a layerpart can be defined as a separated area inside a single layer which does not touch any other layerparts.



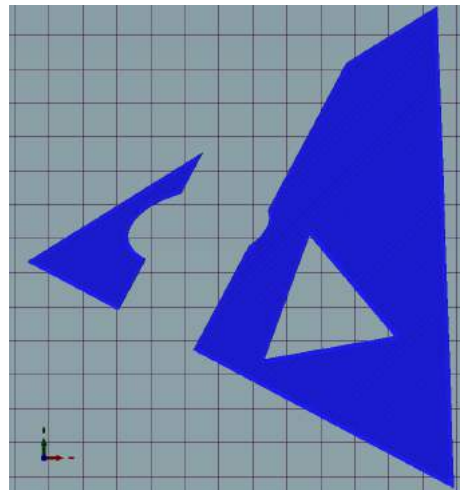
(a) original 3D model in CAD



(b) 20 layers of part in slicer



(c) 2nd layer with 1 layerpart



(d) 9th layer with 2layerparts

**Figure 3.3:** A part with complex geometry in slicer software(CuraEngine)

In the polygon of one layerpart, the external and internal perimeters are defined as the wall type. The inside area will be defined as the infill area. The lists of polygons will be obtained after a series of boolean calculation with the help of clipping-offsetting algorithms in computer graphics.

In G-code file generator, the lists of polygons in previous slicer procedure will be sorted with optimized order by solving Travelling Salesman Problem. Then the infill pattern in one layer part will be generated, resulting in a group of path vectors. Finally all the paths will be integrated as one G-code file which includes most of the information of the path detail in AM process.



## 3.2 Pre-processing for 3D model with complex geometry

The additive manufacturing process is simulated at three different scales: line scale, layer scale, part scale. All of them are macroscopic simulations and the commercial FEM software can be used for these kinds of simulations with some special modifications and developments of codes. In our study, we use ABAQUS as the basic FEM software and develop some python scripts for it.

The ABAQUS software has some advantages for AM multi-scale simulation. First, ABAQUS supports Model Change keyword for element progressive activation during material deposition. Furthermore, free surfaces of convection (FFS) and radiation (RFS) in the thermal analysis should be updated after each time of material deposition. The previous free surfaces exposed in shield gas may be covered with new material deposit. From the version 2017, ABAQUS is able to recognize the free surfaces after each material deposition. Thirdly, one of the difficulties in AM simulation is the definition of multi-steps simulating the material deposition processing. AM simulation involves lots of definition operation for element sets, multiple analysis steps, etc. It is impossible to complete manually this special treatment of FEM pre-process in ABAQUS graphical user interface (GUI) called ABAQUS CAE. The FEM software ABAQUS provides an application programming interface (API) based on python object-oriented programming language. The readability of python scripts is much better than INP file and makes it possible to generate automatically INP file for AM simulation. So we write some python scripts for automatic pre-processing of our AM simulation (see Appendix B and AppendixC).

### 3.2.1 Analysis G-code file and extraction of scan path information

G-code is the programming language widely used in numerical control of CAM, for example, the control of automated machine tools. The G-code files provide some information to the motor of machine tool where to move, which path to follow, and how fast to move. Because of the similarity between the toolpath in machine tools and material deposit/laser beam path in AM machines, some AM systems also accept G-code format file as the input control file for their hardware. On account of the features of AM systems, the material deposition feeding speed may also be added to G-code file, accompanying with the basic trajectory information. In our study, we analysed the keywords and syntax of G-code file generated by CuraEngine. This makes it possible for us to extract the trajectory and the line deposition orders, which is essential information for AM simulation at layer scale.

CuraEngine generates material deposit path in three types: WALL-INNER, WALL-OUTER, SKIN. In G-code file, the redundancy keywords make it difficult to extract the trajectory of each deposition. With the help of some regular expression (REGEX) libraries, we can define certain string search patterns to find the vectors which compose the deposition path. In our study, this text-processing is automatically done by python scripts.

**Table 3.1:** Some G-code keywords in CuraEngine

Cura code	function
G0	rapid linear positioning
G1	linear interpolation movement
F	movement speed
E	feed rate of extruder
X,Y,Z	target coordinates
M140	set bed target temperature
M106	fan on
M204	set default acceleration
M205	advanced settings for jerk

```

;LAYER:1
M140 S60
M106 S85
M204 S2812
M205 X18
G1 F1500 E93.87138
G0 F9642.9 X163.317 Y93.738 Z10.27
G0 X159.543 Y95.402
G0 X156.621 Y95.49
M204 S750
M205 X7.5
;TYPE:WALL-INNER
G1 F1500 E100.37138
G1 X156.62 Y95.491 E100.37205
G1 X156.572 Y95.498 E100.39486
G1 X156.346 Y95.51 E100.50129
G1 X154.869 Y95.7 E101.20159
G1 X154.345 Y95.731 E101.44844
G1 X152.769 Y95.927 E102.19528
G1 X152.508 Y95.94 E102.31818
G1 X152.453 Y95.924 E102.34511
G1 X150.513 Y96.16 E103.26415
G1 X150.243 Y96.171 E103.39123
G1 X150.182 Y96.149 E103.42172
G1 X149.893 Y96.183 E103.55856
G1 X149.577 Y96.195 E103.70728

```

**Figure 3.4:** G-code generated by CuraEngine

The G-code file can't be directly used for pre-processing of AM simulation due to its verbose information like Figure 3.4. We should first extract the scan path vectors (type SKIN), scan path of polygons (type WALL-INNER, type WALL-OUTER), and scan speed from G-code file with some text-processing scripts. Then we can use this information to reconstruct the partition in a layer. Here are some keywords for one layer in Table 3.2.1, similar to that of machine tools. Before the AM simulation of the deposition process in one layer, we need to reconstruct the 3D geometry of one layer where each line should be distinguished. However the initial CAD file (format STL) is only a geometrical description of the whole workpiece to build, the CAD detail in one layer should be re-drawn after the operations in slicer and path generator likes CuraEngine. Instead of

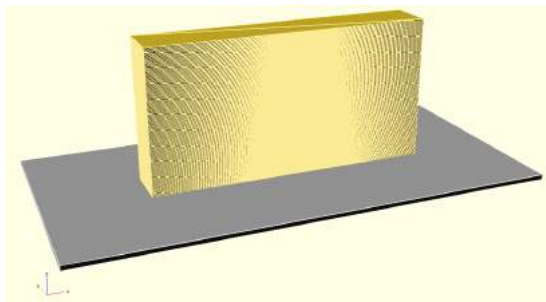
CAD software, some CAD libraries provide an alternative of drawing the 2D CAD file (format DXF) of each layer. For example, *dxfwrite* is a Python library to create DXF R12 drawing. This tool facilitates the automatic CAD drawing of each layer. It is almost impossible to draw manually one layer by one layer since enormous layers and their path lines are generated in additive manufacturing.

The information included in G-code file isn't sufficient to reconstruct the line path in one layer, thus inverse boolean operations opposite to path generator should be executed. The CAD redrawing by *dxfwrite* library combines with a series of boolean operations by *Clipper* library. When the material deposition path is extracted from G-code file by python scripts, the path vectors composing WALL-OUTER type path will first be connected into a closed curve. Then this curve will be offset by the radius of material deposit. The new curve is exactly the polygon of one layer obtained in the slicer. We repeat the similar offset operation for the WALL-INNER path vectors and then these curves will enclose the polygon to infill which can be extracted after subtraction using *Clipper*. The internal polygon then will be hollowed by a rectangle enveloping one path vector. After subtracting the rectangle in the internal polygon, a new rectangle enveloping path vector is eliminated from the new internal polygon using *Clipper*. Repeating this operation, the one layer polygon partition is created while multi-tracks are redrawn on this polygon. Note that there are gaps between tracks in CAD drawing, like the real situation of AM process. In fact, the *Clipper* library represents coordinates as integers by default. Even though conversion between float and integer can be partially solved by scaling function in *Clipper*, the error of number type conversion is hardly avoided. This numerical error coincides exactly with the gaps in AM deposition process.

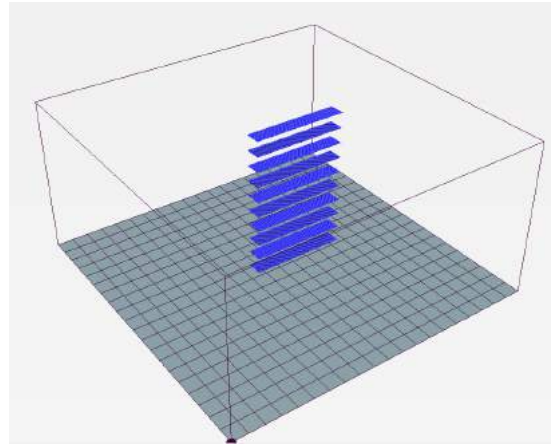
After obtaining the 2D DXF files of numerous layers, the 3D geometrical model of the whole workpiece will be reconstructed by extruding the 2D drawing and stacking assembly. This task is automatically completed by script in Figure 3.2.1. Here we use OpenSCAD, a free 3D CAD software based on constructive solid geometry (CSG), in which all the operation can be executed by a script. The new 3D geometry model file then can be imported into FEM software for further AM simulation.

#### **3.2.2 Reconstruction of 3D model at layer size: offsetting and clipping**

In CuraEngine, a part's geometry file in format STL is converted into CAM file which is compatible with AM machine's hardware. Most of the current software bonded with AM machine adopt some geometry algorithms [DIN 16a] [DIN 14] to offer pre-processing tool for users, especially the generation of scan path. In terms of workflow, the 3D model reconstruction that we conduct is actually the inverse operation in contrast with these software. Thus we used the same algorithms in this task: offsetting and clipping. The basic idea of them is illustrated in Figure 3.6 and Figure 3.7



(a) A thin-wall consist of 100 layers (in OpenSCAD)



(b) 10 layers of scan path after slicing

**Figure 3.5:** Reconstruction of a 3D thin-wall structure

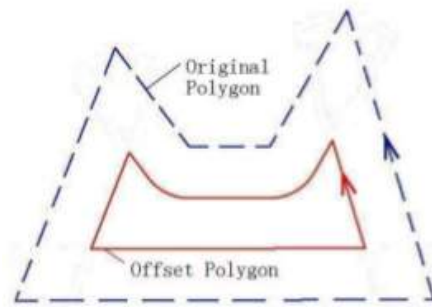


**Figure 3.6:** Inner offsetting of a polygon[CHÉ 05]

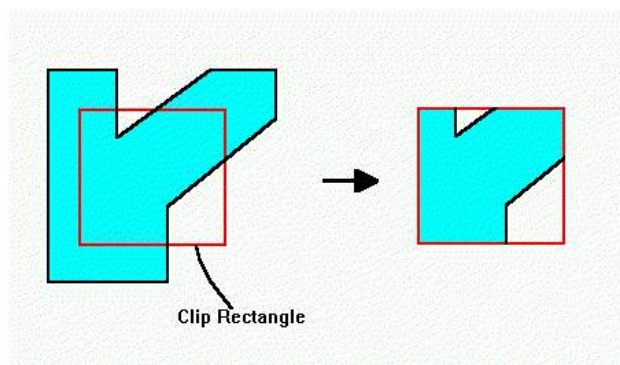


**Figure 3.7:** Clipping for a rectangle[HSI 95]

### Polygon-Offsetting

Polygon-offsetting is one of the fundamental problems in CAD/CAM for additive manufacturing. 3D model is first sliced into a set of 2D contours. For each layer, the contours are offset to construct the nozzle deposition or laser scanning path, especially the path along the external or internal perimeters [YAN 02]. In CuraEngine software, the direction parallel path generation strategy is applied. The path generated by this approach includes the parallel line segments inside and the offset boundaries lines. Both of two type lines are equidistant and the distance is the radius of material deposit in AM systems.

In a polygon generated by AM slicer, the algorithm for construct inner offset curve for the polygon can be resumed as follow [CHE 05]. Each edge is offset opposite to its normal direction while the offset segments keep the same orientation (clockwise/counter-clockwise) as their original edges. Then we connect the endpoints of two offset edges directly or indirectly depending on whether the vertex shared by their two original edges is concave or convex. Then a special number called winding number will be calculated for each region formed by this offset curve. Regions with positive winding numbers mean the interior area of the inner offset polygon, thus the boundary of their union is the inner offset polygon. The algorithm to construct offset curve for the outer offset polygon is similar to that for the inner offset polygon, only with small modifications.

In AM path generation, polygon-offsetting algorithm is mainly used for contour parallel spiral infill strategy, and partially used for the perimeter wall in parallel line-segments infill strategy.

#### **Polygon-Clipping**

Mathematically, to clip one set against another means to find their intersection. The subject polygons are clipped based on the window (clip polygon). Then the portion which is inside the window is kept as it is, while the outside portions are clipped. Polygon-clipping algorithm is important in computer graphics and it is widely applied for 2D boolean operations of complex geometry in CAD/CAM.

There are already several well-known polygon-clipping algorithms. CuraEngine uses the Vatti polygon clipping algorithm [VAT 92] [AGO 05] and one of its open-source libraries called Clipper. In the procedure of AM path generation, lots of boolean operations is based on this algorithm. For instance, parallel line-segments infill strategy can be simplified as the clipping operation. A large polygon filled with parallel lines is placed under one polygon generated by the slicer. The parallel lines in the underlying polygon then will be trimmed by the edges of the polygon above. Finally, the trimmed lines-segments can be organized by the connection of vectors, which will be translated into the G-code file for CAM.

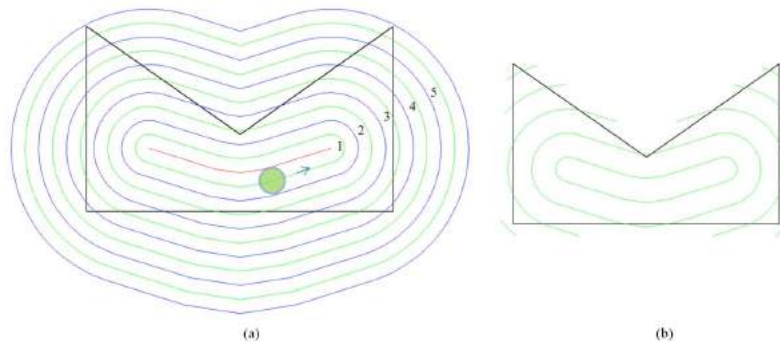


**Figure 3.8:** Generation scan path in one layer, (a) is the background paths before clipping (b) is the final path [DIN 15a]

The basic procedures of scan path generation in Figure 3.8 are helpful to understand our inverse manipulation in this reconstruction of one layer. In the algorithm shown in Figure 3.8(a), the medial axis transformation (MAT) is first generated in this polygon. Then the scan paths are generated by recursively offsetting contour-clockwise and clockwise around MAT. Inward and outward offset compose background loops larger than the contour of original polygon after iterative procedures. Finally, only the paths in the area of original polygon's boundary are retained after clipping. This set of trimmed paths (Figure 3.8(b)) become a set of scan paths for a layer in additive manufacturing.

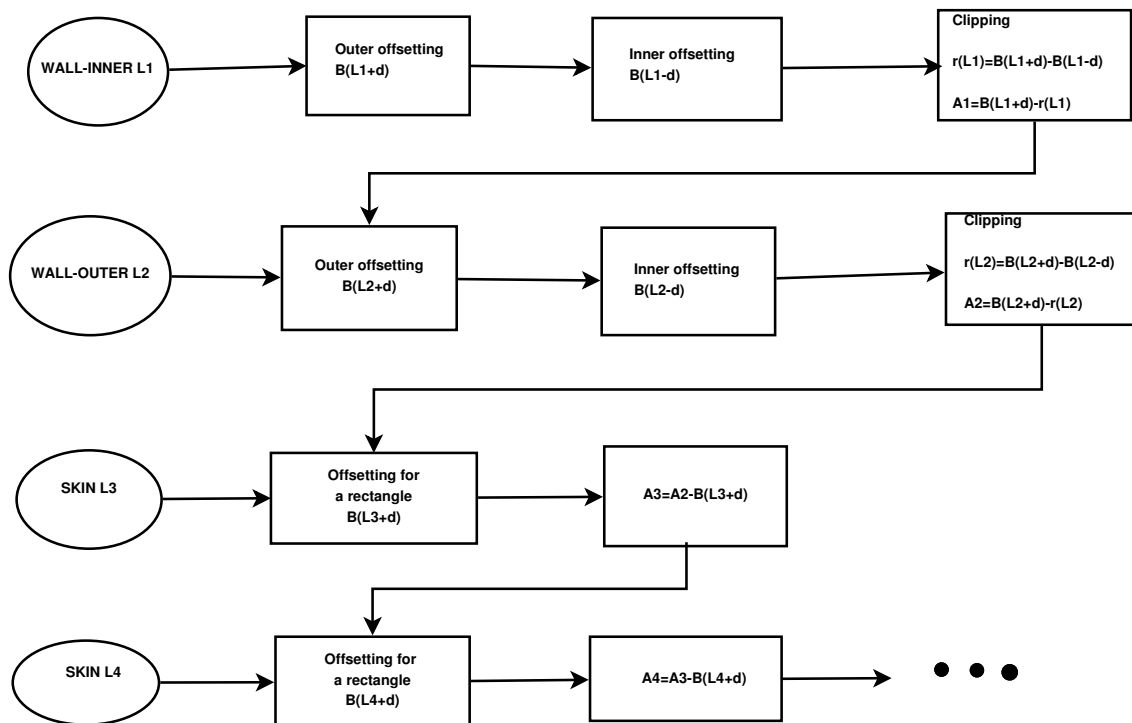


**Figure 3.9:** Flowchart for partitions in one layer, opposite to slicer's manipulation

### 3. Macroscopic AM simulation for multiphysics fields

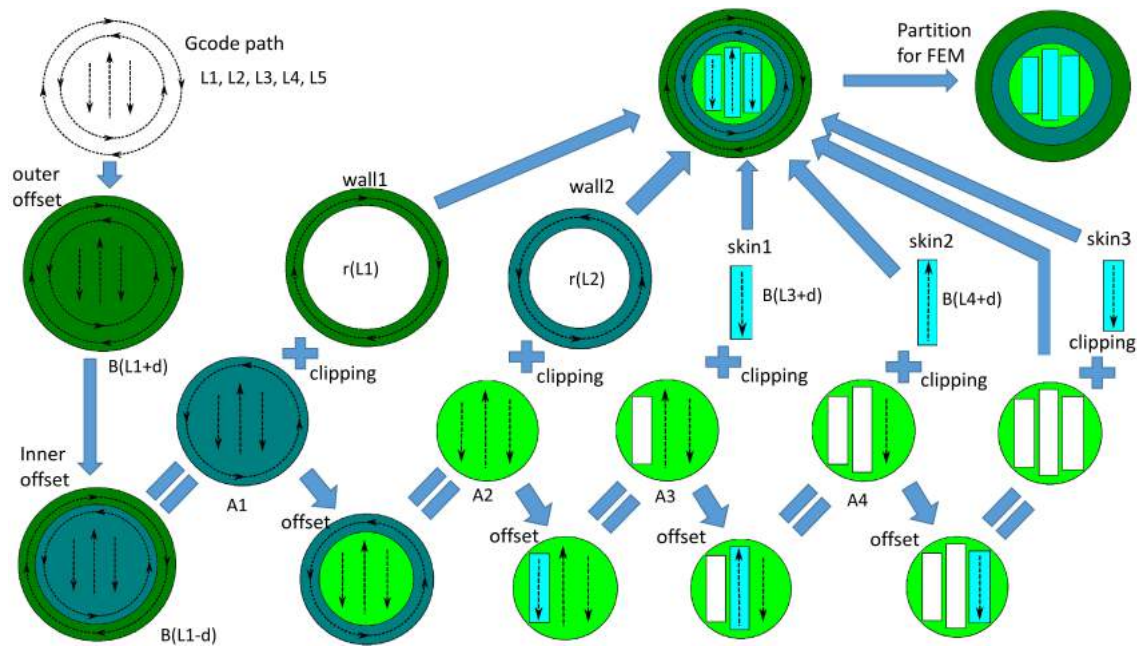


**Figure 3.10:** Generation of the partition for FEM simulation from gcode scan paths

Our algorithm of reconstruction is illustrated in Figure 3.9 and Figure 3.10. In the beginning, we have only a scan path G-code file for one layer, which consists of 3 segments and 2 closed circles. This information can't be imported into FEM software as a normal CAD model.  $L1$  and  $L2$  are two closed polygons representing the WALL-type scan paths.  $L3$ ,  $L4$ , and  $L5$  are three vectors representing the SKIN-type scan paths. We assume that the width of material deposition equals  $2d$ .  $B(L1 + d)$  is the area inside the boundary of polygon ( $L1$ ) after outer offsetting.  $B(L3 + d)$  is the rectangle around the vector  $L3$ , generated by inner and outer offsetting.  $r(L1) = B(L1 + d) - B(L1 - d)$  is the ring around the polygon  $L1$ .  $A1 = B(L1 + d) - r(L1)$  is the rest area after the first clipping manipulation. By a series of Boolean operation of geometry like this, the partition of one layer can be accomplished. The real G-code file is usually more complex than the example in these illustrations above, but the principle of its partition will be similar.

In this thesis, we take the layers in a thin-wall structure as an example. The scan path of a layer (Figure 3.2.2(a)) is reconstructed into a 2D CAD file (Figure 3.2.2(b)), in which the partition of this layer consists of all its tracks. Then we can import this 2D CAD file into some CAD software or the CAD module of FEM software. When this 2D CAD is extruded by the thickness of one layer, the 3D layer which generates G-code will be recreated and added with path scan partition (see 3.2.2(c)). Then we can generate the mesh (see 3.2.2(d)) of this layer's 3D model. These procedures are essential for the AM simulation at layer-level if we want to combine the real scan strategy with FEM's birth and death technique.



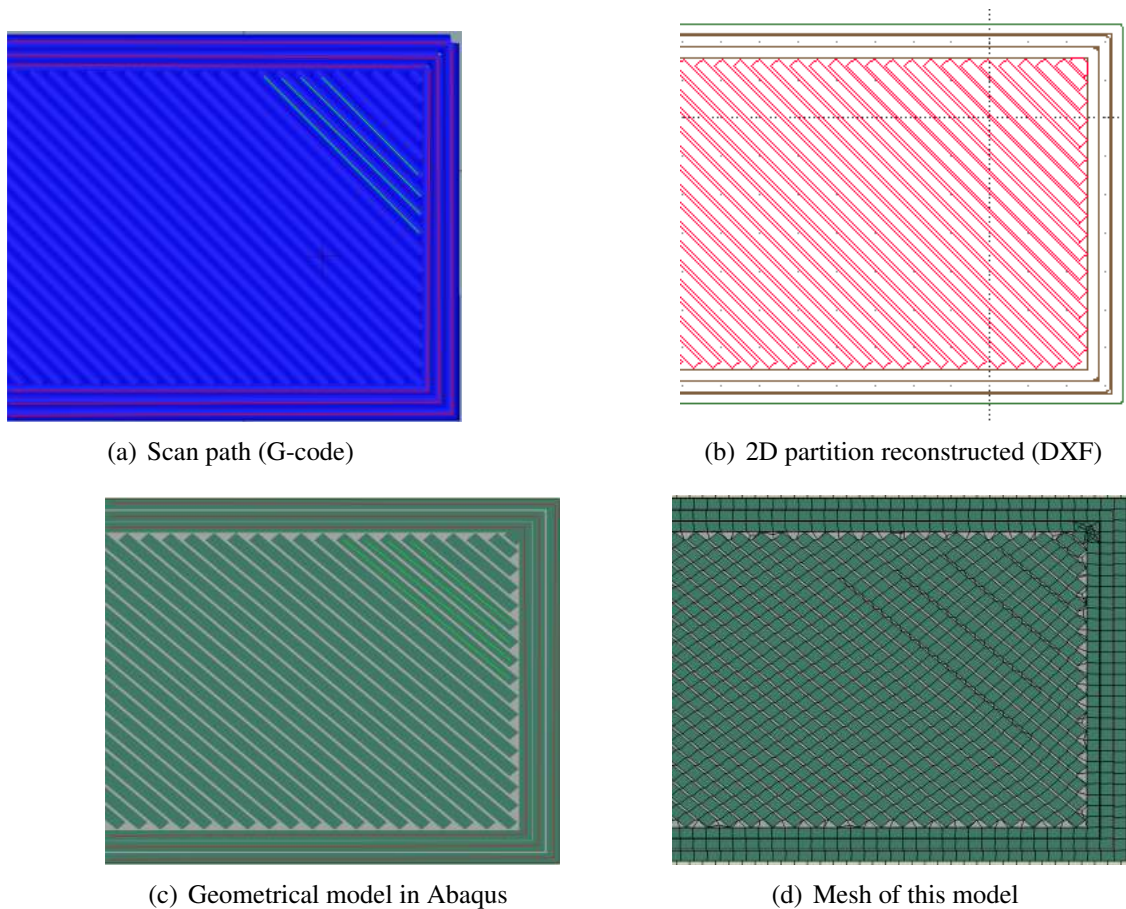


**Figure 3.11:** Detailed view of one layer in a thin wall during the pre-process

### 3.2.3 Map of sets in orphan FEM mesh and in CAD geometry

There are also some problems concerning mesh generation in the pre-process of AM simulation. In the following FEM simulation, a hatch of material deposit, usually called *ElementSet*, should be defined as a set of elements which locate inside the bounding volume of this hatch. Nevertheless, connecting the geometry volumes in CAD systems with element sets in mesh generator isn't straightforward. Boundary representation (B-rep) is ubiquitous in the geometric modelling of 3D CAD systems, such as the solid modelling kernel ACIS. Boundary representation is an essential representation methodology. B-rep representation connects faces, edges and vertices and it organises these shapes into logical units called geometric features. In CAD system, the main topological items (faces, edges and vertices) is different from that in an orphan mesh generated by some FEM software (in which only information about nodes, elements and their connectivity are included), even though they may be two descriptions for the same object [MA 01b].

In our pre-process of AM simulation on software ABAQUS, the geometry file (in STEP format) for the whole part and the geometry files (DXF file) for each layer are im-



ported. The part's geometry is separated into layers. 3D Partition operation is completed for each layer with extrusion of 2D path CAD drawing (see Figure 3.5). Mesh is generated respectively in each layer. The ElementSets of material deposit hatch line can be defined easily in one layer part. Then the meshes of numerous layer parts are assembled into the orphan mesh of the whole workpiece.

However, the definition of ElementSet in each layer part can't be retained in this orphan mesh. This problem makes it impossible to use orphan mesh in AM process simulation where the elements in one hatch line should be activated progressively one ElementSet by one ElementSet. In conclusion, it is a problem caused by the difference between a geometric set in CAD system and its corresponding ElementSet in FEM system. In Figure 3.12, an ElementSet (elements in red) in the 2nd layer is defined before assembly, but its definition disappears in the assembled orphan mesh. We need to re-establish the link of the same ElementSet in different reference frames.

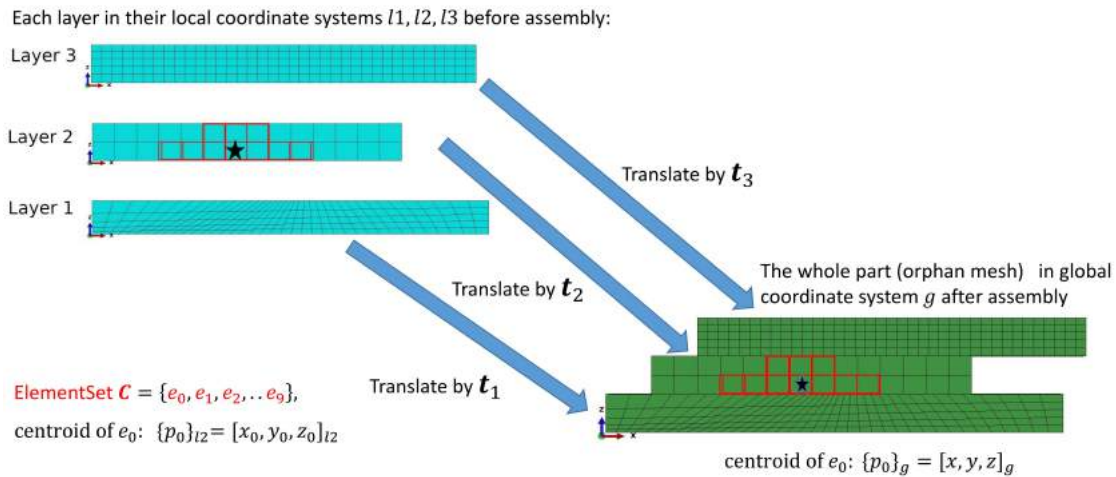


**Figure 3.12:** Loss of ElementSet definition during assembly between different coordinates

In order to solve this information loss problem during assembly, we use a database for each element at the cost of data store space. As the total element quantity is probably considerable for one workpiece, this data library should be established in a specific data format. In our study, Structured Query Language (SQL) is used for this objective. An SQLite library integrating SQL with python is an useful tool under ABAQUS python environment (see Appendix B).

In fact, the geometry of an element doesn't deform after the assembly. Only its attachment to its ElementSet is lost in the orphan mesh. As the orphan mesh is assembled by stacking of layers, one layer's position in CAD system is translated regularly from the layer's position in FEM system by a certain distance in Z direction. The element label in form of integer number has already changed from local layer reference frame to global

workpiece reference frame. But if we calculate the coordinates of an element barycentre before and after assembly, the two positions of barycentre can be linked by a translation. This property makes the coordinates of element barycentre an ideal identified label for elements.

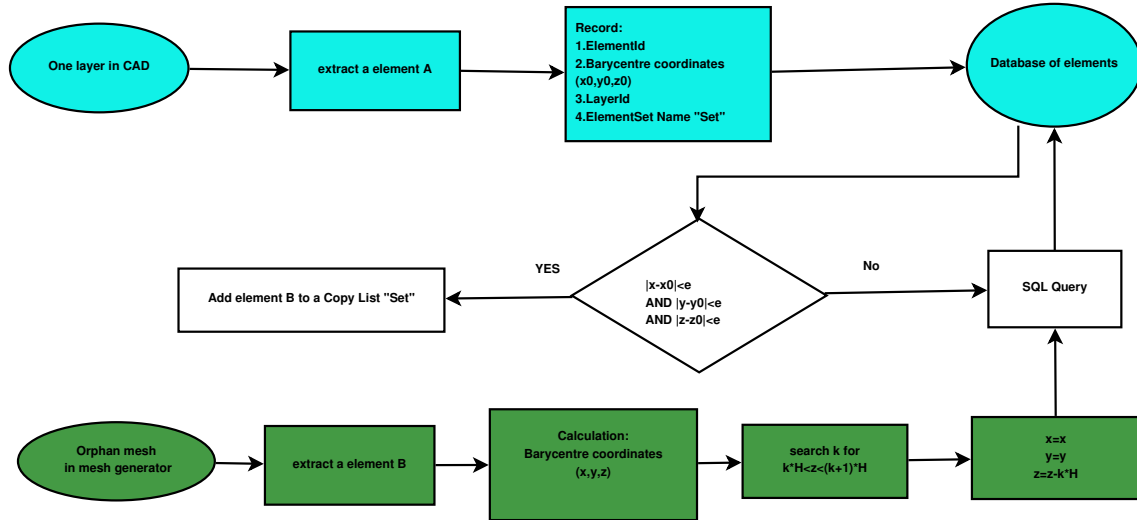


**Figure 3.13:** Flowchart of the algorithm to map ElementSet between two coordinates

Our algorithm for this problem is shown in Figure 3.13. First, in the local layer reference frame, we calculate the barycentre of each element in one layer and record these information below: barycentre coordinates, element ID, the label of the layer to which this element belongs, the label of element set which encloses this element. The database SQL works like an Excel file but with higher performance. This input manipulation is respectively accomplished for every layer.

We can take a simple example in Figure 3.12. Before the assembly, meshes are generated respectively in three layers with their local coordinate systems ( $l_1, l_2, l_3$ ). These meshes are incompatible to each other in three layers. An elementSet  $C = e_0, e_1, e_2, \dots, e_9$  is defined as a material chunk which includes 10 elements. The element  $e_0$  (element with star) belongs to ElementSet  $C$ , and ElementSet  $C$  belongs to the 2th layer. In AM simulation using birth and death technique, the elements in  $C$  will become activated/deactivated at the same time. Before the assembly, the relation  $e_0 \in C$  is known.

There is a bijection  $e_0 \leftrightarrow p_0$  between the element  $e_0$  and its centroid  $p_0 =$ . This centroid under coordinates system  $l_2$  is expressed as

$$\{p_0\}_{l_2} = [x_0, y_0, z_0]_{l_2} \tag{3.1}$$

Then the three layers are assembled into a whole part after three translation  $\mathbf{t}_1, \mathbf{t}_2, \mathbf{t}_3$  for each layer. In the global reference frame of a workpiece  $g$ , an orphan mesh represents the workpiece part assembled from layer parts. For an element in orphan mesh, its centroid's

coordinates is recalculated. As the thickness of each layer is known as  $H$ , it is easy to acquire the translation distance  $k * H$  of each layer in  $Z$  direction during stacking assembly. So we can assume the translating vector  $\mathbf{t}_2$  under global reference frame  $g$  as:

$$\mathbf{t}_2 = [t_x, t_y, 2H]_g \quad (3.2)$$

With the help of translating vector  $\mathbf{t}_2$  of each layer, we can query the bijection relation of an element between its old coordinate  $[x_0, y_0, z_0]_{l2}$  and new coordinates  $[x, y, z]_g$  in the database. This coordinates transformation is simply expressed as:

$$[x, y, z]_g = [t_x, t_y, 2H]_g + [x_0, y_0, z_0]_{l2} \quad (3.3)$$

If we find an element whose centroid is  $[x, y, z]_g$ , we can conclude naturally that it is used to be the element  $e_0$  before the assembly and it belongs to the ElementSet  $C$ . Now the elements in  $C$  are refound in the global reference frame  $g$ .

Correspondingly, the ElementSet can be re-defined in the orphan mesh. Although our algorithm is conducted in CAD module and Mesh module of ABAQUS, it can be extended to similar problems between different CAD software and mesh generators in additive manufacturing.

#### 3.2.4 Reconstruction of 3D model at part size: voxelization

Voxel representation is a method for 3D modelling of a geometric object. Most of the geometric models obtained by CAD drawing are generally represented in continuous form. This model can be converted into a set of voxels as an approximation. Voxel models are very effective and flexible in representing interior details of complex geometric object, such as the medical or biological morphology in surgery simulation and implant design. In fact, the 3D geometric model fabricated by AM technologies is initially represented in an STL file, a set of continuous tessellated triangular facets. The FEM simulations for AM process with traditional geometry models are usually restricted by their complicated geometries. Especially in mesh generation, conventional mesh generation technique often needs delicate operations such as partition of a part, define seed along an edge, etc. For the AM simulation at the scale of the whole part, voxelization is one of the suitable tools with more flexibilities, as it is insensitive to the object's geometric complexity.

Voxelization has already become a mature technique of computer graphics, mainly in volume rendering scene of PC games (ex. Minecraft) and rendering medical imaging of tomography. Some voxelization tools provide us with the possibility of conversion STL file into voxel files. For example, the geometry processing library PyMesh, voxel editor Qubicle, and voxelizer program binvox [NOO 03]. In our study, we use binvox as a FEM mesh generator and then slice the 3D voxel mesh with python scripts. During this pre-processing, we should configure an appropriate resolution to achieve a compromise between the discretization error of modelling and the cost of memory.

Although the voxelization algorithm of AM workpiece is different from most of FEM mesh generator software, it can be simply explained as judging a point whether locates

inside or outside of a given 3D volume. The basic scheme of voxelization is illustrated in Figure 3.17(b). Each facet in STL file stores the coordinate values of its three vertices and an outward normal vector. First, the box bounding space around the complex B-Rep geometry (in STL format) will be filled with regularly voxel grid. Voxels of this background grid are partially enclosed in the B-Rep manifold geometry and they can be classified into two groups according to the parity count method. The voxelisation is often based on ray-tracing algorithm [BEC 16] [SIS 02]. When a ray is emitted from the centre of a voxel, we count the number of times that this ray intersects B-Rep manifold geometry. An even number of intersection means the voxel is exterior to B-Rep manifold geometry while an odd number indicates that the voxel is inside. After the classification by ray-tracing, the geometry of STL will approximatively become a collection of voxels, which can be used as the mesh for FEM simulation.

For the implementation of voxelization, We use the code *binvox*, a tool in computer graphics[NOO 03]. The scheme of file voxel is shown in Figure 3.14.



**Figure 3.14:** File format conversion in voxelization

In this thesis, we used an example of a turbine blade (see Figure 3.15) to test the feasibility of combining voxelization with the pre-processing of AM simulations. The voxelization can be also considered as a special method for mesh generation. The coordinates of each node are known in voxelized mesh, and it is relatively easy to create partitions (ElementSet) of this blade using the bounding box method. This is convenient for AM simulation at part-level.

For the 3D model of this blade, its geometry is twisted along the vertical direction with variable airfoil section, which makes it much more complex than the normal wall structure in AM simulation. It is not easy for traditional mesh generation technique to create a mesh of blade with layer partitions. Here we apply the voxelization technique with 44107 small voxels. The size of each voxel cube is  $1.333\text{mm} \times 1.333\text{mm} \times 1.333\text{mm}$ .

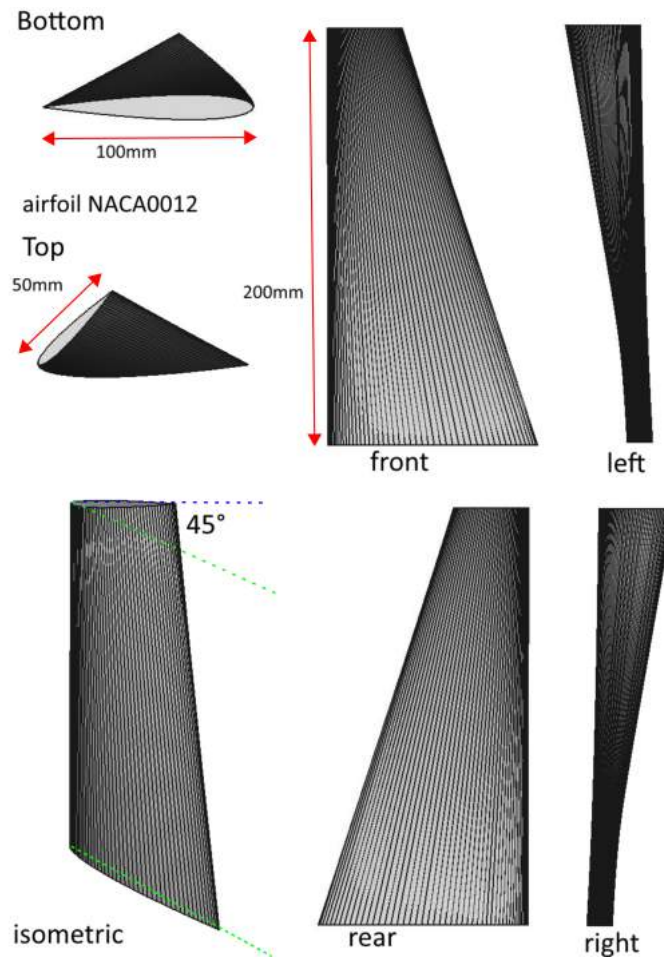


**Figure 3.15:** 3D model of a turbine blade with a twist in vertical direction

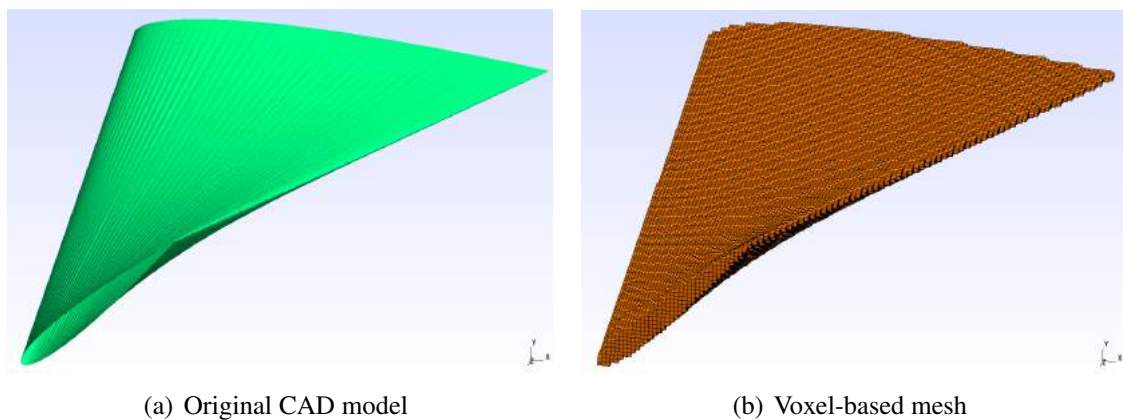


**Figure 3.16:** Approximation of a blade by voxelization (length of voxel is 1.333mm)

In Figure 3.17, it is obvious that the geometrical approximation of an object relies on

the background grid resolution in voxelization. Voxelization with high resolution requires a considerable computational resource, but some techniques in computer graphics, such as depth buffer technique [KAR 99], have already been applied to accelerate voxelization.

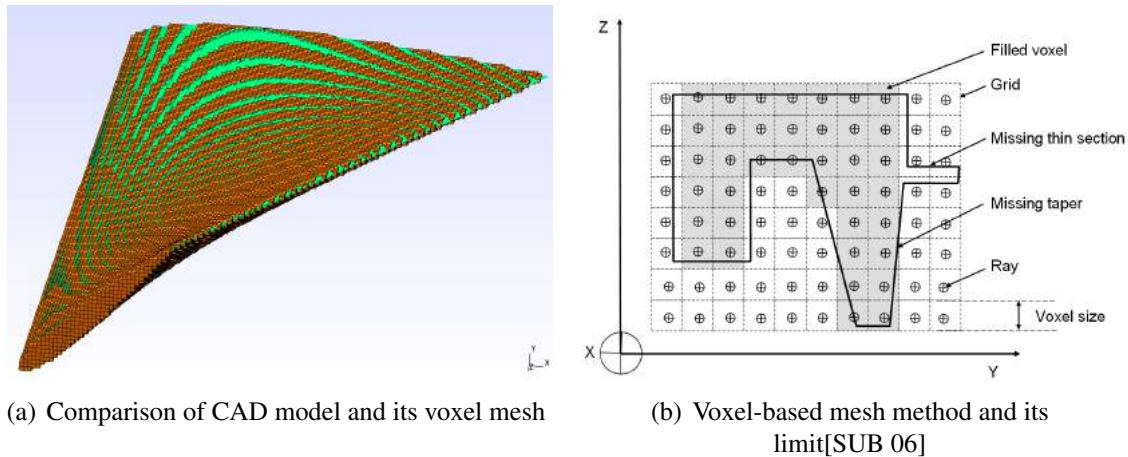


**Figure 3.17:** Geometrical approximation of voxelization

In this thesis, we use this voxel mesh for the AM simulation of this turbine blade, while the compromise of geometry similarity, licenses limit of Abaqus2017 and calculation efficiency is taken into consideration. In fact, the resolution of mesh can be increased if the calculation resource is abundant, thus voxelization technique is a useful tool for the pre-process of complex geometry part in AM simulation

### 3.3 FEM simulation for multi-physics fields

Calculating of new free surfaces is often memory-consuming, since an element's neighbour elements should be searched before indicating the exposed elementFace Id number. For researchers and engineers using a FEM software, this search algorithm is challenging because of the lack of access to software's internal framework. The ABAQUS Welding Interface (AWI) is a plug-in defining automatically the welding passes and generating multiple analysis steps in ABAQUS. By analogy with welding, we attempt to use this plugin for AM simulation in ABAQUS 6.14.

However, there are still some difficulties for mesh partitioning with AWI plug-in. The AWI plug-in only supports the definition of element set and surface set in a substrate which is a boundary representation (B-rep) geometry instead of an orphan mesh. If the model imported into ABAQUS is an orphan mesh without B-rep information, there isn't suitable object-oriented python functions for partition in ABAQUS. Due to these limitations, the AWI plug-in can hardly be applied directly to our AM simulation in the pre-processing aspect. AWI plug-in's methodology is still helpful for ABAQUS users to create their own scripts for AM simulation, though free surface's recognition isn't a problem any more when ABAQUS releases the 2017 version.



### 3. Macroscopic AM simulation for multiphysics fields

---

In our study, the additive manufacturing simulation involves coupled thermal-stress analysis. There are normally two kinds of implementation procedures in FEM software: Sequentially coupled analysis and fully coupled analysis. In coupled thermal-stress problems, the stress/displacement solution is dependent on the temperature field, but the inverse dependency may not be always considered in the simulation. In some cases, such as rapid metalworking or contact problems, the thermal field and mechanical field may affect each other. The Fully coupled thermal-stress analysis can be conducted for the case where the stress/displacement and the temperature fields need to be solved simultaneously. Nevertheless, the sequentially coupled thermal-stress analysis can be conducted if the impact of mechanical field on thermal field is negligible so that substantial computational resource will be saved. In the sequentially coupled thermal-stress analysis, the pure heat transfer problem is first solved, then the temperature result is imported into stress analysis as a predefined field. In our study, we adopt the sequentially coupled thermal-stress analysis in our AM simulation.

Special attention should be paid to some technical details of the AM simulation. The element sets are deactivated/activated successively simulating the process of material deposition[MIC 14]. This birth and death may lead to some divergence problems. In the stress procedure of a sequentially coupled thermal-stress analysis, the material is removed at the start of analysis and then deposited back. Its surrounding material may have displaced in the meantime. If the removed nodes are then replaced to their original position, the elements may be distorted. For AM simulation, we can take advantage of a particular hypothesis that the material deposit is a high temperature. The stiffness of this deposit will be low due to high temperature [SMI 12]. In this case, the material chunk isn't removed initially before its deposition. During the simulation of the deposition process, the material is first removed and then inserted back without stress or strain. The mechanical analysis steps created in this way helps the FEM calculation to avoid the divergence problem.

Another detail contributing to divergence is the heat flux load. In the real process of powder jetting based AM system, the material deposition occurs synchronously while the deposit is heated by heat source likes laser. Naturally, we define the activation of element set representing the new deposit and the load of external heat flux in the same thermal analysis step. The temperature ramped up during the whole time period of this thermal step. However, this definition of the thermal step in AM simulation often results in divergence. In practice, we can define respectively two thermal analysis step for simulating the process (see Figure 3.18). The periods of these two steps are obviously different. In the first period, we only define the activation of the material chunk in a very short period. It seems that the deposition happens instantaneously. In the second period, we only define the heating load on the material chunk which is already deposited in the first step. The second step will take a relatively long period equal to that of the real deposition process. This method can reduce the possibility of divergence in thermal analysis of AM simulation.

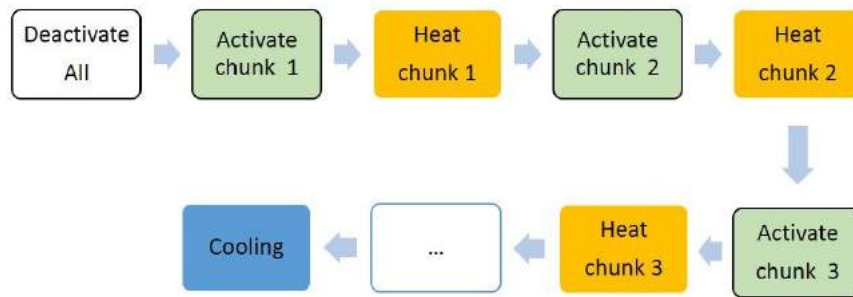


**Figure 3.18:** Basic steps of AM simulation using birth and death technique

In this thesis, we concentrate the macroscopic process in additive manufacturing, and our simulations are conducted at different levels, such as line-level, layer-level and part-level. All of these simulations are based on birth and death technique in Abaqus.

### 3.3.1 Thermal simulation at layer-level

In this simulation, we study the temperature evolution during the fabrication of 4 layers (see Figure 3.19). This is the beginning of a thin wall's manufacturing process (see Figure 3.5(a)). The objective of this simulation is the thermal field between neighbour layers, whose thickness is relatively much smaller than a part's global size. In this simulation, the heat transfer between tracks in neighbour layers can be observed. From the temperature field at layer-level, we can find some features in the vertical direction, from which we may profit as a simplification for a part-level simulation. In a part-level simulation, the detail deposition process in one layer should be neglected if it needs huge calculation resource. So the simulation at layer-level is implemented first in this thesis.

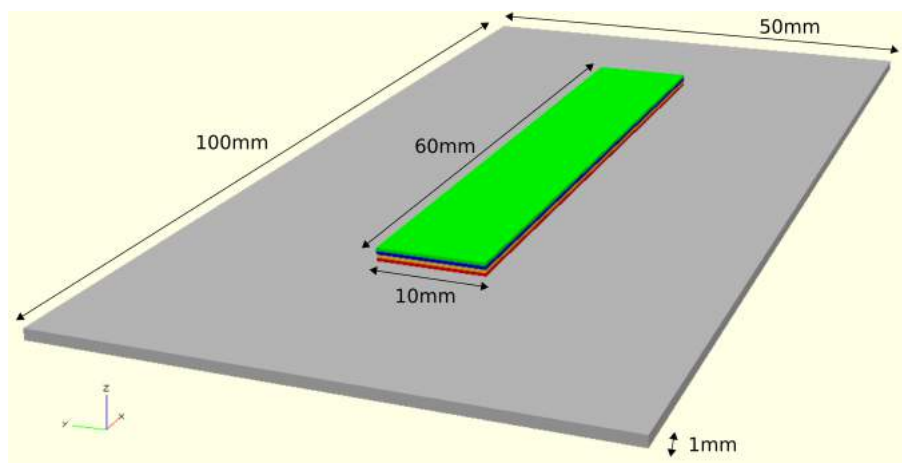


**Figure 3.19:** The first 4 layers of a wall structure (red, yellow, blue, green)

The thickness of each layer is 0.3mm. This 3D model's partition is reconstructed



### 3. Macroscopic AM simulation for multiphysics fields

---

based offsetting and clipping algorithm from G-code file. There are totally 546 lines in these 4 layers. The ElementSets of track lines are activated one by one to simulate the material deposition in a layer. The heat transfer between two layers is treated by predefined contact pairs because the meshes of neighbour layers don't conform to each other. Usually, the infill patterns of scan path are different between two neighbour layers.

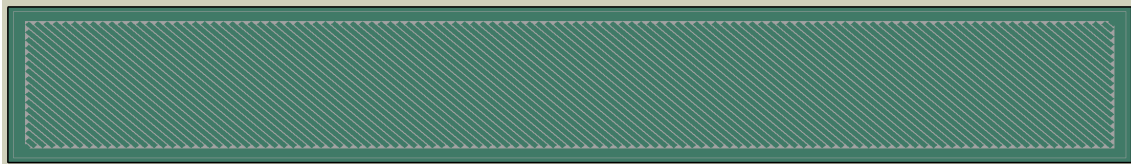


**Figure 3.20:** The scan path partition for the 4th layer

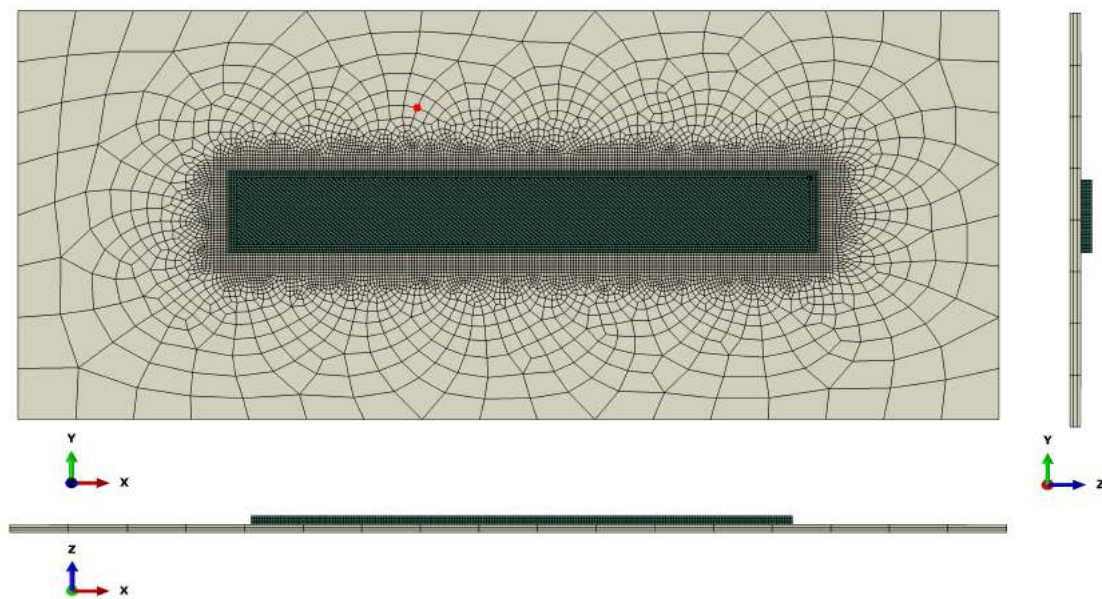
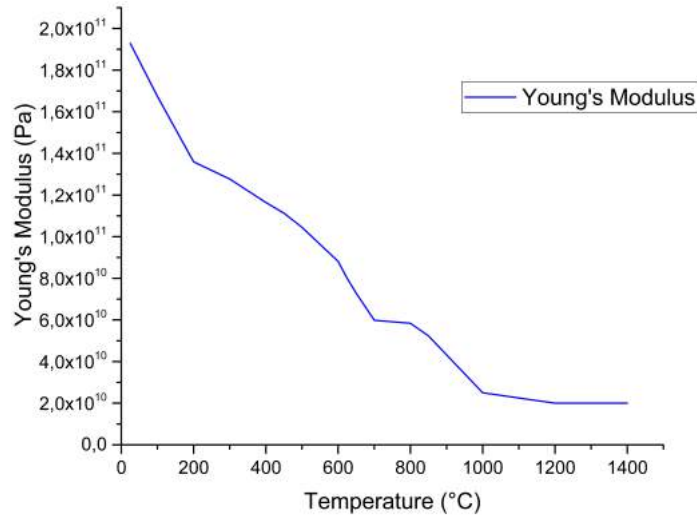


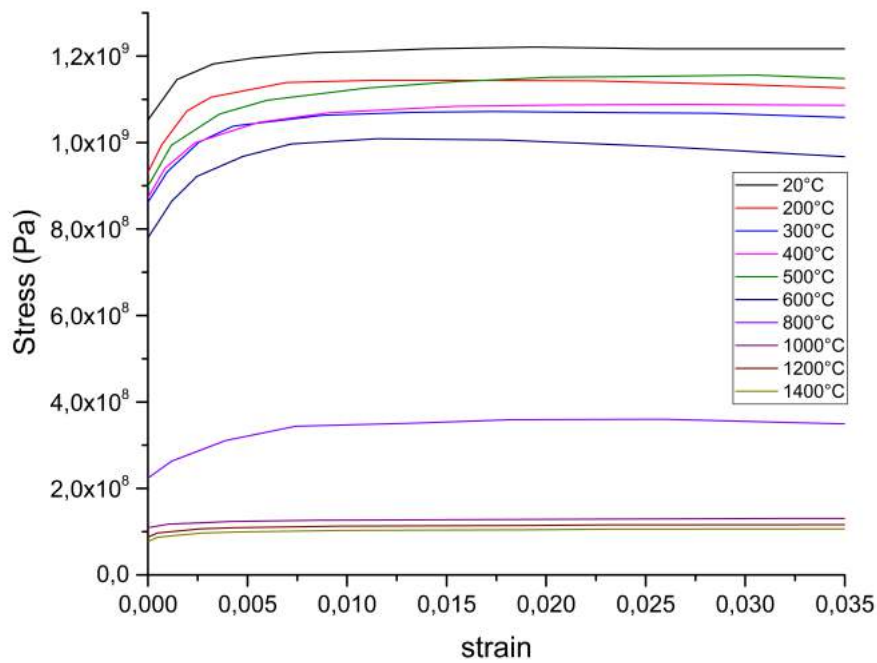
**Figure 3.21:** The mesh of 4 layers and their substrate.

The heating time for each material chunk depends on its length, which can be read from gcode file while we create the 3D partition. Mesh element type is DC3D6 and DC3D8. The activation time for each material chunk is  $1.0 \times 10^{-6}$ s. The preheat temperature  $T_{pre}$  for substrate and metal powder is  $240^\circ\text{C}$ . The volumic heat source's power is  $15000 \text{ mW}/\text{mm}^3$ .

For both the 4 layers and the substrate, the material which we used in this simulation is Maraging steel [VAN 13]. Its material property is shown in Table 3.2. Some of the mechanical properties are also shown in Figure 3.22:



(a) Young's Modulus



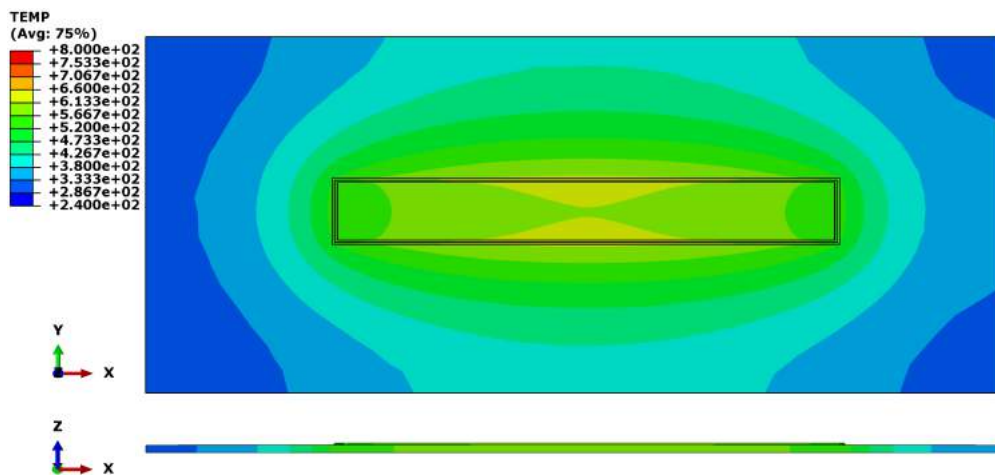
(b) Curve of  $\sigma - \epsilon^{plastic}$

**Figure 3.22:** Mechanical property of Maraging steel at different temperatures[VAN 13]

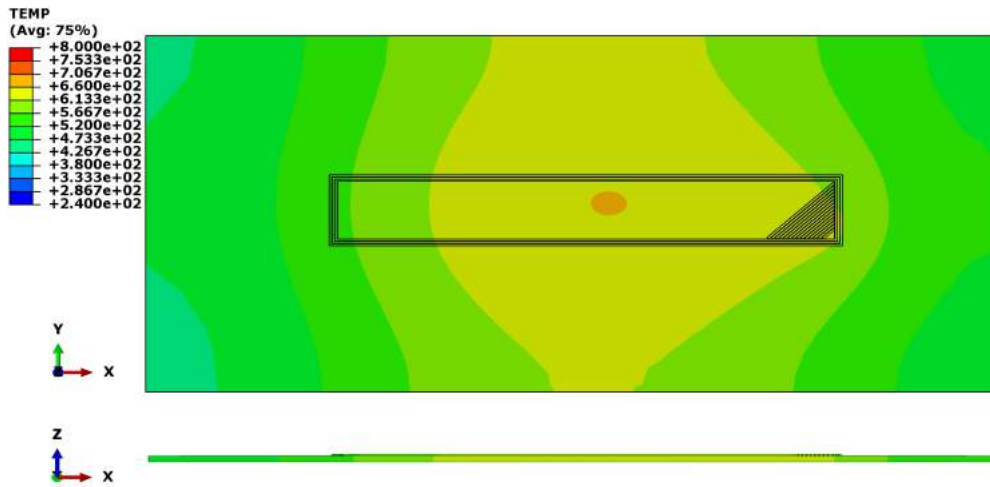
**Table 3.2:** Material property and process parameters in simulation

Parameter	Value
density $\rho$	$7.8 \times 10^{-9} \text{tonne/mm}^3$
poisson $\nu$	0.3
expansion coefficient $\alpha$	$1.6 \times 10^{-5} \text{K}^{-1}$
convection coefficient $h$	$0.001 \text{mW/mm}^2/\text{K}$
conductivity $C_d$	$48.0 \text{mW/mm/K}$
specific heat $C_p$	$4.5 \times 10^8 \text{mJ/ton/K}$
preheat temperature $T_{pre}$	$240^\circ\text{C}$
inert gas temperature $T_{atm}$	$40^\circ\text{C}$
radiation coefficient $\epsilon$	1.0
print scan speed $v$	$10 \text{mm/s}$
volumetric heat source $P_{input}$	$15000 \text{mW/mm}^3$

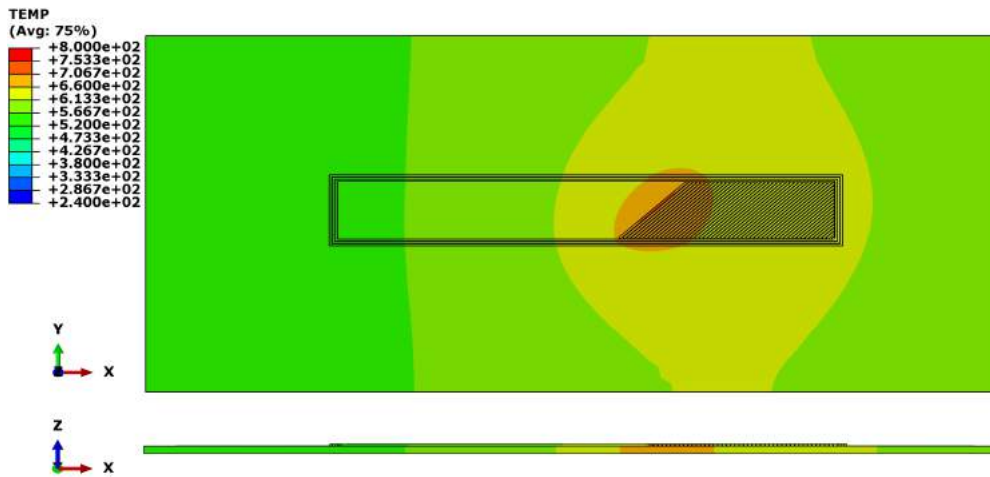
As a simulation of the AM process, the evolution of temperature distribution is investigated in Figure 3.23. This 3D model is observed from its top face xOy and its middle section face xOz. Here are some screenshots of AM thermal simulation for the whole process:



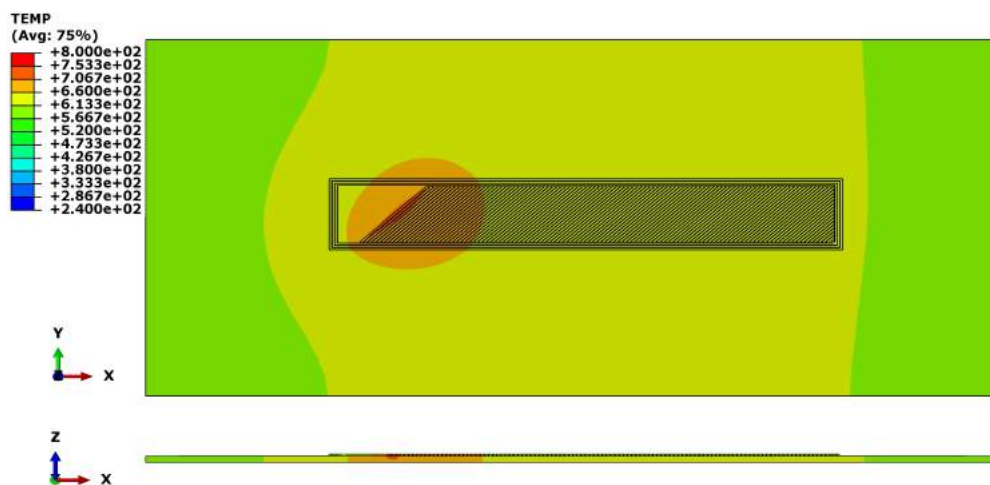
(a) 2nd line (in the 1st layer, WALL type)



(b) 17th line (in the 1st layer, SKIN type)



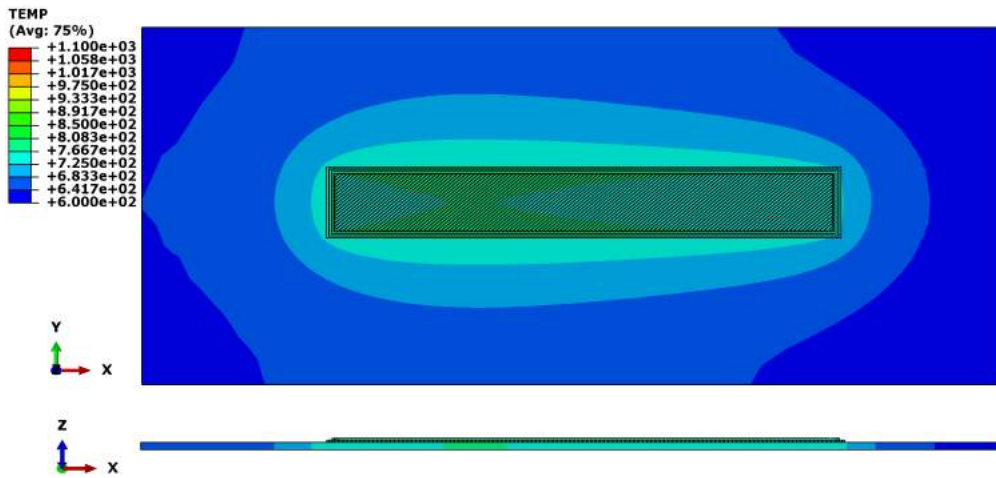
(c) 54th line (in the 1st layer, SKIN type)



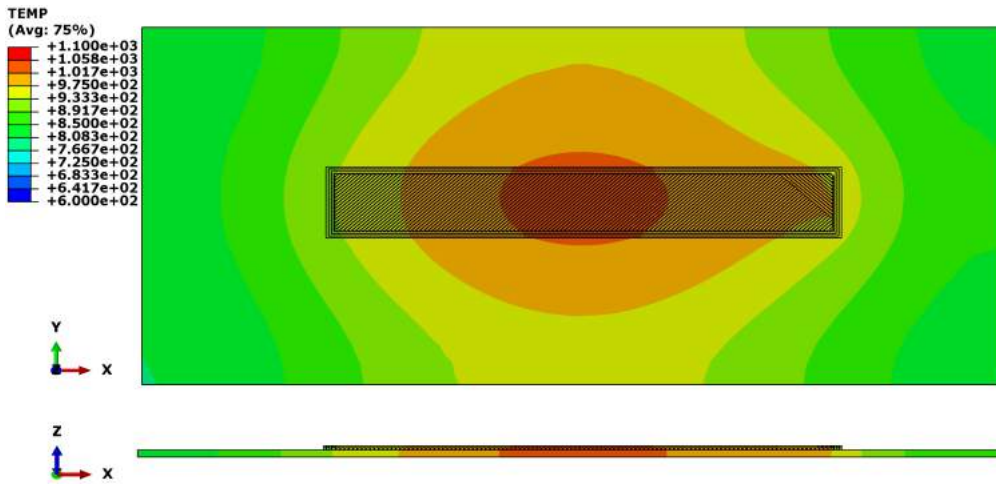
(d) 115th line (in the 1st layer, SKIN type)

### 3. Macroscopic AM simulation for multiphysics fields

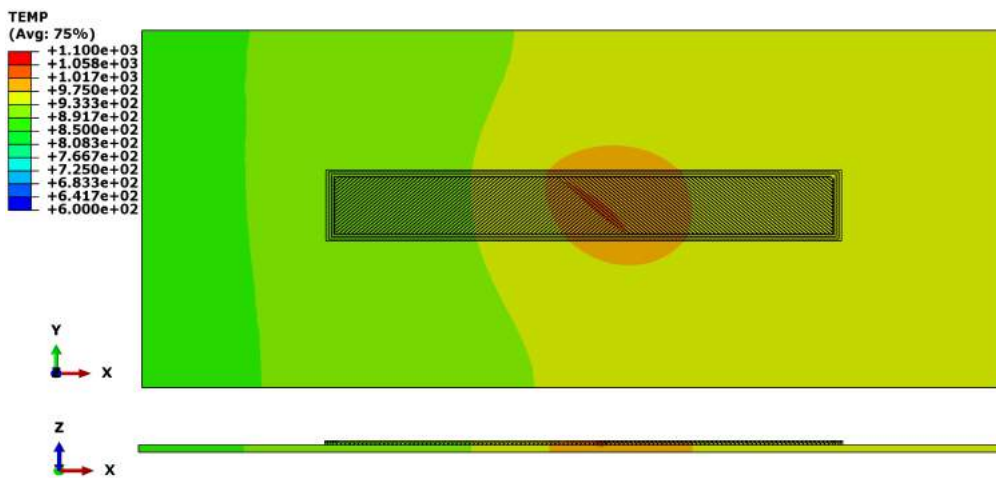
---



(e) 137th line (in the 2nd layer, WALL type)

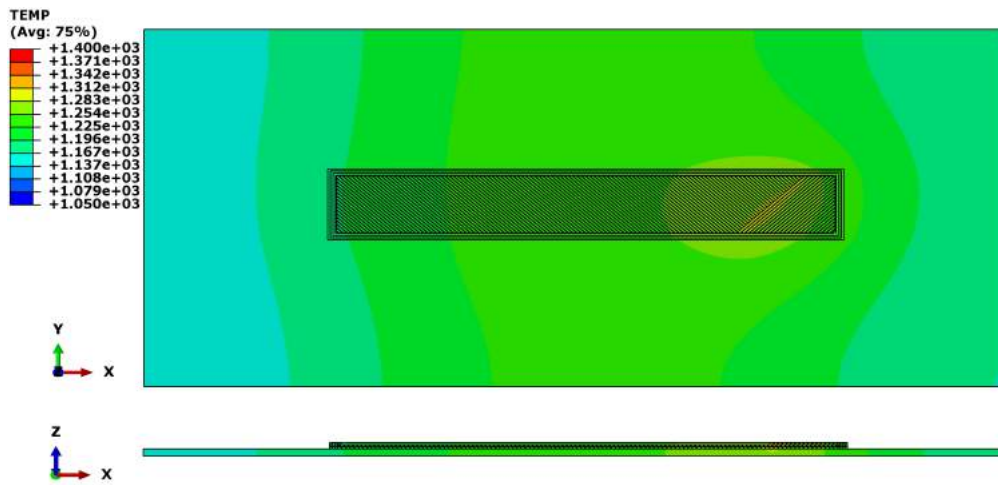


(f) 152th line (in the 2nd layer, SKIN type)

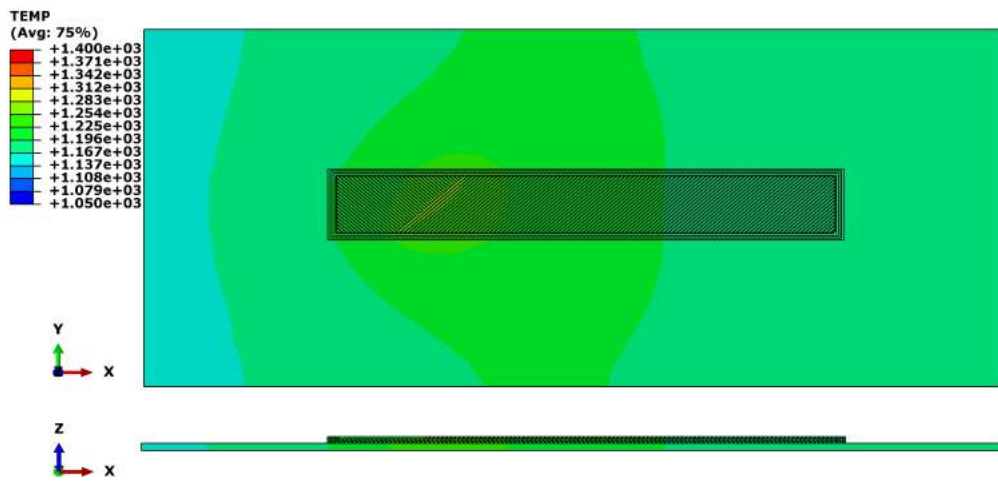


(g) 204th line (in the 2nd layer, SKIN type)

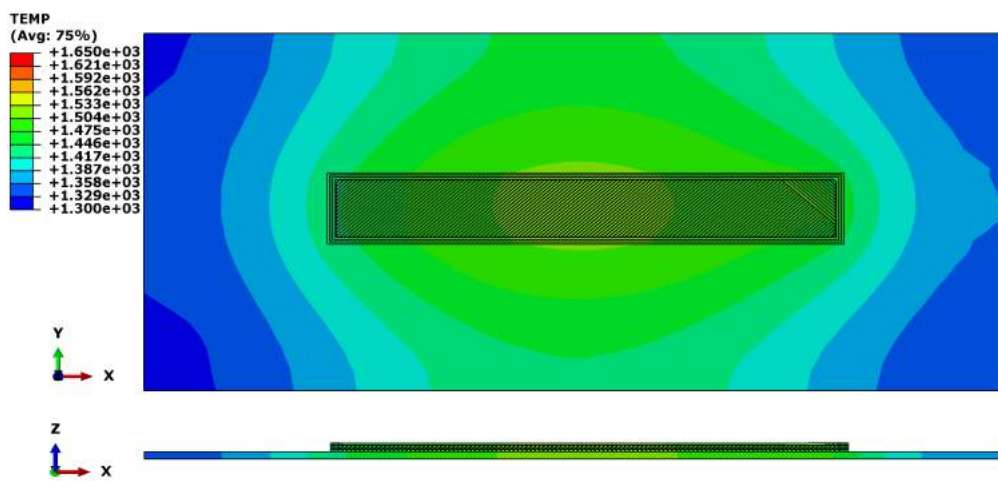




(h) 299th line (in the 3rd layer, SKIN type)

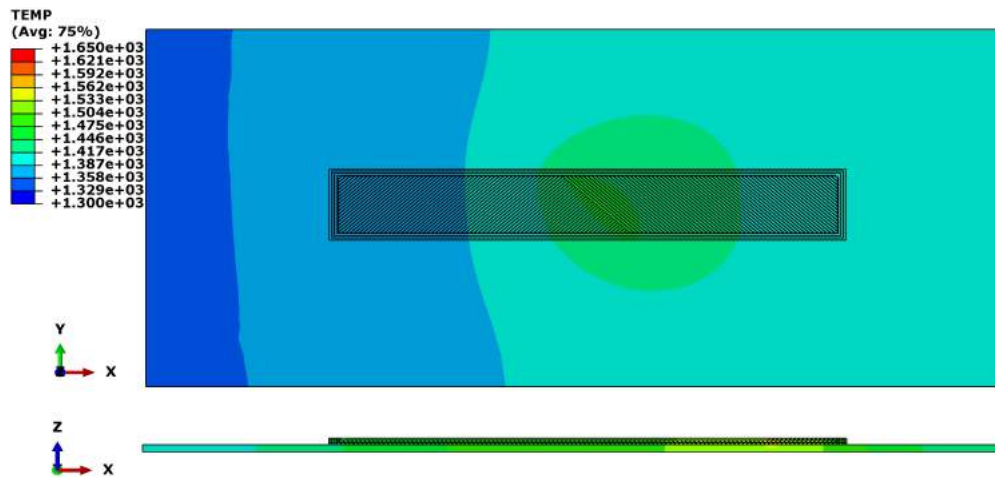


(i) 379th line (in the 3rd layer, SKIN type)

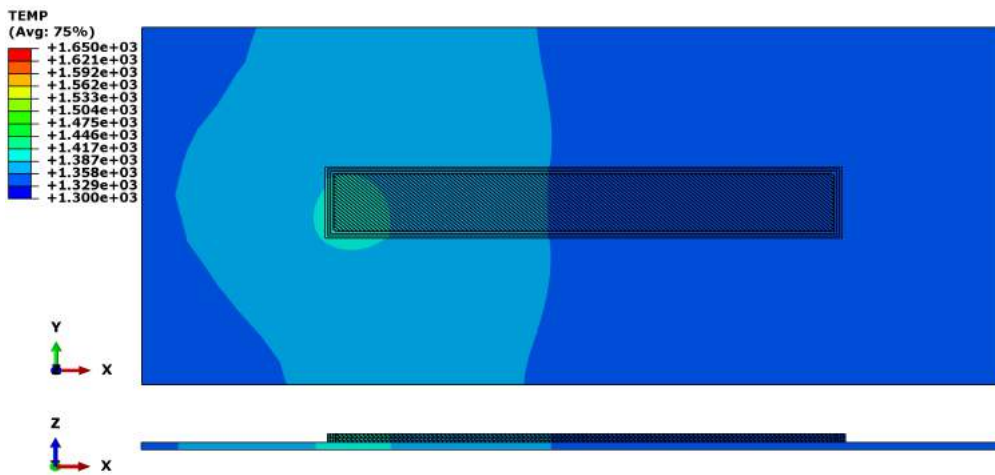


(j) 425th line (in the 4th layer, SKIN type)

### 3. Macroscopic AM simulation for multiphysics fields



(k) 477th line (in the 4th layer, SKIN type)



(l) 546th line (in the 4th layer, WALL type)

**Figure 3.23:** Screenshots of the AM deposition process (546 lines in total, 4 layers), the temperature unit is  $^{\circ}\text{C}$

We can observe the temperature distribution's evolution during the AM process. In a layer of thin wall structure, the WALL type scan paths around the surface is much longer than the SKIN type path. The heat of the WALL path has a larger influence area than the SKIN path. The radiation and convection occur on the surface while the heat source moves. The heat transfer leads to the evolution of thermal distribution. With the movement of heat source, the temperature gradient occurs obviously around the melting pool on the face  $xOy$ . However, the temperature gradient in vertical direction  $z$  is much smaller because of the small thickness of layers. The heat flux can easily transfer from the melting pool to its underlying neighbour layers.

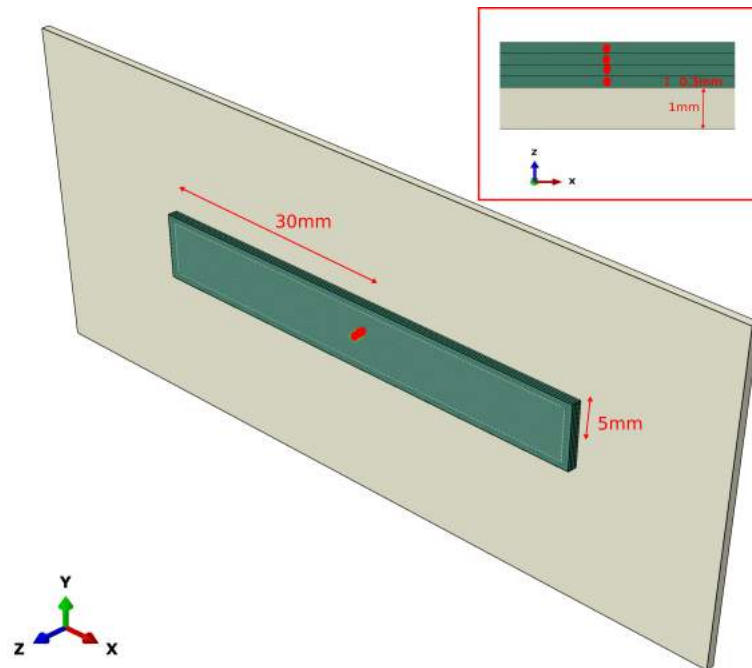


**Figure 3.24:** Position of 4 sensor points (yellow circles) in the centre of each layer

We can select the central points in 4 layers as 4 "sensor points" (see the 4 red circles in Figure 3.24), in order to record representatively the temperature evolution during the AM process. The evolution of the thermal field can be observed from the figure 3.25, the melting zone above will reheat the deposited zone below. Because of the layer's small thickness, the superposition of temperature curves demonstrates that the thermal transfer between two layers is quite fast, and the temperature gradient is negligible in the vertical direction if the thickness is small enough. In other words, the temperature of the 1st sensor point can be used to represent the 4th point's temperature evolution if the vertical distance is small enough (here is  $0.3\text{mm} \times 3$ ) between them.

This neighbourhood thermal behaviour of thin layers in AM process makes it possible to simplify the numerous thin layers of an AM object into several thicker layers. The AM object can be sliced into real deposition layers or simulation regrouped layers. Each group of thicker layers in AM simulation is composed of several layers in real AM process. This simplification is useful to realize a compromise between the precision and calculating speed in AM simulation. For an AM object, the simulation can be implemented at different levels according to the scale we want to observe. At the level of material line chunk, the detail of scan path in one layer can be simulated. However, for a simulation at part level, the scan strategy in one real AM layer will be neglected. Only the deposition of regrouped layers is simulated with larger thickness rather than every thin layer in the real AM process.



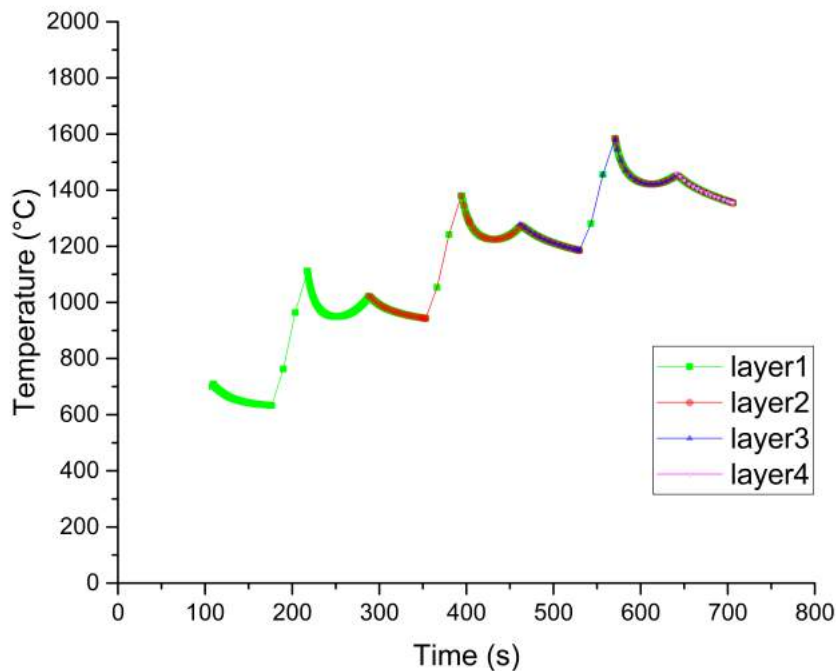


**Figure 3.25:** Temperature evolution at 4 sensor points

#### 3.3.2 Thermal-mechanical-metallurgical simulation at part-level

The macroscopic simulation at part-level is an important tool for AM technology, but it is rarely studied by academic researchers because of a real part's complex geometry. For further study on the residual stress or other problem of an AM part, we need to first construct a platform as a basic tool where the methodology of AM macroscopic FEM simulation is demonstrated.

The feasibility of voxel-based AM simulation is demonstrated in this work. This thermal simulation is conducted at part-level. We use the 3D geometry model of a turbine blade introduced in Figure 3.15 as a part constructed by AM technology. The deposition and heating processes are simulated to obtain first the thermal field, then the metallurgical field and mechanical field are sequentially calculated in Abaqus.

The mesh of this blade and its substrate is shown in Figure (3.26). The geometry of this part is relatively much complex than normal AM simulation. In our work, this macroscopic simulation dedicates to investigate the evolution of temperature field of a part with complex geometry. Without voxelization, the birth and death technique is normally difficult to be applied for such an object in FEM simulation. With higher voxel resolution and more computation resource, an object with more complex form can be simulated in the same way.

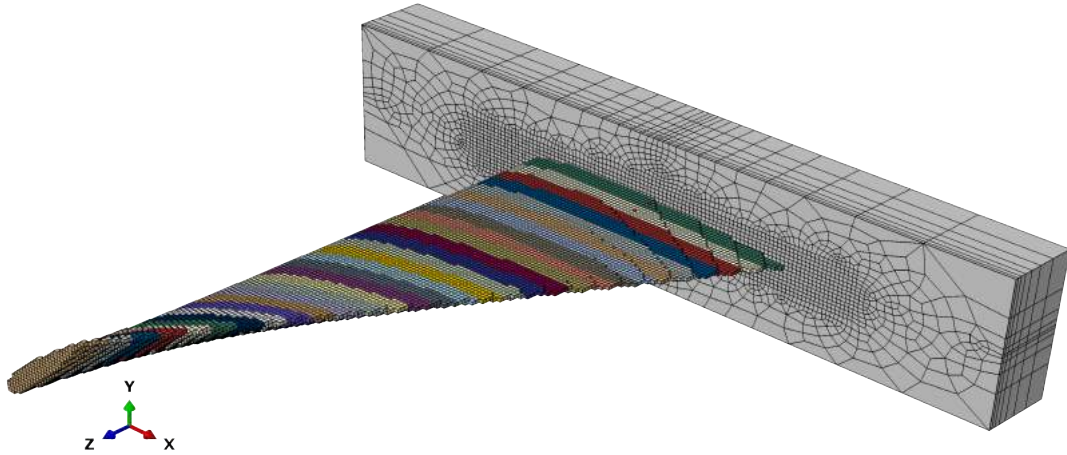


**Figure 3.26:** Mesh of the turbine blade (partition of 30 layers) and its substrate

In the voxel-based mesh, we regroup the part's voxels into 30 layers with different colours. This partition will be used as material chunks in each deposition. In fact, this regrouped layer is not the real material layer in AM process since their thickness is obviously far more than that of the metal powder layer. We simplify the whole AM process into 30 times of deposition, with the hypothesis proved in the simulation at layer-level above. In limited computational resource, the simulation at part-level can be achieved when a part's partition is based on regrouped voxel layer instead of the real powder chunk. The elements in one regrouped layer are considered to be heated with the same power and at the same time, since the temperature gradient can be partially negligible, which is proved before.

In this mesh, each voxel cube's length is  $l_{voxel} = 1.33mm$ , much larger than the size of metal powder. In this macroscopic simulation at part-level, 44107 elements are regrouped into 30 partition layers. For thermal and metallurgical field simulation, the mesh element type is DC3D8. For mechanical field simulation, the mesh element type is C3D8R. The material in our simulation is the titanium alloy Ti6Al4V, whose material properties are shown in Table 3.3, and Figure 3.27. The preheat temperature  $T_{pre}$  for substrate and metal powder is  $240\text{ }^{\circ}\text{C}$ . The initial metallurgical phases are  $\alpha$  and  $\beta$ , and their initial volume fractions are respectively  $f_{\alpha} = 0.92474$  and  $f_{\beta} = 0.07526$ .

The heat time for each partition layer is different. We suppose that the heat time  $t_i^{heat}$  of the  $i$ th layer depends on its volume which can be expressed by the number of voxel  $n_i$  included this layer.

$$t_i^{heat} = \frac{n_i l_{voxel}}{v_{scan}} \quad (3.4)$$

where  $l_{voxel}$  is the size of every voxel and  $v_{scan}$  is the scan speed in AM process. In our AM simulation with birth and death technique, the deposition of material spends also a very

### 3. Macroscopic AM simulation for multiphysics fields

---

short time. In the thermal and metallurgical simulation, this activation time is  $1.0 \times 10^{-6}s$  for each layer. In the mechanical simulation, this activation time is  $1.0 \times 10^{-7}s$  for each layer.

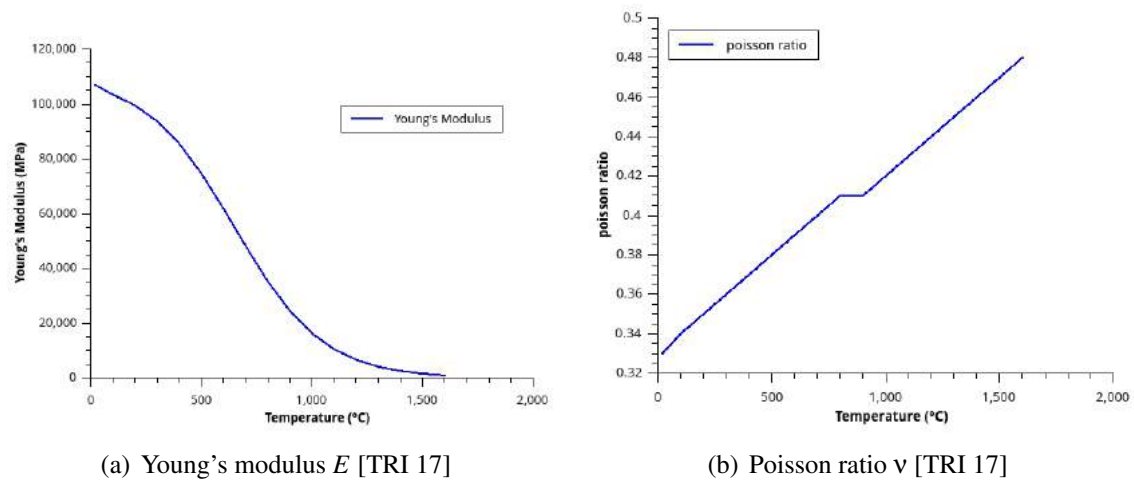
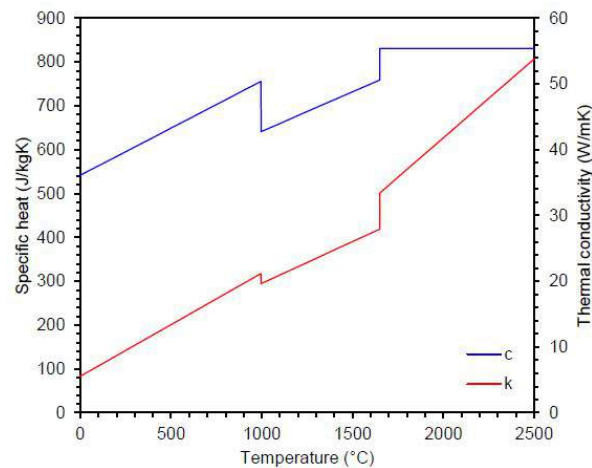
**Table 3.3:** Ti6Al4V's material parameters and AM process parameters

Parameter	Value
density $\rho$	$4.512 \times 10^{-9} \text{tonne}/\text{mm}^3$
expansion coefficient $\alpha$	$9.1 \times 10^{-6} \text{K}^{-1}$
convection coefficient $h$	$0.001 \text{mW}/\text{mm}^2$
preheat temperature $T_{pre}$	$240^\circ \text{C}$
atmosphere temperature $T_{atm}$	$40^\circ \text{C}$
Radiation coefficient $\epsilon$	0.9
print scan speed $v_{scan}$	$20 \text{mm}/\text{s}$
cooling Time after AM	$6.0 \times 10^5 \text{s}$
volumetric heat source $P_{input}$	$600.0 \text{mW}/\text{mm}^3$
initial $\alpha$ phase $f_\alpha$	0.92474
initial $\alpha'$ phase $f_{\alpha'}$	0.0
initial $\beta$ phase $f_\beta$	0.07526

The theory basis of Johnson-Cook plastic model has already been introduced in Chapter 2. The Johnson-Cook model's coefficient for Ti6Al4V at high temperature is shown in Table 3.4.

**Table 3.4:** Johnson-Cook plastic properties for Ti6Al4V[ZHA 15]

A	B	n	m	Melt temp( $^\circ\text{C}$ )	transition temp ( $^\circ\text{C}$ )
1098	1092	0.93	1.1	1630	25

(a) Young's modulus  $E$  [TRI 17](b) Poisson ratio  $\nu$  [TRI 17](c) Specific heat  $C_p$  and thermal conductivity  $C_d$  [AHN 16]**Figure 3.27:** Ti6Al4V's material properties which depend on temperature

The mechanical boundary condition is illustrated in Figure 3.28. The bottom surface of the substrate and its four corners are fixed. We create a tie between the substrate's top surface and part's inferior surface since their meshes aren't compatible.

Like the methodology in the simulation above at layer-level, we can define some "sensor points" inside the part to observe the evolution of multi-physics fields in each layer. The position of 30 sensor points is shown in Figure 3.29.

Now we begin to simulation the AM process, where the coupling of three multi-physics fields (thermal-metallurgical-mechanical) should be sequentially decoupled.

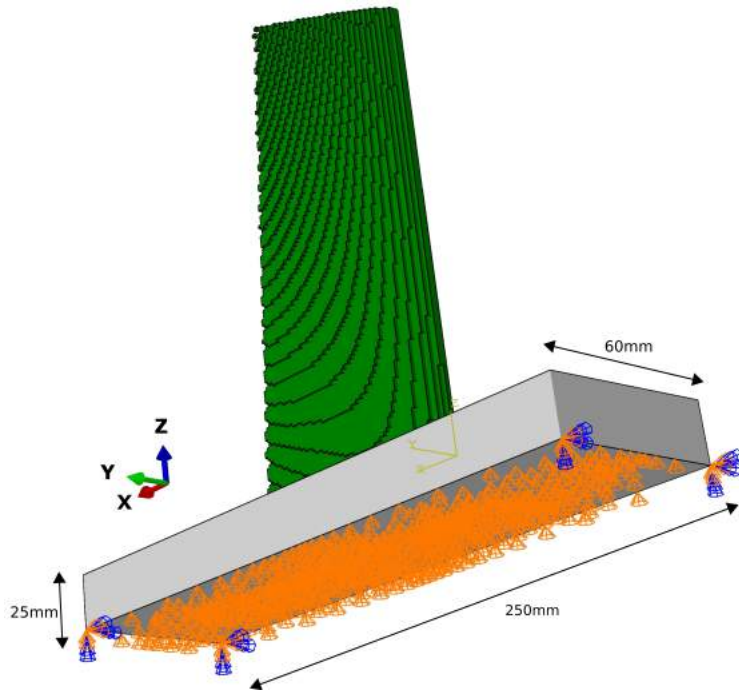


**Figure 3.28:** Mechanical boundary condition at the substrate's bottom face

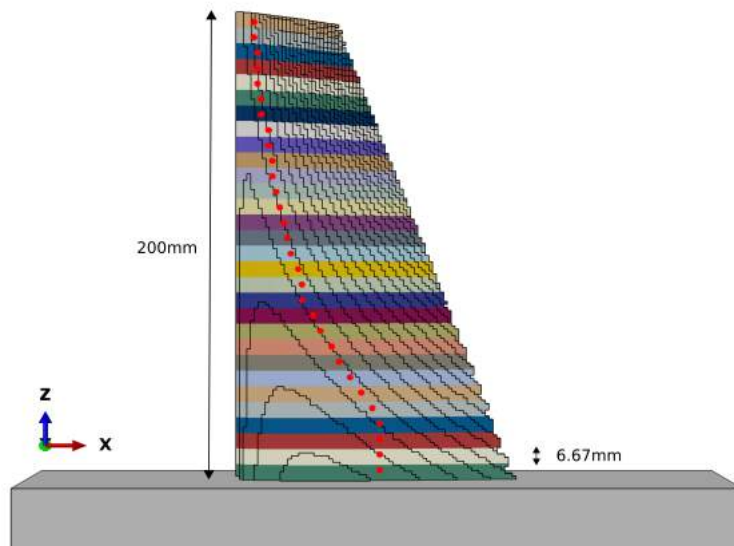
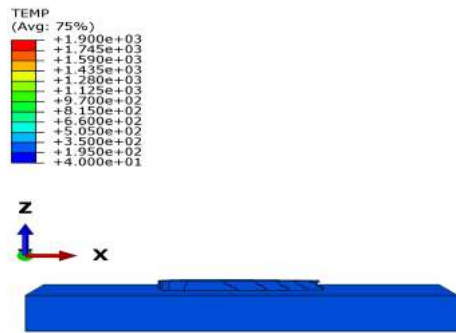


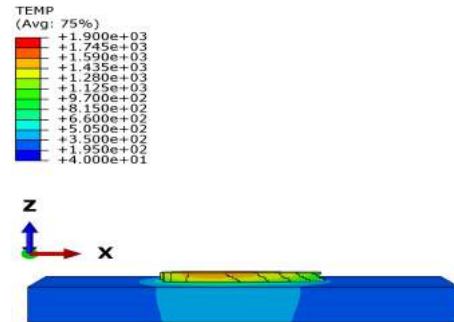
**Figure 3.29:** Position of 30 sensor points in each layers of the blade

### Thermal field simulation

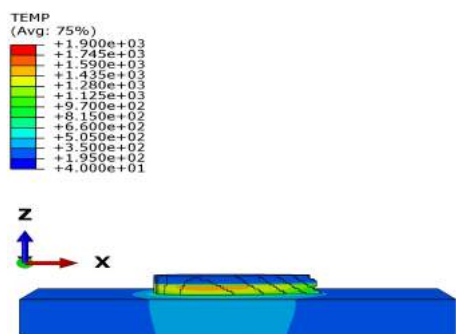
We first simulate the temperature field in AM process since it is the base for the later simulations of metallurgical and mechanical fields. The temperature field's evolution is recorded by a series of screenshots below:



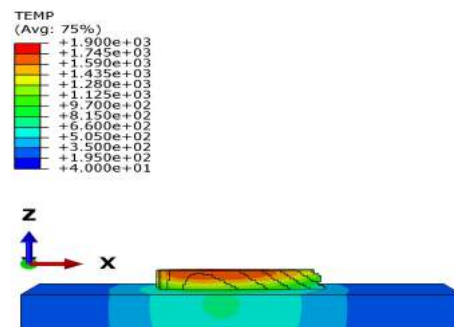
(a) 1st layer's deposition



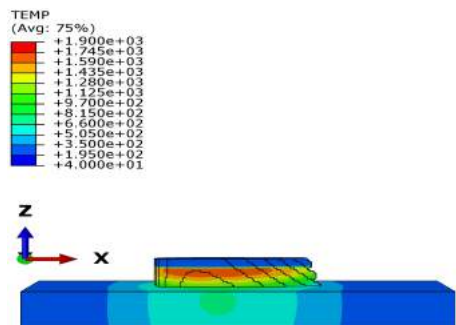
(b) 1st layer's heating



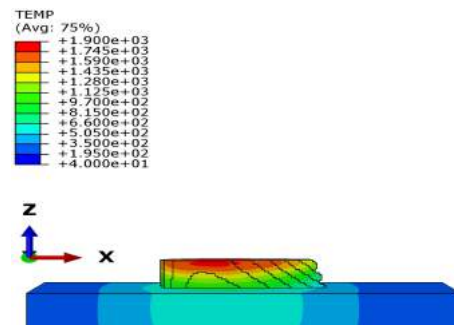
(c) 2nd layer's deposition



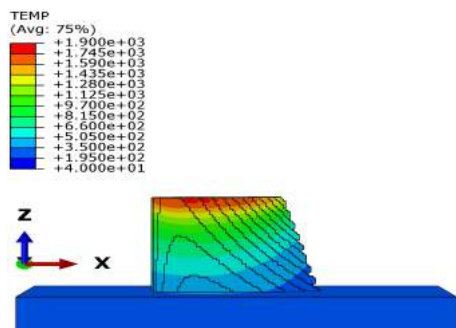
(d) 2nd layer's heating



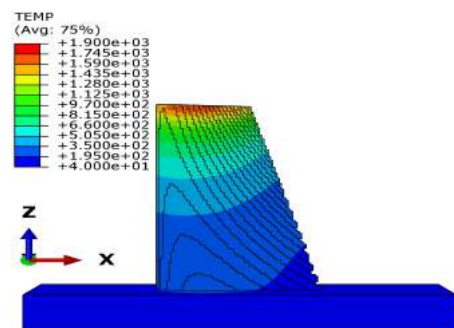
(e) 3rd layer's deposition



(f) 3rd layer's heating



(g) 10th layer's heating



(h) 20th layer's heating



### 3. Macroscopic AM simulation for multiphysics fields

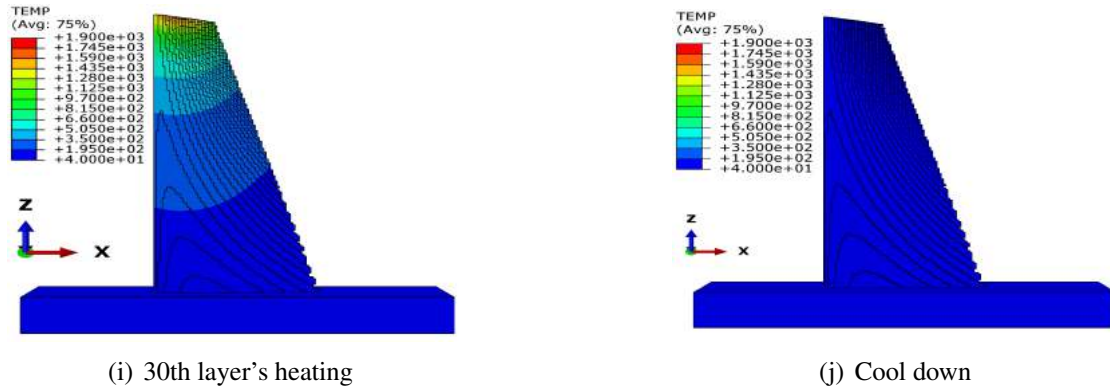


**Figure 3.30:** Screenshots of thermal simulation ( $^{\circ}\text{C}$ ) in part-level for a blade

The AM simulation is the repetition of two steps: deposition ( $1.0 \times 10^{-6}\text{s}$ ) and heat. Finally the part cools down in the environment of inert gas ( $40^{\circ}\text{C}$ ). The screenshots of Figure 3.30 (c) are captured at the instant of the 2nd layer's deposition. The newly deposited material isn't heated yet, thus the temperature of the 2nd layer looks less than that of the 1st layer at that moment. In fact, the final temperature field at the end of the 2nd layer's heating is illustrated in Figure 3.30(d).

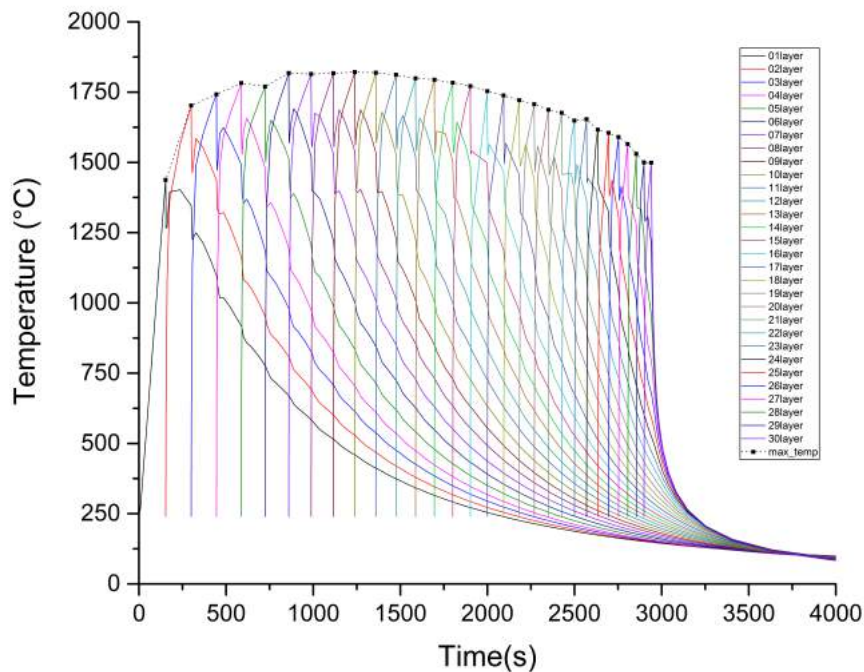


**Figure 3.31:** Temperature evolution at 30 sensor points

The temperature evolution record of 30 sensor points is illustrated in Figure 3.31. For one layer, the temperature curve arrives its maximum value just before the next deposition. For 30 layers, the maximum value of temperature rises first then declines during the building process instead of a constant value. This phenomenon demonstrates the complexity of thermal behaviour in AM process. The maximum temperature depends on the heat accumulation effect. Two aspects, heat source and heat loss, should be considered to explain this effect.

### 1. Effect of substrate heat conduction:

Since the  $k$ th layer is heated on the  $(k - 1)$ th layer, we suppose that each layer ( $k = 1, 2, 3$ ) has the same original temperature which is higher than that of the substrate (0th layer). The deposition in AM process can be considered as a series of connection of layers. When the 1st chunk is added on the substrate, the heat flux flows from the hotter 1st layer to the cooler substrate. The volume of substrate is relatively much larger than that of the 1st layer (see the simplified model in Figure 3.32). The influence of heat conduction between neighbour layers varies during the material deposition process. The maximum temperature of the  $k$ th layer  $T_{max}(k)$  depends on its neighbour layer below  $T_{max}(k - 1)$  and the distance from the substrate. The farther this distance is, the weaker effect of substrate heat conduction will be.

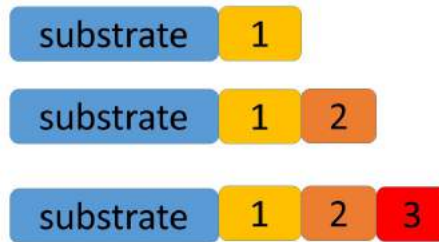


Figure 3.32: Simple example of substrate effect

### 2. Effect of convection and radiation:

When layers are separately observed, their heat accumulation effects are different. In our AM simulation, a volumetric heat source is applied for all elements in this part. As the AM part is protected by inertia gas, convection and radiation occur on its surface. For a chunk whose volume is  $V$ , its surface can be approximatively estimated as  $(\sqrt[3]{V})^2$ . During a period of heating, the ratio between heat loss of convection/radiation and the heat source can be approximatively expressed as

$$\frac{\dot{Q}_{loss}}{\dot{Q}_{generate}} \propto \frac{(\sqrt[3]{V})^2}{V} \quad (3.5)$$

If the volume  $V$  diminished, the ratio  $\dot{Q}_{loss}/\dot{Q}_{generate}$  will increase and less volumetric heat  $\dot{Q}_{generate} - \dot{Q}_{loss}$  will be accumulated. The part is a twisted blade in this macroscopic simulation, its geometrical size decreases with the height. Since we adopt a voxel-based mesh, the element size is uniform. Here is the Figure 3.33 illustrating the  $i$ th layer's



volume  $V_i$  in comparison with the total volume  $V_{all}$ . This fraction can be easily calculated from the number of voxel element included in each layer. From this figure, we can see the volume of each layer decreases when the material is deposited layer by layer.

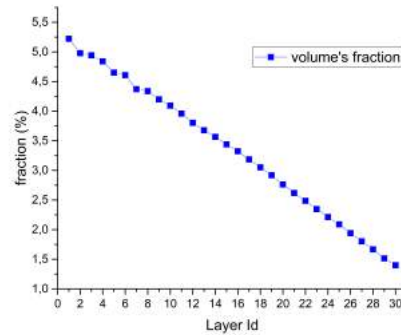


**Figure 3.33:** Fraction of each layer's volume  $V_i$  in whole part  $V_{all}$ .

Totally, the two effects above occur simultaneously during the AM process. The effect of substrate heat conduction will make temperature maximum values increase while the effect of convection/radiation makes them decrease. The evolution of maximum temperature is in fact a superposition of these two effects, thus the final curve first increases then decreases.

After the thermal AM simulation, we can use the temperature evolution of the whole as a base for further metallurgical and mechanical simulation. This decoupling is shown in Figure 3.34

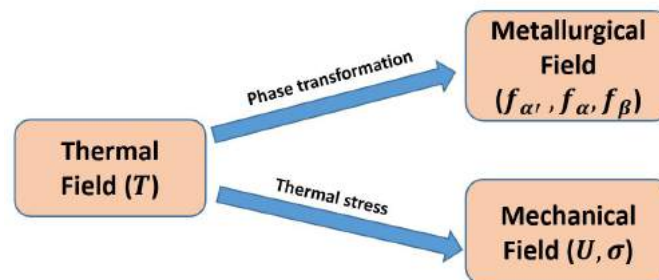


**Figure 3.34:** Decoupling of three multi-physics field in this thesis.

#### Metallurgical field simulation

The initial volume fraction of  $\alpha$  phase,  $\beta$  phase, martensite phase  $\alpha'$  of Ti6Al4V will be influenced by AM thermal process. In this thesis, we study the phase transformation during AM process, based on the temperature evolution obtained from AM thermal simulation. At the initial state there are two basic phases in Ti6Al4V  $f_{\alpha} = 0.92474$ ,  $f_{\alpha'} = 0.0$  and  $f_{\beta} = 0.07526$ . The martensite phase may be generated from austenite phase  $\beta$  under certain condition.

From the Figure 3.35 and Figure 3.36, we can observe the phase transformation  $\alpha \rightarrow \beta$  in the high temperature zone, which moves with the new material deposition. This diffusional transformation occurs during the heating process. The new generated phase  $\beta$  doesn't retain stable during the cooling process. In the layer far away from the moving heat source, the new generate  $\beta$  will then change into phase  $\alpha$ .

The cycle of heating and cooling happens frequently in AM process. This cycle makes the volume fractions  $f_\alpha$  and  $f_\beta$  vary in different layers of the whole part during the printing. The heating leads to  $\alpha \rightarrow \beta$  while the cooling leads to  $\beta \rightarrow \alpha$ . We can observe the evolution of volume fractions by the Figure3.38 and the Figure3.39. Both of the phase  $\alpha$  and  $\beta$  will finally return to their initial state after the AM process.

The volume fractions  $f_{\alpha'}(\mathbf{x},t), f_\alpha(\mathbf{x},t), f_\beta(\mathbf{x},t)$  vary spatially and temporally during the additive manufacturing process, but they obey always the relation between them in material Ti6Al4V:

$$f_{\alpha'}(\mathbf{x},t) + f_\alpha(\mathbf{x},t) + f_\beta(\mathbf{x},t) = 1.0 \quad (3.6)$$

where  $\mathbf{x}$  is a fixed position in the part,  $t$  is the instant. We will take the 30 sensor points as the fixed values  $x$  in Figure 3.38 and Figure 3.39. The basic algorithms for phase transformation of Ti6Al4V have already introduced in Chapter 2 and its subroutine is shown in Appendix E.

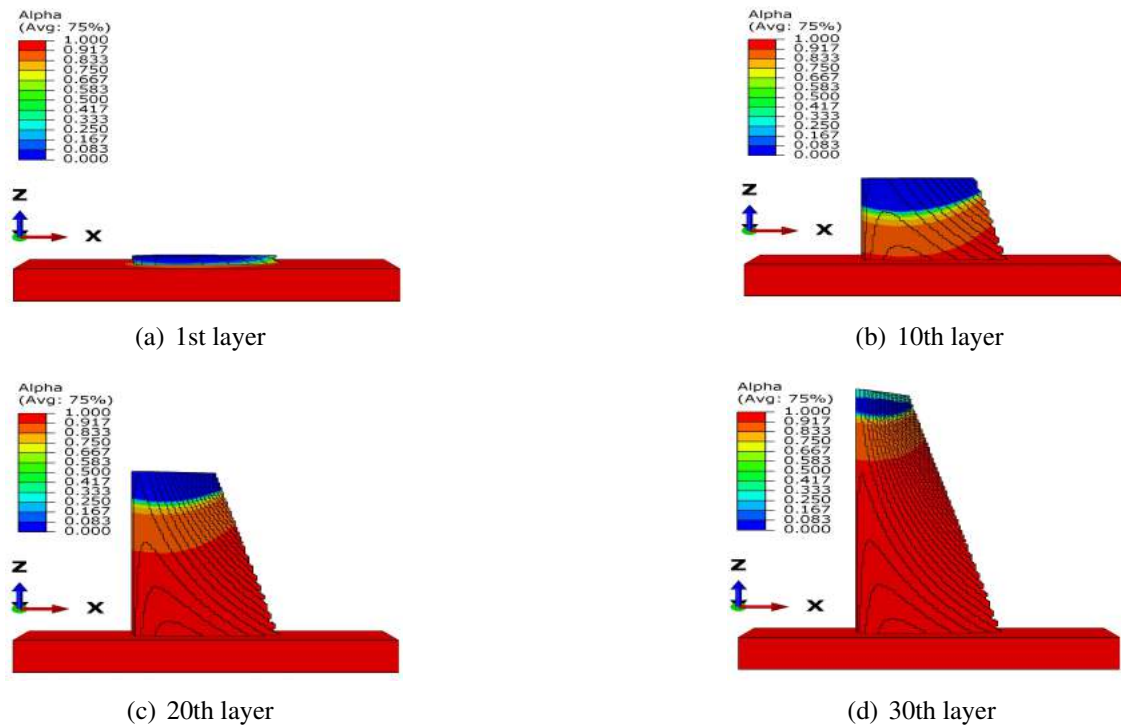


**Figure 3.35:** Screenshots of the simulation for  $\alpha$  phase during AM process

### 3. Macroscopic AM simulation for multiphysics fields

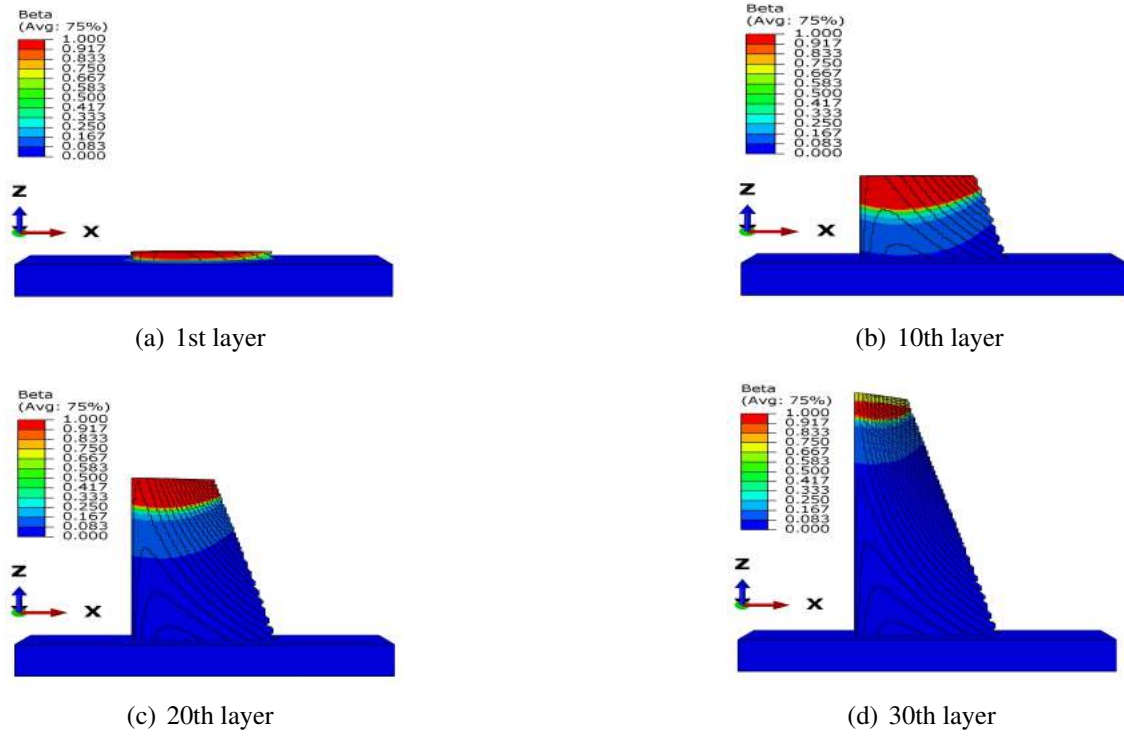


**Figure 3.36:** Screenshots of the simulation for  $\beta$  phase during AM process

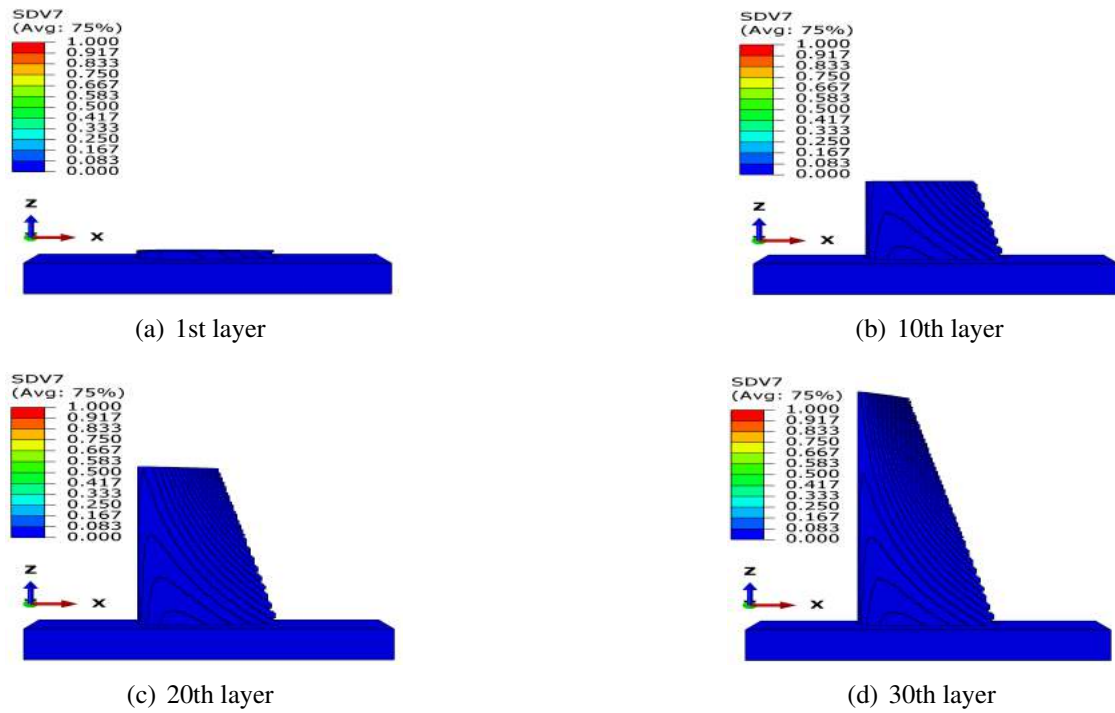


**Figure 3.37:** Screenshots of the simulation for martensite  $\alpha'$  during AM process

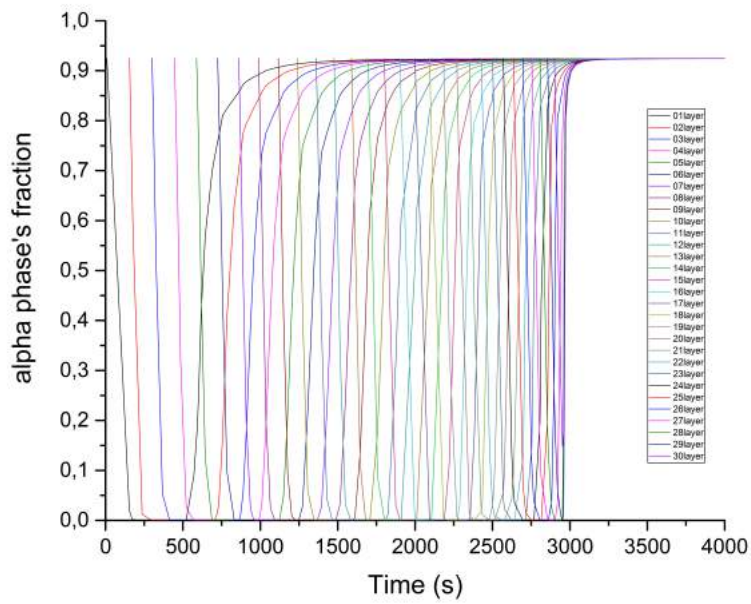


**Figure 3.38:**  $\alpha$  phase's evaluation at 30 sensor points

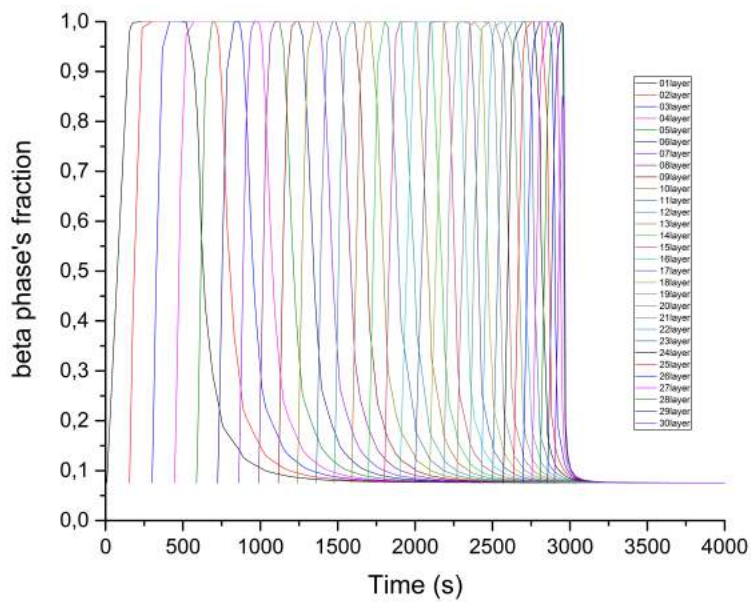


**Figure 3.39:**  $\beta$  phase evaluation's at 30 sensor points

We note that no martensite phase  $\alpha'$  is generated from phase  $\beta$  in the whole AM

process (see Figure 3.37). Martensitic transformation isn't observed in this macroscopic simulation at part-level. In fact, this diffusionless transformation only happens under a rapid cooling process. From the temperature change rate record of 30 sensor points in Figure 3.40, the magnitude of cooling speed is always lower than  $410^{\circ}\text{C}$ , which is the critical cooling speed for this kind of transformation. This figure explains why the generation of martensite phase  $\alpha'$  isn't observed in our macroscopic AM simulation.

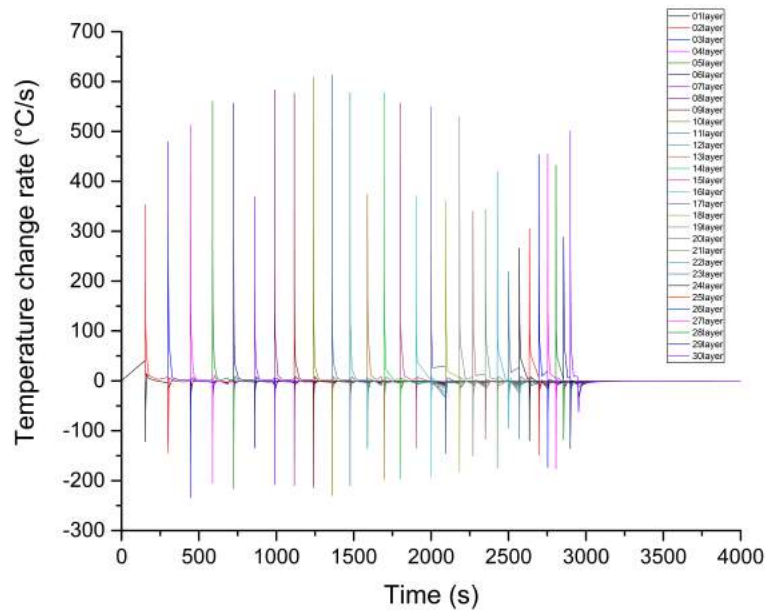


**Figure 3.40:** Evolution of temperature rate  $dT/dt$  at 30 sensor points

#### **Mechanical simulation**

Based on the thermal simulation above, we simulate the mechanical field in AM part using the temperature evolution data of \*.odb file. The temperature history of each node is imported into the mechanical simulation. The complex AM thermal process leads to the non-homogeneous effect in the mechanical field. For example, the final displacement at environment temperature is non-isotropic in this blade part, shown in Figure 3.41(b), 3.41(c) and 3.41(d). The extreme values of displacement are usually located near the edge of this blade part, where the thickness in Y direction is smaller because of the airfoil section's geometry. Since the length and width of the airfoil are much longer than the thickness of a layer, the displacement in X and Y directions (xOy horizontal face) is globally more noticeable than that in Z vertical direction.



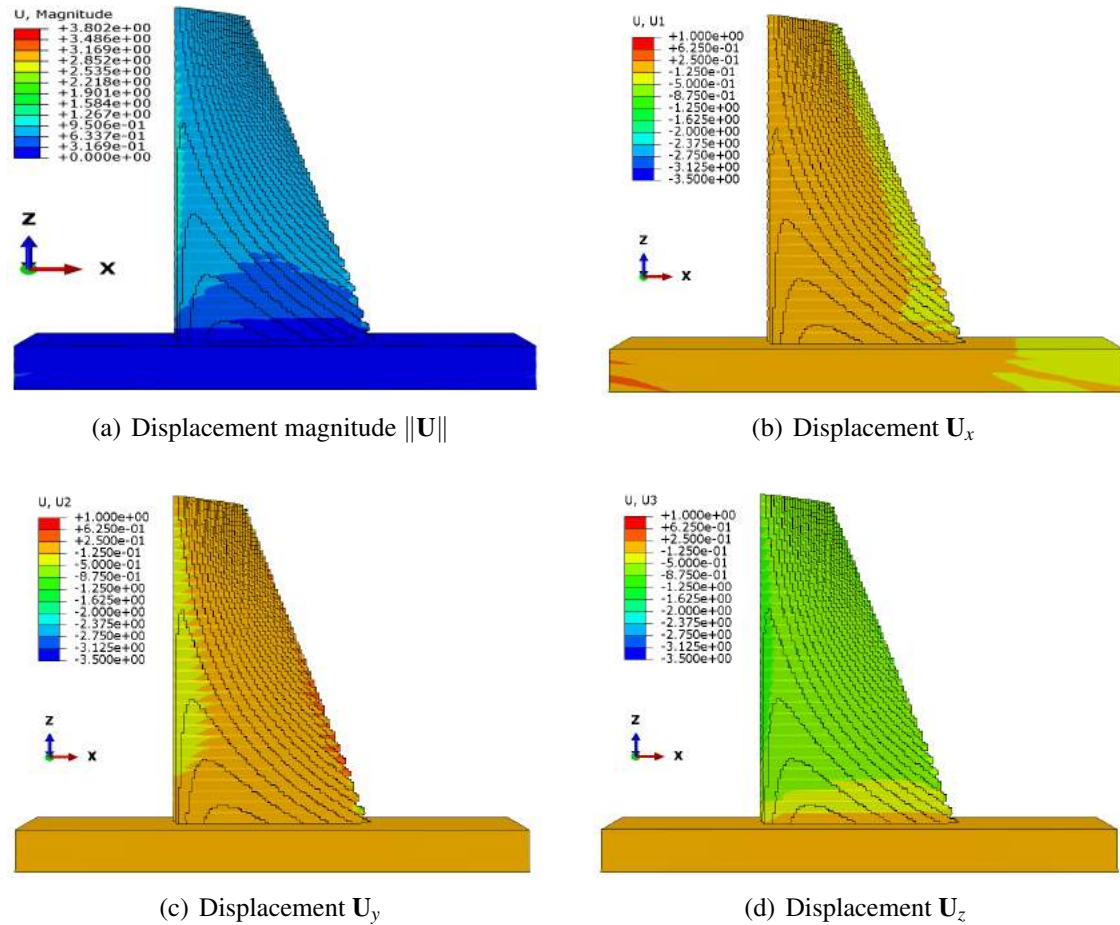


**Figure 3.41:** Final displacement ( $mm$ ) at environment temperature

The residual stress of a part at environment temperature can be also observed from different views. Here we choose the von Mises stress to illustrate the distribution of residual stress. The residual stress not only exists in the near-surface area, but also in the centre of a part. From the outside view of this part (Figure 3.42(a)), we find that the residual stress near the thin edge is relatively higher than other zones. These thin edge zones contact directly with inert gas have fiercer temperature change, so their residual stresses have higher magnitudes than thicker central zone. Profiting from the convenience of simulation, we can virtually cut the part and observe the residual stress distribution inside the part. In Figure 3.42(b)(c), we create two cutting section faces parallel to  $xOz$  face at the  $y$  depth  $y = 30mm$  and  $y = 33mm$ . Similarly, we create in Figure 3.42 a cutting face parallel to  $yOz$  face at the depth  $x = 105$  in  $X$  axis. From the Figure 3.42(b)(c)(d), we can find the residual stress exists not only near the thin edge zone, but also inside the part, especially near the interface of two neighbour layers. Before the next deposition of a new layer, an interface contacts directly with inert gas as the external surface. After the next deposition, this interface is covered by the new layer, whose initial temperature is colder than the max temperature of the older layer. As a result, the temperature changes more

### 3. Macroscopic AM simulation for multiphysics fields

violently at the interface of two layers than the centre zone of one layer. This temperature change history makes the residual stress non-homogeneous throughout the blade part.

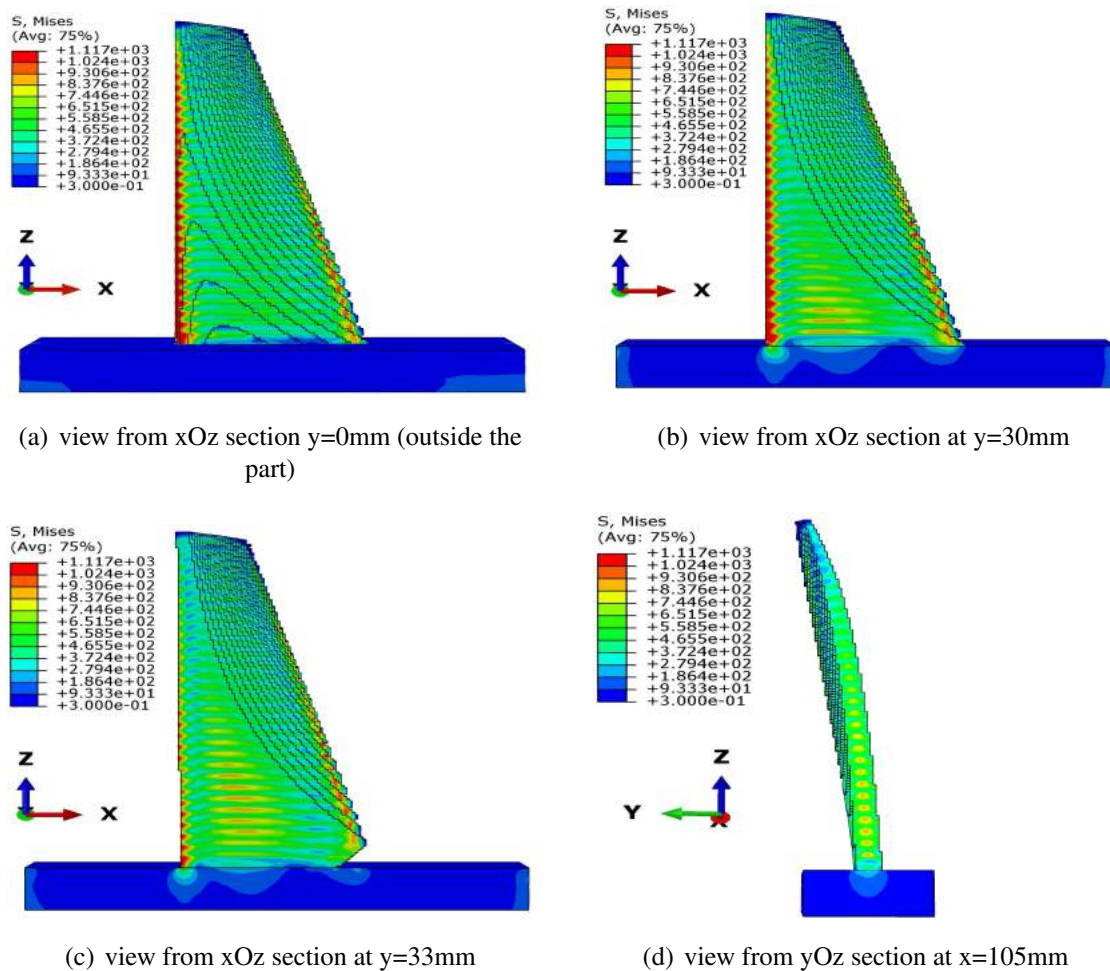


**Figure 3.42:** Final von Mises residual stress (MPa) at environment temperature with different views

### 3.4 Study on AM process parameters for a part's residual stress

The blade part's von Mises residual stress is demonstrated in Figure 3.42 after cooling to the environmental temperature  $40^\circ\text{C}$ . In fact, many factors in AM system have influences on the final part's residual stress. We can consider the AM simulation in Figure 3.42 as a reference case to investigate how to reduce the residual stress of a part built by metal AM technologies.

In this section, we study different additive manufacturing case using our macroscopic

simulation tool, mainly in two directions: first, the preheat temperature, then the process parameters (input power-heating time).

Mathematically, the reduction of residual stress  $\sigma$  is an optimization problem for the function  $f$  who can determinate  $\sigma$ .

### 3.4.1 Influence of preheat temperature

As is discussed in Chapter 1, increasing the preheat temperature in AM system is a method for many commercial AM machines to improve the part's quality, especially to reduce the residual stress. For advanced AM machine,  $500^{\circ}\text{C}$  is one of the best records. The arrival of such a high temperature is still difficult today for most of AM machine without special modification. In our work, we will simulate the AM process at preheat temperature  $T_{pre} = 500^{\circ}\text{C}$ . Then we will compare this result with the reference case at preheat temperature  $T_{pre} = 240^{\circ}\text{C}$ , which has already been calculated before (see the Figure 3.42). From this comparison, we can understand better why the AM machine manufacturer company adapt the increase of preheating temperature as one technique direction.

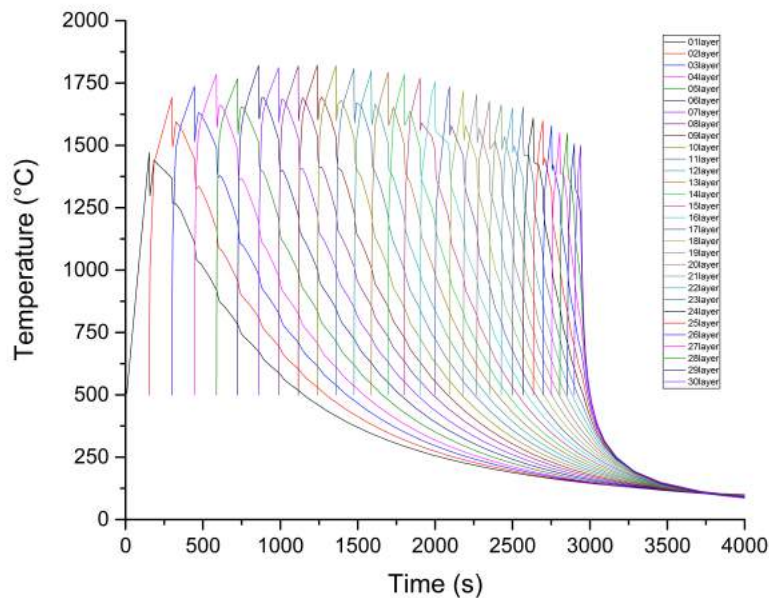


**Figure 3.43:** Temperature evaluation of the case in which the preheat temperature  $T_{pre}$  is  $500^{\circ}\text{C}$ .

Before AM simulation, the only input difference between the new case ( $T_{pre} = 500^{\circ}\text{C}$ ) and the reference case ( $T_{pre} = 240^{\circ}\text{C}$ ) is their preheat temperatures. Like the Figure 3.31, we can obtain the temperature evolution (Figure 3.43) during AM process in new case.



### 3. Macroscopic AM simulation for multiphysics fields

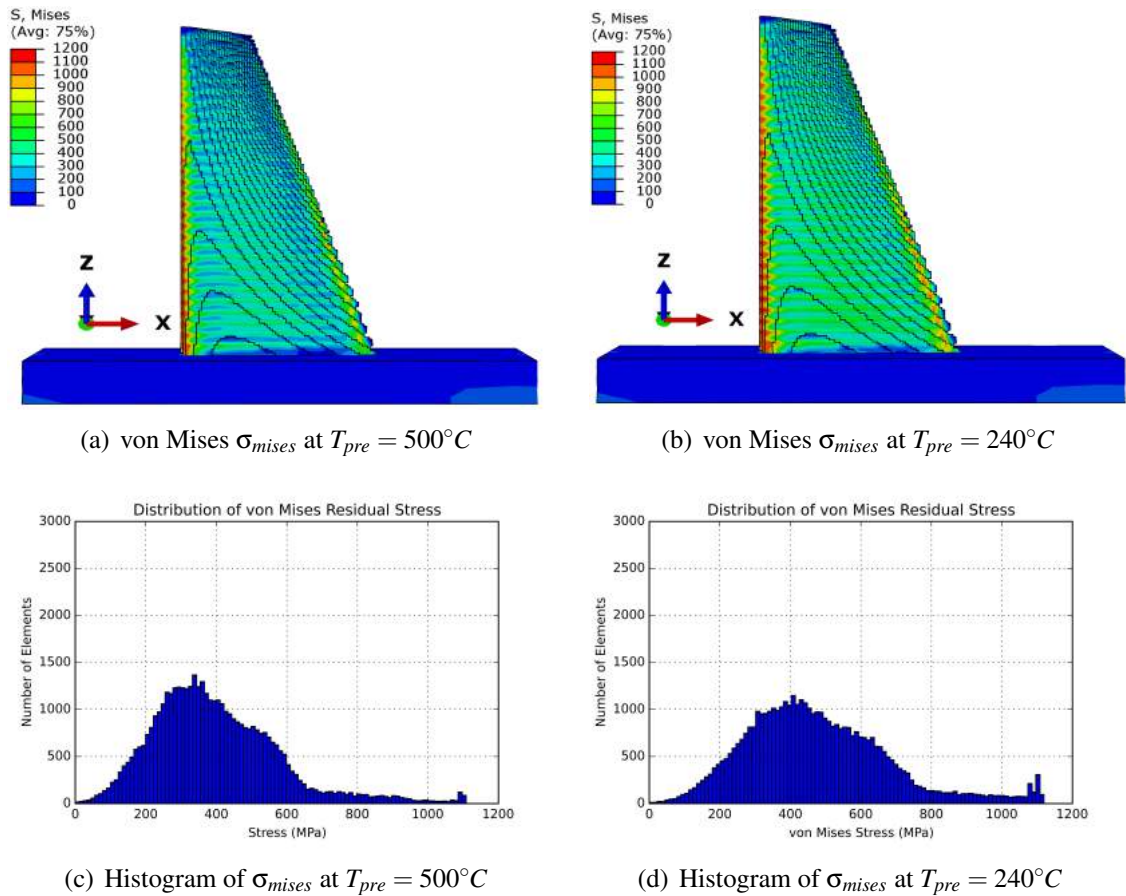


**Figure 3.44:** Final residual stress (MPa) with different preheat temperature  $T_{pre} = 500^{\circ}C$  and  $T_{pre} = 240^{\circ}C$  (Reference case)(Other AM process parameters are the same)

From the Figure 3.44(a) and the Figure 3.44(b), we can see some slight differences between the cases with different preheat temperatures  $500^{\circ}C$  and  $240^{\circ}C$ . The residual stress in case of  $500^{\circ}C$  is globally less severe than the case of  $240^{\circ}C$ . Distinguishing the two stress field is qualitative from Figure 3.44(a)(b) and this outside view restrain us from observing the stress inside the part.

In this simulation, voxel-based mesh is applied to describe the blade's geometry and the size of each voxel is the same. Profiting from this feature, we can use a histogram for all elements to study quantitatively the stress distribution in this complex geometry. This post-processing is implemented by C++ (see Appendix F) and python. From the Figure3.44(c) and the Figure3.44(d), we can find easily the maximum value of the von Mises residual stress  $\sigma_{mises}$  and its average value. The difference in the maximum values of residual stress isn't obvious, one reason is the maximum stress locates principally at the thin edge of blade part, which is locally influenced more by inert gas around. However, in terms of the histogram's overall profile, the increase of preheat temperature is indeed useful for reducing globally the residual stress in one part. We will analyse these histograms in further study (see Table 4.2).

### 3.4.2 Influence of AM process parameters ( $P_i, t_i$ )

The process parameters in additive manufacturing have also influences on the final residual stress. However, this kind of research is relatively rare because of its complexity. In this thesis, we simulate AM cases with different process parameters. Even though these parameters are subjectively chosen, we can still find the potential value of optimising AM process parameters for reducing one part's residual stress.

The residual stress  $\sigma$  of the blade part can be expressed as a function  $f$  of AM process parameters in 30 layers. In this work, we choose the input power  $P_i$  and heating time  $t_i$  (sometimes it can be calculated from printing speed) as two representative variables of all the AM process parameters, since it is relatively easy for AM machine's hardware to adjust these two parameters in real-time.

In mathematics, the target of reduce residual stress  $\sigma$  in a metal part built by AM machine is an optimisation problem. The relation between input power and heating time:

$$\sigma = f(P_1, t_1, P_2, t_2, P_3, t_3, \dots, P_i, t_i, \dots, P_{30}, t_{30}) \quad (3.7)$$

where  $i = 1, 2, 3, \dots, 30$  represents 30 layers in the blade part. We attempt to adjust AM process parameters to find a group  $(P_i^k, t_i^k)$  such that  $\max(\sigma^k) < \max(\sigma^{ref})$ , where  $i$  is the number of layer in  $k$  th simulation ( $k$  is the label of case). Here we suppose some groups of AM process parameters to investigate their performance on reducing the residual stress. It should be noticed that all of these cases below are simulated under the same preheat temperature  $T_{pre} = 240^\circ C$  as the reference case. Here is the four cases of different AM process parameters:

**Table 3.5:** Some cases for AM process parameters adjustment

Case	Power ( $i = 1, 2, 3, \dots, 30$ )	Heat Time ( $i = 1, 2, 3, \dots, 30$ )
Reference	$P_i^{ref}$	$t_i^{ref}$
A	$P_i^A = 0.5P_i^{ref}$	$t_i^A = 2t_i^{ref}$
B	$P_i^B = 0.2P_i^{ref}$	$t_i^B = 5t_i^{ref}$
C	$P_i^C = 0.1P_i^{ref}$	$t_i^C = 10t_i^{ref}$
D	$P_i^D = C_iP_i^{ref}$	$t_i^D = t_i^{ref}$

In these cases A, B, C, the strategy of adjustment is to decrease print speed (to extend heating time) while the input power is decreased to retain the input energy  $P_i \times t_i$  as same as that in the reference case (see Figure 3.45). The heating process in A,B,C cases are slower than that in the reference case. This may be helpful for heat transfers more smoothly between neighbour layers.

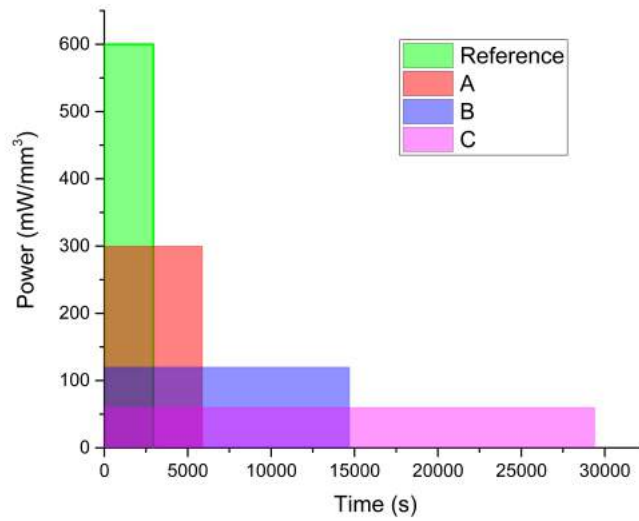


**Figure 3.45:** The input power and heating time for different AM simulation cases.

In the reference case, the maximum temperature curve is concave, as is shown in Figure 3.31. We attempt to increase input energy at the beginning and near the end of AM fabrication in Case D, so as to make the maximum layer temperature curve less concave. In Case D,  $C_i$  is a coefficient of adjustment for each layer (shown in Figure 3.46).

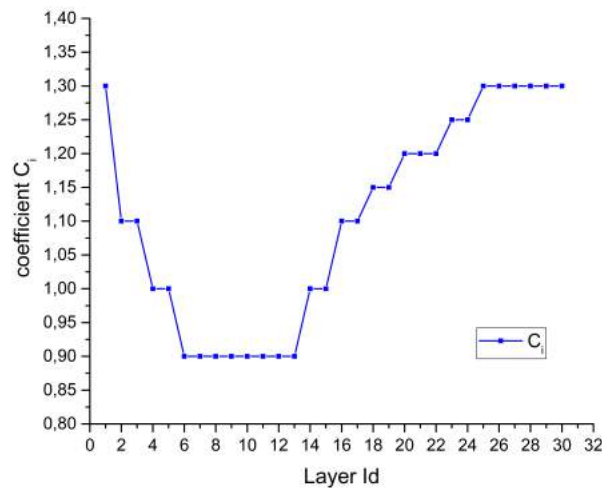


**Figure 3.46:** The coefficient  $C_i$  for the input power of the case D.

We simulate separately the four cases, the temperature evolution curve of each case is shown in Figure 3.47.

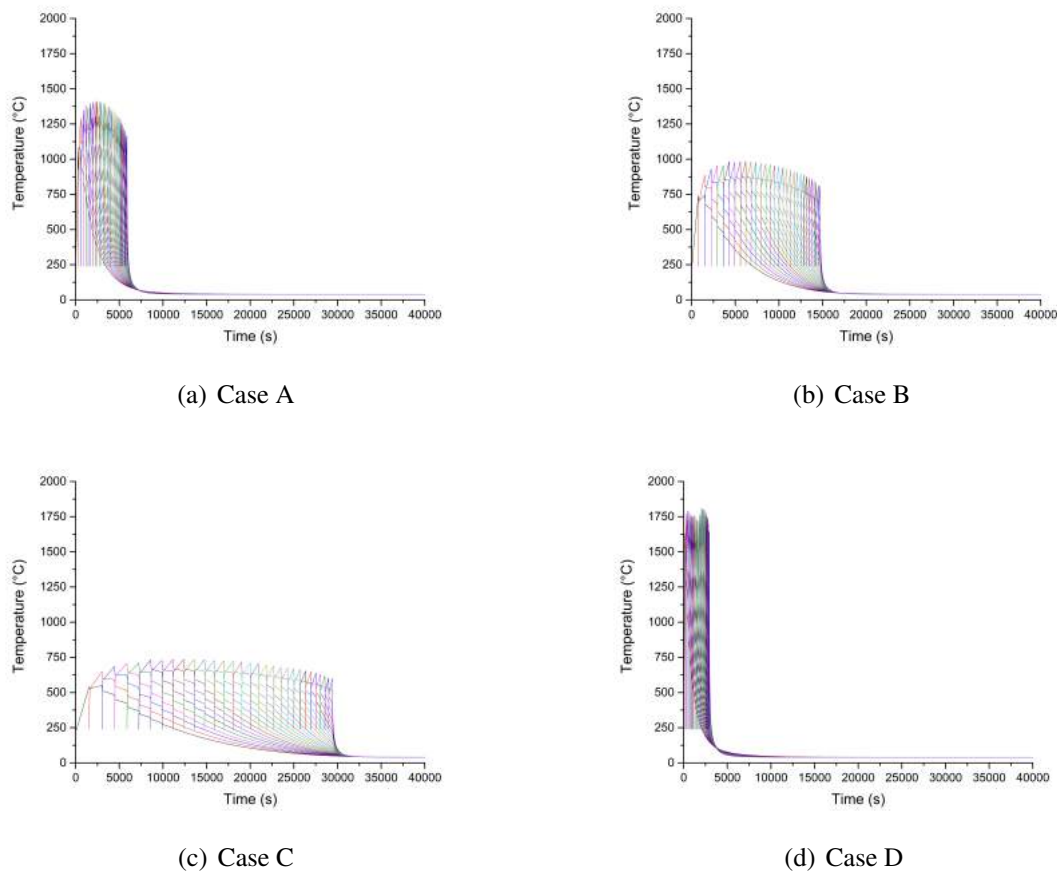


**Figure 3.47:** Temperature evolution at 30 sensor points for different simulation cases (Each different colour represents one layer.)

The temperature varies in different cases because all of these cases are macroscopic simulations without any temperature control loop. During the heating process, the heat transfers inside the blade and with the inert gas. The Figure 3.47(a), the Figure 3.47(b) and the Figure 3.47(c) correspond to the input power-heat time relations of case A,B,C shown in Figure 3.45. If we pick the maxima values of temperature in 30 layers from Figure 3.47(d), we can obtain the temperature maxima curve in Figure 3.48 below.

In comparison with the reference case (see Figure 3.31), the heat time in Case D retains the same without adjustment. but the maximum temperature curve becomes less concave as we expect (see Figure 3.48 ), after reducing the difference between maximum and minimum values on this curve.

### 3. Macroscopic AM simulation for multiphysics fields

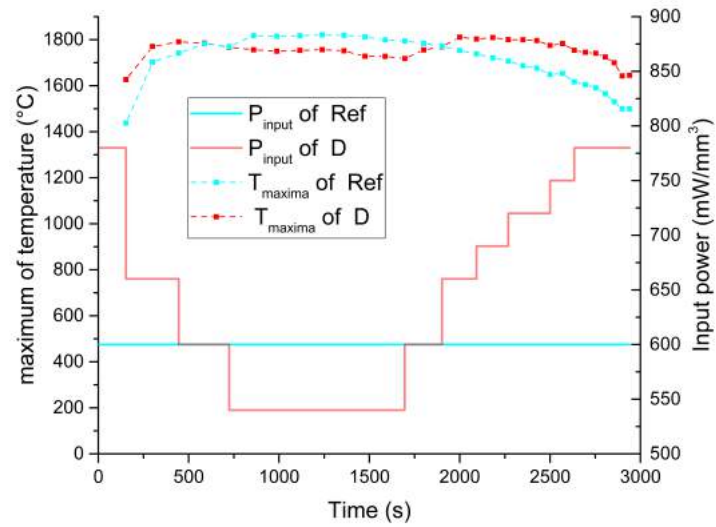


**Figure 3.48:** The AM thermal process of Case Ref and Case D.

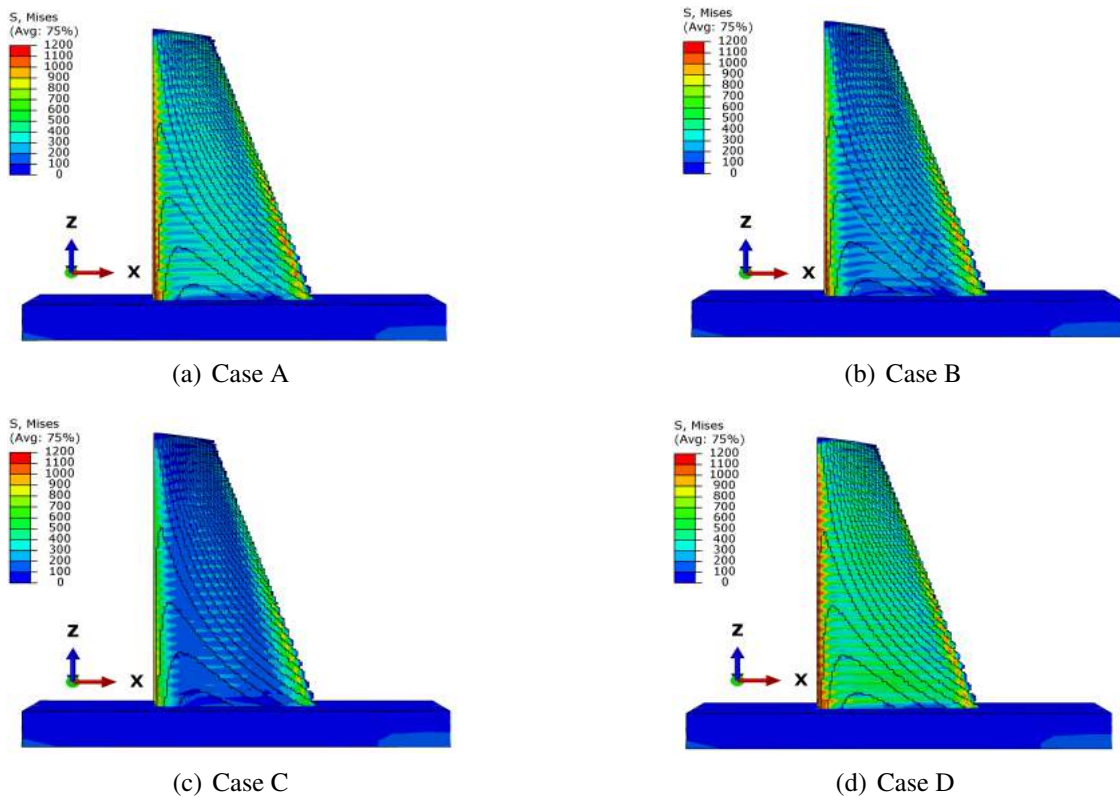


**Figure 3.49:** Residual stress  $\sigma_{vonMises}$  (MPa) distribution for different simulation cases

Comparing the four results (see Figure 3.49) with the reference case in Figure 3.44(b), we find the process parameters have indeed influences on the final residual stress. In order to estimate their overall field inside the part, we extract the von Mises stress of every voxel element in this blade part and create 4 histograms (see Figure 3.50) for further study.

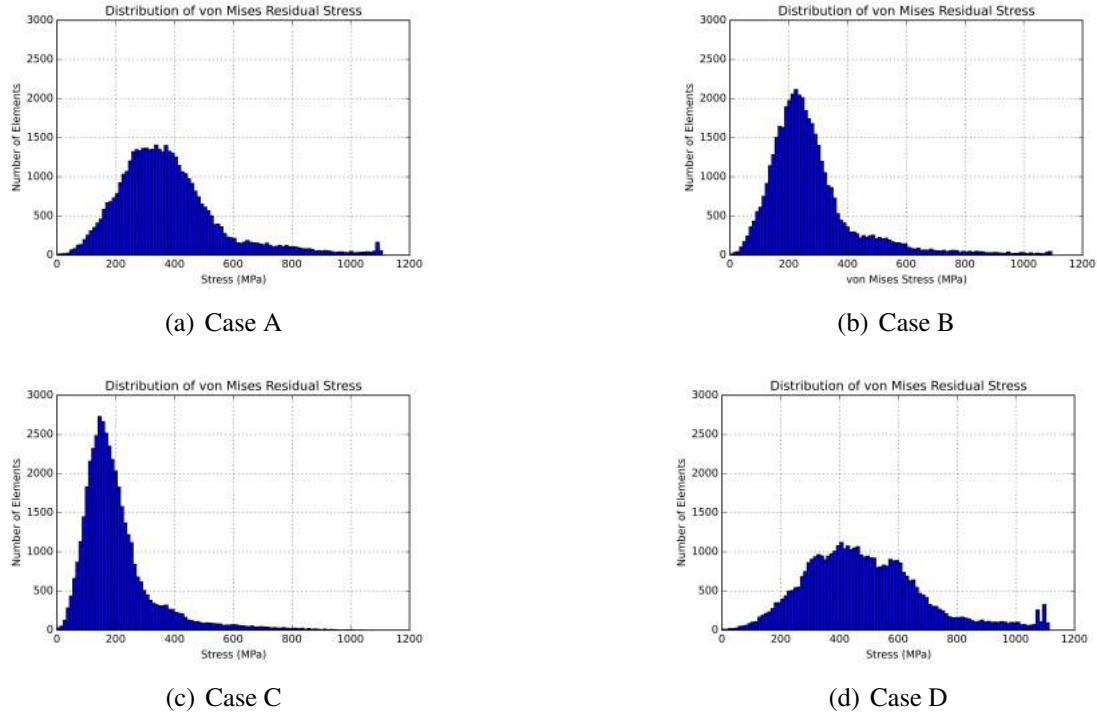


**Figure 3.50:** Histogram of  $\sigma_{vonMises}$  throughout the blade for different simulation cases

Although the simulation is a deterministic system, we can still use some mathematical tool to describe the histograms by calculate its probability density function (pdf). In this work, Burr type XII distribution is applied to fit the histogram. Burr type XII distribution is defined as a function of three coefficients  $a, c, k$  :

$$f(x|a, c, k) = \frac{\frac{kc}{a} \left(\frac{x}{a}\right)^{c-1}}{\left(1 + \left(\frac{x}{a}\right)^c\right)^{k+1}}, x > 0, a > 0, c > 0, k > 0 \quad (3.8)$$

The probability density function of the histogram of residual stress is useful to evaluate the efficacy of different AM parameters optimisation. After function fitting operation for these histograms above (Figure 3.44, Figure 3.50), we obtain their Burr XII coefficients, basic statistic mean and standard deviation in Table 4.2. From the probability density function (pdf) of von Mises residual stress, the efficacy of each technical strategies can be quantitatively evaluated for the whole part.

**Table 3.6:** Statistic results and Burr XII coefficients

Case	Mean (MPa)	Standard deviation(MPa)	$c$	$k$	$a(\text{MPa})$
Reference	477.3	204.3	3.096	2.729	678.3
A	378.9	178.1	3.393	1.526	411.5
B	277.3	156.5	3.613	0.975	241.6
C	203.9	125.4	3.505	0.906	168.7
D	486.4	203.3	3.147	2.804	694.3
Preheat 500°C	397.4	179.2	3.079	2.297	524.4

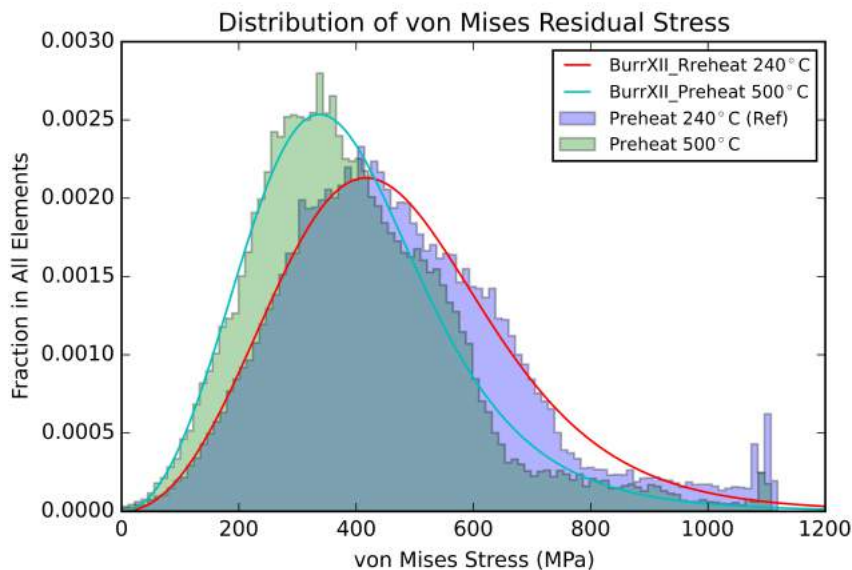


**Figure 3.51:** PDF of AM case with different preheat temperature  $T_{pre} = 500^{\circ}\text{C}$  and  $T_{pre} = 240^{\circ}\text{C}$  (Reference case).

The Figure 3.51 illustrates the efficacy of the strategy in which the preheat temperature should be increased to reduce residual stress. The difference between the maximum residual stresses in these two cases is quite small. However, it is noticeable that the residual stress value is globally reduced in case of  $T_{pre} = 500^{\circ}\text{C}$ . This proves why some AM machine manufacturers are always trying to increase the preheat temperature as high as possible.

Now we begin to evaluate the strategies in which the preheat temperature is  $240^{\circ}\text{C}$ : Case A, B, C, D and the reference case.



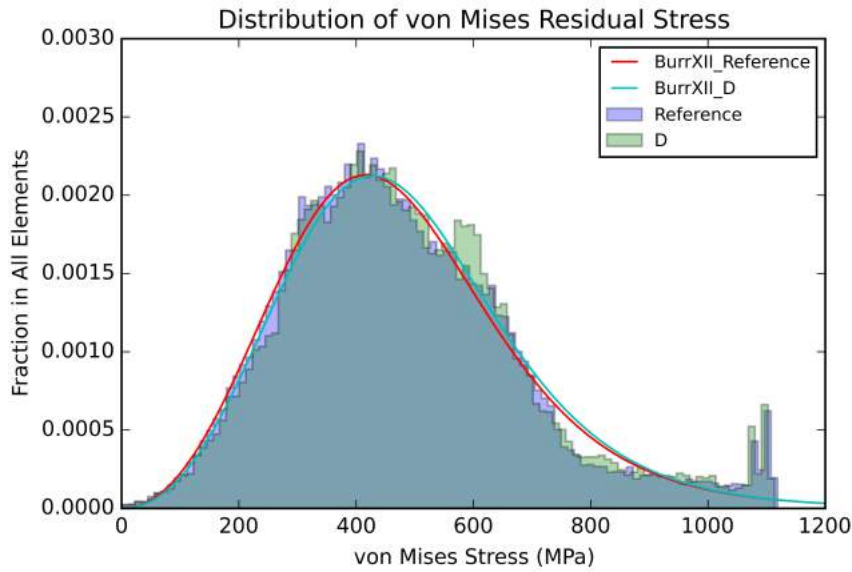


**Figure 3.52:** PDF of AM cases (Case D and Reference Case).

Comparing with the reference case, we find that the strategy in Case D isn't efficacious enough to reduce residual stress (see Figure 3.52). The overlapping of histograms makes it quite difficult to distinguish reference case and Case D. Nevertheless, we can find their Burr type XII distribution coefficients approach respectively in Table 4.2. The group of process parameters in case D have no evident improvement for reducing residual stress in comparison with the reference case.

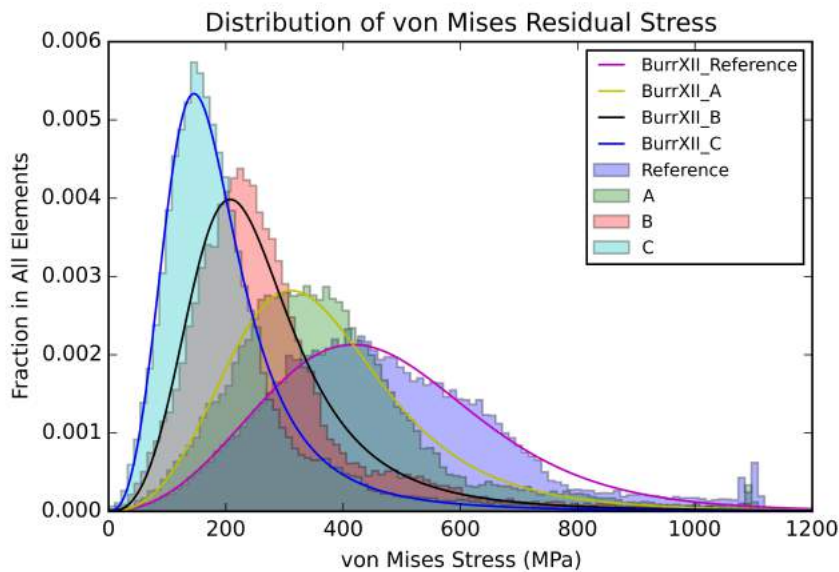


**Figure 3.53:** PDF of AM cases (Case A, Case B, Case C and Reference Case).



When the histograms of reference case and cases A, B, C are analysed together (see Figure 3.53), we can find this strategy can reduce residual stress, both its extreme maximum value and its global statistic level (mean value and variance). The slower the heating time of each layer (the printing speed) is, the less residual stress will be in the AM part. This strategy demonstrates the possibility of reducing residual stress with lower preheat temperature, if we can apply an appropriate group of AM process parameters.

These AM simulation results imply a potential technique direction for reduction of residual stress in additive manufacturing. Nevertheless, the group of process parameters are subjectively chosen in this chapter, and we can't conclude that the parameters in Case C is the best solution among all the possible optimisation parameters, we study in Chapter 4 more about the optimisation problem of residual stress.

The control of AM process parameters, mainly input power and heat time (printing speed), is difficult and very delicate because of the complex heat transfer and hardware's physic limits (e.g. melting point) in AM system. In Chapter 5, we investigate further some problems on temperature control as basic preparation for realizing this potential technique.

## 3.5 Conclusion

In this chapter, the methodology of study multi-physics fields in the AM process is introduced. We apply FEM simulation at the macro scale for the thermal-metallurgical-mechanical coupling phenomenon in AM system. The main conclusions are listed as follows :

- 1. For AM simulation at layer level, some approaches are proposed to solve the special pre-processing problems. When we import scan path information into the material deposition partition, the partition from a G-code file is conducted based on a series of inverse calculation of polygon offsetting and clipping. When a part's separated layers are assembled in FEM software, incompatibility of 3D element set occurs between CAD B-Rep system and mesh generator. This problem is solved by a database based technique: injective mapping of the element set from CAD system to orphan mesh.
- 2. For AM simulation at part level, the voxelization is a promising method where the voxel mesh can be considered as the approximation of a 3D object's shape. This approach is suitable for a part with complex geometry and its macroscopic simulation. This voxel-based has also convenience for the analysis using histograms.
- 3. The temperature evolves coincidentally in the vertical direction for neighbour layers with a very small thickness. The heat transfers fast through a group of thin layers. By regrouping these neighbour thin layers into a thicker layer, this feature makes it possible to simplify a part with fewer layer numbers to accelerate the calculation in AM simulation.

- 4. The residual stress exists not only on the surface of a part built by an AM system, but also inside the part. The histogram of residual stress obeys approximately the Burr type XII distribution.
- 5. The increase of preheating temperature before the material deposition is indeed favourable for reducing residual stress. This can be validated by AM simulation. However, we can reduce residual stress in another way: adjusting the input power and heating time of each layer. While keeping the total input energy is kept the same as the case without adjustment, we can reduce residual stress with a lower preheat temperature.



## Chapter 4

# Regression between process parameters and residual stress

*In this chapter, we generate a series of data from cases of AM simulations at line-level. Then some regression analysis is conducted to reveal the statistic relation between AM process parameters and the final quality of the product made by additive manufacturing. Artificial neural network and other algorithms are compared as post-processing for data acquired from AM macroscopic simulation.*

## Contents

---

<b>4.1</b>	<b>Influence of multi-parameters on residual stress . . . . .</b>	<b>113</b>
<b>4.2</b>	<b>A basic thermal-mechanical AM simulation of a zigzag line . . . . .</b>	<b>115</b>
<b>4.3</b>	<b>Post-processing of AM simulation with regression . . . . .</b>	<b>120</b>
<b>4.4</b>	<b>Regression implementations . . . . .</b>	<b>122</b>
<b>4.5</b>	<b>Artificial neural network for regression . . . . .</b>	<b>123</b>
4.5.1	Fundamentals of back-propagation algorithm . . . . .	124
4.5.2	Construction of artificial neural network . . . . .	125
4.5.3	Regression after AM simulations . . . . .	126
<b>4.6</b>	<b>Conclusion . . . . .</b>	<b>128</b>

---

In Chapter 3, the relation  $f$  between a part's AM process parameters and its residual stress is studied by simulating several cases. However, the AM process parameters in these cases are subjectively determined and the numbers of cases is also limited. A better understanding of the relation  $f$  will be helpful for us to complete the optimisation of  $f$ . If the global behaviour of  $f$  is known, the reduction of residual stress can be achieved more objectively with the best group of process parameters.

## 4.1 Influence of multi-parameters on residual stress

The quality of the final part made by additive manufacturing involves generally two aspects, its property and shape. In practice, it is relatively easier to monitor the shape quality during or after fabrication, such as distortion and surface roughness. However, measuring directly the mechanical and metallurgical properties of a part is usually non-feasible during the process of AM fabrication. A part with the desired shape may have unsatisfactory properties which are detected after it has been removed outside from AM machine. Hence, foreseeing part's final quality and controlling AM process parameters in time require rich experiences of AM machine operators. A better understanding of the influence of AM parameters on part's quality will help us to facilitate the configuration before fabrication and to realise real-time control on AM machine rapidly[FAR 16].

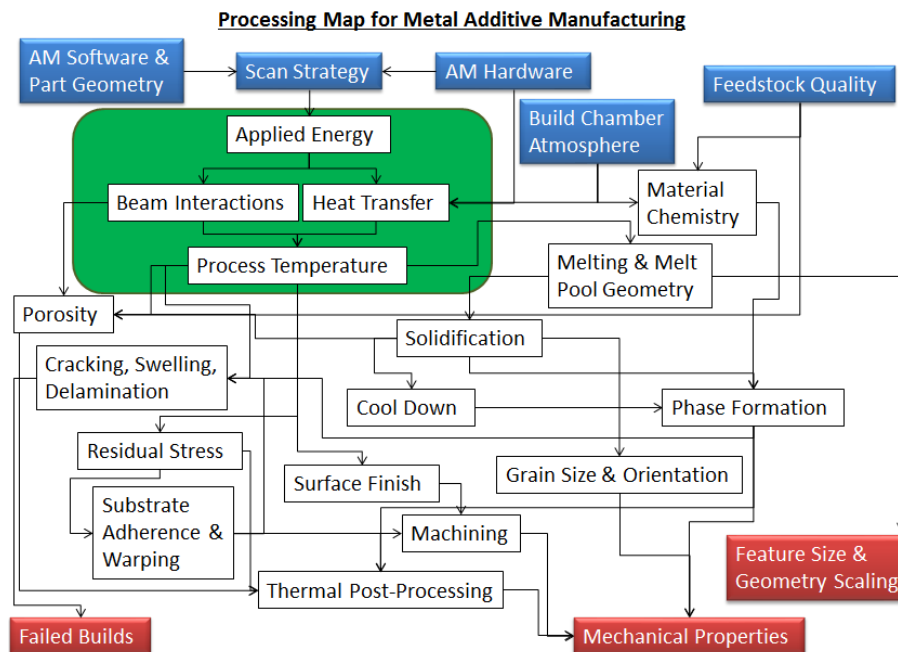


Figure 4.1: Quality control in powder bed fusion[SAM 16]

The residual stress is one of the most important property criteria for the quality control of metallic product in additive manufacturing. In this thesis, we choose the maximum

residual stress as the quality criteria. This work is a simple example of the application of multivariate analysis (MVA) in additive manufacturing. In fact, our methodology of post-processing can be expanded to more AM parameter variables and more criteria of quality. The residual stress depends on different factors in fabrication, mainly in two catalogues as follows:

**material**

The properties of material make a difference in residual stress. Some of them are actually temperature-dependent or state-dependent, such as thermal conductivity, specific heat capacity, density, coefficient of thermal expansion, elastic modulus, yield limit, etc.

**machine process parameters**

Some process parameters on AM machines can impacts residual stress as well, such as heat source power and spot size, scan speed and pattern [HAG 17], layer thickness, support structure, removal manipulation from the substrate, etc.

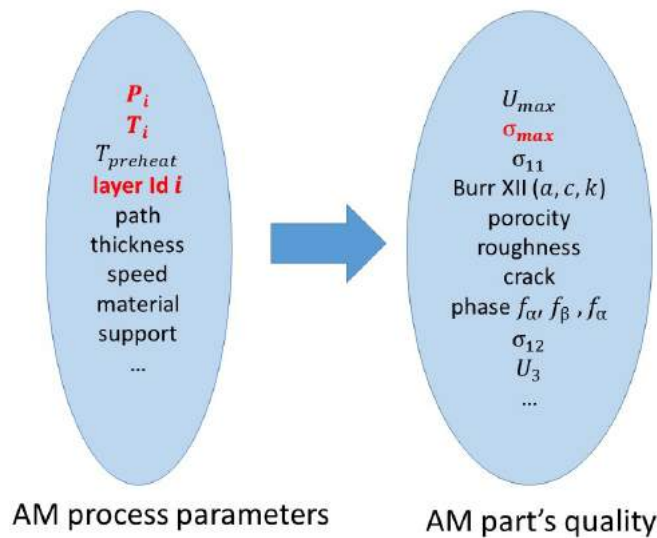


**Figure 4.2:** Influence of process parameters on the final quality of a part in additive manufacturing

In this chapter, we choose the layer label  $i$ , input power  $p_i$ , heating time  $t_i$  as the input AM process parameters. The maximum value of von Mises is chosen as the output AM quality criteria. We will try to use the cases of AM simulation at line level to demonstrate the methodology of establishing the function between the input values  $(i, p_i, t_i)$  and the output value  $(\sigma_{vonmises})$ . The features and problems of this regression-based method can be investigated in this chapter.

Engineers often conduct destructive or non-destructive testing [WIT 07] [WAN 17] to measure the residual stress of the parts made on AM machine. In numerical simulations, the final distribution of residual stress can be acquired virtually as basic post-processing work. This convenience makes it possible to produce virtually and inexpensively a great number of parts with the help of AM macroscopic simulation.

## 4.2 A basic thermal-mechanical AM simulation of a zigzag line

The regression method is often based on a big quantity of data, thus we use a zigzag line as an AM simulation at line-level. This object's AM process is still simulated by birth and death technique. So the methodology can be similarly expanded to simulations at layer-level and at part-level, without the loss of generality. This zigzag line's geometry is relatively simpler than that of a twisted turbine blade. Correspondingly, the zigzag line's simulation (line-level) will spend less time than the blade part (part-level). This change of simulation level is important for us to generate more cases for regression work with limited computational resource.

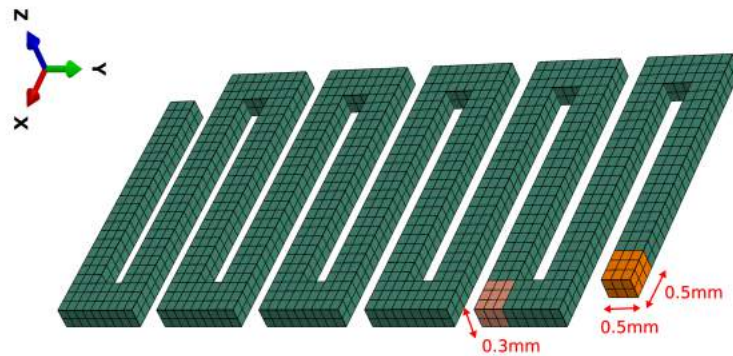


**Figure 4.3:** Detailed view of the zigzag track's mesh

The object that we studied is a zigzag track line in one layer (see Figure 4.3). In this zigzag line, there are 107 depositions. Each material chunk consists of several elements. These chunks will be progressively activated in AM process with birth and death technique. The central deposition zone on the substrate is first preheated to  $200^{\circ}\text{C}$ , then the material is deposited. The activation time for each chunk is  $1.0 \times 10^{-7}\text{s}$ . With the moving volumetric heat source whose input power  $P_{input}$  is  $6 \times 10^{11}\text{W}/\text{m}^3$ , every chunk is activated and heated in  $t = 0.025\text{s}$  one by one before the final cooling to the environment temperature  $20^{\circ}\text{C}$ . As the material in Chapter 3's simulation at layer level, the material in this simulation is steel, whose mechanical properties are shown in Table 3.2 and in the Figure 3.22.

The mesh of this zigzag track line and its substrate is illustrated in Figure 4.5. In the thermal simulation, the element type is DC3D8. In the mechanical simulation, the element type is C3D8R. In terms of boundary conditions, the inferior surface of substrate and its four corners are fixed, as is shown in Figure 4.5.



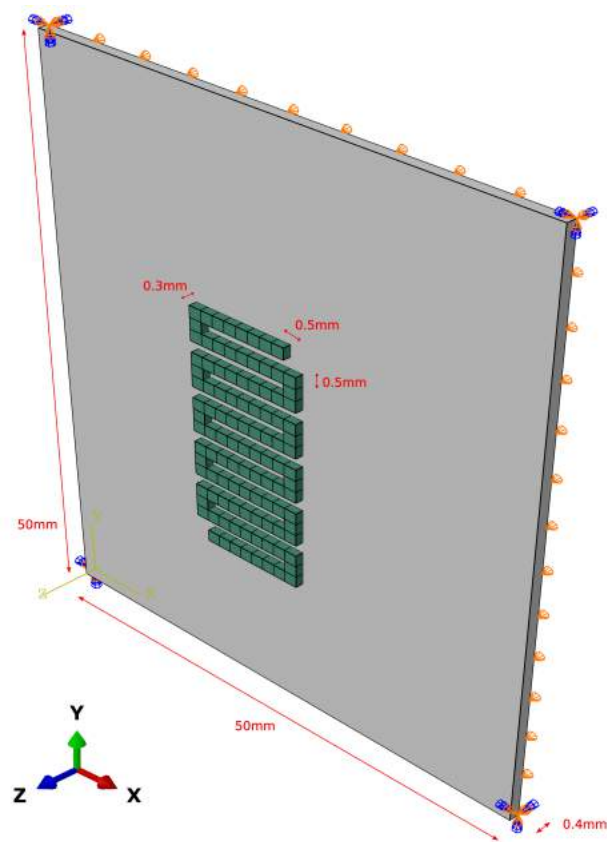


**Figure 4.4:** A zigzag track and its substrate

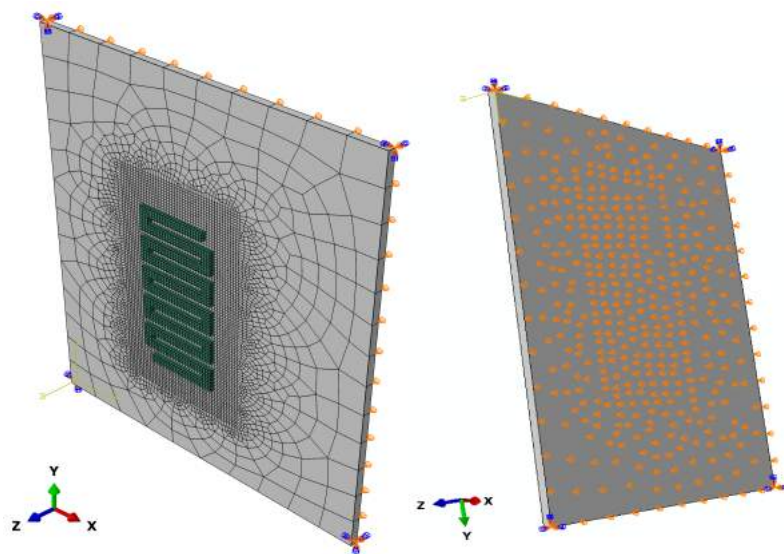
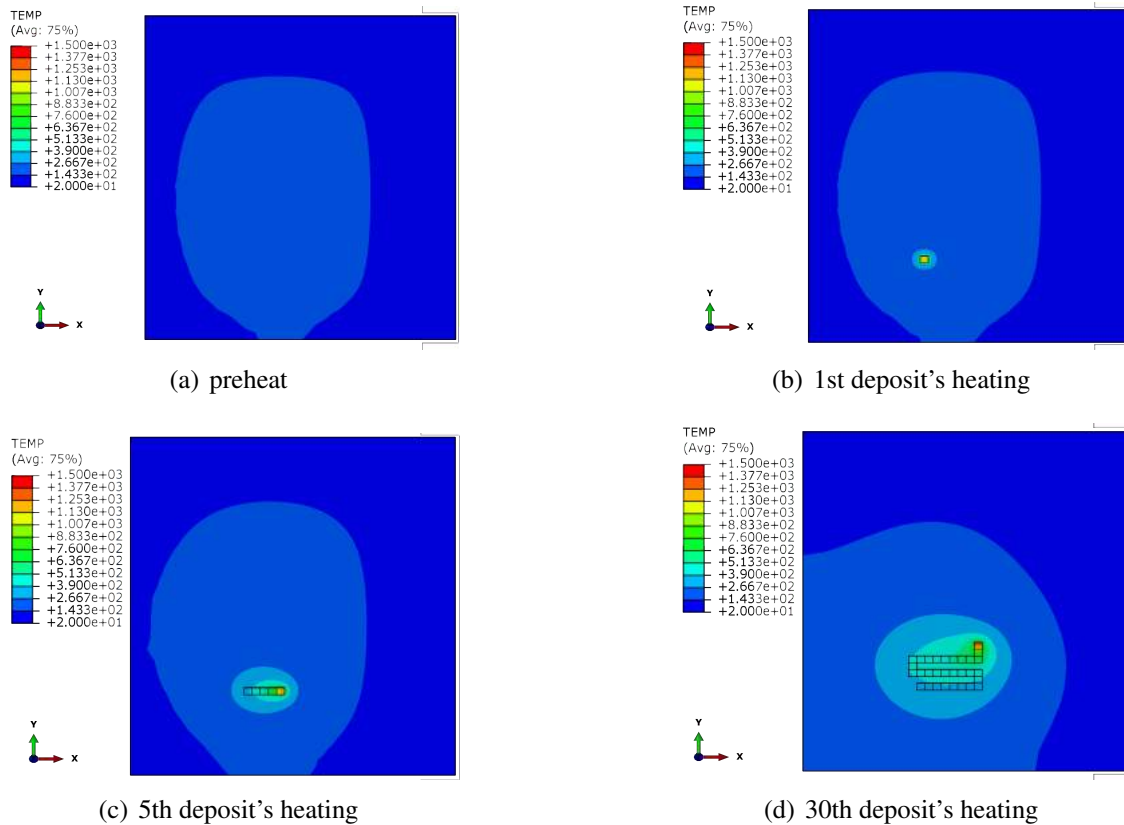


**Figure 4.5:** Mesh and mechanical boundary condition

**Table 4.1:** Steel parameters and some process parameters

Parameter	Value
density $\rho$	$7800\text{kg}/\text{m}^3$
expansion coefficient	$1.6 \times 10^{-5}\text{K}^{-1}$
conductivity $C_d$	$50.0\text{W}/\text{m}/\text{K}$
specific heat $C_p$	$451.0\text{J}/\text{kg}/\text{K}$
scan speed	$0.02\text{m}/\text{s}$
cooling Time	$36000\text{s}$
initial powder temperature	$20^\circ\text{C}$
volumetric heat source	$6 \times 10^{11}\text{W}/\text{m}^3$

In this simulations, we first begin the thermal simulation, then simulate mechanical field using temperature evolution in \*.odb file. Temperature field is the predefined input for mechanical analysis. The AM process can be recorded by a series of screenshots shown in Figure 4.6



#### 4. Regression between process parameters and residual stress

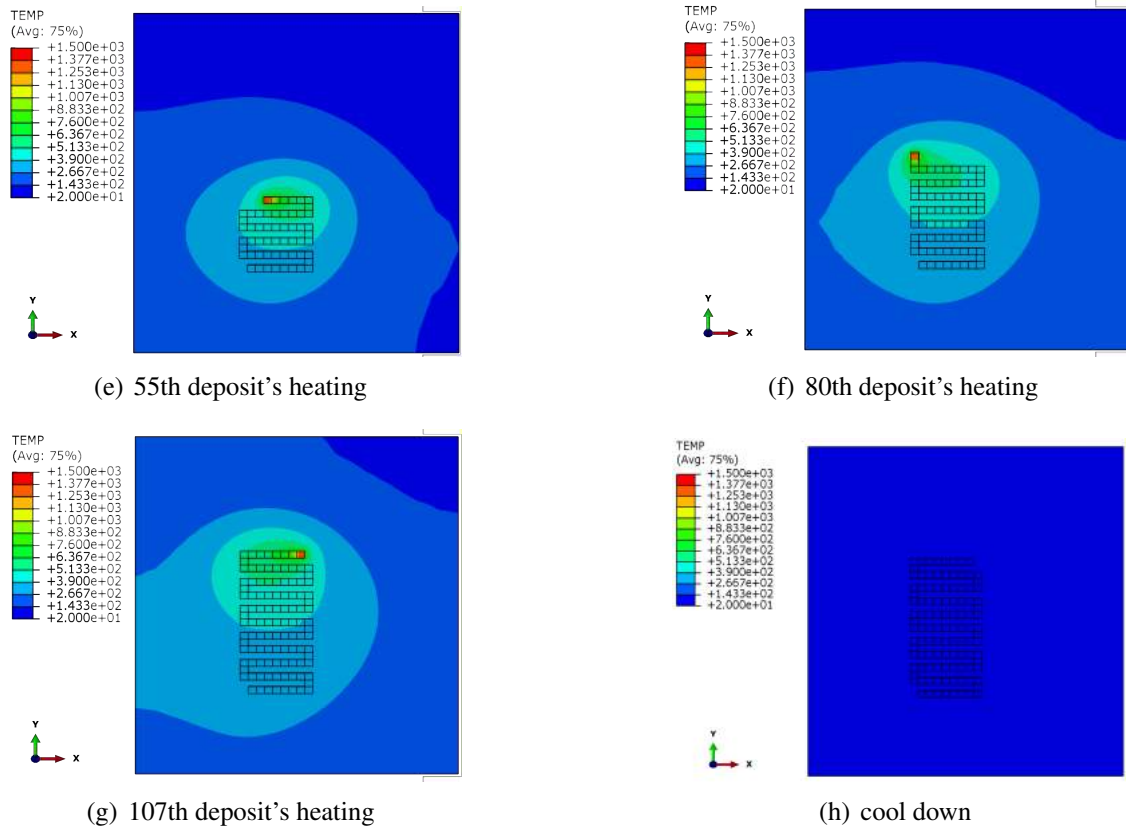


**Figure 4.6:** Screenshots of thermal simulation ( $^{\circ}\text{C}$ ) for a zigzag track in AM process

After this sample's temperature is cooled to environmental temperature, its mechanical field, such as residual stress, can be observed. Figure 4.8 illustrates the residual stress in zigzag line and its substrate. Even though the geometry of zigzag is only one thin layer in this line-level simulation, not a huge part, we can still find the non-homogeneous distribution of stress. In segments of zigzag line, the segments in x direction (8 or 9 chunks) is longer than the segments in y direction (3 chunks). This geometrical difference makes the von Mises stress isn't uniform in chunks of zigzag line. Furthermore, we can find non-isotropic effect in stress distribution if the stress is observed using tensor form in Figure 4.7.

The stress tensor's components are shown in Figure 4.7. Since the Z thickness (0.3mm) of zigzag line is smaller than the length in X and Y. The stress with Z direction  $\sigma_{zz}$ ,  $\sigma_{xz}$ ,  $\sigma_{yz}$  are globally less noticeable. Because of the difference in the lengths of X and Y segments, the normal stress  $\sigma_{xx}$  is more obvious than  $\sigma_{yy}$ . Since the deposition process happens on the xOy surface of the substrate, the shear stress  $\sigma_{xy}$  is severer than the other two shear stress  $\sigma_{xz}$  and  $\sigma_{yz}$ .

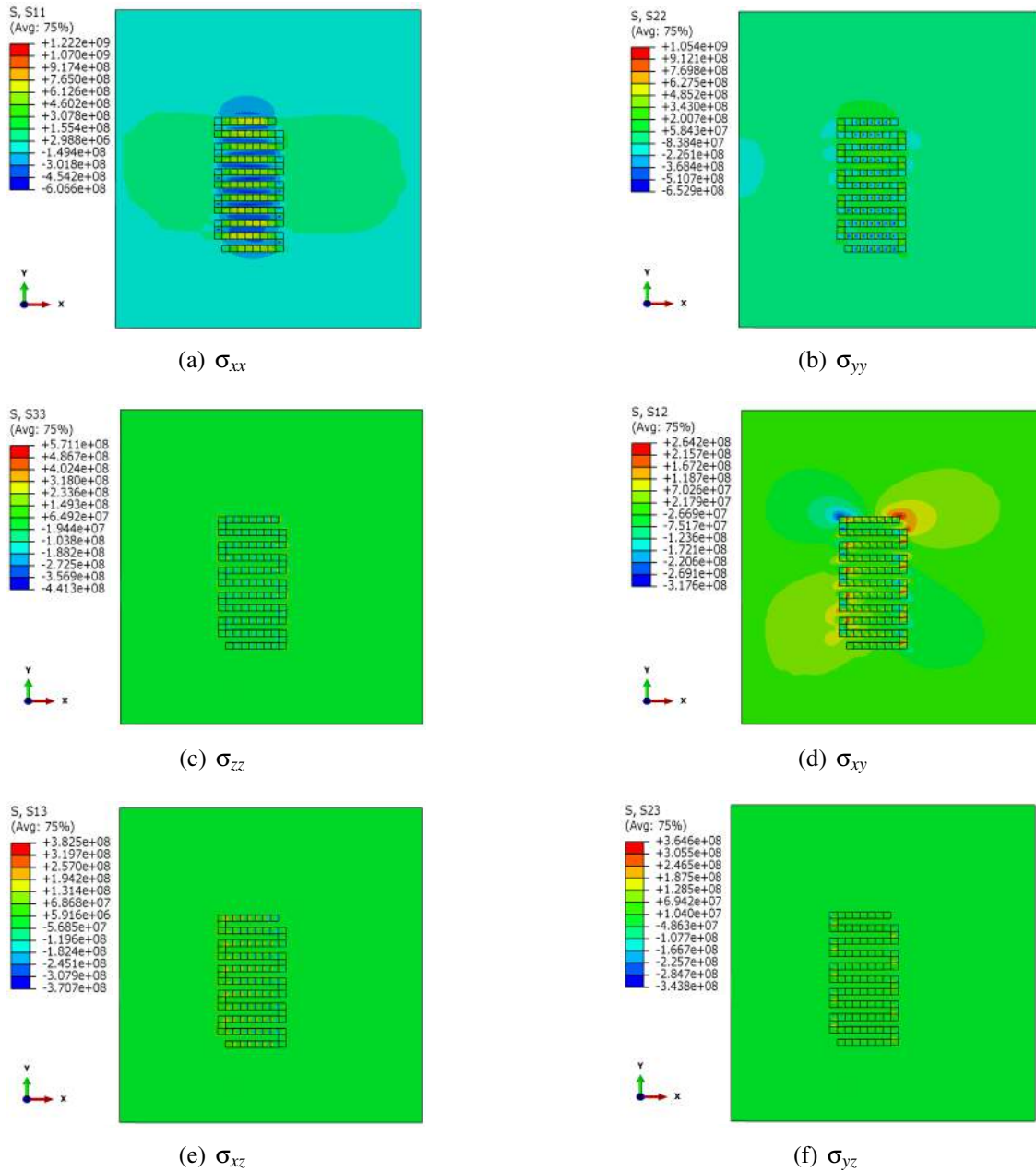


**Figure 4.7:** Residual stress (Pa) as tensor components

Although the mechanical field can be described as different tensor fields. In this work, we choose the von Mises  $\sigma_{Mises}$  stress as the only output data, because we concentrate on a MISO (Multiple input single output) problem instead of the more complex MIMO(multiple input multiple output)[CAO 15] problems.

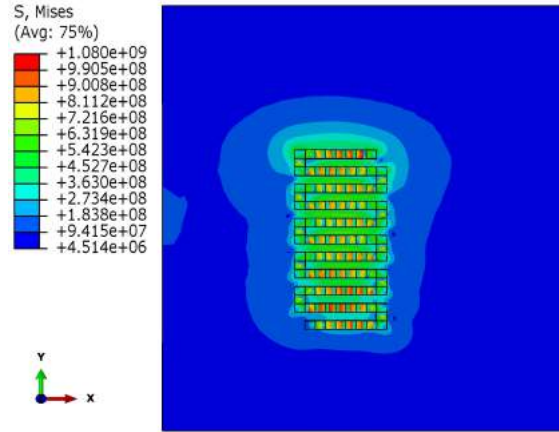


**Figure 4.8:** Residual stress  $\sigma_{vonMises}$  (Pa) for a zigzag track line

### 4.3 Post-processing of AM simulation with regression

Regression analysis is a tool for estimating the relationships among variables from statistical datum [KUB 15]. Sometimes computing the exact value of a dependent variable  $Y$  from the potential independent variables  $X$  is time-consuming or even impossible, if the precise functions between  $X$  and  $Y$  is complex or unknown. For additive manufacturing process where the relation between the final quality of workpiece and AM process parameters, regression analysis can be applied to explore this relation which is probably hardly expressed in normal forms because of the complexity of AM process [GAR 16][CHO 16]. Usually it is unavoidable to carry out lots of experiments or simulations in AM technologies before obtaining a workpiece with satisfactory quality. No matter whether they are built on AM machines or simulated virtually on CAE software, the rejected products aren't useless any more, when their quantity is sufficient for regression analysis. If we can estimating the regression function, the prediction of final quality with a given group of process parameters will be beneficial for AM engineers and researchers, even though we can't acquire direct explanation from this phenomenological forecasting. Based on better understanding the influence of different AM process parameters on workpiece's quality, a guide using regression will facilitate and improve the determining of appropriate process parameters [XIO 14b].

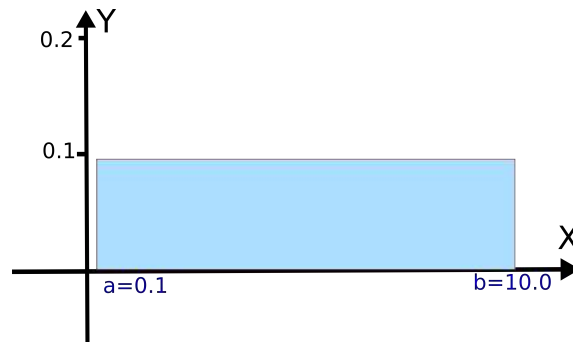
In our study, we used the basic case mentioned in Chapter 4 to simulate the construction of a zigzag line in AM system. Although many process parameters have influences on the final quality of workpiece fabricated by AM technologies, we simplify our AM simulation and only choose some features among them to explain our methodology. For the  $i$ th material deposit, the heat source power  $P_i$  and heating time  $(\Delta t)_i$  for  $i$ th deposit are supposed to vary randomly obeying the following formulae

$$\begin{cases} P_i = P_{set} \exp(u) \\ (\Delta t)_i = (\Delta t)_{set} \exp(u) \end{cases} \quad (4.1)$$

**Table 4.2:** The input parameters and output criteria in 1 time of AM simulation

Input processing parameters	deposit $i$	power $P_i$	heating time $t_i$
	1	$P_1$	$\Delta t_1$
	2	$P_2$	$\Delta t_2$
	3	$P_3$	$\Delta t_3$
	...	...	...
107	$P_{107}$	$\Delta t_{107}$	
Output quality criteria		$\sigma_{max}$	

where  $P_{set} = 6 \times 10^{11} W/m^3$  and  $(\Delta t)_{set} = 0.0125s$  are two predefined values of heat source power and heating time,  $u$  is a random variable which obeys the uniform distribution  $U[a, b]$  ( $u \sim U[a, b]$ ),  $a$  equals to 0.1 and  $b$  equals to 10.0. The probability density function (PDF) of this uniform distribution  $U[0.1, 10.0]$  is illustrated in the Figure 4.9.


**Figure 4.9:** PDF of the uniform distribution  $U[0.1, 10.0]$ 

The continuous random variable  $u$  can be automatically generated by Python codes (the library numpy). This generation of random variable  $u$  obeys the expression between the probability  $p$  and its value  $u$  as following:

$$p(u < x) = \begin{cases} 0, & \text{for } x < 0.1 \\ \frac{x-0.1}{10.0-0.1}, & \text{for } 0.1 \leq x \leq 10.0 \\ 1, & \text{for } x > 10.0 \end{cases} \quad (4.2)$$

According this description in  $[0.1, 10.0]$ , this uniform random variable  $u$  has the same probability of appearance in two intervals which have the same lengths. This can be observed by calculating the definite integral in Figure 4.9.

Naturally, these two AM process parameters (power and heating time) can be considered as two features of a deposit. The order of material deposition  $i$  in AM may also impact on workpiece's final quality, since the locations of deposits are different on one layer where heat accumulation effect is heterogeneous in one hatch line. The heat transfer history of each deposit leads to the non-uniform thermal and mechanical fields. As

a result, we take the order of each deposit into account as the third feature of a deposit. In total, this AM simulation's input variables are the  $3N = 321$  processing parameters if there are  $N = 107$  chunks in a hatch line. In the  $L$ th experiment or simulation ( $L$  is a label for one simulation), we can define

$$X_L = \{i, P_i, (\Delta t)_i\} = \{X_i\} \quad \text{for } i = 1, 2, 3, \dots, 107 \quad (4.3)$$

The final quality of a workpiece in additive manufacturing includes residual stress, max strain, metallurgical micro-structure, etc. In our study, we extract the max value of residual stress  $\sigma_{max}$  as the criterion of quality after finishing the whole AM simulation. Thus we define in the  $k$ th experiment of simulation

$$Y_L = (\sigma_{max})_L \quad (4.4)$$

In fact, determining AM process parameters is normally a problem of multi-objective optimization. Because our methodology can be expanded to more complex situations, with loss of generality, here we simplify the output variables of AM system by extract only residual stress.

## 4.4 Regression implementations

There is some open-source software for regression analysis [GÉR 17]. With the help of them, researchers are capable of completing regression analysis more easily and avoiding concentrating on the detail of code implementation.

Scikit-learn is a python library for machine learning. This library includes many kinds of algorithms for classification, clustering and regression. Tensorflow, written in C++, python, CUDA programming languages, is a symbolic math library used for machine learning applications. In Tensorflow, generalized back-propagation algorithm is implemented facilitating the generation of artificial neural networks (ANN). Keras is a python interface of TensorFlow's core library with better user-friendliness.

Normally, the linear regression based on least square method is broadly applied. However, our regression problem for additive manufacturing may not belong to the generalized linear model. In addition, the AM process parameters include two types, categorical and numerical. These types correspond to the Boolean/string and integer/float types in code. This mixture of data types makes the regression analysis more complex. Consequently, we also attempt to apply other approaches for regression including Support Vector Regression (SVR), Decision Tree, Random Forest, Adaptive Boosting (AdaBoost), Gradient Boosting, k-nearest neighbours algorithm(k-NN) [MÜL 16]. Even though the sample population is the same, different regression approaches result in obviously different performances. As a kind of post-process of AM simulation, regression analysis is able to find which AM parameter has the most of influence on the final quality since the weights of parameters are calculated.



## 4.5 Artificial neural network for regression

Artificial neural network (ANN) is a computing technique [BAS 00] for tasks where the prior knowledge isn't sufficient about a system with complex behaviours[ÖZE 05][ACH 11][LIU 00][KAR 09]. It is often difficult to describe the influences of AM process parameters on the final quality of workpiece since the multi-variables problems involves the complicated interactions of different process parameter [DIN 16c]. Some researchers have attempted to use this technique in data analysis after AM experiments [DIN 16b][GAR 15]. In our study, we attempt to establish an ANN and to estimate the regression model from datum generated by AM simulation. In ANN, an artificial neuron which receives one or more input signals can calculate the responding output signal. When the responding output value exceeds the threshold, this artificial neuron will transmit the signal to its neighbour neuron according to its connection edges. An artificial neural network consists normally at least three layers: input layer, hidden layer, and output layer. Different layers include different numbers of artificial neurons and the rules of signal transformation  $\phi$  in each layer are also different.

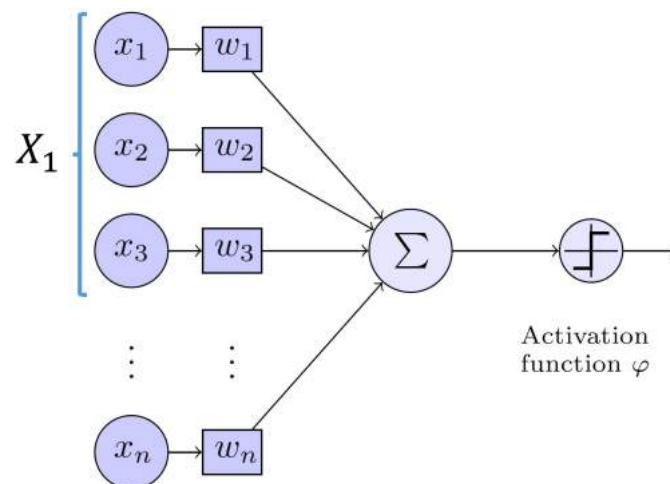


**Figure 4.10:** Basic structure of an artificial neuron

The figure above is the basic structure of an artificial neuron. For the case in this thesis, we can take an example of the input layer and one neuron in the 1st hidden layer.  $n$  equals  $3 \times N = 321$ .  $x_j$  represents the AM processing parameters. For the 1st chunk in the zigzag line, three variables  $x_1 = 1$ ,  $x_2 = P_1$ ,  $x_3 = (\Delta t)_1$  constitute the variable  $X_1$ . The information of 107 chunks, from  $X_1 = \{x_1, x_2, x_3\}$  to  $X_{107} = \{x_{319}, x_{320}, x_{321}\}$ , will be captured by this neuron.

An artificial neuron is a mathematical function receiving aggregated signal inputs. Each input has a weight. The artificial neuron sums its inputs with weight and the sum is passed into an activation function. The activation function is a differentiable non-linear



function which is used to detect if the weighted sum exceeds the predetermined threshold.

$$o_k = \Phi \left( \sum_{j=1}^m w_{kj} x_j \right) \quad (4.5)$$

In this thesis, we adopt the Rectified Linear Unit (ReLU) function[DAH 13] as the activation function. This ReLU function can be also replaced by other functions easily in Tensorflow codes.

In the learning's forward propagation process, the input signal traverses the hidden layers from the input layer, then it arrives to the output layer. The value of output  $\tilde{Y}$  estimated from the training set isn't equal to the true value  $Y$  obtained from experiments or simulations. A loss function  $\zeta$  is defined using the mean squared error (MSE) as follows:

$$\zeta = \frac{1}{2} (Y - \tilde{Y})^2 \quad (4.6)$$

Mathematically, the learning by ANN becomes an optimization problem whose objective is to find the minimum of loss function. This optimization can be solved by the gradient descent algorithm based on back-propagation (BP) technique.

#### 4.5.1 Fundamentals of back-propagation algorithm

In artificial neural network, we need to calculate the gradient of loss function with respect to the weight, then the weight can be adjusted according to this gradient. This is the fundamental algorithm of back-propagation method[MEL 18]. Calculating the gradient of loss can be realized by using the chain rule of partial derivative when the activation function of each artificial neuron is predefined.

$$\frac{\partial \zeta}{\partial w_{ij}} = \frac{\partial \zeta}{\partial o_j} \frac{\partial o_j}{\partial s_j} \frac{\partial s_j}{\partial w_{ij}} \quad (4.7)$$

In Equation 4.7 above, the weighted sum at the  $j$ th node is

$$s_j = \sum_{k=1}^K w_{kj} o_k \quad (4.8)$$

where  $o_k$  is the output value of  $k$ th nodes in precedent layer and this precedent layer has  $K$  neutral nodes.

In Equation 4.7, the output value of the the  $j$ th node is define as

$$o_j = \Phi(s_j) \quad (4.9)$$

The weight  $w_{ij}$  will be updated by gradient descent algorithm.

$$\Delta w_{ij} = -\eta \frac{\partial \zeta}{\partial w_{ij}} \quad (4.10)$$

In the formula, the learning rate  $\eta$  is of importance for the learning of ANN. If it is too large, the missing of minimum may occur. Nevertheless, the training may become unacceptably slow. The choice of  $\eta$  can be achieved using an adaptive learning rate when necessary. The repeating weight modification can reduce the loss when the number of iteration is abundant.

#### 4.5.2 Construction of artificial neural network

In our AM simulation, we choose the power and heating time of each deposit as the input of a sample pair. However, the orders of magnitude are different for these two parameters. In order to improve the performance of back-propagation algorithm, we accomplish the normalization of data  $z$  before the ANN learning.

$$z^* = \frac{z - z_{min}}{z_{max} - z_{min}} \quad (4.11)$$

where  $z$  represents the original value of a kind of feature in one of the AM simulations. For example, we can normalise the original power  $P$  into  $P^*$  after finding the extreme values  $P_{max}$  and  $P_{min}$  among  $P_1, P_2, P_3, \dots, P_{107}$ :

$$P_i^* = \frac{P_i - P_{min}}{P_{max} - P_{min}} \quad (4.12)$$

Similarly, the other features, such as the heating time and the stress, can also be normalised in this way before the regression operation.

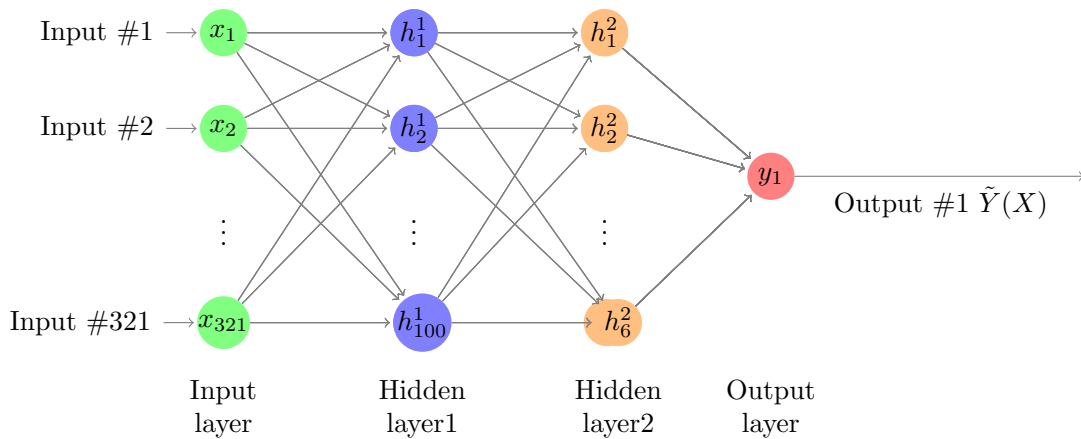


**Figure 4.11:** Artificial neural network with multiple neurons and layers

The AM process parameters and the maximum of residual stress compose an input-output pair in an AM simulation. When input value is modified for every AM simulation

and the repeated mapping  $X \mapsto Y$  will create samples constituting the statistical population  $(X, Y)$  for supervised learning after  $M = 120$  times simulations is the dataset of 120 groups of mapping:

$$\begin{cases} f : & (X_1, X_2, X_3, \dots, X_c, \dots, X_{107})_k \mapsto Y_k \quad \text{for } k = 1, 2, 3, \dots, 120 \\ \tilde{f} : & (X_1, X_2, X_3, \dots, X_c, \dots, X_{107})_k \mapsto \tilde{Y}_k \quad \text{for } k = 1, 2, 3, \dots, 120 \end{cases} \quad (4.13)$$

where  $X_c$  is the process parameters of the  $c$ th chunk in the zigzag line and  $\tilde{Y}_k$  is the predicted value of  $Y_k$ . The regression is a task of fitting the real relation  $f$  by the predicted regression relation  $\tilde{f}$  while the real relation  $f$  can't be obtained easily and directly by traditional manner.

These 120 samples are independent between each other. The total sampling population  $(X, Y)$  will be stochastically split into at least two data sets: the training set (normally 70% of the total population), the validation dataset/testing dataset. After the partition of population, we can use the cross-validation technique to avoid over-fitting problems and to generalize the regression model to an unknown dataset. First, the training of regression is run only on training and we acquire a predictive model  $\tilde{f}$ . Then this model will be tested on the validation dataset. After observing the model's ability to predict new data which doesn't participate in estimating before, we can estimate how accurately our regression model will perform in practice.

### 4.5.3 Regression after AM simulations

In this thesis, we create a dataset after 120 simulations with different input process parameters. We first use Keras (Tensorflow) to establish an artificial neural network of two hidden layers (100 neurons for the 1st hidden layer and 6 neurons for the 2nd hidden layer) for post-processing. The prediction is shown in Figure 4.12, the scatter points of dataset (predicted value  $\tilde{Y}$ -true value  $Y$ ) aggregates weakly around the standard line (true value  $Y$ -true value  $Y$ ).

Next, we use Scikit-learning to conduct some other regression algorithms for the dataset from AM simulations. In fact, there are already many kinds of regression algorithms, such as linear regression, support vector regression (SVR), random forest, gradient boosting, decision tree, and adaptive boosting (AdaBoost), etc. These algorithms can be easily implemented using Scikit-learning codes and then be evaluated automatically with a score. It is obvious that the performances of these algorithms are different in Figure 4.13 even though they use the same dataset. Only the testing dataset (30% of the total dataset) is used here to evaluate the performance of algorithms, we compare the true value  $Y$  (in green) and predicted value  $\tilde{Y}$  (in red) of each data point.

Note that we apply the cross-validation technique here, the performances of one algorithm may vary in two evaluations. This work reveals the importance of the choice of regression algorithms. In AM simulation's post-processing, researchers should be careful and try to compare different algorithms for the same dataset before acquiring a credible correlation.

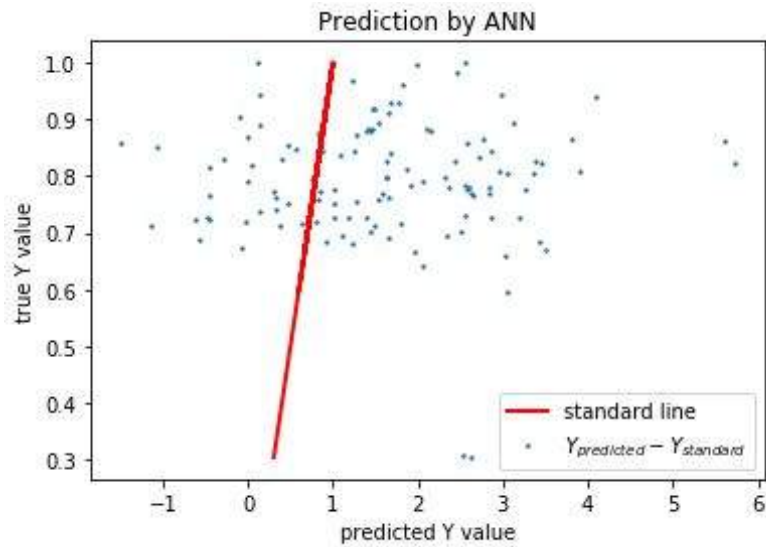


**Figure 4.12:** Regression using artificial neural network in Tensorflow

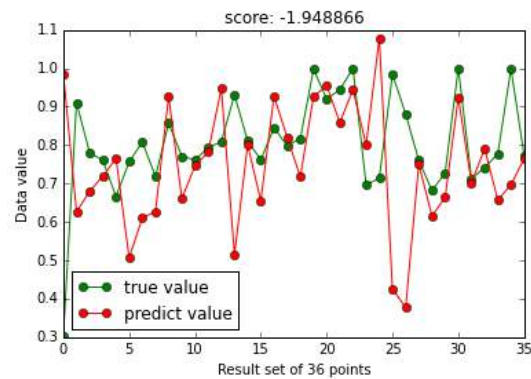
Although we didn't acquire an excellent correlation curve in these regressions, there are still some interesting details in this work. With some improvements in both simulation and regression post-processing, our basic methodology can be expanded to other studies of multi-objective optimization problems in additive manufacturing.

First, we generate the dataset from AM simulations using the expression of Equation 4.1, in order to enlarge the cover range of AM process parameters  $P$  and  $\Delta t$  for the problem of optimization. However, the probability distributions of  $P$  and  $\Delta t$  don't mathematically obey the uniform distribution, even though  $u$  is a uniform random variable. Because of this generation method for the dataset, the scatter points are relatively far from the standard line in Figure 4.12. In fact, the fluctuation of process parameters in an automatic control problem often obeys the Gaussian distribution, according to the law of large numbers in statistics. This is the case more universal in AM experiments.

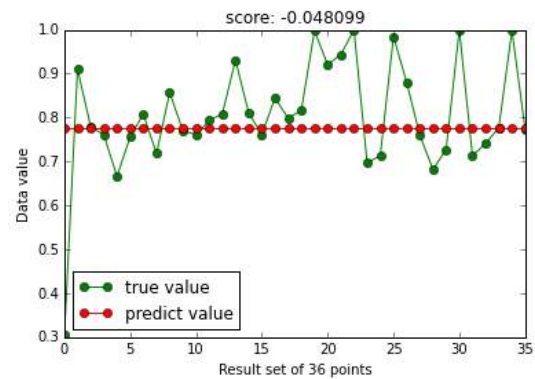
Second, we use the results from  $M = 120$  times of AM simulations, and this number of samples is relatively insufficient for a precise regression analysis[DIN 16b][GAR 15].

Third, the cross-validation technique is applied in our evaluation. This technique is helpful for avoiding overfitting problems in supervised learning but it's stricter than the normal regression evaluation. Last, there are still some mathematical problems for ANN. In this black-box-like method, we use an input data  $X$  with 321 parameters to indicate the scheme of multi-parameters regression. However, the numerous parameters may also lead to some severe problems in the ANN method, which are still being studied by researchers currently.

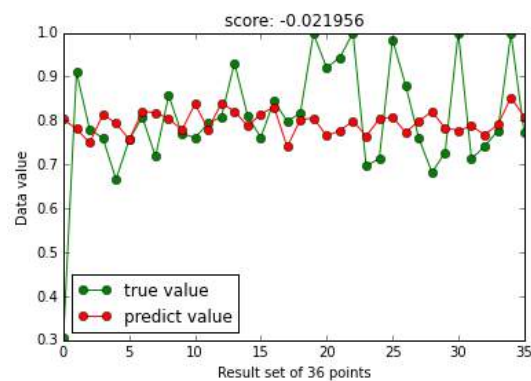
## 4. Regression between process parameters and residual stress



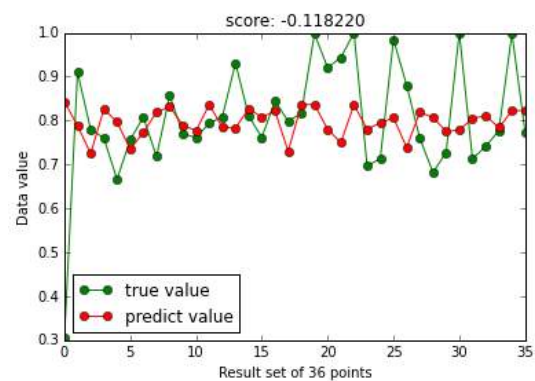
(a) Linear regression



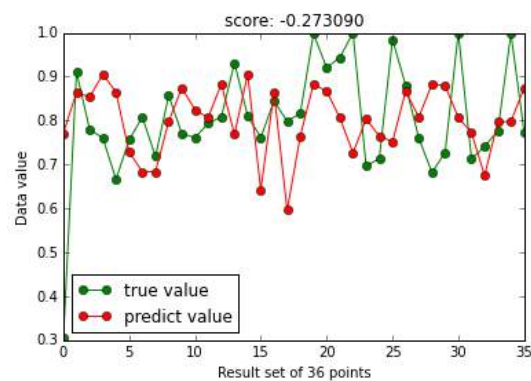
(b) Support Vector Regression (SVR)



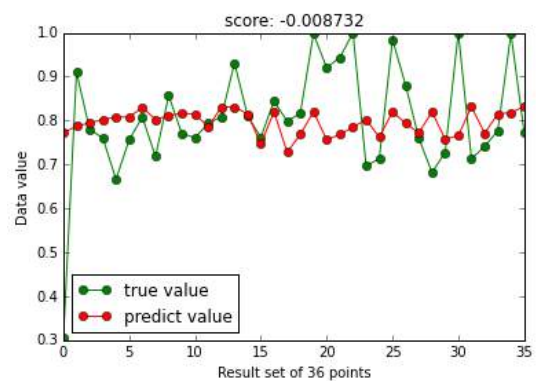
(c) Random Forest



(d) Gradient Boosting



(e) Decision Tree



(f) Adaptive Boosting (AdaBoost)

**Figure 4.13:** Regression using different algorithms in Scikit-learn

## 4.6 Conclusion

In this chapter, the study of a zigzag track line's AM process is performed at line level. This work is a simple benchmark to explain the regression-based methodology that we can

analyse part's residual stress and its potentially dependent factors. The main conclusions are the following :

- 1. The non-isotropic effect is observed in the final stress field of AM simulation. Even though the zigzag line is a simple geometry in only one layer, its stress tensor components are different because of the difference of its edge lengths and thickness in three X, Y, Z axes.
- 2. We investigate the relation between the maximum residual stress of part  $\sigma_{max}$  and three process parameters (deposition order  $i$ , heat source power  $P_i$  and heating time  $(\Delta t)_i$ ) during the  $i$ th material deposition. In order to obtain the phenomenological relation between residual stress and its dependent parameters, we apply the artificial neural network and other regression algorithms in this thesis. The performances of these algorithms are quite different after training. This indicates the importance of the prudential choice of regression algorithm before the application of this kind approach.



## Chapter 5

# Simulation for the control of the process in additive manufacturing

*In this chapter, the evolution of temperature in an AM thermal field is simulated to demonstrate the feasibility of simulating the feedback control loop in additive manufacturing. PID controller and its parameter auto-tuning are investigated by iterations of calculating and post-processing.*



## Contents

---

<b>5.1</b>	<b>Preparation for the study of AM thermal system's control . . . . .</b>	<b>133</b>
<b>5.2</b>	<b>PID controller in feedback loop . . . . .</b>	<b>139</b>
<b>5.3</b>	<b>AM simulation with PID power controller for temperature . . . . .</b>	<b>142</b>
<b>5.4</b>	<b>PID parameters tuning . . . . .</b>	<b>143</b>
5.4.1	Manual PID tuning . . . . .	143
5.4.2	Auto-tuning . . . . .	143
<b>5.5</b>	<b>Conclusion . . . . .</b>	<b>149</b>

---

In Chapter 3, we find the process parameters have influences on the final residual stress of a part printed by additive manufacturing. This implies the potential technique to reduce residual stress by controlling the AM process parameters instead of increase the preheat temperature. In Chapter 4, we try some regression-based methods to discovery more quantitatively the relation between AM process parameters and the residual stress. In this chapter, we will study the temperature control in additive manufacturing by macroscopic AM simulation. For realizing this new technique of residual stress reduction in real AM machine, a better understanding of this unavoidable problem of temperature control is of great importance.

## 5.1 Preparation for the study of AM thermal system's control

The control of additive manufacturing machine plays an important role in the final quality of workpiece[XIO 16][DEV 16][MAH 14]. The predefined processing parameter configurations in most of AM machine are obeyed during the manufacturing without real-time correction. However, it is possible for some AM machines to adjust process parameters according to the real-time result[EVE 16]. The process monitor of AM process is one of the most significant modules for sophisticated industrial metal AM systems[WEI 14], such as LENS (see Figure 5.1). With the help of control loop, the advanced AM machine can modify automatically some parameters[XIO 14a] to better respond to the perturbation which isn't foreseen before workpiece's AM building.

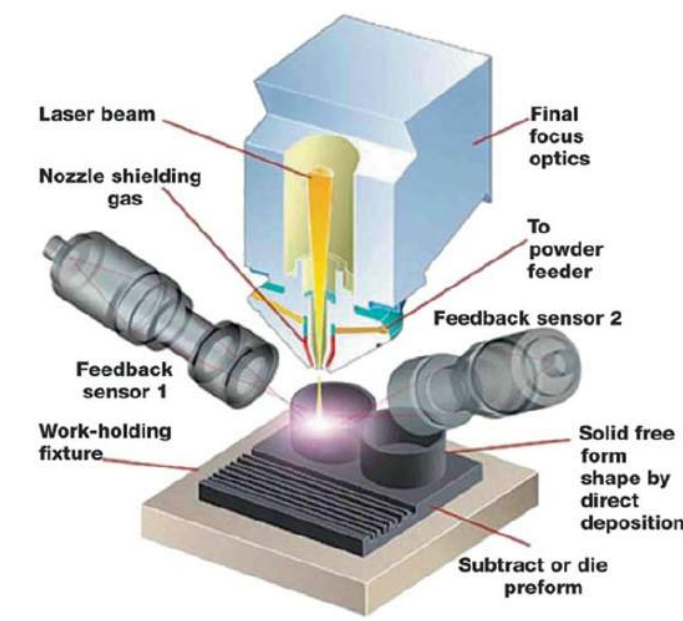


**Figure 5.1:** Powder-injection based AM system (LENS)[GU 15]

## 5. Simulation for the control of the process in additive manufacturing

Among the processing parameters of additive manufacturing, as is shown in Figure 5.2, the heat source power and heating time are two of adjustable factors most feasible in industrial practice [LEE 16][HU 03]. Generally in AM machine, the power control device has faster responding speed than mechanical modules, as mechanical modules like material jetting nozzle often have inertia effect. For powder bed based AM system, the deposition of powder layer and powder melting/sintering doesn't synchronize and laser or electron beam power controlled by an electric circuit is almost the only corrigible factor in one layer's building procedure. The other factor like shield gas temperature is hardly regulated during AM process. In our study, we concentrate on the AM process simulation for the close-loop control of power, which will be helpful to understand better the behaviour of a control loop before the real manufacturing on AM machines. Our investigation is one of the examples demonstrating the value of AM process simulation in macro scale because of its potential to reduce the expense of real AM experiments.

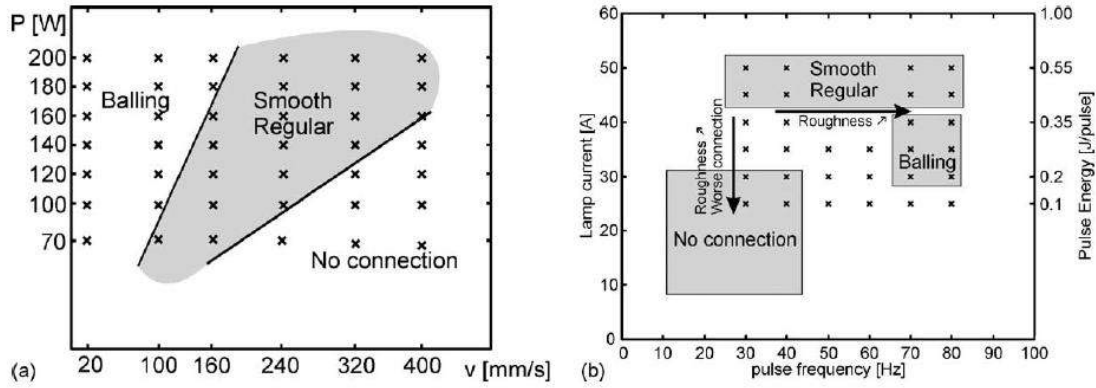


**Figure 5.2:** Influence of process parameters (Heat source control) on the quality of component made by AM [VAN 13]

The further proposal of control AM process is a MIMO (multiple input multiple output) problem [CAO 15]. The law control for some thermal fields, such as the temperature gradient (to calculate it, temperature field should be captured at least two points), is complex and indirect. As is shown in a simple example, the initial temperature fields in Figure 5.3(a) and Figure 5.3(b) are the same, the left side is cooler than the right side. Nevertheless their scan paths are different. A formula of temperature gradient between two points A and B is defined as:

$$\left( \frac{\partial T(t)}{\partial \mathbf{x}} \right)_{AB} = \frac{T_A(t) - T_B(t)}{x_A - x_B} \mathbf{i} + \frac{T_A(t) - T_B(t)}{y_A - y_B} \mathbf{j} \quad (5.1)$$

where  $(x_A, y_A)$  and  $(x_B, y_B)$  are the coordinates of points A and B,  $T_A(t)$  and  $T_B(t)$  are their temperature at the instant  $t$ .

If we want to reduce the temperature gradient  $\partial T(t)/\partial \mathbf{x}$  between the points A and B, the next input power in Figure (b) should be increased while the next input power in

Figure (a) should be decreased. From this example, we can understand that the control law of overall fields is not only temporal but also spatial. Additionally, there are also some hardware difficulties for AM machines to capture the overall field of an AM being built. The camera is now able to capture the temperature in the narrow melting zone around the laser focus. This temperature is an one-point datum, not the data for a surface or a volume. The control of one point's temperature is fundamental and unavoidable for the further whole thermal field control.

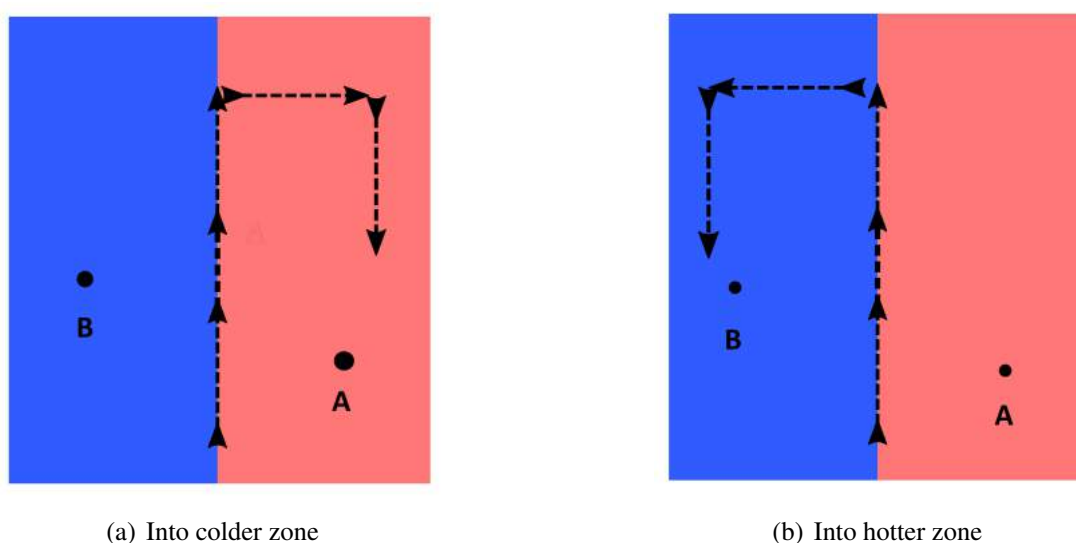


**Figure 5.3:** Whole field (multiple points)'s control depends on scan path for an AM system

In this chapter, we concentrate on a SISO (single input and single output) problem as a basic step for the research in the control of AM system. This is a control problem of one point: The input value is the power for each deposition, and the output value is the corresponding maximum temperature of each melt deposition. Furthermore, this work isn't only important for reducing residual stress, but also quite practical for avoiding the phenomenon of balling effect and lack of fusion, which are introduced in Chapter 1. The control of melting temperature will be helpful to ameliorate the shape quality and property of an AM object.

We simulate the AM building process of a zigzag track line in one layer, where each material deposit in this line consists of several elements (see Figure 4.3 and Figure 4.6). It is the same thermal simulation case which we have already used in Chapter 4. Although this simulation is quite straightforward, it can sufficiently indicate the feasibility of our idea and can be expanded to more complex case of layer-level or part-level AM simulation.

The intrinsic property of a system has influences on the implementation of a control loop. Most of the classic control theories are based on LTI (linear time invariant) system.

For LTI systems, there are already many mathematical tools for its control, such as Fourier transform and Laplace transform, etc. These tools are also integrated into software like Simulink.



**Figure 5.4:** Difference in temporal response between LTI system and non-LTI system

One of the differences between LTI systems and non-LTI systems is the time invariance (see Figure 5.4). In an LTI system, whether we apply an input to the system now or a delay  $\tau$  from now, the output will be identical except for a time delay of  $\tau$ . If the output due to input power  $P(t)$  is the temperature  $T(t)$ , then the output temperature due to input power  $P(t + \tau)$  is  $T(t + \tau)$ . Therefore, the system is time invariant because the output does not depend on the particular time the input is applied. We use a group of input power to verify whether this simple AM system is an LTI system. The open-loop structure of this simulation is shown in Figure 5.5. Using the zigzag model, some simulations at line-level are studied to discover the behaviour of AM system.

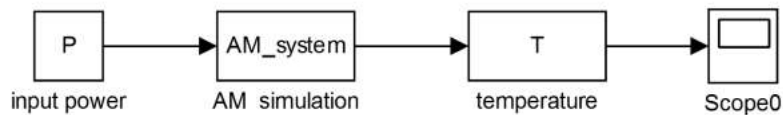
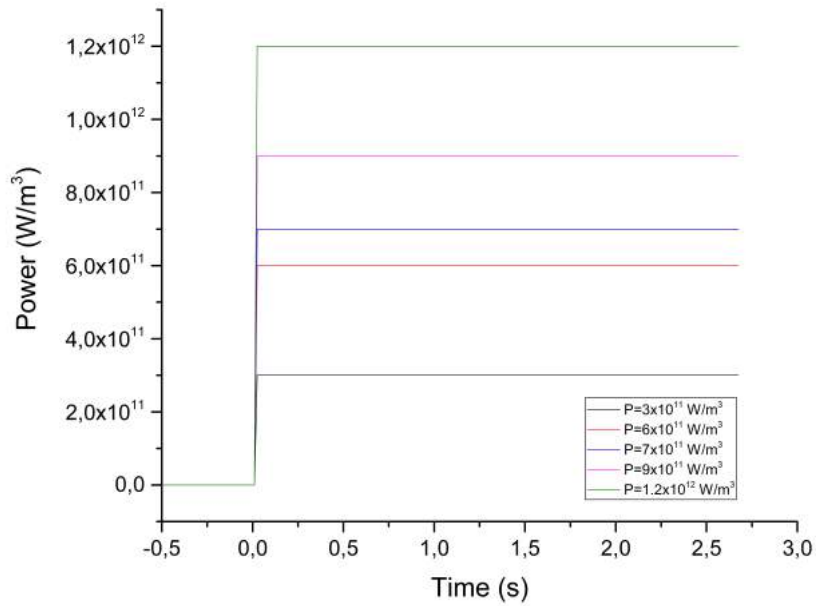


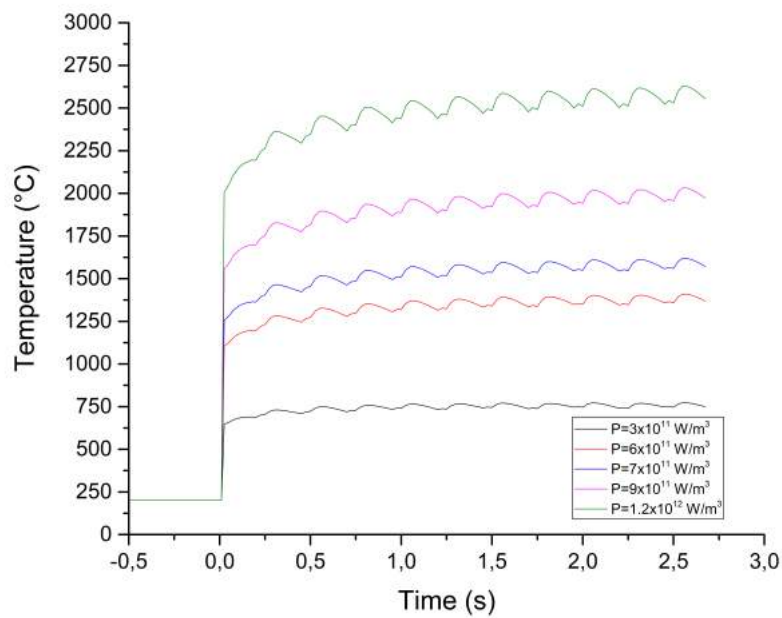
**Figure 5.5:** Block diagram of an open-loop AM system

From Figure 5.6(a), we observed the responding output temperature under different input power (see Figure 5.6). Different step functions are used as input powers ( $3.0 \times 10^{11} \text{W/m}^3$ ,  $6.0 \times 10^{11} \text{W/m}^3$ ,  $7.0 \times 10^{11} \text{W/m}^3$ ,  $9.0 \times 10^{11} \text{W/m}^3$ ,  $1.2 \times 10^{12} \text{W/m}^3$ ) for the same geometry. For one input curve, the value retains constant during the deposition of 107 chunks. However, its output temperature response isn't constant and it varies with the AM building process. We can find the output temperature curves have always fluctuations. The higher the input power, the severer this fluctuation will be. This fluctuating curve demonstrates obviously that this AM system isn't an LTI system, even though its geometry structure is quite simple.

In fact, real systems are usually more complex as they are exactly non-LTI systems, which makes it difficult to implement the control loop in practice. For most of the heating cases such as a furnace, the heat transfer obeys normally process model which has delay effect in the time since it is usually a relatively slow process. However, we adopt a high value of input power to simulate the laser heat source whose power density is much higher than a furnace. The delay effect is relatively weak.



(a) Input powers



(b) Responding output temperature

**Figure 5.6:** 5 simulations for the open-loop AM system

The output curve Figure 5.6(b) is not a strict constant. This can be explained by the complexity of AM process. First, this curve can't reach its maximum value immediately because of the substrate effect. At the beginning of the deposition, the substrate's temperature is only 200 °C, much lower than the heated chunk, This temperature difference makes the conduction more remarkable between the deposited chunk and the substrate.

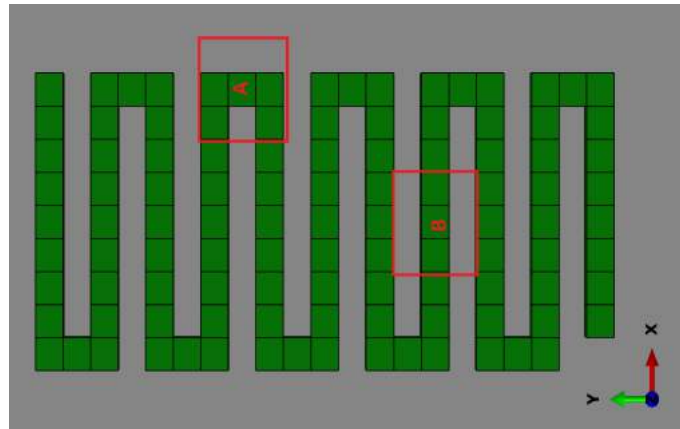


**Figure 5.7:** The difference of crowdedness for two deposits

Second, the zigzag line's geometry also has influences on the heating process. The temperature of one deposition depends on its position in the zigzag line, especially its crowdedness with its neighbour depositions. For example, we take a square (1.5mm × 1.5mm) to study the crowdedness along the zigzag line (see Figure 5.7). 2 neighbour chunks are around the deposit B in its square while 4 chunks surround the deposit A. This crowdedness leads to different heat accumulation effect in two squares, so the temperature reach a maximal value at the deposit A (the material in this square is heated 5 times) and the B deposit 's temperature (material is heated 3 times its square) is one of minimal value in the curve. In total, the substrate effect and geometrical crowdedness effect makes the AM system non-LTI with notable fluctuation.

After measuring and recording the temperature of new deposit after each deposition, we will find this temperature may vary during the whole AM process without feedback control. The temperature distribution around a new deposit will change because of the complex thermal transfer in additive manufacturing. Suppose that the power absorbed by new deposit is always unique, the new deposit laid on the location where the magnitude of accumulated heat is higher has naturally a higher temperature. If the power can be flexibly regulated according to the temperature of the previous deposit, we are able to keep the temperature of deposits quasi-unique during the AM process. This retaining of temperature is very important for reducing porosity and lack of fusion for an AM system. What's more, the ideal power configuration for a new kind of material is difficult to be determined at the beginning of additive manufacturing. With only several times experiments on AM machine, how to reach the ideal temperature of this material as fast as possible is often troublesome for AM researchers. Before we adopt new process parameters control

technique to reduce an AM part's residual stress, the behaviour of control loops in AM thermal system must be investigated.

## 5.2 PID controller in feedback loop

Our simulation is mainly based on a small size code for additive manufacturing, then we integrate PID controller and PID auto-tuning algorithm with this code. The power magnitude closed control loop can be realized by different controllers. PID controller is a kind of conventional feedback controller and it has become, in fact, the most universal controller for industrial application [FAT 07][BI 06]. Instead of more advanced algorithms such as state space[LIM 17][SON 12], we use a PID controller to regulate power in the building of one layer.

A proportional-integral-derivative (PID) controller continuously first calculates an error value  $e(t) = T(t) - T_{preset}$  as the difference of a output temperature between its desired goal temperature  $T_{preset}$  and its measured real temperature  $T(t)$ . Based on proportional, integral, and derivative terms of this output error  $e(t)$ , then the PID controller calculates a correction  $\Delta P(t)$  for input power. The PID controller attempts to minimize the output error over time by adjustment of input power to a new value determined by a weighted sum of the control terms.

$$\Delta P(t) = K_p e(t) + K_i \int_0^t e(t') dt' + K_d \frac{de(t)}{dt} \quad (5.2)$$

Three control terms of the PID controller have different effects in automatic feedback loop[WAN 07]. The proportional term generates compensation according to the magnitude of error. If the error is positive and large, the control output will be proportionately positive and large. The final real value regulated by a proportional controller will have a constant error from the set-value instead of arrival at the desired set-value. This residual error is an inherent problem of feedback loop with only proportional controller[SAE 16]. The integral term takes the historic cumulative errors into account by integrating them. This term can eliminate the residual error caused by the proportional term. To some extent, the performance of a PI controller has already been satisfactory for many industrial automatic applications to achieve a stable control loop, but the oscillation accompanies with PI controller should be diminished in some cases[RAH 12]. The derivative term is used for this purpose due to its dampening effect. This term generates response according to the rate of error change. The more rapid the rate changes, the greater the dampening effect. This feature of the derivative controller can reduce the overshoot in oscillation.



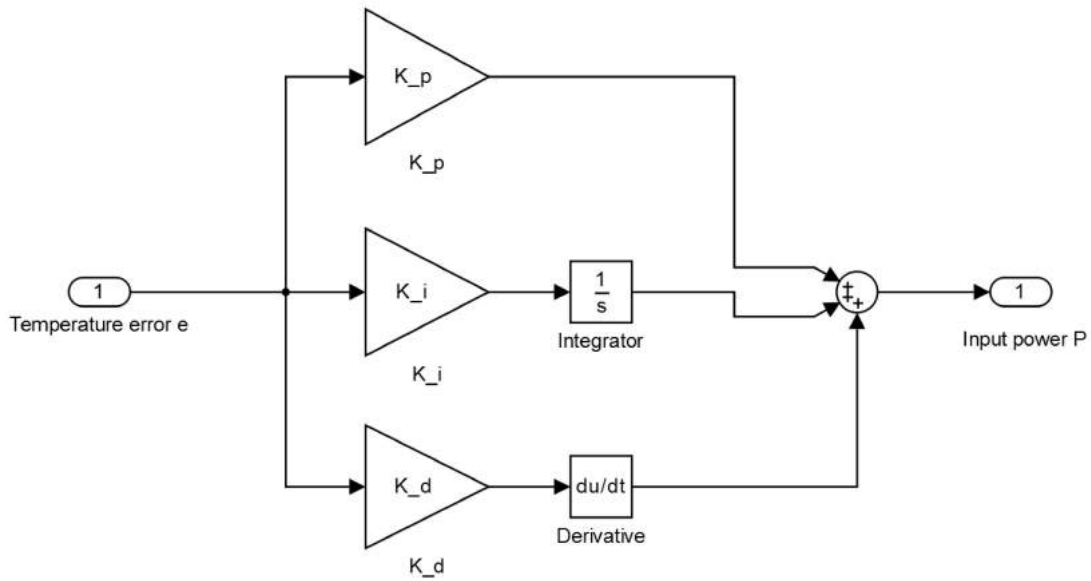


**Figure 5.8:** Block diagram of PID controller's internal structure

The PID controller can be integrated into our AM macroscopic simulation like Figure 5.9. The discrete expression of the input power correction term  $\Delta P_k$  at the  $k$ th step in PID controller can be expressed as:

$$\Delta P_k = K_p e_k + K_i \sum_{j=0}^k e_j + K_d \frac{e_k - e_{k-1}}{\Delta t} \quad (5.3)$$

where  $e_k = T_k - T_{preset}$  is the temperature error,  $T_{preset}$  is the preset temperature to which we adjust the temperature,  $\Delta t$  is the time step.  $K_p$ ,  $K_i$  and  $K_d$  are three constant coefficients of PID controller.

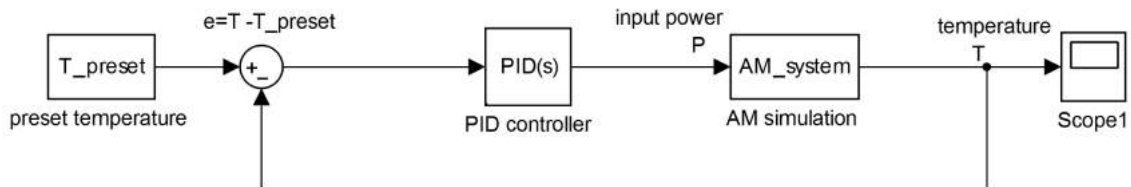


**Figure 5.9:** Block diagram of a close-loop AM system with a PID controller

This PID closed-loop can be implemented in AM simulation using the algorithm in Figure 5.10.

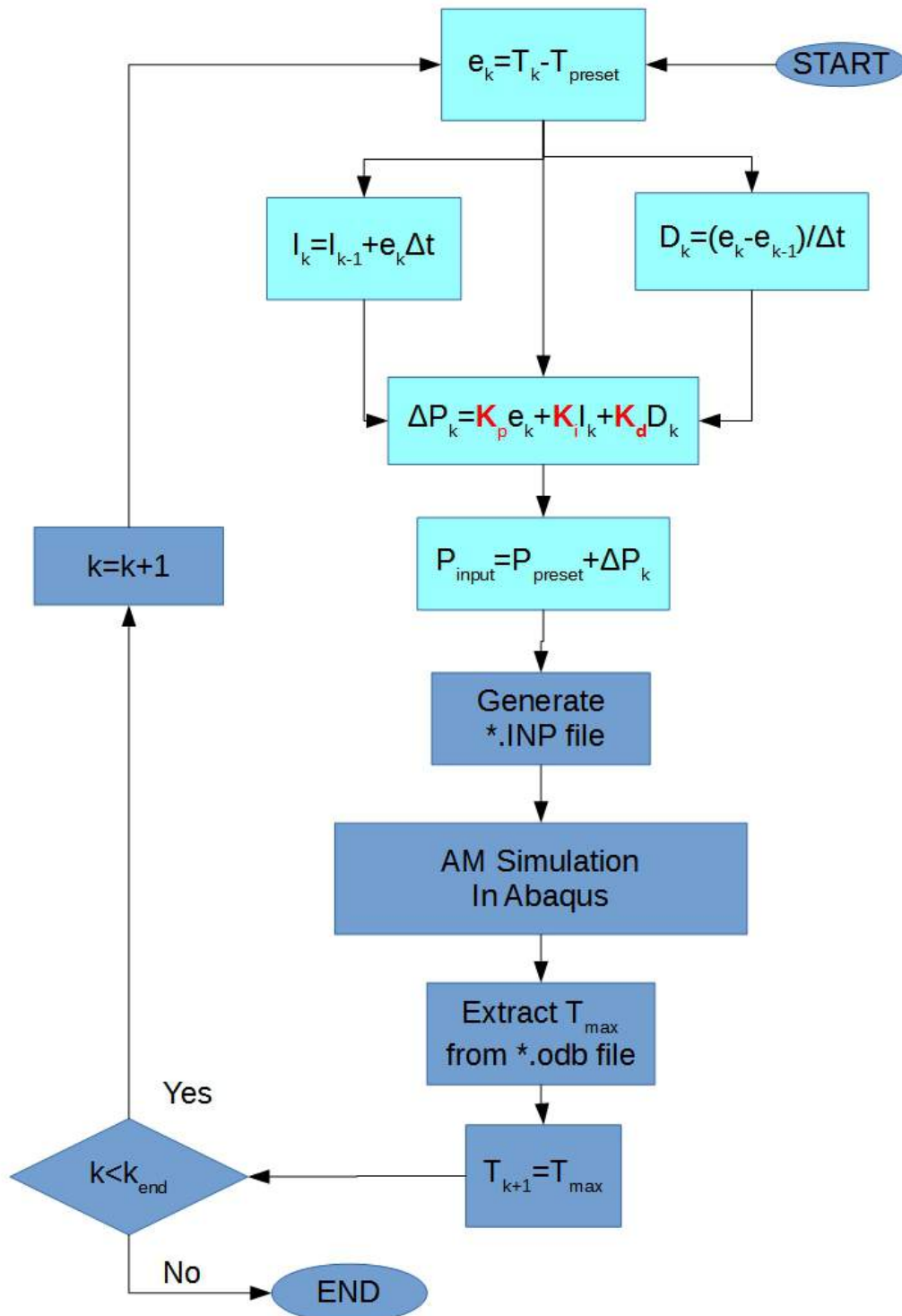


Figure 5.10: Flow chart of PID controller's algorithm

The three terms ( $K_p$ ,  $K_i$  and  $K_d$ ) in PID controller should be adjusted to achieve a balance of three different effects. This adjustment is called PID tuning in control theory. Even though there are only three constant coefficients to determine, it is still not easy to accomplish PID tuning due to the different behaviours of different systems. In practice, this conceptually intuitive work needs lots of iterative experiments before establishing acceptable closed-loop[FIT 14].

In additive manufacturing, these heuristic experiments mean the considerable expense for scrapped sample fabrication as the initial PID parameters need to be adjusted repeatedly[GAN 16]. Even though there is already some software for the study of automatic control such as Simulink, they often rely on the understanding of the transfer function of AM system, still based on lots of data obtained from experiments. With AM simulation in macro scale, designers and engineers are able to reduce the times of PID tuning experiments on AM machines. Moreover, some PID tuning method depends on offline loop, thus not all PID tuning methods can be directly operated on AM machines. For the safety factors in industry, modifying the hardware configuration of AM systems for PID tuning may lead to some risks such as the over-bounding of some process parameters. For example, a fast PID tuning usually leads to an overshoot in order to reach the set-value more quickly, nevertheless AM system may not accept an excessive or a sudden response of power, and the overshoot of temperature may be harmful to AM machine. In this case, AM process simulation can replace real experiment on AM machine. For other types of automatic controllers, the AM simulation platform with PID controller can serve as a fundamental tool after some modifications.

### **5.3 AM simulation with PID power controller for temperature**

The FEM simulation of feedback loop needs to combine the pre-processing, FEM calculation and post-processing together. In our study, a python script generates the input file for the first deposit and submits this file to ABAQUS. After finishing the thermal analysis of the first deposit, we create another python script to extract the maximum temperature value of the whole part. Then the next input power is corrected by the automatic controller according to the maximum temperature. We use the new heat source power to generate the second input file for the second material deposit. The FEM simulation is continued with the new input file by using ABAQUS job restart option. While repeating these steps, we record the values of maximum temperature, time instant and input heat source power. AM simulation with an automatic controller can be implemented in this manner[HAE 05]. All of these procedures above can be integrated into a DOS batch file on Microsoft Windows or a Shell script on Linux.

## 5.4 PID parameters tuning

### 5.4.1 Manual PID tuning

The manual PID tuning methods can be relatively time-consuming but straightforward. The system remains online during tuning. This means that the PID controller is integrated into the feedback loop at the beginning of regulation.

First, the gain coefficients of integral term and derivative term are set to zero. Only the proportional gain coefficient is increased until the output value begins to oscillate. From the oscillating output curve, the values of local maximums and local minimum are recorded. Then the first and second values of peak derivation from the final stable output value are calculated. When the second peak derivation is approximately 1/4 of the first peak derivation, the feedback loop reaches a quarter amplitude decay response. Engineers should record the proportional gain at this moment, then the  $K_p$  should be set to half of that value.

Second, the integral coefficient should be increased until the output value can reach the set-value within sufficient time despite its oscillation. This term can flatten the curve of PI controller.

Third, increase derivative coefficient until the system can reach the set-value at an acceptable rising rate while keeping the proportional and integral coefficient.

### 5.4.2 Auto-tuning

Manual tuning is only one method to create a stable PID feedback loop, in fact, this tuning can be completed automatically with less trial and error. There are already some special patents and commercial software for PID tuning in industry, but the accessible algorithms are more feasible for academic researchers' explorations. The auto-tuning methods include two kinds: open-loop tuning (e.g. Cohen-Coon method) and closed-loop tuning (e.g. Ziegler-Nichols method, Tyreus-Luyben method) [HAU 13]. In our study, we take the Ziegler-Nichols method as an example to explain the PID autotuning method.

The first procedure of Ziegler-Nichols tuning method is similar to that of manual procedure. The gains of integral and derivative terms are set to zero. The proportional coefficient gain is increased until the critical situation, where the output curve has stable and consistent oscillation. In the critical situation, the proportional gain is defined as ultimate gain  $K_u$  and the oscillation period is the critical period  $P_u$ . With these two critical values, the coefficients in different controllers are determined according to Table 5.14 below.

The critical situation in Ziegler-Nichols tuning is still difficult to reach because the tedious adjustment of  $K_p$  coefficient needs also lots of trial and error. So as to facilitate the appearance of critical situation, Karl Johan Åström and Tore Hägglund proposed the relay method [ÅST 95] to obtain the ultimate gain  $K_u$  and the critical period  $P_u$  more efficiently. The feedback loop of the relay method uses temporarily a bang-bang controller instead of a PID controller.

**Table 5.1:** Ziegler-Nichols auto-tuning method for PID controller

controller	$K_p$	$K_i$	$K_d$
P	$0.5K_u$		
PI	$K_u/2.2$	$0.55K_u/P_u$	
PID	$0.6K_u$	$1.2K_u/P_u$	$0.075K_uP_u$
no overshoot PID	$0.2K_u$	$0.4K_u/P_u$	$0.067K_uP_u$

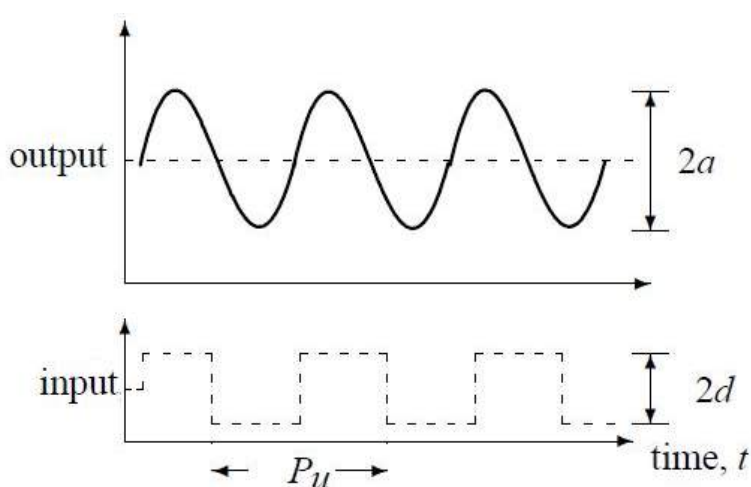


**Figure 5.11:** Relay method for auto-tuning [WIL 05]

The loop regulated by bang-bang controller switches abruptly between an upper and a lower bound. Mathematically, bang-bang controller using Heaviside step function generates a square wave of control input power  $p(t)$  according to the output temperature output  $T(t)$ :

$$p(t) = \begin{cases} p_{preset} - d & T(t) > T_{preset} \\ p_{preset} + d & T(t) < T_{preset} \end{cases} \quad (5.4)$$

where  $p_{preset}$  is a preset power around which the power is discontinuously adjusted using two values,  $d$  is a constant value to correct the initial  $p_{preset}$   $T_{preset}$  is a temperature threshold.

In the first procedure of the relay method, we should deactivate the PID controller (Figure 5.9) and switch the feedback loop to a bang-bang controller, as is shown in Figure 5.13. This offline tuning may be difficult for AM machines due to their complicated hardware systems, but it is relatively more easy for the implement in AM simulation. When the heat source's power input retains an upper actuation value  $p_{preset} + d$ , the temperature at melting pool tends to increase as output value  $T(t)$  because of the heat accumulation effect. If the temperature begins to exceed the set value of temperature  $T_{preset}$ , the power

input will decrease discontinuously in the opposite direction reaching and keeping a lower amplitude  $p_{preset} - d$ . Repeating this adjustment manipulation during the process, we will obtain the respond curve of temperature with oscillation, like Figure 5.11.

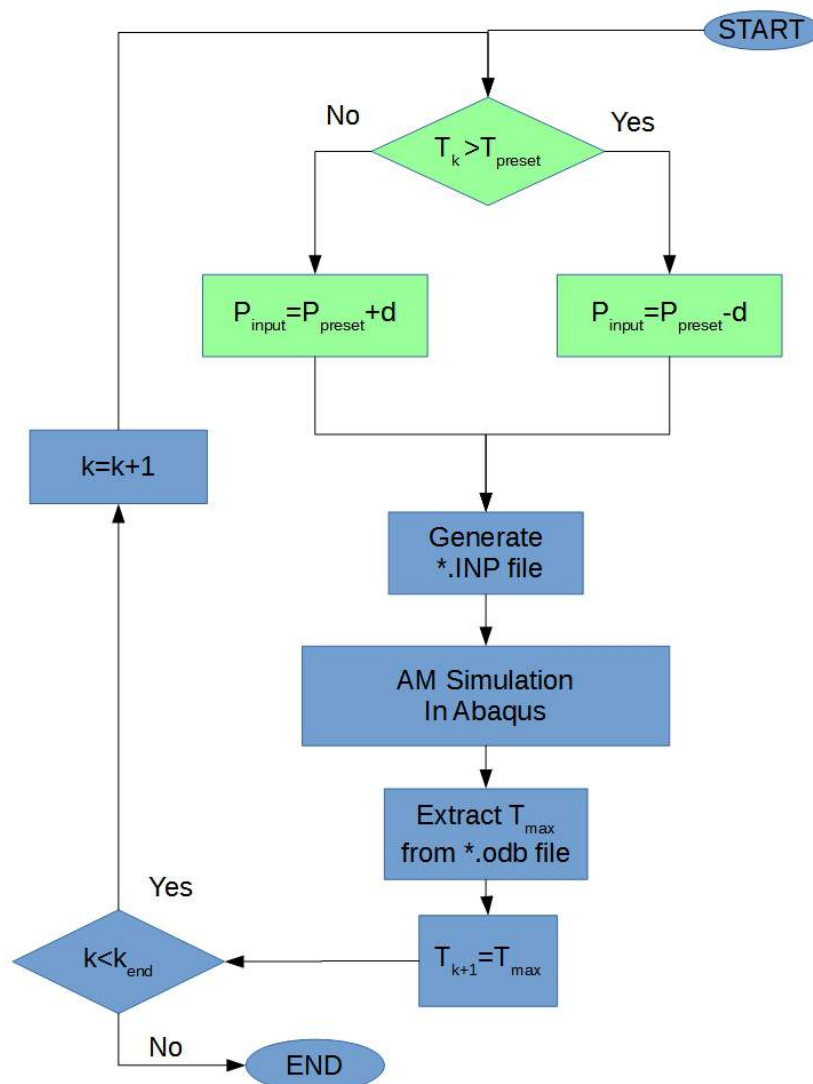


**Figure 5.12:** Flow chart of relay method for a PID controller's auto-tuning

Some of the system characteristics are independent on an automatic controllers. From

## 5. Simulation for the control of the process in additive manufacturing

this curve, we can acquire directly the values of ultimate gain  $K_u$

$$K_u = \frac{4d}{\pi a} \quad (5.5)$$

and critical period  $P_u$ , which can be applied for determining the three coefficients of PID according to the parameter table of Ziegler-Nichols tuning 5.14. Then the bang-bang controller is switch off in the closed-loop and the PID controller is reactivated with suitable parameters. From the Figure 5.14 we can read the output values  $a$ :  $a_1 = 111.949^\circ\text{C}$  for Figure 5.14(a) and  $a_2 = 367.852^\circ\text{C}$  for Figure 5.14(b).

Then we use the Table 5.14 to calculate controller's parameters by

$$K_u = 0.5 \left( \frac{4d_1}{\pi a_1} + \frac{4d_2}{\pi a_2} \right) = 1.030994846 \times 10^9 \text{W/m}^3 / ^\circ\text{C} \quad (5.6)$$

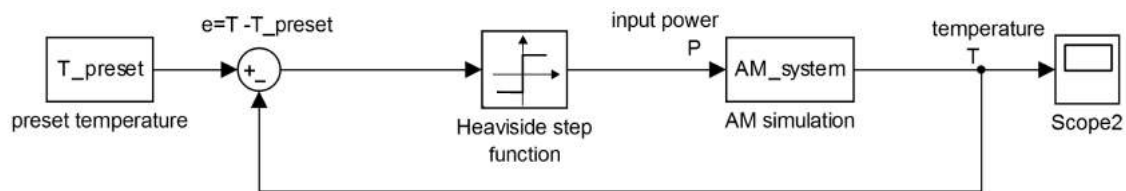
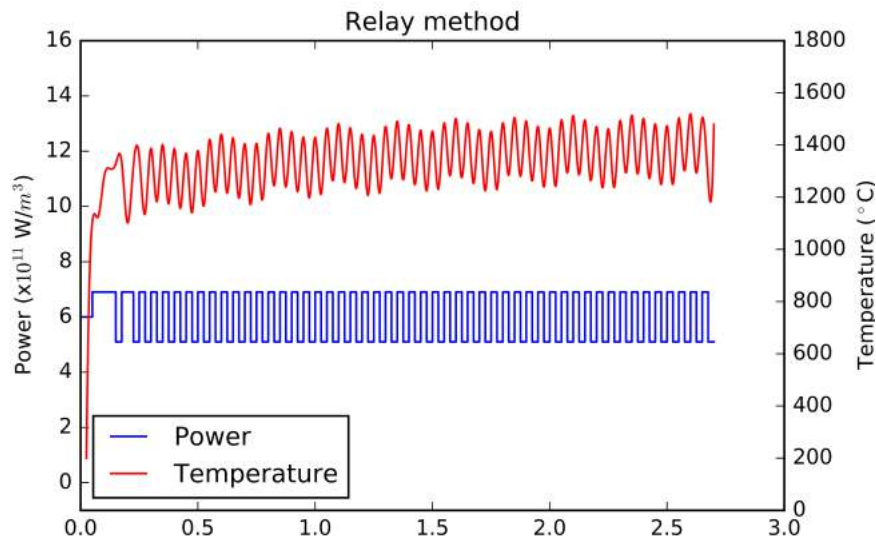
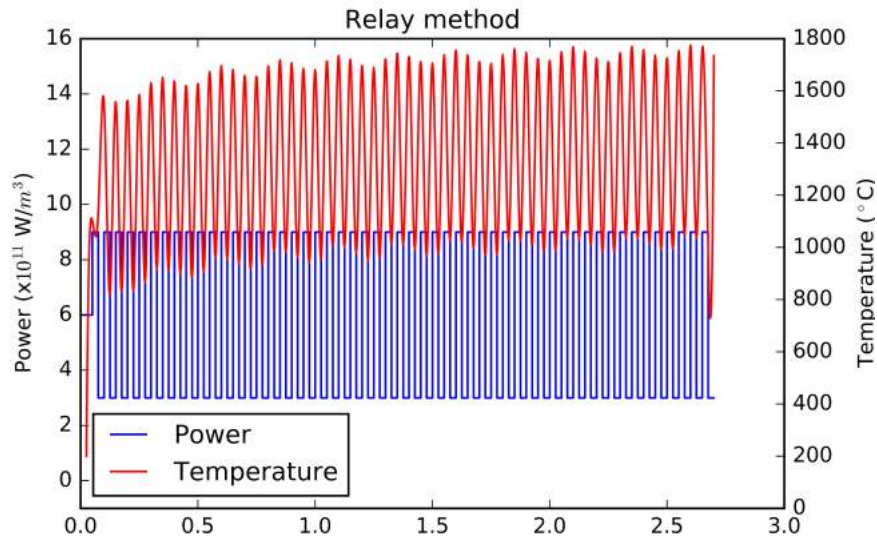


**Figure 5.13:** Block diagram of a close-loop with relay method for PID auto-tuning



(a)  $d_1 = 9.0 \times 10^{10} \text{W/m}^3$



$$(b) d_2 = 3.0 \times 10^{11} \text{W/m}^3$$

**Figure 5.14:** Relay method,  $P_{preset} = 6.0 \times 10^{11} \text{W/m}^3$ ,  $T_{preset} = 1600^\circ\text{C}$

Then we switch off the bang-bang controller in the feedback loop and turn on the PID-based controller. Some performances of controllers are compared in AM simulation in Figure 5.15.

The maximum temperature of melting zone is extracted and recorded in Figure 5.15(a) after each deposition and heating. This control includes two steps: First, with the help of a controller, this temperature arrives rapidly to the preset value  $1600^\circ\text{C}$ . Second, when the temperature has reached near  $1600^\circ\text{C}$ , the input power is controlled to keep this temperature stable around the preset value.

In practice, there are some limits because of the hardware of an AM machine, such as the maximum limits of temperature, power or overshoot, etc. In our work, we set  $1.2 \times 10^{12} \text{W/m}^3$  as the input power limit. Inappropriate PID parameters may cause saturation of control as the PID controller in Figure 5.15(b). In fact, Ziegler-Nichols tuning is just one of many guides for PID tuning. Based on the rough suggestion of Ziegler-Nichols method, more delicate tunings are necessary, if the curves of input power or output temperature are expected to be far away from hardware limits. This result can be an example to demonstrate one advantage of AM simulation. If these PID parameters are executed on real AM machine, there will perhaps be a risk of hardware damage since the input power reaches the maximum limit.

All these three controllers can achieve the temperature control function in AM simulation, but their performances are different in many aspects, such as the overshoot value of temperature, oscillation frequency before the arrival of stable temperature, and the time spent to achieve stability. These results indicate the importance of the choice of controller in the design of feedback in additive manufacturing system. The no-overshoot controller

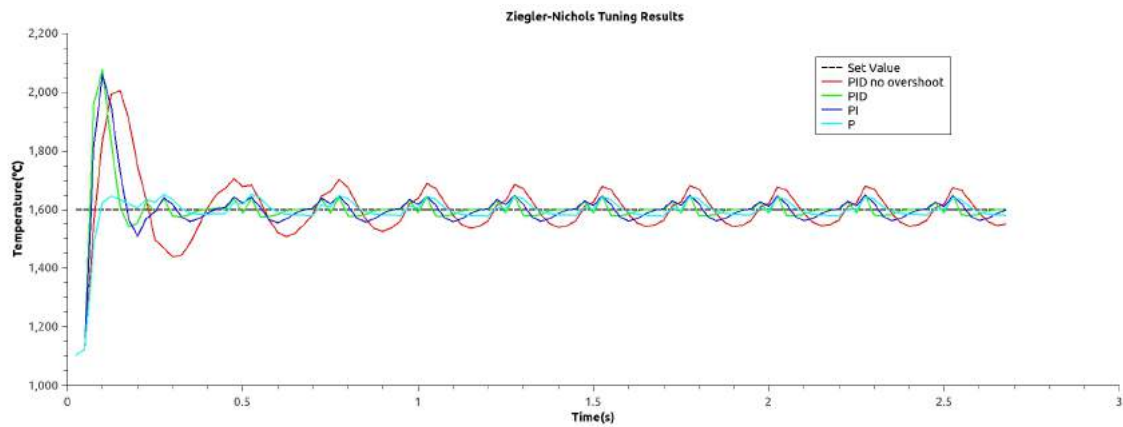


## 5. Simulation for the control of the process in additive manufacturing

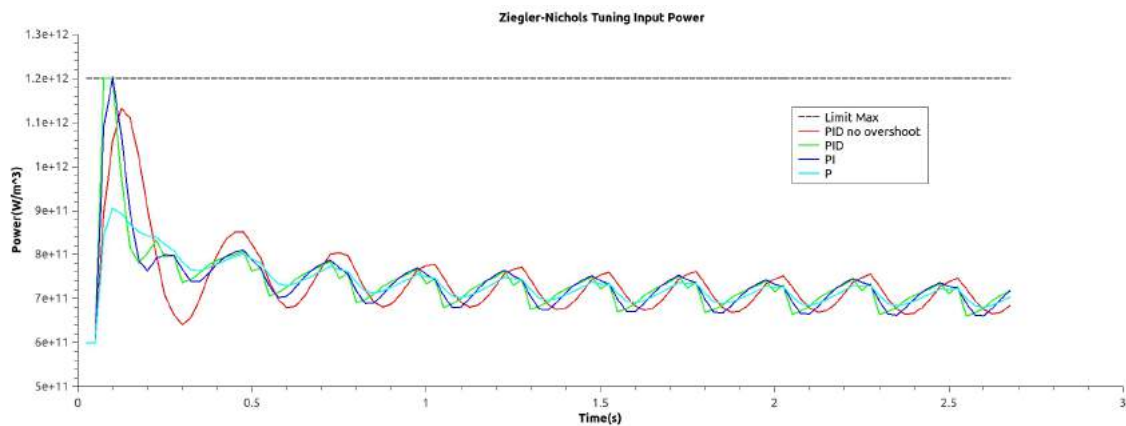
doesn't behave as its ideal function. This may be caused by the sampling frequency which is determined by material deposition speed and the temporal resolution in post-processing. Although the objective of our work is to demonstrate the methodology for the integration of feedback loop in AM simulation, this should be studied in further research.

**Table 5.2:** Different kinds of PID controllers

controller	$K_p(10^8 W/m^3/^\circ C)$	$K_i(10^9 W/m^3/^\circ C/s)$	$K_d(10^6 J/m^3/^\circ C)$
P	5.15497423		
PI	4.63947681	11.134744338	
PID	6.18596908	24.743876307	3.866231
no overshoot PID	2.06198969	8.247958769	3.436649



(a) Output: maximum temperature during AM process



(b) Input: heat source power

**Figure 5.15:** PID control in AM simulation with different controllers

## 5.5 Conclusion

For an advanced AM machine, The capacity to control the temperature at one point during AM dynamic process is fundamental for residual stress reduction. To demonstrate how to combine control-loop with AM simulation, we take a PID controller as an example. This work is performed by simulating a zigzag line at line level. In this chapter, The main conclusions are following:

- 1. The AM system is a non-LTI (linear time invariant) system. Using an open-loop simulation, we can discover it from observing the corresponding output temperature of input power in step function. The complexity of the zigzag line's geometry leads to the corresponding temperature's fluctuation. This feature implies the simplification is necessary for a real AM system if researchers want to study its control loop. Some tools for LTI can't be applied directly for a real AM system.
- 2. The heat source power is regulated to control the maximum temperature of the whole part. Since the PID controller's manual tuning is tedious, auto-tuning is conducted based on Ziegler-Nichols method and relay method, which is more efficient. However, the Ziegler-Nichols is only one of the rough guides for PID auto-tuning. Some more delicate tuning should be performed if the performance of PID loop needs to be further ameliorated. From the comparison of different controllers (All of them belongs to PID controller family), we can choose an appropriate controller according to the AM system's constraint.



# General conclusions and perspectives

## General conclusions

In this thesis, we investigate some problems of additive manufacturing numerical simulation. The procedures to overcome these problems demonstrate the basic workflow in AM simulation in macro scale. The quality of a metal part fabricated by AM technology isn't always satisfactory in industrial applications due to many reasons. In order to better understanding the process of additive manufacturing, numerical simulations using the FEM method are employed in our study. Some interesting conclusion can be revealed from this thesis, which we hope to be useful for researchers in this area:

- New potential technique direction for reducing the residual stress

Instead of benchmarks with relatively simple geometry, our work concerns to 3D objects with complex geometry which are generated from AM slicer software. Thanks to the simplification of regrouping neighbour thin layers into a thicker layer, we can simulate in Chapter 3 the thermal-metallurgical-mechanical fields of a twisted turbine blade. The residual stress of such a complex geometry is normally difficult for previous simulations.

According to the simulation results, we conclude that the residual stress exists both on the surface and inside the part built by an AM system. The histogram of residual stress throughout a part obeys approximately the Burr XII distribution. While the total input energy is kept the same as the reference case, we can reduce residual stress with a lower preheat temperature. In this potential technique, the input power is decreased for each layer and the heating time is correspondingly elongated. This process adjustment may allow the heat to transfer more homogeneously. This adjustment of input process parameters indicates a new residual stress reduction at lower preheat temperature, rather than the higher preheat temperature which has disadvantages in the limit of material and energy consumption. Since the AM machine manufacturers are approaching the limit of preheating temperature nearer and nearer, the role of AM process control will become important as a new technique direction.

- Methodology for special pre-processing problems of AM simulation

Some AM simulation cases have been performed in this thesis to demonstrate the feasibility of pre-processing. In Chapter 3, the pre-processing methodology is investigated at two levels, layer level and part level.

In layer-level simulation, two algorithms are proposed. It is proved that the inverse calculation of polygon offsetting and clipping can serve as a tool for extracting AM scan path information from G-code. Between CAD B-Rep system and mesh generator, the incompatibility of 3D element set can be solved with database technique. In this database, local and global coordinates transformation is conducted. This method can be expanded to similar problems in AM simulation.

In part-level simulation, voxelization method is adopted in our work. Different from ordinary mesh generation procedures, voxelization is proved to be a useful and convenient tool for AM simulation in macro scale. With the help of these methodologies and practical tools that we mentioned above, academic researchers are able to simulate less laboriously the intricate AM processes of an object with complex geometry.

- Implementation for the parameters optimisation of residual stress

For revealing the relation between AM process parameters and part's final residual stress at environment temperature, the basic framework of regression analysis is implemented combining with AM macroscopic simulation of a zigzag track line. In Chapter 4, we make use of some regression codes to analyse data generated from AM simulation. Our work is simplified with an assumption that the maximum residual stresses of a part  $\sigma_{max}$  is impacted by three process parameters (deposition order  $i$ , heat source power  $P_i$  and heating time  $(\Delta t)_i$ ). Without empirical formulas for a certain part, we attempt to statistically predict this relation. The role of AM simulation in Chapter 4 is to generate virtually multiple parts as the raw data for regression instead of real fabrication on AM machine. The differences in performance of artificial neural network and other regression algorithms are also observed in our study. These differences indicate the importance of the prudential choice of regression algorithm before the application of this kind approach. Our methodology for residual stress in this work can be the essential step for further study using regression-based phenomenological tool.

- Integration of control loop into AM simulation

Before the application of the adjustment of AM process parameters for residual stress reduction, the AM system must be equipped with a control loop. The one-point temperature control is the fundamental preparation for realizing new residual stress technique which is implied in Chapter 3. From the fluctuation response in open-loop simulation, we can reveal some complexity of AM system. The AM system is non-LTI (linear time invariant). This feature prevents us from applying directly most of the mathematical automation tools if the AM system isn't appropriately simplified yet. In Chapter 5, we integrate a PID controller into AM simulation and attempt to obtain a stable desired temperature by regulating input power.

Instead of operation on AM machine, the PID auto-tuning is achieved in AM numerical simulation with Ziegler-Nichols method and relay method. The different performances for many kinds of controllers ( in PID family) are compared. The Ziegler-Nichols method is one of the rough auto-tuning methods. If the controller needs to be further optimised, finer tuning should be executed. The choice of a suitable controller depends on the requirements of the AM system. In this thesis, we proposed the basic control loop combining with AM simulation. We can intuitively perceive the advantage of simulating a part's AM process, such as avoid the risk of overshoot.

## Perspectives

Aiming at solving some special problems in the FEM simulation of additive manufacturing, our study is a prototype for demonstrating the feasibility of some methodologies. After this thesis, future work could be considered in these aspects:

- Experiment validations

In this work, we have no access to a real metal AM machine because of the lack of expensive hardware. In fact, the experiment validations on an AM machine will be useful and interesting when it is combined with AM macroscopic simulation. First, the PID feedback loop simulation may be a guide of the first step before the experiment on the expensive hardware. Second, the process records of defective parts fabricated in AM experiment can serve as initial data set for regression. This supplementary data set can be mixed with data set generated by relatively accurate AM simulation. In an AM system with a control loop, infra-red or CCD cameras are often installed. Some technology based on image identification might be also studied comparing with the result of AM simulation.

- Further numerical simulations

Some tasks need to be completed for the coupling fields in additive manufacturing. In this thesis, our thermo-mechanical-metallurgical simulation is simplified, excluding some phenomenon (such as plastic dissipation, latent heat, interaction between phase transformation and strain). Some coefficients in AM simulation depends on temperature or certain phase's volume fraction, not only in the metallurgical field but also in the thermo-mechanical field. Most of these coefficients can be expressed as empirical formulae. If we integrate material database into our AM simulation platform. The input coefficient can be dynamically updated during the simulation. This database of metallurgy models will facilitate the research of different materials in AM simulation. Since we have studied the pre-processing of 3D models with complex geometry. Some typical AM test, such as lattice structure [HUS 13b], cases may be also simulated as further validation.

- Acceleration of simulation

Even though the cases in this thesis are already simplified during the 3D reconstruction from initial \*.stl file, the time consumption is still considerable both in pre-processing and FEM calculation. AM simulation should be accelerated for achieving the equilibrium between high resolution and calculating speed. By analogy with welding simulation, some special numerical methods, such as inherent strain method[FRA 16] and model order reduction [LU 18], can be applied in AM simulation with suitable modifications. These algorithms often use principal component analysis(PCA) to approximate the exact FEM model. This may be helpful for calculating rapidly a complex model with multiple parameters.

- Combining with micro-scale simulation The properties of material depends strongly on their initial state. Although numerical simulations often adopt solid metal parameters for the whole part, granulometry experiment should be conducted to acquire precise properties of metal powder. In this thesis, simulations are conducted in macro-scale levels: line level, layer level, part level. Nevertheless, the micro-structure simulation at welding pool is an important focus for many AM researchers in recent years[SHR 18][MEI 17][YAN 17a]. This microscopic simulation usually uses visco-plastic model and computational fluid dynamics. The calculating speed and accuracy may be improved, if the different simulations are combined across multi-scales in continuum mechanics.

# Appendix A

## Additive manufacturing's workflow in industry

In Figure A.1, powder bed fusion is taken as an example to illustrate the workflow of additive manufacturing in industry.

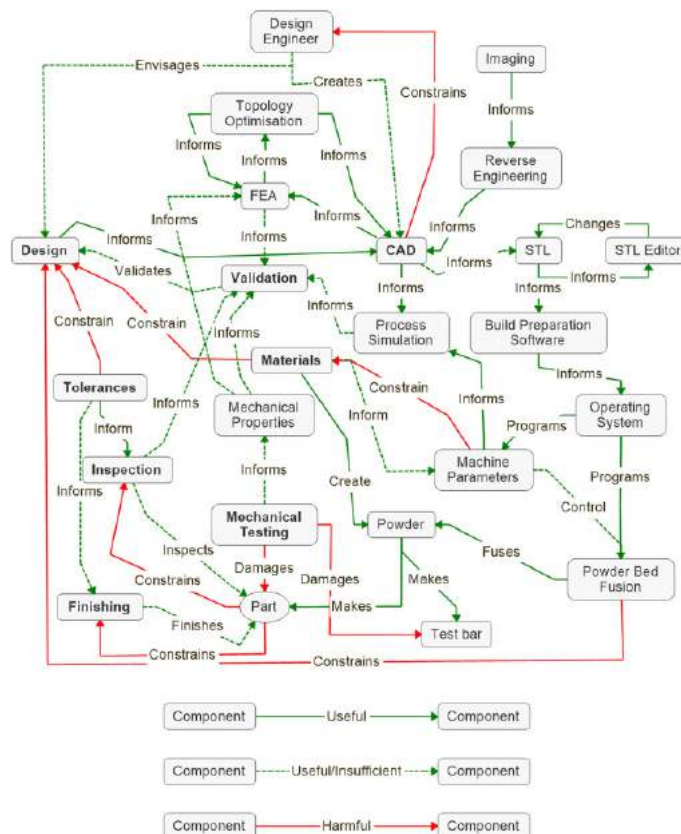


**Figure A.1:** Additive manufacturing's workflow in industry[THO 18]





## Appendix B

# Python codes for mesh incompatibility problem

These codes dedicate to solve the incompatibility problem in Abaqus. This tool has the potential to be extend to similar problem in different CAD software, mesh generators, FEM software. When the definition of ElementSet in one coordinates frame disappeared in the other coordinates frame after assembly, a dataset based on SQL language can be established profiting from features in additive manufacturing.

```
import sqlite3
from abaqus import *
from abaqusConstants import *
import __main__
from caeModules import *
from driverUtils import executeOnCaeStartup
def average_center (Element) :
    ns=Element.getNodes ()
    c_x=0.0
    c_y=0.0
    c_z=0.0
    for i in range (len (ns)) :
        c_x=c_x+ns [i].coordinates [0]
        c_y=c_y+ns [i].coordinates [1]
        c_z=c_z+ns [i].coordinates [2]
    c_x=c_x/len (ns)
    c_y=c_y/len (ns)
    c_z=c_z/len (ns)
    return (c_x, c_y, c_z)

def CreateNativeMeshDB () :
    conn = sqlite3.connect ('native_mesh.db')
    c = conn.cursor ()
    c.execute ("CREATE TABLE NATIVEMESH (ID3D INTEGER PRIMARY KEY,
                                         NATIVEELEMENTID INT NOT NULL, X
                                         REAL NOT NULL, Y REAL NOT NULL,
                                         Z REAL NOT NULL, LAYERID INT
                                         NOT NULL, CELLNAME CHAR (50));")
```

## B. Python codes for mesh incompatibility problem

---

```
conn.commit()
conn.close()

def CreateOrphanMeshDB():
    conn = sqlite3.connect('orphan_mesh.db')
    c = conn.cursor()
    c.execute("CREATE TABLE ORPHANMESH (ORPHANELEMENTID INT PRIMARY KEY
        NOT NULL, X REAL NOT NULL, Y
        REAL NOT NULL, Z REAL NOT NULL)
        ;")

    conn.commit()
    conn.close()

def CreateAssociativityDB():
    conn = sqlite3.connect('associativity.db')
    c = conn.cursor()
    c.execute("CREATE TABLE ASSOCIATIVITY (ORPHANELEMENTID INT PRIMARY
        KEY NOT NULL, NATIVEELEMENTID
        INT, SETNAME CHAR(50));")

    conn.commit()
    conn.close()

def NativeMesh2DB(partName, LayerID, derivation): #layerID=0 base
    conn = sqlite3.connect('native_mesh.db')
    #print "Opened database successfully";
    c = conn.cursor()
    p = mdb.models['Model-1'].parts[partName]
    oldE = p.elements
    for ele in oldE:
        eleCenter=average_center(ele)
        OldId=ele.label
        z_real=eleCenter[2]-derivation*(LayerID+1)
        c.execute("INSERT INTO NATIVEMESH (ID3D,NATIVEELEMENTID,X,Y,Z,
            LAYERID) VALUES (NULL
            ,?,?,?,?), (OldId,
            eleCenter[0],eleCenter[1],
            z_real,LayerID))

    conn.commit()
    conn.close()

def OrphanMesh2DB(partName):
    conn = sqlite3.connect('orphan_mesh.db')
    c = conn.cursor()
    p = mdb.models['Model-1'].parts[partName]
    newE = p.elements
    for ele in newE:
        eleCenter=average_center(ele)
        NewId=ele.label
        c.execute("INSERT INTO ORPHANMESH (ORPHANELEMENTID,X,Y,Z)
            VALUES (?, ?, ?, ?)", (NewId,
            eleCenter[0],eleCenter[1],
            eleCenter[2]))
```

```

conn.commit ()
conn.close ()

def AddCell2NativeDB (CellObj, layerID) :
    #p = mdb.models['Model-1'].parts[partName]
    conn = sqlite3.connect ('native_mesh.db')
    CellName="Cell_"+str (layerID)+"_"+str (CellObj.index)
    c = conn.cursor ()
    eleArray=CellObj.getElements ()
    for e in eleArray:
        c.execute ("UPDATE NATIVEMESH set CELLNAME=? where
                    NATIVEELEMENTID=? AND
                    LAYERID=?", (CellName, e.
                    label, layerID))

    conn.commit ()
    conn.close ()

def AssociateNative_Orphan (tolerant) :
    conn1 = sqlite3.connect ('native_mesh.db')
    c1 = conn1.cursor ()
    conn2 = sqlite3.connect ('orphan_mesh.db')
    c2 = conn2.cursor ()
    conn3 = sqlite3.connect ('associativity.db')
    c3 = conn3.cursor ()
    cursor2 = c2.execute ("SELECT ORPHANELEMENTID,X,Y,Z FROM ORPHANMESH
                          ")

    for row in cursor2:
        orphanEleId=row [0]
        orphanX=row [1]
        orphanY=row [2]
        orphanZ=row [3]
        cursor1 = c1.execute ("SELECT NATIVEELEMENTID,CELLNAME from
                              NATIVEMESH where abs (x-?)<?
                              AND abs (y-?)<? AND abs (z
                              -?)<?", (orphanX, tolerant,
                              orphanY, tolerant, orphanZ,
                              tolerant))

        for row in cursor1:
            nativeEleId=row [0]
            setName=row [1]
            if nativeEleId!=None:
                cursor3 = c3.execute ("INSERT INTO ASSOCIATIVITY (
                                      ORPHANELEMENTID,
                                      NATIVEELEMENTID,
                                      SETNAME) VALUES
                                      (?, ?, ?) ", (
                                      orphanEleId,
                                      nativeEleId, setName)
                                      )
            else:
                print 'The '+str (orphanEleId)+' Element in OrphanMesh
                       has no corresponding

```

## B. Python codes for mesh incompatibility problem

---

```

                                                                 element in
                                                                 NativeMesh!'

conn3.commit()
conn3.close()
conn2.close()
conn1.close()

def PickOrphanElementsFromNativeCell (CellObj, layerId, OrphanPartName) :
    SetName="Cell_"+str(layerId)+"_"+str(CellObj.index)
    p= mdb.models['Model-1'].parts[OrphanPartName]
    e=p.elements
    tmp=e[0:0]
    conn = sqlite3.connect('associativity.db')
    c = conn.cursor()
    cursor= c.execute("SELECT ORPHANELEMENTID, NATIVEELEMENTID FROM
                                                                ASSOCIATIVITY WHERE SETNAME=?"
                                                                ,(SetName,))

    for row in cursor:
        elelabel=row[0]
        eleId=elelabel-1#!!!!!!!!!!!!!!e[0].label=1,e[1].label=2,e[2].
                                                                label=3.....!!!!!!!!!!!!

        tmp=tmp+e[eleId:eleId+1]
    conn.close()
    return p.Set(name=SetName, elements=tmp)

def PickElementOfBaseFromOrphanPart (OrphanPartName) :
    p= mdb.models['Model-1'].parts[OrphanPartName]
    e=p.elements
    tmp=e[0:0]
    conn = sqlite3.connect('orphan_mesh.db')
    c = conn.cursor()
    cursor=c.execute("SELECT ORPHANELEMENTID FROM ORPHANMESH where z<0"
                                                                )

    for row in cursor:
        elelabel=row[0]
        eleId=elelabel-1#!!!!!!!!!!!!!!e[0].label=1,e[1].label=2,e[2].
                                                                label=3.....!!!!!!!!!!!!

        tmp=tmp+e[eleId:eleId+1]
    conn.close()
    return p.Set(name='Base', elements=tmp)
```

## Appendix C

# Reconstruction of tracks in one layer from G-code

This tool conduct inverse operations opposite to slicer software. After importing the basic data of scan vectors from G-code, we can reconstruct the tracks in one layer, and this layer's partition information will be used for defining ElementSet. The DXF files of each layer are drawn automatically by dxfwrite library.

```
#!/usr/bin/python
# -*- coding: utf-8 -*-
import numpy as np
from dxfwrite import DXFEngine as dxf
import pyclipper
import os
import linecache

def rectangle(vector, radius):
    coeff=0.8
    p0=np.array([vector[0][0],vector[0][1],0])
    p1=np.array([vector[1][0],vector[1][1],0])
    v=p1-p0
    #print v
    nz=np.array([0,0,1])
    n=np.cross(v,nz)
    n=n/np.linalg.norm(n)
    #print n
    nv=v/np.linalg.norm(v)
    p0=p0+coeff*radius*nv
    p1=p1-coeff*radius*nv
    tmp0=p0+radius*n
    tmp1=p0-radius*n
    tmp2=p1-radius*n
    tmp3=p1+radius*n
    rectangle_vertex=[]
    rectangle_vertex.append((float("%.3f"%tmp0[0]),float("%.3f"%tmp0[1]
    )))
    rectangle_vertex.append((float("%.3f"%tmp1[0]),float("%.3f"%tmp1[1]
```

## C. Reconstruction of tracks in one layer from G-code

---

```
    ))
rectangle_vertex.append((float("%.3f"%tmp2[0]), float("%.3f"%tmp2[1]
    ))
rectangle_vertex.append((float("%.3f"%tmp3[0]), float("%.3f"%tmp3[1]
    ))
return rectangle_vertex

def multilines(drawing, points, layerName, layerColor):
    for i in range(len(points)-1):
        drawing.add(
            dxf.line(start=(points[i][0], points[i][1]), end=(points[i+1][0]
                , points[i+1][1]), layer=
                    layerName, color=layerColor
                )
        )
    drawing.add(
        dxf.line(start=(points[len(points)-1][0], points[len(points)-1][1]
            ), end=(points[0][0], points[0]
                [1]), layer=layerName, color=
                    layerColor)
    )

def squarebrackets2parentheses(listData, IfReturnList):
    tmp=[]
    for i in range(len(listData)):
        tmp.append(tuple(listData[i]))
    if IfReturnList==False:
        return tuple(tmp)
    else:
        return tmp

def reverse_clipper_inner(background_list, vectors, deposition_radius):
    Blocks=[]

    Big0=tuple(background_list)
    for i in range(len(vectors)):
        vector=vectors[i]
        rectangle_tmp=rectangle(vector, deposition_radius)
        rectangle_clipper=tuple(rectangle_tmp)
        pyclipper.SCALING_FACTOR = 1000
        pc = pyclipper.Pyclipper()
        A=pyclipper.scale_to_clipper(Big0, pyclipper.SCALING_FACTOR)
        B=pyclipper.scale_to_clipper(rectangle_clipper, pyclipper.
            SCALING_FACTOR)

        pc.AddPaths(A, pyclipper.PT_SUBJECT, True)
        pc.AddPath(B, pyclipper.PT_CLIP, True)
        intersection = pc.Execute(pyclipper.CT_INTERSECTION, pyclipper.
            PFT_EVENODD, pyclipper.
            PFT_EVENODD)

        solution = pyclipper.scale_from_clipper(intersection, pyclipper.
            .SCALING_FACTOR)

        Blocks.append(solution)
```

```

pyclipper.SCALING_FACTOR = 1000
pc = pycclipper.Pyclipper()
pc.AddPaths(A, pycclipper.PT_SUBJECT, True)
for i in range(len(solution)):
    small=solution[i]
    C=pyclipper.scale_to_clipper(small,pyclipper.SCALING_FACTOR
                                )
    pc.AddPath(C, pycclipper.PT_CLIP, True)
tmp1=pc.Execute(pycclipper.CT_DIFFERENCE, pycclipper.PFT_EVENODD,
                pycclipper.PFT_EVENODD)
tmp2=pyclipper.scale_from_clipper(tmp1, pycclipper.
                                  SCALING_FACTOR)

Big0=tuple(tmp2)
return Blocks

def collect_skin_vectors(datfileName):
    if os.path.isfile(datfileName)==False:
        return
    vectors=[]
    VectorStart=False
    VectorContinue=False
    fo = open(datfileName, "r")
    lineNb=0
    for line in fo:
        lineNb=lineNb+1
        if line=='$\n':
            VectorStart=True
            VectorContinue=False
        elif line=='*\n':
            VectorStart=False
            VectorContinue=False
        else:
            if VectorContinue==False:
                pstr=line.split()
                p=map(float,pstr)
                if VectorStart==True:
                    VectorTmp=[]
                    VectorTmp.append((p[0],p[1]))
                else:
                    VectorTmp.append((p[0],p[1]))
            else:
                VectorStart=False
                up=linecache.getline(datfileName,lineNb-1)
                pstr_up=up.split()
                p_up=map(float,pstr_up)
                pstr=line.split()
                p=map(float,pstr)
                VectorTmp=[]
                VectorTmp.append((p_up[0],p_up[1]))
                VectorTmp.append((p[0],p[1]))
            VectorContinue=True
    if VectorStart==False and len(VectorTmp)!=1:

```



## C. Reconstruction of tracks in one layer from G-code

---

```
        vectors.append(VectorTmp)
    fo.close()
    return vectors

def collect_wall_vectors(datfileName):
    if os.path.isfile(datfileName)==False:
        return
    BlockNb=0
    p_tmp=[]
    p_tmp0=[]
    fo = open(datfileName, "r")
    for line in fo:
        if line=='*\n':
            if BlockNb!=0:
                p_tmp.append(p_tmp0)
                BlockNb=BlockNb+1
                p_tmp0=[]
            else:
                pstr=line.split()
                p=map(float,pstr)
                p_tmp0.append((p[0],p[1]))
    p_tmp.append(p_tmp0)
    fo.close()
    return p_tmp

def wall_offset(polygon_list, radius):
    new_polygon_list=[]
    tmp=tuple(polygon_list)
    pyclipper.SCALING_FACTOR = 1000
    subj = pyclipper.scale_to_clipper(tmp,pyclipper.SCALING_FACTOR)
    pco = pyclipper.PyclipperOffset()
    pco.AddPaths(subj, pyclipper.JT_ROUND, pyclipper.ET_CLOSEDPOLYGON)
    solution = pco.Execute(radius*pyclipper.SCALING_FACTOR)
    tmp1 = pyclipper.scale_from_clipper(solution, pyclipper.
                                        SCALING_FACTOR)

    for i in range(len(tmp1)):
        new_polygon = squarebrackets2parentheses(tmp1[i], True)
        new_polygon_list.append(new_polygon)
    return new_polygon_list

def polygon_dxf(drawing, Kind, polygons_list):
    layerName={'wall_inner':'WALL-INNER','wall_outer':'WALL-OUTER','
              skin':'SKIN'}
    layerColor={'wall_inner':37,'wall_outer':97,'skin':240}
    colorNb=layerColor[Kind]
    layer_name=layerName[Kind]
    drawing.add_layer(layer_name)
    for i in range(len(polygons_list)):
        polygon=polygons_list[i]
        multilines(drawing,polygon,layer_name,colorNb)

deposition_radius=0.285/2
```

---

```
data_skin=collect_skin_vectors('layer_skin.dat')
data_wall_inner=collect_wall_vectors('layer_inner.dat')
data_wall_outer=collect_wall_vectors('layer_outer.dat')

skin_polygons_group=reverse_clipper_inner(data_wall_outer,data_skin,
                                          deposition_radius)
add_wall_outer=wall_offset(data_wall_outer,2*deposition_radius)
drawing = dxf.drawing('one_layer.dxf')
skin_vectors=[]
for i in range(len(skin_polygons_group)):
    skin_polygons=skin_polygons_group[i]
    small_rectangle=squarebrackets2parentheses(skin_polygons[0],True)
    skin_vectors.append(small_rectangle)
    polygon_dxf(drawing,'skin',skin_vectors)
polygon_dxf(drawing,'wall_inner',data_wall_inner)
polygon_dxf(drawing,'wall_inner',data_wall_outer)
polygon_dxf(drawing,'wall_outer',add_wall_outer)
drawing.save()
```



## Appendix D

### Script for simulating a feedback loop

In this Bash Shell script on Linux, pre-processing, FEM calculation, post-processing and PID controller's regulation are automatically submitted one by one. Though these procedures are executed with ABAQUS and python scripts, the schema can be also used in similar case after some modifications

**Code Listing D.1:** Shell script

```
#!/bin/bash
step=1
startNb=9
endNb=26
abaqus cae noGUI=main.py
abaqus analysis job=Job-1 input=Job-1.inp user=subroutine.f
cpus=8 memory='17gb' interactive
python ./PIDcontrol_power.py -- 1
echo "Job-1_has_finished"
for ((i=${startNb};i<${endNb}+1;i=i+${step}));
do
    j='expr ${i} - 1'
    echo ${j}
    power=$(cat power_tmp.txt)
    echo "Power=_${power}"
    abaqus cae noGUI=generateRestart.py -- ${power} ${i}
    echo 'Inp file is generated'
    abaqus analysis job=Job-${i} input=Job-${i}.inp oldjob=Job-${j} user=subroutine.f
    fil=new cpus=8 memory='17gb' interactive
    echo "JobNumber:_${i}"
    abaqus cae noGUI=odb_analysis.py -- ${i}
    python ./PIDcontrol_power.py -- ${i}
done
```



## Appendix E

# Subroutines for simulating Ti6Al4V phase transformation

In these FORTRAN subroutines of Abaqus, volume fractions of the three Ti6Al4V phases  $\alpha'$ ,  $\alpha$ ,  $\beta$  are first initialized by SDVINI subroutine. Then the phase transformation between different metallurgical phases is calculated in USDFLD subroutine, with both diffusionless process (Koistinen-Marburger model) and diffusional process (modified Johnson-Mehl-Avrami model). Note that the JMA model is modified here to adapt to real non-isothermal process in simulation.

### Code Listing E.1: SDVINI and USDFLD subroutine

```
SUBROUTINE SDVINI(STATEV,COORDS,NSTATV,NCRDS,NOEL,NPT,  
1 LAYER,KSPT)  
C  
  INCLUDE 'ABA_PARAM.INC'  
C  
  DIMENSION STATEV(NSTATV),COORDS(NCRDS)  
    STATEV(4)=0.00D0  
    STATEV(5)=0.07526D0  
    STATEV(6)=0.92474D0  
    STATEV(7)=0.00D0  
    STATEV(8)=0.00D0  
    STATEV(9)=STATEV(5)  
    STATEV(10)=STATEV(6)  
  RETURN  
  END  
C=====
```

```
SUBROUTINE USDFLD(FIELD,STATEV,PNEWDT,DIRECT,T,CELENT,  
1 TIME,DTIME,CMNAME,ORNAME,NFIELD,NSTATV,NOEL,NPT,LAYER,  
2 KSPT,KSTEP,KINC,NDI,NSHR,COORD,JMAC,JMATYP,MATLAYO,LACCFLA)  
C
```

```

INCLUDE 'ABA_PARAM.INC'
C
CHARACTER*80 CMNAME,ORNAME
CHARACTER*3 FLGRAY(15)
DIMENSION FIELD(NFIELD),STATEV(NSTATV),DIRECT(3,3), T(3,3),TIME(2)
C-----Ti-6Al-4V Phase Transformation during AM-----
DIMENSION ARRAY(15),JARRAY(15),JMAC(*),JMATYP(*),COORD(*)
C-----
C USFLD routine to calculate change due to phase transformation.
C Solution dependant state variables – must be defined and initialised
C in the ABAQUS input file.
C STATEV(1) Current temp stored as previous temp
C STATEV(2) Time increment DTIME
C STATEV(3) Heating or Cooling rate dT/dt
C STATEV(4) Update Field(1) to store max Temp
C STATEV(5) Beta Phase
C STATEV(6) Alpha Phase
C STATEV(7) Martensite Phase
C STATEV(8) Old Martensite Phase
C STATEV(9) Old Beta Phase
C STATEV(10) Old Alpha Phase
C FIELD(1) Current Temp
C FIELD(2) DTIME
C FIELD(3) DT/Dt
C FIELD(4) Connect SDV7 and SDV8
C-----
real*4 k1, n1, k2, n2, m_gamma, m_s, m_cool_rate
C USER CODE START
C Reading instantaneous temperature in direction 11
CALL GETVRM('TEMP',ARRAY,JARRAY,FLGRAY,JRCD,JMAC,JMATYP,MATLAYO,
1 LACCFLA)
FIELD(1)=ARRAY(1) !temp as field variable
DTEMP=FIELD(1)-STATEV(1) !dT Current temp – previous stored temp
FIELD(2)=DTIME !dt
FIELD(3)=DTEMP/FIELD(2) !dT/dt
if (jrct == 1) then
write(6,*) "GETVRM_routine_error!!!"
call XIT
endif
! define JMA coefficients k and n
an=2.5D0 !(n)
xc=734.59204D0
y=3.84D-05

```

---

```

H=0.01375D0
wi=58.38677D0
we=35.81163D0
EE=2.7182818D0

IF (FIELD(1).LT.xc) THEN
  ak=y+(H*EE**(-0.5*(FIELD(1)-xc)**2.0/(wi**2.0)))
  ako=y+(H*EE**(-0.5*(STATEV(1)-xc)**2.0/(wi**2.0)))
ELSE
  ak=y+(H*EE**(-0.5*(FIELD(1)-xc)**2.0/(we**2.0)))
  ako=y+(H*EE**(-0.5*(STATEV(1)-xc)**2.0/(we**2.0)))
ENDIF
C Additivity rule k = k1 (new) and ko = k0 (old)
C Eps = additional step added at t1 (t1f)
C FAEQ and FBEQ FMEQ are equilibrium fractions at t1 (new, current), FAEQ0+FBEQ0=1.0
C
C=====
C Store the current temp as a solution dependent state (previous, old)
  STATEV(1)=FIELD(1)
  STATEV(2)=FIELD(2)
  STATEV(3)=FIELD(3)
C=====
C !max temperature
  IF (FIELD(1).LT.STATEV(4)) THEN
    STATEV(4)=STATEV(4)
  ELSE
    STATEV(4)=FIELD(1)
  ENDIF
C=====
k1=ak
n1=an
k2=ak
n2=an
m_gamma=0.015
m_s=650.0
m_cool_rate=-410.0
c1=450.0
c2=80.0
c3=0.925
c4=0.0085
b_transus=980.0
if (STATEV(9).LT.0.25) then
  f_b_r=STATEV(9)

```

---



```

else
  f_b_r=0.25*(1.0-STATEV(9))
endif

if ((FIELD(3).LT.m_cool_rate).AND. (FIELD(1).LT.M_s).AND.
& (STATEV(4).GT.1200.0))then! fast cooling
  STATEV(7)=STATEV(8)+(STATEV(9)-f_b_r)*(1.0-EE**(-m_gamma*(M_s
& -FIELD(1))))!martensite
  IF (STATEV(7) .GE. 1.00) THEN
    STATEV(7)=1.00
  ELSEIF (STATEV(7) .LE. 0.00) THEN
    STATEV(7)=0.00
  ENDIF
  STATEV(6)=STATEV(10)!alpha
  STATEV(5)=1.0-STATEV(6)-STATEV(7)!beta
C !slow cooling or heating
elseif (FIELD(3).GT.m_cool_rate)then
  FMEQ=0.5*(1.0+tanh((c1-FIELD(1))/c2))!Martensite equilibre T1
C write(7,*) 'FMEQ', FMEQ!!!!
  IF (FMEQ .GE. 1.00) THEN
    FMEQ=1.00
  ELSEIF (FMEQ .LE. 0.00) THEN
    FMEQ=0.00
  ENDIF
  if (FIELD(1).LT.b_transus)then!alpha equilibre T1
    FAEQ0=c3*(1.0-EE**(-c4*(b_transus-FIELD(1))))
C write(7,*) 'FAEQ0', FAEQ0
  else
    FAEQ0=0.0
  endif
  IF (FAEQ0 .GE. 1.00) THEN
    FAEQ0=1.00
  ELSEIF (FAEQ0 .LE. 0.00) THEN
    FAEQ0=0.00
  ENDIF
  FBEQ0=1.0-FAEQ0
  FBEQ=FBEQ0*(1.0-STATEV(8))
  FAEQ=FAEQ0*(1.0-STATEV(8))

  if ((FIELD(3).GT.0.0).AND.(STATEV(8).GT.0.0)) then!heat: martensit->alpha+beta
    if (STATEV(8).GT.FMEQ)then
      Eps_M=(-log((STATEV(8)-FMEQ)/(1.0-FMEQ)))/k1)**(1.0/n1)
C write(7,*) '1-FMEQ', 1.0-FMEQ

```

---

```

C      write(7,*) 'Eps_M', EPS_M
      STATEV(7)=1.0-(1.0-EE**(-k1*(Eps_m+DTIME)**n1))*(1-FMEQ)
C      write(7,*) 'SDV7', STATEV(7)
      else
      STATEV(7)=STATEV(8)
      endif
      IF (STATEV(7) .GE. 1.00) THEN
      STATEV(7)=1.00
      ELSEIF (STATEV(7) .LE. 0.00) THEN
      STATEV(7)=0.00
      ENDIF
      endif

      if (STATEV(8).LT.1.0) Then!beta<->alpha heating or slow cooling
      f_a_star=STATEV(10)*(1.0-STATEV(7))/(1.0-STATEV(8))
      f_b_star=STATEV(9)*(1.0-STATEV(7))/(1.0-STATEV(8))
C      write(7,*) 'f_a_star', f_a_star,'f_b_star', f_b_star,'eps_b',
C      write(7,*) 'SDV9-FBEQ',STATEV(9)-FBEQ
C      write(7,*) '1-SDV7-FBEQ',1.0-STATEV(7)-FBEQ
C      write(7,*) 'eps_b', eps_b
      if((f_b_star.GT.FBEQ).AND.(STATEV(9).GT.FBEQ).AND.
      & ((1.0-STATEV(7)).GT.FBEQ))then!beta->alpha
      Eps_B1=(-log((STATEV(9)-FBEQ)/(1.0-STATEV(7)-FBEQ))/k2)**(1.0/
      & n2)
      STATEV(5)=1.0-STATEV(7)-(1.0-EE**(-k2*(Eps_B1+DTIME)**n2))*
      & (1.0-STATEV(7)-FBEQ)
C      write(7,*) 'BPS_B1', EPS_B1
C      write(7,*) 'baSDV5', STATEV(5)
      elseif((f_b_star.LT.FBEQ).AND.(STATEV(9).LT.FBEQ))then!alpha->beta
      Eps_B2=(-log((FBEQ-STATEV(9))/FBEQ)/k2)**(1.0/n2)
      STATEV(5)=(1.0-EE**(-k2*(Eps_B2+DTIME)**n2))*FBEQ
C      write(7,*) 'EPS_B2',EPS_B2
C      write(7,*) 'abSDV5',STATEV(5)
      else
      STATEV(5)=f_b_star
      endif
      else
      STATEV(5)=0.0
      endif
      STATEV(6)=1.0-STATEV(7)-STATEV(5)
      else!no change
      STATEV(5)=STATEV(9)
      STATEV(6)=STATEV(10)

```

---

```
STATEV(7)=STATEV(8)
endif! record history
FIELD(4)=STATEV(7)
STATEV(8)=FIELD(4)
STATEV(9)=STATEV(5)
STATEV(10)=STATEV(6)
```

```
RETURN
END
```

## Appendix F

# Abaqus post-process program to extract von Mises stress

This C++ program is applied to extract the extracting von Mises stress of each element, which is a basic preparation step before analysing quantitatively the residual stress in a voxel part. This program can be easily modified to adapt itself to different Abaqus post-processing tasks, such as extract the maximum temperature from an \*.odb file. In fact, the post-processing of Abaqus can be implemented by both python and C++ (usually more faster than python for a huge mesh). We compile this source code, then an executable binary file \*.exe will be generated. This \*.exe file can be used for reading and analysing an \*.odb result file.

**Code Listing F.1:** C++ program for extracting von Mises stress of each element

```
/*  
/*****  
#if (defined(HP) && (! defined(HKS_HPUXI)))  
#include <iostream.h>  
#else  
#include <iostream>  
using namespace std;  
#endif  
  
#include <odb_API.h>  
#include <sys/stat.h>  
/*  
*****  
utility functions  
*****  
*/  
#include <string>  
#include <vector>  
#include <fstream>
```

```

#include <sstream>
/*****/
bool fileExists(const odb_String &string);
void rightTrim(odb_String &string,const char* char_set);
/*****/

int ABQmain(int argc, char **argv)
{
    odb_String odbPath;
    bool ifOdbName = false;
    // Initialize maximum values.
    float maxMises = -0.1;
    int maxElem = 0;
    odb_String maxStep = "__None__";
    int numBD = 0,numElems = 0, numIP = 0, numComp = 0, position = 0;
    /*****/
    ofstream outFile;
    outFile.open("mises_all_elements.csv", ios::out);
    outFile << "ElementId" << ',' << "Mises" << endl;

    for (int arg = 0; arg<argc; arg++)
    {
        if (strcmp(argv[arg],"-o**",2) == 0)
        {
            arg++;
            odbPath = argv[arg];
            rightTrim(odbPath,".odb");
            if (!fileExists(odbPath))
            {
                cerr << "**ERROR**_output_database_" << odbPath.CStr()
                    << "_does_not_exist\n" << endl;
                exit(1);
            }
            ifOdbName = true;
        }
    }

    odb_Odb& myOdb = openOdb(odbPath);
    odb_Instance& instance = myOdb.rootAssembly().instances()["PART-1-1"];
    odb_Set& myEleSet= instance.elementSets()["AMPART"];
    odb_Step& lastStep = myOdb.steps()["Step-Cooling"];
    odb_SequenceFrame& allFramesInLastStep = lastStep.frames();
    int numFrames = allFramesInLastStep.size();

```

---

```

odb_Frame& lastFrame = allFramesInLastStep[numFrames-1];
odb_FieldOutputRepository& fieldOutputRep = lastFrame.fieldOutputs();
odb_FieldOutput& fieldS = fieldOutputRep.get("S");
odb_FieldOutput partStress = fieldS.getSubset(myEleSet);
const odb_SequenceFieldBulkData& seqVal = partStress.bulkDataBlocks();
int numBlocks = seqVal.size();
for ( int iblock=0; iblock<numBlocks; iblock++)
{
    const odb_FieldBulkData& bulkData = seqVal[iblock];
    numBD = bulkData.length();
    numElems = bulkData.numberofElements();
    numIP = numBD/numElems;
    float* mises = bulkData.mises();
    int* elementLabels = bulkData.elementLabels();
    for (int elem=0; elem<numElems; elem++)
    {
        for (int ip=0; ip<numIP; ip++)
        {
            position = elem*numIP+ip;
            float misesData = mises[position];
            outFile<< position <<','<< misesData <<endl;
            if (misesData > maxMises)
            {
                maxMises = misesData;
                maxElem = elementLabels[elem];
                maxStep = lastStep.name();
            }
        }
    }
}
outFile.close();
cout <<"The number of integration points for each element" << numIP <<endl;
cout << "Maximum von Mises stress at integration point" << " is " << maxMises
    << " in element" << maxElem << endl;
cout << " step:" << maxStep.CStr() << endl;
// close the output database before exiting the program

myOdb.close();
return(0);
}

bool fileExists(const odb_String &string)
{

```

```
bool exists = false;  
struct stat buf;  
if (stat(string.CStr(),&buf)==0)  
    exists = true;  
return exists;  
}  
  
void rightTrim(odb_String &string,const char* char_set)  
{  
    int length = string.Length();  
    if (string.Find(char_set)==length)  
        string.append(odb_String(char_set));  
}
```

# Bibliography

- [ABH 18] A BHAGAVATAM A RAMAKRISHNAN V. A., DINDA G.  
Laser Metal Deposition of Aluminum 7075 Alloy. *International Journal of Material Science and Research*, , 2018.
- [ACH 11] ACHERJEE B., MONDAL S., TUDU B., MISRA D.  
Application of artificial neural network for predicting weld quality in laser transmission welding of thermoplastics. *Applied soft computing*, vol. 11, n° 2, 2011, p. 2548–2555, Elsevier.
- [AGO 05] AGOSTON M. K., AGOSTON M. K.  
*Computer graphics and geometric modeling*, vol. 1. Springer, 2005.
- [AHN 16] AHN J.  
Experimental characterisation and numerical simulation of fibre laser welding of AA 2024-T3 and Ti-6Al-4V. Thèse de doctorat, Imperial College London, 2016.
- [AHN 18] AHNEMAN D. T., ESTRADA J. G., LIN S., DREHER S. D., DOYLE A. G.  
Predicting reaction performance in C–N cross-coupling using machine learning. *Science*, vol. 360, n° 6385, 2018, p. 186–190, American Association for the Advancement of Science.
- [AHS 11] AHSAN M. N.  
Modelling and analysis of laser direct metal deposition of Ti-6Al-4V alloy. Thèse de doctorat, The University of Manchester (United Kingdom), 2011.
- [ALI 17] ALI H., MA L., GHADBEIGI H., MUMTAZ K.  
In-situ residual stress reduction, martensitic decomposition and mechanical properties enhancement through high temperature powder bed pre-heating of Selective Laser Melted Ti6Al4V. *Materials Science and Engineering: A*, vol. 695, 2017, p. 211–220, Elsevier.
- [ANS ] ANSYS  
ANSYS Advanced Analysis Techniques.
- [ÅST 95] ÅSTRÖM K. J., HÄGGLUND T.  
*PID controllers: theory, design, and tuning*, vol. 2. Instrument society of America Research Triangle Park, NC, 1995.



- [AUT 18] AUTODESK  
Autodesk Netfabb Simulation Utility Tutorial, 2018.
- [AVE 17] AVERSA A., LORUSSO M., TREVISAN F., AMBROSIO E., CALIGNANO F., MANFREDI D., BIAMINO S., FINO P., LOMBARDI M., PAVESE M.  
Effect of process and post-process conditions on the mechanical properties of an A357 alloy produced via laser powder bed fusion. *Metals*, vol. 7, n° 2, 2017, p. 68, Multi-disciplinary Digital Publishing Institute.
- [BAD 18] BADER C., KOLB D., WEAVER J. C., SHARMA S., HOSNY A., COSTA J., OXMAN N.  
Making data matter: Voxel printing for the digital fabrication of data across scales and domains. *Science Advances*, vol. 4, n° 5, 2018, American Association for the Advancement of Science.
- [BAE 17] BAEK G. Y., LEE K. Y., PARK S. H., SHIM D. S.  
Effects of substrate preheating during direct energy deposition on microstructure, hardness, tensile strength, and notch toughness. *Metals and Materials International*, vol. 23, n° 6, 2017, p. 1204–1215, Springer.
- [BAS 00] BASHEER I. A., HAJMEER M.  
Artificial neural networks: fundamentals, computing, design, and application. *Journal of microbiological methods*, vol. 43, n° 1, 2000, p. 3–31, Elsevier.
- [BEC 16] BECKERS B., PICO T., JIMENEZ S.  
A robust smoothed voxel representation for the generation of finite element models for computational urban physics. *First International Conference on Urban Physics*, 2016.
- [BEN 14] BENNETT J.  
Voxel octree intersection based 3D scanning. Master's thesis, Lethbridge, Alta.: University of Lethbridge, Dept. of Mathematics and Computer Science, 2014.
- [BI 06] BI G., GASSER A., WISSENBACH K., DRENKER A., POPRAWA R.  
Characterization of the process control for the direct laser metallic powder deposition. *Surface and Coatings Technology*, vol. 201, n° 6, 2006, p. 2676 - 2683.
- [BIC 07] BICANIC N.  
*Discrete Element Methods*, Chapter 11. American Cancer Society, 2007.
- [BOS 18] BOSE A., SCHUH C. A., TOBIA J. C., TUNCER N., MYKULOWYCZ N. M., PRESTON A., BARBATI A. C., KERNAN B., GIBSON M. A., KRAUSE D., BRZEZINSKI T., SCHROERS J., FULOP R., MYERBERG J. S., SOWERBUTTS M., CHIANG Y.-M., HART A. J., SACHS E. M., LOMELI E. E., LUND A. C.  
Traditional and additive manufacturing of a new Tungsten heavy alloy alternative. *International Journal of Refractory Metals and Hard Materials*, vol. 73, 2018, p. 22 - 28.

- [BRA 16] BRANDT M.  
*Laser Additive Manufacturing: Materials, Design, Technologies, and Applications*. Woodhead Publishing, 2016.
- [BRO 13] BROWN A. C., DE BEER D.  
Development of a stereolithography (STL) slicing and G-code generation algorithm for an entry level 3-D printer. *2013 Africon*, Sept 2013, p. 1-5.
- [BUC 14] BUCHBINDER D., MEINERS W., PIRCH N., WISSENBACH K., SCHRAGE J.  
Investigation on reducing distortion by preheating during manufacture of aluminum components using selective laser melting. *Journal of laser applications*, vol. 26, n° 1, 2014, p. 012004, LIA.
- [BUR 15] BURKERT T., FISCHER A.  
The effects of heat balance on the void formation within marage 300 processed by selective laser melting. *Proc of SFF Symposium*, 2015, p. 745–757.
- [CAO 15] CAO X., AYALEW B.  
Control-oriented MIMO modeling of laser-aided powder deposition processes. *2015 American Control Conference (ACC)*, July 2015, p. 3637-3642.
- [CAP 18] CAPRIO L., CHIARI G., DEMIR A., PREVITALI B.  
Development of Novel High Temperature Laser Powder Bed Fusion System for the Processing of Crack-Susceptible Alloys. *The Twenty-ninth Annual International Solid Freeform Fabrication (SFF) Symposium—An Additive Manufacturing Conference*, 2018, p. 2275–2285.
- [CAR 15] CARROLL B. E., PALMER T. A., BEESE A. M.  
Anisotropic tensile behavior of Ti-6Al-4V components fabricated with directed energy deposition additive manufacturing. *Acta Materialia*, vol. 87, 2015, p. 309 - 320.
- [CAS 66] CASTRO R S. L.  
CONTRIBUTION TO METALLOGRAPHIC AND STRUCTURAL STUDY OF TITANIUM ALLOY TA6V. *MEMOIRES SCIENTIFIQUES DE LA REVUE DE MET-ALLURGIE*, vol. 63(12), 1966, p. 1025.
- [CAS 11] CASAVOLA C., PAPPALETTERE C., TURSI F.  
Residual Stress on Aisi 300 Sintered Materials. *Experimental and Applied Mechanics, Volume 6*, p. 201–208 Springer, 2011.
- [CAS 18] CASATI R., HAMIDI NASAB M., CODURI M., TIRELLI V., VEDANI M.  
Effects of Platform Pre-Heating and Thermal-Treatment Strategies on Properties of AlSi10Mg Alloy Processed by Selective Laser Melting. *Metals*, vol. 8, n° 11, 2018, p. 954, Multidisciplinary Digital Publishing Institute.

- [CHE 05] CHEN X., MCMAINS S.  
POLYGON OFFSETTING BY COMPUTING WINDING NUMBERS. *ASME 2005 International Design Engineering Technical Conferences & Computers and Information in Engineering Conference*, 2005.
- [CHE 18] CHEN Q., GUILLEMOT G., GANDIN C.-A., BELLET M.  
Finite Element Modeling of Ceramic Deposition by LBM(SLM) Additive Manufacturing. MEBOLDT M., KLAHN C., Eds., *Industrializing Additive Manufacturing - Proceedings of Additive Manufacturing in Products and Applications - AMPA2017*, Cham, 2018 Springer International Publishing, p. 49–58.
- [CHO 16] CHOWDHURY S., ANAND S.  
Artificial neural network based geometric compensation for thermal deformation in additive manufacturing processes. *ASME 2016 11th International Manufacturing Science and Engineering Conference* American Society of Mechanical Engineers, 2016, p. V003T08A006–V003T08A006.
- [CHU 14] CHUA C. K., LEONG K. F.  
*3D Printing and Additive Manufacturing: Principles and Applications*. WORLD SCIENTIFIC, 4th edition, 2014.
- [COM 17] COMPANY R.  
. « Design for metal AM-a beginner's guide ». <https://www.renishaw.com/en/design-for-metal-am-a-beginners-guide-42652>, 8 2017.
- [COO 18] COOPER K., STEELE P., CHENG B., CHOU K.  
Contact-Free Support Structures for Part Overhangs in Powder-Bed Metal Additive Manufacturing. *Inventions*, vol. 3, n° 1, 2018.
- [COR 16] CORBIN D., NASSAR A., REUTZEL E., KISTLER N., BEESE A., MICHALERIS P.  
Impact of directed energy deposition parameters on mechanical distortion of laser deposited Ti-6Al-4V. *Solid Freeform Fabrication*, , 2016, p. 670–679.
- [COR 17] CORBIN D. J., NASSAR A. R., REUTZEL E. W., BEESE A. M., KISTLER N. A.  
Effect of directed energy deposition processing parameters on laser deposited Inconel® 718: External morphology. *Journal of Laser Applications*, vol. 29, n° 2, 2017, p. 022001, LIA.
- [COR 18] CORBIN D. J., NASSAR A. R., REUTZEL E. W., BEESE A. M., MICHALERIS P.  
Effect of Substrate Thickness and Preheating on the Distortion of Laser Deposited Ti-6Al-4V. *Journal of Manufacturing Science and Engineering*, vol. 140, n° 6, 2018, p. 061009, American Society of Mechanical Engineers.

- [COZ 10] DEL COZ DÁAZ J., RODRÁGUEZ P. M., NIETO P. G., CASTRO-FRESNO D. Comparative analysis of TIG welding distortions between austenitic and duplex stainless steels by FEM. *Applied Thermal Engineering*, vol. 30, n° 16, 2010, p. 2448 - 2459. Selected Papers from the 12th Conference on Process Integration, Modelling and Optimisation for Energy Saving and Pollution Reduction.
- [CRE 09] CRESPO A., DEUS A., VILAR R. Modeling of phase transformations and internal stresses in laser powder deposition. *XVII International Symposium on Gas Flow, Chemical Lasers, and High-Power Lasers*, vol. 7131 International Society for Optics and Photonics, 2009, p. 713120.
- [CRE 11] CRESPO A. Modelling of Heat Transfer and Phase Transformations in the Rapid Manufacturing of Titanium Components. AHSAN A., Ed., *Convection and Conduction Heat Transfer*, Chapter 15 IntechOpen, Rijeka, 2011.
- [CUE 18] CUELLAR J. S., SMIT G., PLETTENBURG D., ZADPOOR A. Additive manufacturing of non-assembly mechanisms. *Additive Manufacturing*, vol. 21, 2018, p. 150 - 158.
- [DAH 13] DAHL G. E., SAINATH T. N., HINTON G. E. Improving deep neural networks for LVCSR using rectified linear units and dropout. *2013 IEEE international conference on acoustics, speech and signal processing IEEE*, 2013, p. 8609–8613.
- [DAL 16] DAL M., FABBRO R. An overview of the state of art in laser welding simulation. *Optics & Laser Technology*, vol. 78, 2016, p. 2 - 14. The year of light: optical fiber sensors and laser material processing.
- [DAS 15] DAS P., CHANDRAN R., SAMANT R., ANAND S. Optimum Part Build Orientation in Additive Manufacturing for Minimizing Part Errors and Support Structures. *Procedia Manufacturing*, vol. 1, 2015, p. 343 - 354. 43rd North American Manufacturing Research Conference, NAMRC 43, 8-12 June 2015, UNC Charlotte, North Carolina, United States.
- [DAS 17] DAS P., MHAPSEKAR K., CHOWDHURY S., SAMANT R., ANAND S. Selection of build orientation for optimal support structures and minimum part errors in additive manufacturing. *Computer-Aided Design and Applications*, vol. 14, n° sup1, 2017, p. 1-13, Taylor & Francis.
- [DEM 17] DEMIR A. G., PREVITALI B. Investigation of remelting and preheating in SLM of 18Ni300 maraging steel as corrective and preventive measures for porosity reduction. *The International Journal of Advanced Manufacturing Technology*, vol. 93, n° 5-8, 2017, p. 2697–2709, Springer.

- [DEN 15] DENLINGER E. R.  
thermo-mechanical model development and experimental validation for metallic parts in additive manufacturing. Thèse de doctorat, Pennsylvania State University, 2015.
- [DEV 16] DEVESSE W., DE BAERE D., HINDERDAEL M., GUILLAUME P.  
Hardware-in-the-loop control of additive manufacturing processes using temperature feedback. *Journal of Laser Applications*, vol. 28, n° 2, 2016, p. 022302, LIA.
- [DIN 14] DING D., PAN Z. S., CUIURI D., LI H.  
A tool-path generation strategy for wire and arc additive manufacturing. *The International Journal of Advanced Manufacturing Technology*, vol. 73, n° 1, 2014, p. 173–183.
- [DIN 15a] DING D., PAN Z., CUIURI D., LI H.  
A practical path planning methodology for wire and arc additive manufacturing of thin-walled structures. *Robotics and Computer-Integrated Manufacturing*, vol. 34, 2015, p. 8 - 19.
- [DIN 15b] DING D., PAN Z., CUIURI D., LI H.  
Wire-feed additive manufacturing of metal components: technologies, developments and future interests. *The International Journal of Advanced Manufacturing Technology*, vol. 81, n° 1, 2015, p. 465–481.
- [DIN 16a] DING D., PAN Z., CUIURI D., LI H., LARKIN N.  
Adaptive path planning for wire-feed additive manufacturing using medial axis transformation. *Journal of Cleaner Production*, vol. 133, 2016, p. 942 - 952.
- [DIN 16b] DING D., PAN Z., CUIURI D., LI H., VAN DUIN S., LARKIN N.  
Bead modelling and implementation of adaptive MAT path in wire and arc additive manufacturing. *Robotics and Computer-Integrated Manufacturing*, vol. 39, 2016, p. 32–42, Elsevier.
- [DIN 16c] DING D., SHEN C., PAN Z., CUIURI D., LI H., LARKIN N., VAN DUIN S.  
Towards an automated robotic arc-welding-based additive manufacturing system from CAD to finished part. *Computer-Aided Design*, vol. 73, 2016, p. 66–75, Elsevier.
- [DIN 16d] DING Y., WARTON J., KOVACEVIC R.  
Development of sensing and control system for robotized laser-based direct metal addition system. *Additive Manufacturing*, vol. 10, 2016, p. 24 - 35.
- [DOM 11] DOMAŃSKI T., BOKOTA A.  
Numerical models of hardening phenomena of tools steel base on the TTT and CCT diagrams. *Archives of Metallurgy and Materials*, vol. 56, n° 2, 2011, p. 325–344, Versita.

- [DUB 17] DUBROV A., MIRZADE F. K., DUBROV V.  
Mathematical modeling of thermal behavior for additive manufacturing with metal powder injection. *Procedia Engineering*, vol. 201, 2017, p. 478–488, Elsevier.
- [ELM 04] ELMER J. W., PALMER T. A., BABU S. S., ZHANG W., DEBROY T.  
Phase transformation dynamics during welding of Ti-6Al-4V. *Journal of Applied Physics*, vol. 95, n° 12, 2004, p. 8327-8339.
- [EVE 16] EVERTON S. K., HIRSCH M., STRAVROULAKIS P., LEACH R. K., CLARE A. T.  
Review of in-situ process monitoring and in-situ metrology for metal additive manufacturing. *Materials & Design*, vol. 95, 2016, p. 431 - 445.
- [EVE 18] EVERAERTS J., SONG X., NAGARAJAN B., KORSUNSKY A. M.  
Evaluation of macro- and microscopic residual stresses in laser shock-peened titanium alloy by FIB-DIC ring-core milling with different core diameters. *Surface and Coatings Technology*, vol. 349, 2018, p. 719 - 724.
- [FAL 11] FALLAH V., ALIMARDANI M., CORBIN S. F., KHAJEPOUR A.  
Temporal development of melt-pool morphology and clad geometry in laser powder deposition. *Computational materials science*, vol. 50, n° 7, 2011, p. 2124–2134, Elsevier.
- [FAN 93] FAN Z.  
On the Young's moduli of Ti-6Al-4V alloys. *Scripta Metallurgica et Materialia; (United States)*, vol. 29:11, 1993.
- [FAR 06] FARJAS J., ROURA P.  
Modification of the Kolmogorov-Johnson-Mehl-Avrami rate equation for non-isothermal experiments and its analytical solution. *Acta Materialia*, vol. 54, n° 20, 2006, p. 5573 - 5579.
- [FAR 16] FARSHIDIANFAR M. H., KHAJEPOUR A., GERLICH A.  
Real-time control of microstructure in laser additive manufacturing. *The International Journal of Advanced Manufacturing Technology*, vol. 82, n° 5-8, 2016, p. 1173–1186, Springer.
- [FAT 07] FATHI A., KHAJEPOUR A., TOYSERKANI E., DURALI M.  
Clad height control in laser solid freeform fabrication using a feedforward PID controller. *The International Journal of Advanced Manufacturing Technology*, vol. 35, n° 3, 2007, p. 280–292.
- [FIT 14] FITZPATRICK C. K., BALDWIN M. A., CLARY C. W., MALETSKY L. P., RULLKOETTER P. J.  
Evaluating knee replacement mechanics during ADL with PID-controlled dynamic finite element analysis. *Computer Methods in Biomechanics and Biomedical Engineering*, vol. 17, n° 4, 2014, p. 360-369, Taylor & Francis. PMID: 22687046.

- [FRA 14] FRAZIER W. E.  
Metal Additive Manufacturing: A Review. *Journal of Materials Engineering and Performance*, vol. 23, n° 6, 2014, p. 1917–1928.
- [FRA 16] FRANSEN M.  
Eigenstrain reconstruction of residual stresses induced by selective laser melting. Master's thesis, Technische Universiteit Delft, 2016.
- [FRA 17] FRADL D., PANDITARATNE J., BI J., FU R., OANCEA V.  
Finite Element Simulation of the Multi Jet Fusion (MJF) Process using Abaqus. *NAFEMS World Congress*, 2017.
- [FRU 15] DE FRUTOS G. M.  
Product development process for additive manufacturing. Considerations on the design of final products for 3D printing. Master's thesis, Instituto Superior Técnico, 2015.
- [GAN 16] GAN Z., YU G., LI S., HE X., CHEN R., ZHENG C., NING W.  
A novel intelligent adaptive control of laser-based ground thermal test. *Chinese Journal of Aeronautics*, vol. 29, n° 4, 2016, p. 1018 - 1026.
- [GAO 15] GAO W., ZHANG Y., RAMANUJAN D., RAMANI K., CHEN Y., WILLIAMS C. B., WANG C. C., SHIN Y. C., ZHANG S., ZAVATTIERI P. D.  
The status, challenges, and future of additive manufacturing in engineering. *Computer-Aided Design*, vol. 69, 2015, p. 65 - 89.
- [GAR 15] GARG A., LAM J. S. L., SAVALANI M.  
A new computational intelligence approach in formulation of functional relationship of open porosity of the additive manufacturing process. *The International Journal of Advanced Manufacturing Technology*, vol. 80, n° 1-4, 2015, p. 555–565, Springer.
- [GAR 16] GARDAN J.  
Additive manufacturing technologies: state of the art and trends. *International Journal of Production Research*, vol. 54, n° 10, 2016, p. 3118–3132, Taylor & Francis.
- [GEO 07] GEORGE P. L., BOROUCHEKI H., FREY P. J., LAUG P., SALTEL E.  
*Mesh Generation and Mesh Adaptivity: Theory and Techniques*, Chapter 17. American Cancer Society, 2007.
- [GÉR 17] GÉRON A.  
*Hands-on machine learning with Scikit-Learn and TensorFlow: concepts, tools, and techniques to build intelligent systems.* " O'Reilly Media, Inc.", 2017.
- [GHO 18] GHOSH S.  
Predictive modeling of solidification during laser additive manufacturing of nickel superalloys: recent developments, future directions. *Materials Research Express*, vol. 5, n° 1, 2018, p. 012001.

- [GOL 84] GOLDAK J., CHAKRAVARTI A., BIBBY M.  
A new finite element model for welding heat sources. *Metallurgical Transactions B*, vol. 15, n° 2, 1984, p. 299–305.
- [GU 15] GU D.  
*Laser Additive Manufacturing (AM): Classification, Processing Philosophy, and Metallurgical Mechanisms*, p. 15–71. Springer Berlin Heidelberg, Berlin, Heidelberg, 2015.
- [HAE 05] HAEMMERICH D., WEBSTER J. G.  
Automatic control of finite element models for temperature-controlled radiofrequency ablation. *BioMedical Engineering OnLine*, vol. 4, 2005, p. 42 - 42.
- [HAG 17] HAGEDORN-HANSEN D., BEZUIDENHOUT M., DIMITROV D., OOSTHUIZEN T.  
THE EFFECTS OF SELECTIVE LASER MELTING SCAN STRATEGIES ON DEVIATION OF HYBRID PARTS. *The South African Journal of Industrial Engineering*, vol. 28, n° 3, 2017, p. 200–212.
- [HAU 02] HAUMONT D., WARZÄ©E N.  
Complete Polygonal Scene Voxelization. *Journal of Graphics Tools*, vol. 7, n° 3, 2002, p. 27-41, Taylor & Francis.
- [HAU 13] HAUGEN F., LIE B.  
Relaxed Ziegler-Nichols Closed Loop Tuning of PI Controllers. *Modeling, Identification and Control*, vol. 34, n° 2, 2013, p. 83–97, Norwegian Society of Automatic Control.
- [HEJ 17] HEJTMANEK M.  
Additive Manufacturing Technologies Utilization in Process Engineering. Master's thesis, Czech Technical University in Prague, 2017.
- [HIL 09] HILLER J. D., LIPSON H.  
Stl 2.0: A proposal for a universal multi-material additive manufacturing file format. *In Mechanical and Aerospace Engineering*, 2009, p. 266–278.
- [HSI 95] HSIEH H.  
. « Computer Graphics Courseware-Clipping », 1995.
- [HU 03] HU D., KOVACEVIC R.  
Sensing, modeling and control for laser-based additive manufacturing. *International Journal of Machine Tools and Manufacture*, vol. 43, n° 1, 2003, p. 51 - 60.
- [HU 09] HU B., ZHANG Q. H., WANG F., ZHANG J. H.  
FEM Analysis of EDM in Gas Based on Birth and Death of Element. *Advances in Materials Manufacturing Science and Technology XIII Volume I*, vol. 626 *Materials Science Forum* Trans Tech Publications, 11 2009, p. 599–604.



- [HU 15] HU K., JIN S., WANG C. C.  
Support slimming for single material based additive manufacturing. *Computer-Aided Design*, vol. 65, 2015, p. 1 - 10.
- [HUA 16] HUANG Y., KHAMESEE M. B., TOYSERKANI E.  
A comprehensive analytical model for laser powder-fed additive manufacturing. *Additive Manufacturing*, vol. 12, 2016, p. 90 - 99.
- [HUS 13a] HUSSEIN A., HAO L., YAN C., EVERSON R.  
Finite element simulation of the temperature and stress fields in single layers built without-support in selective laser melting. *Materials & Design (1980-2015)*, vol. 52, 2013, p. 638 - 647.
- [HUS 13b] HUSSEIN A., HAO L., YAN C., EVERSON R., YOUNG P.  
Advanced lattice support structures for metal additive manufacturing. *Journal of Materials Processing Technology*, vol. 213, n° 7, 2013, p. 1019 - 1026.
- [HUY 15] HUYAN F., HEDSTRÅM P., BORGSTAM A.  
Modelling of the Fraction of Martensite in Low-alloy Steels. *Materials Today: Proceedings*, vol. 2, 2015, p. S561 - S564. International Conference on Martensitic Transformations, ICOMAT-2014.
- [IAN 15] IAN GIBSON DAVID ROSEN B. S.  
*Additive Manufacturing Technologies: 3D Printing, Rapid Prototyping, and Direct Digital Manufacturing*. Springer-Verlag New York, 2 edition, 2015.
- [JÄR 14] JÄRVINEN J.-P., MATILAINEN V., LI X., PIILI H., SALMINEN A., MÄKELÄ I., NYRHILÄ O.  
Characterization of Effect of Support Structures in Laser Additive Manufacturing of Stainless Steel. *Physics Procedia*, vol. 56, 2014, p. 72 - 81. 8th International Conference on Laser Assisted Net Shape Engineering LANE 2014.
- [JIA 17] JIAWEN XIE V. OANCEA J. A. H.  
Phase Transformations in Metals during Additive Manufacturing Processes. *NAFEMS World Congress, Stockholm, 2017*.
- [JON 13] JONES R. O.  
Additive Manufacturing of Functional Engineering Components. Thèse de doctorat, University of Bath, 2013.
- [KAR 99] KARABASSI E.-A., PAPAIOANNOU G., THEOHARIS T.  
A fast depth-buffer-based voxelization algorithm. *Journal of graphics tools*, vol. 4, n° 4, 1999, p. 5-10, Taylor & Francis.
- [KAR 09] KARATAŞ C., SOZEN A., DULEK E.  
Modelling of residual stresses in the shot peened material C-1020 by artificial neural

- network. *Expert Systems with Applications*, vol. 36, n° 2, 2009, p. 3514–3521, Elsevier.
- [KEM 14] KEMPEN K., VRANCKEN B., BULS S., THIJS L., VAN HUMBEECK J., KRUTH J.-P.  
Selective laser melting of crack-free high density M2 high speed steel parts by base-plate preheating. *Journal of Manufacturing Science and Engineering*, vol. 136, n° 6, 2014, p. 061026, American Society of Mechanical Engineers.
- [KIN 15] KING W. E., ANDERSON A. T., FERENCZ R. M., HODGE N. E., KAMATH C., KHAIRALLAH S. A., RUBENCHIK A. M.  
Laser powder bed fusion additive manufacturing of metals; physics, computational, and materials challenges. *Applied Physics Reviews*, vol. 2, n° 4, 2015, p. 041304.
- [KIR 17] KIRKA M. M., NANDWANA P., LEE Y., DEHOFF R. R.  
Solidification and solid-state transformation sciences in metals additive manufacturing. *Scripta Materialia*, vol. 135, 2017, p. 130 - 134.
- [KIS 17] KISTLER N. A., NASSAR A. R., REUTZEL E. W., CORBIN D. J., BEESE A. M.  
Effect of directed energy deposition processing parameters on laser deposited Inconel® 718: Microstructure, fusion zone morphology, and hardness. *Journal of Laser Applications*, vol. 29, n° 2, 2017, p. 022005, LIA.
- [KLE 15] KLEIN J., STERN M., FRANCHIN G., KAYSER M., INAMURA C., DAVE S., WEAVER J. C., HOUK P., COLOMBO P., YANG M. et al.  
Additive manufacturing of optically transparent glass. Master's thesis, Massachusetts Institute of Technology, 2015.
- [KOL 17] KOLLATAJ J.  
Additive Manufacturing (3D Printing)-A Potential Future for Tennis Racket Production: Could 3D Printing/Additive Manufacturing eventually replace the current manufacturing method? Master's thesis, Arcada University of Applied Sciences, 2017.
- [KUB 15] KUBAT M.  
*An introduction to machine learning*, vol. 681. Springer, 2015.
- [LAB 17] DE LA BATUT B., FERGANI O., BROTON V., BAMBACH M., EL MANSOURI M.  
Analytical and Numerical Temperature Prediction in Direct Metal Deposition of Ti6Al4V. *Journal of Manufacturing and Materials Processing*, vol. 1, 2017.
- [LEE 98] LEE W.-S., LIN C.-F.  
Plastic deformation and fracture behaviour of Ti-6Al-4V alloy loaded with high strain rate under various temperatures. *Materials Science and Engineering: A*, vol. 241, n° 1, 1998, p. 48 - 59.

- [LEE 15] LEE Y., ZHANG W.  
Mesoscopic simulation of heat transfer and fluid flow in laser powder bed additive manufacturing. *Proceedings of the Annual International Solid Freeform Fabrication Symposium, Austin, TX, USA*, 2015, p. 10–12.
- [LEE 16] LEE J., PRABHU V.  
Simulation modeling for optimal control of additive manufacturing processes. *Additive Manufacturing*, vol. 12, 2016, p. 197 - 203. Special Issue on Modeling & Simulation for Additive Manufacturing.
- [LI 15] LI Y., XU M., JIN Y., LU H.  
Finite-element Simulation of Low-alloy High Strength Steel Welding Incorporating Improved Martensite Transformation Kinetics and Recrystallization Annealing. *ISIJ International*, vol. 55, n° 7, 2015, p. 1448-1453.
- [LI 16] LI W., LIU J., ZHOU Y., WEN S., WEI Q., YAN C., SHI Y.  
Effect of substrate preheating on the texture, phase and nanohardness of a Ti–45Al–2Cr–5Nb alloy processed by selective laser melting. *Scripta Materialia*, vol. 118, 2016, p. 13–18, Elsevier.
- [LIM 17] LIM I., HOELZLE D. J., BARTON K. L.  
A multi-objective iterative learning control approach for additive manufacturing applications. *Control Engineering Practice*, vol. 64, 2017, p. 74 - 87.
- [LIO 14] LIOU J., EL-WARDANY T.  
Finite Element Analysis of Residual Stress in Ti-6Al-4V Alloy Plate Induced by Deep Rolling Process under Complex Roller Path. *International Journal of Manufacturing Engineering*, vol. 2014, 2014, Hindawi.
- [LIO 15] LIOU F., NEWKIRK J., FAN Z., SPARKS T., CHEN X., FLETCHER K., ZHANG J., ZHANG Y., KUMAR K. S., KARNATI S.  
Multiscale and multiphysics modeling of additive manufacturing of advanced materials. rapport, 2015, National Aeronautics and Space Administration.
- [LIU 00] LIU J., CHANG H., HSU T., RUAN X.  
Prediction of the flow stress of high-speed steel during hot deformation using a BP artificial neural network. *Journal of materials processing technology*, vol. 103, n° 2, 2000, p. 200–205, Elsevier.
- [LIU 15] LIU H., SPARKS T., LIOU F., DIETRICH D. M.  
Residual stress and deformation modelling for metal additive manufacturing processes. *Proc. World Congr. Mech. Chem. Mater. Eng.(MCM 2015)*, , 2015.
- [LIV 17] LIVESU M., ELLERO S., MARTÍNEZ J., LEFEBVRE S., ATTENE M.  
From 3D models to 3D prints: an overview of the processing pipeline. *Computer Graphics Forum*, vol. 36, n° 2, 2017, Wiley.

- [LU 18] LU Y., BLAL N., GRAVOUIL A.  
Space-time POD based computational vademecums for parametric studies: application to thermo-mechanical problems. *Advanced Modeling and Simulation in Engineering Sciences*, vol. 5, n° 1, 2018, p. 3.
- [MA 01a] MA D., LIN F., CHUA C. K.  
Rapid Prototyping Applications in Medicine. Part 2: STL File Generation and Case Studies. *The International Journal of Advanced Manufacturing Technology*, vol. 18, n° 2, 2001, p. 118–127.
- [MA 01b] MA D., LIN F., CHUA C.  
Rapid Prototyping Applications in Medicine. Part 1: NURBS-Based Volume Modelling. *The International Journal of Advanced Manufacturing Technology*, vol. 18, n° 2, 2001, p. 103–117.
- [MAH 14] MAHAMOOD R. M., AKINLABI E. T., SHUKLA M., PITYANA S.  
Revolutionary additive manufacturing: an overview. *Lasers in Engineering*, , 2014, Old C: ily Publishing Croup.
- [MAL 01] MALINOV S., GUO Z., SHA W., WILSON A.  
Differential scanning calorimetry study and computer modeling of  $\beta \rightarrow \alpha$  phase transformation in a Ti-6Al-4V alloy. *Metallurgical and Materials Transactions A*, vol. 32, n° 4, 2001, p. 879–887.
- [MAN 15] MANI M., FENG S., LANE B., DONMEZ A., MOYLAN S., FESPERMAN R.  
*Measurement science needs for real-time control of additive manufacturing powder bed fusion processes*. US Department of Commerce, National Institute of Standards and Technology, 2015.
- [MAR 14] MARION G., CAILLETAUD G., COLIN C., MAZIÈRE M.  
A finite element model for the simulation of direct metal deposition. *33rd International Congress on Applications of Lasers & Electro-Optics (ICALEO)*, San Diego, CA, Oct, 2014, p. 19–23.
- [MCG 17] MCGINNIS A.  
Opportunities and Challenges with Additive and Subtractive Manufacturing. *Global product data interoperability summit*, 2017.
- [MEG 16] MEGAHEM M., MINDT H.-W., N'DRI N., DUAN H., DESMAISON O.  
Metal additive-manufacturing process and residual stress modeling. *Integrating Materials and Manufacturing Innovation*, vol. 5, n° 1, 2016, p. 4.
- [MEI 17] MEIER C., PENNY R. W., ZOU Y., GIBBS J. S., HART A. J.  
Thermophysical Phenomena in Metal Additive Manufacturing by Selective Laser Melting: Fundamentals, Modeling, Simulation and Experimentation. *CoRR*, vol. abs/1709.09510, 2017.

- [MEK 16] MEKONNEN B. G., BRIGHT G., WALKER A.  
A Study on State of the Art Technology of Laminated Object Manufacturing (LOM).  
MANDAL D. K., SYAN C. S., Eds., *CAD/CAM, Robotics and Factories of the Future*,  
New Delhi, 2016 Springer India, p. 207-216.
- [MEL 14] MELLOR S.  
An implementation framework for additive manufacturing. Thèse de doctorat, University of Exeter, 2014.
- [MEL 18] DE MELLO R. F., PONTI M. A.  
*Machine Learning: A Practical Approach on the Statistical Learning Theory*. Springer, 2018.
- [MER 06] MERCELIS P., KRUTH J.  
Residual stresses in selective laser sintering and selective laser melting. *Rapid Prototyping Journal*, vol. 12, n° 5, 2006, p. 254-265.
- [MET 17] METAL D.  
Desktop Metal studio sytem brochure. <https://www.desktopmetal.com/products/studio>, 2017.
- [MIC 14] MICHALERIS P.  
Modeling metal deposition in heat transfer analyses of additive manufacturing processes. *Finite Elements in Analysis and Design*, vol. 86, 2014, p. 51 - 60.
- [MIL 17] MILEWSKI J. O.  
*Additive Manufacturing of Metals: From Fundamental Technology to Rocket Nozzles, Medical Implants, and Custom Jewelry*, vol. 258. Springer International Publishing, 1 edition, 2017.
- [MIN 15] MINDT H., DESMAISON O., MEGAHED M.  
Modelling Powder Bed Additive Manufacturing Defects. *EUCASS 2017, Milan, Italy*, 2015.
- [MOR 17] DE MORAES D. A., CZEKANSKI A.  
Thermal Modeling of 304L Stainless Steel for Selective Laser Melting: Laser Power Input Evaluation. *ASME 2017 International Mechanical Engineering Congress and Exposition* American Society of Mechanical Engineers, 2017, p. V002T02A033–V002T02A033.
- [MOY 13] MOYLAN S. P., SLOTWINSKI J. A., COOKE A., JURRENS K., DONMEZ M. A.  
Lessons learned in establishing the NIST metal additive manufacturing laboratory. rapport, 2013, National Institute of Standards and Technology.

- [MUK 17] MUKHERJEE T., ZHANG W., DEBROY T.  
An improved prediction of residual stresses and distortion in additive manufacturing. *Computational Materials Science*, vol. 126, 2017, p. 360–372, Elsevier.
- [MÜL 16] MÜLLER A. C., GUIDO S. et al.  
*Introduction to machine learning with Python: a guide for data scientists*. " O'Reilly Media, Inc.", 2016.
- [NIC 18] NICKELS L.  
Office-based AM now open for business. *Metal Powder Report*, vol. 73, n° 4, 2018, p. 195 - 197.
- [NOO 03] NOORUDDIN F. S., TURK G.  
Simplification and repair of polygonal models using volumetric techniques. *IEEE Transactions on Visualization and Computer Graphics*, vol. 9, n° 2, 2003, p. 191-205.
- [ONS 18] ONSTEIN I. F.  
An Additive Manufacturing Path Generation Method Based on CAD Models for Robot Manipulators. Thèse de doctorat, NTNU, 2018.
- [OTT 10] OTTO A., SCHMIDT M.  
Towards a universal numerical simulation model for laser material processing. *Physics Procedia*, vol. 5, 2010, p. 35 - 46. Laser Assisted Net Shape Engineering 6, Proceedings of the LANE 2010, Part 1.
- [ÖZE 05] ÖZEL T., KARPAT Y.  
Predictive modeling of surface roughness and tool wear in hard turning using regression and neural networks. *International Journal of Machine Tools and Manufacture*, vol. 45, n° 4-5, 2005, p. 467–479, Elsevier.
- [PAL 15] PAL D., STUCKER B.  
A New and Efficient Multi-Scale Simulation Architecture for Prediction of Performance Metrics for Parts Fabricated Using Additive Manufacturing. *TMS 2015 144th Annual Meeting & Exhibition Springer*, 2015, p. 381–388.
- [PAR 07] PARVIZIAN J., DÜSTER A., RANK E.  
Finite cell method. *Computational Mechanics*, vol. 41, n° 1, 2007, p. 121–133.
- [PAT 15] PATIL N., PAL D., RAFI H. K., ZENG K., MORELAND A., HICKS A., BEELER D., STUCKER B.  
A Generalized Feed Forward Dynamic Adaptive Mesh Refinement and Derefinement Finite Element Framework for Metal Laser Sintering-Part I: Formulation and Algorithm Development. *Journal of Manufacturing Science and Engineering*, vol. 137, n° 4, 2015, p. 041001, American Society of Mechanical Engineers.

- [PK 16] P.KHAZAN T. R., WOIZESCHKE P.  
Numerical simulation of distortion in conventional laser and fluxless laser-plasma brazing of aluminum using Simufact.welding. *9th DVS Aluminium Brazing Congress, Dösselndorf*, 2016.
- [PRA 15] PRABHAKAR P., SAMES W., DEHOFF R., BABU S.  
Computational modeling of residual stress formation during the electron beam melting process for Inconel 718. *Additive Manufacturing*, vol. 7, 2015, p. 83 - 91.
- [QI 06] QI H., MAZUMDER J., KI H.  
Numerical simulation of heat transfer and fluid flow in coaxial laser cladding process for direct metal deposition. *Journal of Applied Physics*, vol. 100, n° 2, 2006, p. 024903.
- [QUR 18] QURMOSHI A. I.  
Additive manufacturing of stainless steel. Master's thesis, Western Sydney university, Australia, 2018.
- [RAD 92] RADAJ D.  
*Heat Effects of Welding: Temperature Field, Residual Stress, Distortion*. Springer-Verlag Berlin Heidelberg, 1992.
- [RAH 12] RAHMAN N. U., ALAM M. N.  
Active vibration control of a piezoelectric beam using PID controller: Experimental study. *Latin American Journal of Solids and Structures*, vol. 9, 2012, p. 657 - 673, scielo.
- [RAJ 12] RAJLAXMI N MHETRE S. J.  
FINITE ELEMENT ANALYSIS OF WELDED JOINTS. *International Journal of Instrumentation, Control and Automation (IJICA)*, vol. 1, 2012, p. 2231-1890.
- [RAM 18] RAMIRO P., ALBERDI A., ORTIZ M., LAMIKIZ A., UKAR E. et al.  
Characteristics of Fe-, Ni-and Co-based powder coatings fabricated by laser metal deposition without preheating the base material. *Procedia CIRP*, , 2018, Elsevier BV.
- [ROB 09] ROBERTS I., WANG C., ESTERLEIN R., STANFORD M., MYNORS D.  
A three-dimensional finite element analysis of the temperature field during laser melting of metal powders in additive layer manufacturing. *International Journal of Machine Tools and Manufacture*, vol. 49, n° 12, 2009, p. 916 - 923.
- [ROB 12] ROBERTS I. A.  
Investigation of residual stresses in the laser melting of metal powders in additive layer manufacturing. Thèse de doctorat, University of Wolverhampton, 2012.
- [SAE 16] SAEED M., ALI A., MAHMOOD H.  
A Comparison between Velocity Feedback and Proportional-Integral-Derivative [PID]

- Performance In Active Vibration Control. *Journal of Vibration Analysis, Measurement, and Control*, vol. 4, n° 1, 2016, p. 40–55.
- [SAM 16] SAMES W. J., LIST F. A., PANNALA S., DEHOFF R. R., BABU S. S.  
The metallurgy and processing science of metal additive manufacturing. *International Materials Reviews*, vol. 61, n° 5, 2016, p. 315-360, Taylor & Francis.
- [SHA 15] SHAMSAEI N., YADOLLAHI A., BIAN L., THOMPSON S. M.  
An overview of Direct Laser Deposition for additive manufacturing; Part II: Mechanical behavior, process parameter optimization and control. *Additive Manufacturing*, vol. 8, 2015, p. 12 - 35.
- [SHI 17] SHIM D.-S., BAEK G.-Y., LEE E.-M.  
Effect of substrate preheating by induction heater on direct energy deposition of AISI M4 powder. *Materials Science and Engineering: A*, vol. 682, 2017, p. 550–562, Elsevier.
- [SHR 18] SHRESTHA S., CHOU K.  
Computational Analysis of Thermo-Fluid Dynamics with Metallic Powder in SLM. NASTAC L., PERICLEOUS K., SABAU A. S., ZHANG L., THOMAS B. G., Eds., *CFD Modeling and Simulation in Materials Processing 2018*, Cham, 2018 Springer International Publishing, p. 85–95.
- [SIS 02] SISIAS G., PHILLIPS R., DOBSON C., FAGAN M., LANGTON C.  
Algorithms for accurate rapid prototyping replication of cancellous bone voxel maps. *Rapid Prototyping Journal*, vol. 8, n° 1, 2002, p. 6-24.
- [SMI 12] SMITH M., BOUCHARD P., TURSKI M., EDWARDS L., DENNIS R.  
Accurate prediction of residual stress in stainless steel welds. *Computational Materials Science*, vol. 54, 2012, p. 312 - 328.
- [SON 12] SONG L., BAGAVATH-SINGH V., DUTTA B., MAZUMDER J.  
Control of melt pool temperature and deposition height during direct metal deposition process. *The International Journal of Advanced Manufacturing Technology*, vol. 58, n° 1, 2012, p. 247–256.
- [SON 15] SONK K.  
Development of Additive Manufacturing Based on Functional Requirements. Thèse de doctorat, Tallinn University of Technology, 2015.
- [STA 17] STACKPOLE B.  
. « Materialise Takes the Pain Out of Support Generation for Metal 3D Printing ». Rapid Ready Technology, 11 2017.
- [STA 18] STATATHOS E., VOSNIAKOS G.-C.  
A computationally efficient universal platform for thermal numerical modeling of



- laser-based additive manufacturing. *Proceedings of the Institution of Mechanical Engineers, Part C: Journal of Mechanical Engineering Science*, vol. 232, n° 13, 2018, p. 2317-2333.
- [STE 16a] STEUBEN J. C., ILIOPOULOS A. P., MICHPOULOS J. G.  
Discrete element modeling of particle-based additive manufacturing processes. *Computer Methods in Applied Mechanics and Engineering*, vol. 305, 2016, p. 537 - 561.
- [STE 16b] STEUBEN J. C., ILIOPOULOS A. P., MICHPOULOS J. G.  
Implicit slicing for functionally tailored additive manufacturing. *Computer-Aided Design*, vol. 77, 2016, p. 107 - 119.
- [SUB 06] SUBBURAJ K., PATIL S., RAVI B.  
Voxel-based thickness analysis of intricate objects. *International Journal of CAD/CAM*, , 2006.
- [SUR 16] SURLERAUX A., PERNOT J.-P., BIGOT S.  
A comparative study between NURBS surfaces and voxels to simulate the wear phenomenon in micro-EDM. *Computer-Aided Design and Applications*, vol. 13, n° 6, 2016, p. 792-798, Taylor & Francis.
- [TAG 18] TAGHIPOUR A., PARVIZIAN J., HEINZE S., DÄ $\frac{1}{4}$ STER A.  
The finite cell method for nearly incompressible finite strain plasticity problems with complex geometries. *Computers & Mathematics with Applications*, vol. 75, n° 9, 2018, p. 3298 - 3316.
- [TAN 17] TANG M., PISTORIUS P. C., BEUTH J. L.  
Prediction of lack-of-fusion porosity for powder bed fusion. *Additive Manufacturing*, vol. 14, 2017, p. 39 - 48.
- [TAU 13] TAUFIK M., JAIN P. K.  
Role of build orientation in layered manufacturing: a review. *International Journal of Manufacturing Technology and Management*, vol. 27, n° 1-3, 2013, p. 47-73, Inderscience Publishers Ltd.
- [THO 15] THOMPSON S. M., BIAN L., SHAMSAEI N., YADOLLAHI A.  
An overview of Direct Laser Deposition for additive manufacturing; Part I: Transport phenomena, modeling and diagnostics. *Additive Manufacturing*, vol. 8, 2015, p. 36 - 62.
- [THO 16] THOMPSON M. K., MORONI G., VANEKER T., FADEL G., CAMPBELL R. I., GIBSON I., BERNARD A., SCHULZ J., GRAF P., AHUJA B., MARTINA F.  
Design for Additive Manufacturing: Trends, opportunities, considerations, and constraints. *CIRP Annals*, vol. 65, n° 2, 2016, p. 737 - 760.

- [THO 17] THOMAS B., SUTTON A., LEU M. C., AUSTIN SUTTON D., LEU M., DOIPHODE N.  
Study of Selective Laser Melting for Bonding of 304L Stainless Steel to Grey Cast Iron. *Solid Freeform Fabrication 2017: Proceedings of the 28th Annual International Solid Freeform Fabrication Symposium – An Additive Manufacturing Conference*, 2017.
- [THO 18] THOMAS-SEALE L., KIRKMAN-BROWN J., ATTALLAH M., ESPINO D., SHEPHERD D.  
The barriers to the progression of additive manufacture: Perspectives from UK industry. *International Journal of Production Economics*, vol. 198, 2018, p. 104 - 118.
- [TOF 18] TOFAIL S. A., KOUMOULOS E. P., BANDYOPADHYAY A., BOSE S., O'DONOGHUE L., CHARITIDIS C.  
Additive manufacturing: scientific and technological challenges, market uptake and opportunities. *Materials Today*, vol. 21, n° 1, 2018, p. 22 - 37.
- [TRI 17] TRIPATHY S., CHIN C., LONDON T., ANKALKHOPE U., OANCEA V.  
Process Modeling and Validation of Powder Bed Metal Additive Manufacturing. *NAFEMS World Congress, Stockholm, Sweden*, 2017.
- [UEN 18] UENG S.-K., CHEN L.-G., JEN S.-Y.  
Voxel-based virtual manufacturing simulation for three-dimensional printing. *Advances in Mechanical Engineering*, vol. 10, n° 6, 2018, p. 1687814018781632.
- [VAI 15] VAITHILINGAM J.  
Additive manufacturing and surface functionalisation of Ti6Al4V components using self-assembled monolayers for biomedical applications. Thèse de doctorat, University of Nottingham, December 2015.
- [VAN 13] VAN BELLE L.  
Analysis, modeling and simulation of residual stresses during the SLM process of metallic powders. Theses, INSA de Lyon, novembre 2013.
- [VAN 16] VAN ZYL I., YADROITSAVA I., YADROITSEV I.  
Residual stress in Ti6Al4V objects produced by direct metal laser sintering. *South African Journal of Industrial Engineering*, vol. 27, n° 4, 2016, p. 134–141, The Southern African Institute for Industrial Engineering.
- [VAS 16] VASTOLA G., ZHANG G., PEI Q., ZHANG Y.-W.  
Controlling of residual stress in additive manufacturing of Ti6Al4V by finite element modeling. *Additive Manufacturing*, vol. 12, 2016, p. 231 - 239. Special Issue on Modeling & Simulation for Additive Manufacturing.
- [VAT 92] VATTI B. R.  
A Generic Solution to Polygon Clipping. *Commun. ACM*, vol. 35, n° 7, 1992, p. 56–63, ACM.

- [VOR 17] VORA P., MARTINEZ R., HOPKINSON N., TODD I., MUMTAZ K.  
Customised Alloy Blends for In-Situ Al339 Alloy Formation Using Anchorless Selective Laser Melting. *Technologies*, vol. 5, n° 2, 2017, MDPI. © 2017 by the authors. Licensee MDPI, Basel, Switzerland. This article is an open access article distributed under the terms and conditions of the Creative Commons Attribution (CC BY) license (<http://creativecommons.org/licenses/by/4.0/>).
- [WAH 16] WAHLSTRÖM T., SAHLSTRÖM J.  
Additive Manufacturing in Production-for the Automotive Industry. Master's thesis, Lund University, 2016.
- [WAN 06] WANG D.-X., GUO D.-M., JIA Z.-Y., LENG H.-W.  
Slicing of CAD models in color STL format. *Computers in Industry*, vol. 57, n° 1, 2006, p. 3 - 10.
- [WAN 07] WANG W. R., CHEN G. L., LIN Z. Q., LI S. H.  
Determination of optimal blank holder force trajectories for segmented binders of step rectangle box using PID closed-loop FEM simulation. *The International Journal of Advanced Manufacturing Technology*, vol. 32, n° 11, 2007, p. 1074–1082.
- [WAN 17] WANG Z., DENLINGER E., MICHALERIS P., STOICA A. D., MA D., BEESE A. M.  
Residual stress mapping in Inconel 625 fabricated through additive manufacturing: Method for neutron diffraction measurements to validate thermomechanical model predictions. *Materials & Design*, vol. 113, 2017, p. 169 - 177.
- [WAR 16] WARHOLM M., SÑEGÅRD J.  
Industrialization of Additive Manufacturing - Development of an Additive Manufacturing Design Guide for Metal Laser Powder Bed Fusion. Master's thesis, Chalmers University of Technology, 2016.
- [WAS 17] WASSERMANN B., KOLLMANNNSBERGER S., BOG T., RANK E.  
From geometric design to numerical analysis: A direct approach using the Finite Cell Method on Constructive Solid Geometry. *Computers & Mathematics with Applications*, vol. 74, n° 7, 2017, p. 1703 - 1726. High-Order Finite Element and Isogeometric Methods 2016.
- [WEI 14] WEISS B.  
Closed-loop control of a 3D printer gantry. Master's thesis, University of Washington, 2014.
- [WEN 10] WEN S., SHIN Y. C.  
Modeling of transport phenomena during the coaxial laser direct deposition process. *Journal of Applied Physics*, vol. 108, n° 4, 2010, p. 044908.

- [WIL 05] WILSON D. I.  
Relay-based PID tuning. *Automation and Control*, , 2005, p. 10–11.
- [WIT 01] WITHERS P., BHADESHIA H.  
Residual stress. Part 1 - Measurement techniques. *Materials Science and Technology*, vol. 17, n° 4, 2001, p. 355-365, Taylor & Francis.
- [WIT 07] WITHERS P. J.  
Residual stress and its role in failure. *Reports on Progress in Physics*, vol. 70, n° 12, 2007, p. 2211.
- [WRI 15] WRIGHT S.  
3D printing titanium: Learning to learn from success. rapport, 2015, Layerwise, Belgium.
- [WU 14] WU H. B., ZHANG S. J.  
3D FEM simulation of milling process for titanium alloy Ti6Al4V. *The International Journal of Advanced Manufacturing Technology*, vol. 71, n° 5, 2014, p. 1319–1326.
- [XIE 17] XIE J., OANCEA V., HURTADO J.  
Phase transformations in metals during additive manufacturing processes. *NAFEMS World Congress*, 2017.
- [XIO 14a] XIONG J., ZHANG G.  
Adaptive control of deposited height in GMAW-based layer additive manufacturing. *Journal of Materials Processing Technology*, vol. 214, n° 4, 2014, p. 962 - 968.
- [XIO 14b] XIONG J., ZHANG G., HU J., WU L.  
Bead geometry prediction for robotic GMAW-based rapid manufacturing through a neural network and a second-order regression analysis. *Journal of Intelligent Manufacturing*, vol. 25, n° 1, 2014, p. 157–163, Springer.
- [XIO 16] XIONG J., YIN Z., ZHANG W.  
Closed-loop control of variable layer width for thin-walled parts in wire and arc additive manufacturing. *Journal of Materials Processing Technology*, vol. 233, 2016, p. 100 - 106.
- [YAD 15] YADROITSAVA I., YADROITSEV I.  
Residual stress in metal specimens produced by direct metal laser sintering. *Proceedings of the SFF Symposium, Austin, TX, USA*, 2015, p. 10–12.
- [YAN 02] YANG Y., LOH H., FUH J., WANG Y.  
Equidistant path generation for improving scanning efficiency in layered manufacturing. *Rapid Prototyping Journal*, vol. 8, n° 1, 2002, p. 30-37.

- [YAN 17a] YAN W., QIAN Y., MA W., ZHOU B., SHEN Y., LIN F.  
Modeling and Experimental Validation of the Electron Beam Selective Melting Process. *Engineering*, vol. 3, n° 5, 2017, p. 701 - 707.
- [YAN 17b] YANG L., HSU K., BAUGHMAN B., GODFREY D., MEDINA F., MENON M., WIENER S.  
*Additive Manufacturing of Metals: The Technology, Materials, Design and Production*. Springer, 2017.
- [YAS 18] YASA E.  
UNDERSTANDING ADOPTING SELECTIVE LASER MELTING OF METALLIC MATERIALS. *Solid Freeform Fabrication 2018:Proceedings of the 29th Annual International Solid Freeform Fabrication Symposium*, 2018.
- [ZÄH 10] ZÄH M. F., LUTZMANN S.  
Modelling and simulation of electron beam melting. *Production Engineering*, vol. 4, n° 1, 2010, p. 15–23.
- [ZEL 15] ZELINSKI P.  
Additive's Idiosyncrasies. *Additive Manufacturing Magazine*, , 2015.
- [ZHA 15] ZHANG Y., OUTEIRO J., MABROUKI T.  
On the selection of Johnson-Cook constitutive model parameters for Ti-6Al-4 V using three types of numerical models of orthogonal cutting. *Procedia Cirp*, vol. 31, 2015, p. 112–117, Elsevier.
- [ZHA 18] ZHANG Y., CHEN Q., GUILLEMOT G., GANDIN C.-A., BELLET M.  
Numerical modelling of fluid and solid thermomechanics in additive manufacturing by powder bed fusion: continuum and level set formulation applied to track and part scale simulations. *Comptes Rendus Mecanique*, , 2018.
- [ZUM 17] ZUMOFEN L., BECK C., KIRCHHEIM A., DENNIG H.-J.  
Quality Related Effects of the Preheating Temperature on Laser Melted High Carbon Content Steels. *International Conference on Additive Manufacturing in Products and Applications* Springer, 2017, p. 210–219.



# Résumé étendu

## Introduction du contexte

La fabrication additive (FA) devient de plus en plus importante pour la fabrication de pièces dans l'industrie et est devenue un pôle multidisciplinaire pour les chercheurs académiques au cours de la dernière décennie. Néanmoins la qualité des pièces métalliques obtenues par fabrication additive n'est pas toujours satisfaisante. En effet, dans la fabrication additive métallique, la forme et les propriétés d'une pièce sont directement impactées par de le procédé de fabrication lui-même et certains problèmes peuvent limiter l'utilisation de ces pièces, tels que l'existence de contraintes résiduelles, la précision dimensionnelle, la qualité de surface, les propriétés mécaniques, la porosité / densité, la fatigue, etc. Ces problèmes sont généralement étudiés soit expérimentalement, soit numériquement. La simulation FEM (Finite Element Method) numérique du procédé de FA fournit un moyen important de réaliser "virtuellement" des expériences. Les moyens expérimentaux peuvent se révéler coûteux et longs à mettre en place et présentent souvent des difficultés en terme de techniques de mesure. Bien que la simulation numérique présente de nombreux avantages dans la recherche sur la fabrication additive de pièces métalliques, il reste encore quelques problèmes à résoudre :

### 1. Modélisation multi-échelle pour le procédé de FA

Le procédé de fabrication additive est un phénomène multi-physique et multi-échelle : de la micro-échelle (bain de fusion) à la macro-échelle (piste, couche, pièce). La séparation de ces échelles rend assez difficile la description des phénomènes complexes dans le procédé de FA en tant que modèle unique. Dans la simulation macroscopique, les conditions limites de surface libre constituent un problème inévitable pour l'addition de matériaux et les effets de dépôt des multi-pistes des objets 3D.

### 2. Irrégularité géométrique

Le pré-processing représente souvent un challenge pour la simulation de FA à l'échelle macroscopique. C'est l'une des raisons pour lesquelles la majorité des simulations de FA se sont concentrées sur le procédé de fabrication d'une paroi mince ou d'une ligne simple. Le passage de la CAO à la FAO pour la fabrication additive s'appuie sur des connaissances en infographie. Actuellement, la plupart des logiciels de CAO sont basés sur des systèmes paramétrique NURBS. Ces logiciels conviennent bien à la modélisation des géométries associées aux procédés de fabrication traditionnelle (extrusion, révolution, etc.), mais sont souvent inadaptés aux géométries plus complexes. De plus, il n'est pas facile d'acquérir des modèles géométriques multi-échelles (bain de fusion, piste, couche, pièce, etc.) à partir d'un objet 3D dans un logiciel traditionnel de CAO. En outre le chemin de balayage généré par les algorithmes de tranchage ou « slicer » ne peut pas être directement importé dans la simulation FEM. En

raison de l'irrégularité géométrique d'un objet construit par la FA, il est nécessaire d'appliquer des algorithmes spécifiques pour reconstruire un modèle 3D dans la fabrication additive.

### **3. Boucle de contrôle**

Dans un système de FA à boucle ouverte, les fluctuations des paramètres du procédé (par exemple, la puissance du laser, la vitesse de balayage et le débit de poudre) conduisent souvent à une déviation du procédé de l'état initialement prédéfini, aboutissant à l'apparition de défauts dans les composants finis. Quelques chercheurs ont développé un système de détection et de contrôle pour les systèmes de FA automatiques. La surveillance du procédé permet de garantir la qualité des pièces et l'efficacité du procédé. Néanmoins, ces systèmes en temps réel sont encore à leurs balbutiements, car ils reposent non seulement sur le matériau mais également sur la compréhension des comportements des systèmes de FA correspondant aux paramètres du procédé.

### **4. Optimisation des paramètres du procédé**

La qualité d'un composant fabriqué en FA dépend fortement des paramètres d'entrée du procédé. Par la sélection appropriée des valeurs optimales de ces paramètres, la qualité d'une pièce fabriquée par une FA peut être améliorée. Il est généralement difficile de formuler explicitement les relations entre les paramètres du procédé et les critères de qualité, du fait de la complexité du procédé de FA. Cependant, la boucle d'asservissement en temps réel du système de FA repose fortement sur le calcul rapide de la corrélation entre les paramètres d'entrée et les paramètres de sortie. Cette corrélation doit être acquise avant le début du procédé de FA. La méthode permettant de démontrer la corrélation phénoménologique à partir de l'ensemble des données expérimentales ou numériques sera utile pour le contrôle de la qualité dans la fabrication additive.

### **5. Ecosystème des outils de la simulation de FA**

La fabrication additive est un secteur en plein développement. De nombreuses entreprises adoptent une stratégie de vente de l'ensemble « logiciel-matériau-machine », ce qui rend l'écosystème de la fabrication additive métallique assez complexe. Il n'est pas toujours facile de convertir différents formats de fichier dans le déploiement d'une simulation numérique du procédé de FA. La majorité des logiciels internes ou commerciaux possèdent des sources inaccessibles aux utilisateurs. Les chercheurs académiques ont souvent besoin d'un outil plus flexible pour étudier les détails de la simulation. Donc Il est essentiel de construire des plateformes numériques basées sur des logiciels de FEM à usage général et d'explorer la méthodologie de la simulation numérique du procédé de FA.

\*\*\*\*\*

## **Résumé de chaque chapitre**



Dans cette thèse, nous étudions le procédé macroscopique de FA pour des pièces métalliques par la simulation FEM, afin d'étudier principalement les problèmes évoqués ci-dessus.

## Chapitre 1

Dans le chapitre 1, un état des lieux de la fabrication additive est présenté, ainsi que les avantages (complexité géométrique, moins d'assemblage, moins de gaspillage des matériaux, production personnalisable) et les inconvénients (mauvaises propriétés mécaniques, distorsion excessive, dépense d'appareil, limite de taille des composants, vitesse lente de fabrication, difficulté dans la configuration du procédé et du contrôle) de ce procédé. La classification de la fabrication additive peut être réalisée selon différents aspects : composition chimique du matériau (polymère, métal, céramique), état initial du matériau (liquide, poudre, fil, plaque), méthode technique (Stéréolithographie, Dépôt de fil en fusion, Continuous liquid interface production, Bound metal deposition, Modélisation d'objets laminés). Notamment la fabrication additive métallique utilise deux principales technologies : le lit de poudre (ex. fusion sélective par laser, fusion par faisceau d'électrons, frittage sélectif par laser, etc.) ou l'injection de poudre (ex. direct metal deposition). Ces procédés sont présentés dans ce chapitre ainsi que les problèmes rencontrés lors de la fabrication additive :

1. Distorsion et fissure causées par une contrainte résiduelle
2. Conception du support
3. Interférence de la lame (collision de pale)
4. Surchauffage ou absence de fusion
5. Optimisation de l'orientation des pièces
6. Enlèvement/découpe d'une pièce de son substrat

Certaines tendances, en termes de simulation numérique pour la fabrication additive, sont aussi brièvement présentées. Pour une pièce métallique fabriquée dans les systèmes de FA, sa forme et ses propriétés peuvent ne pas être satisfaisantes comme prévu. Quelques méthodes numériques utilisées pour la simulation macroscopique de la fabrication additive par des chercheurs académiques ainsi que des logiciels propriétaires (exemple : 3DSim, Simufact Additive, Autodesk Netfabb Simulation Utility), sont présentés :

1. Technique de *birth and death* dans la méthode des éléments finis
2. Voxélisation pour la géométrie complexe dans le pré-processing
3. Adaptation du maillage

4. Méthode de *Level-Set* pour la géométrie 3D
5. Méthode de *Volume of fluid* pour la limite libre
6. Méthode des éléments discrets
7. Méthode des cellules finies

## Chapitre 2

Dans le chapitre 2, la fabrication additive est mathématiquement décrite comme un problème de couplage multi-physique. Les comportements macroscopiques d'une pièce fabriquée et de son substrat sont découplés en trois aspects : champ thermique, champ mécanique et champ métallurgique. Même si le logiciel ABAQUS est utilisé comme un outil dans nos simulations, les équations constitutives implémentées dans ce logiciel doivent être d'abord analysées avant tous les travaux de programmation.

Outre l'équation gouvernante (l'équation de la chaleur avec une condition limite complexe en raison de dépôt du matériau dans la fabrication additive), deux modèles de source de chaleur sont introduits dans l'analyse thermique. Le premier modèle (faisceau gaussien) correspond à un mode de laser transverse fondamental, et le second (modèle Goldak) correspond à un modèle de soudage.

Les équations élasto-plastiques sont combinées au modèle d'écrouissage de Johnson-Cook afin de calculer les contraintes résiduelles. Le comportement macroscopique d'une pièce métallique pendant le procédé de la fabrication additive est dominé par l'équation de conservation de la quantité de mouvement, combinée à quelques modifications pour l'expansion thermique.

Pour l'évolution des phases métallurgiques, nous prenons l'alliage de titane Ti6Al4V comme exemple. L'alliage de titane Ti6Al4V qui comprend trois phases (l'austénite cubique centré  $\beta$ , la martensite cubique centré  $\alpha'$ , l'empilement hexagonal compact  $\alpha$ ), se comporte différemment selon le procédé thermique, et notamment selon la vitesse de changement de température. Deux modèles de transformation de phase (sans diffusion et avec diffusion), le modèle Koistinen-Marburger (KM) et le modèle modifié Johnson-Mehl-Avrami (JMA) sont brièvement présentés. Le modèle JMA ne peut pas être directement utilisé dans les transformations non-isothermiques de refroidissement ou de réchauffage. Néanmoins, quelques chercheurs ont proposé des méthodes spécifiques afin de généraliser le modèle JMA pour le cas où le refroidissement continu est remplacé par une série d'étapes consécutives isothermiques.

## Chapitre 3

Le pré-processing du modèle 3D, tel que la génération de maillage, est essentiel pour la simulation FEM. Cependant, quelques problèmes spécifiques limitent l'application de la simulation macroscopique de la fabrication additive. Dans la simulation numérique de FA, les chercheurs académiques sont souvent limités lorsqu'ils importent les fichiers de la géométrie d'une pièce, CAO et G-code, dans le logiciel FEM. En raison de l'absence d'outil et de méthodologie de pré-processing, la simulation d'une pièce en macro échelle reste complexe. La reconstruction du modèle 3D représente une difficulté majeure dans la réalisation des simulations.

Les problèmes spécifiques du pré-processing sont étudiés pour la simulation de FA à différents échelles : à l'échelle de la couche et à l'échelle de la pièce. Nous avons construit une plate-forme pour la simulation macroscopique de FEM, en utilisant un algorithme de *offsetting / clipping* de polygones et la méthode de voxélisation. En raison des nombreuses opérations répétées dans la simulation de FA basée sur la FEM, ces travaux de pré-processing sont complétés par la programmation au lieu de la manipulation manuelle. Dans la simulation à l'échelle de la couche, le traitement de texte sur le fichier G-code et la transformation des coordonnées sur la base de données sont réalisés, ce qui permet de surmonter quelques obstacles dans la simulation d'un objet avec une géométrie complexe. L'incompatibilité de l'ensemble d'éléments 3D a lieu entre le système CAO (B-Rep) et le générateur de mailles. Ce problème est résolu par l'injection des éléments du système de CAO au maillage orphelin.

D'autre part, nous utilisons la représentation de voxélisation comme une approximation d'un objet créé par la représentation de limite (B-Rep). Consécutivement il est montré que la voxélisation est une méthode pratique pour la simulation de la fabrication additive à l'échelle de la pièce.

Subséquentement ces méthodologies de pré-processing peuvent être intégrées à la simulation séquentielle du couplage. Dans ce chapitre, nous vérifions la faisabilité de ces méthodes de pré-processing avec deux cas de test (une paroi mince et une aube de turbine), en se concentrant principalement sur l'évolution des des champs. La transformation de phases  $\alpha$  et  $\beta$  est observée dans la simulation métallurgique de cette aube. La contrainte résiduelle  $\sigma_{residual}$  est analysée pour différents cas. L'efficacité de réduire  $\sigma_{residual}$  en augmentant la température de préchauffage est vérifiée par notre simulation macroscopique. Après les simulations avec les puissances et les temps de chauffage au sein des différentes couches, nous pouvons découvrir un moyen potentiel pour réduire la contrainte résiduelle. Ce moyen dépend de l'optimisation des paramètres du procédé (diminution de puissance et prolongation de temps de chauffage), au lieu d'augmenter la température de préchauffage (ce moyen traditionnel se rapproche actuellement de plus en plus de sa limite physique).

## Chapitre 4

La qualité finale de la pièce construite par la fabrication additive comporte généralement deux aspects : sa propriété et sa forme. En pratique, il est relativement facile de surveiller les qualités de sa forme pendant ou après la fabrication, telles que la distorsion et la rugosité de surface. Cependant, mesurer directement les propriétés mécaniques et métallurgiques de cette pièce est généralement impossible pour le procédé de FA. Une pièce avec la forme désirée peut posséder des propriétés insatisfaisantes, qui sont détectées après son enlèvement de la machine de FA. Par conséquent, prévoir la qualité finale d'une pièce et contrôler les paramètres du procédé de FA en temps réel nécessitent une expérience importante de la part des opérateurs de machine de FA. Une meilleure compréhension de l'influence des paramètres de FA sur la qualité des pièces nous aidera à faciliter la configuration avant la fabrication et à réaliser le contrôle en temps réel sur la machine FA.

La contrainte résiduelle est l'un des critères les plus importants pour le contrôle de la qualité des produits métalliques dans la fabrication additive. Dans cette thèse, nous choisissons le maximum de la contrainte résiduelle comme critère de qualité. Ce travail est un exemple simple pour l'application d'analyse des multivariables (MVA) dans la fabrication additive. À terme notre méthodologie de post-processing pourra être étendue à d'autres paramètres de FA et critères de qualité.

Ce travail de post-processing est un exemple simple pour expliquer la méthodologie permettant d'analyser la qualité d'une pièce et ses facteurs potentiels, en se basant sur une quantité suffisante de fichiers « journal ». Avec son fichier « journal », une pièce obtenue par fabrication additive rejetée sera utile, qu'elle soit construite sur une machine de FA ou simulée par FEM. Un fichier « journal », qui comprend la configuration des multi-paramètres et la qualité finale correspondante, constitue une donnée essentielle pour l'analyse de régression. À partir de ce travail statistique, nous essayons d'imiter l'apprentissage d'un ingénieur par ses essais et erreurs. Même si la valeur prédite n'est pas exacte, il est encore possible de connaître la tendance globale de l'influence des paramètres du procédé sur la qualité finale.

Dans ce chapitre, quelques analyses de régression sont effectuées pour obtenir la relation statistique entre les paramètres du procédé de FA et la qualité finale du produit fabriqué par la fabrication additive. Le réseau neuronal artificiel (la rétro-propagation du gradient) et autres algorithmes (régression linéaire, régression à vecteurs de support, forêts aléatoires, gradient boosting, arbre de décision, adaptive boosting) sont comparés en tant que post-processing pour les données acquises à partir de la simulation macroscopique de FA. La contrainte résiduelle maximale de la pièce est choisie comme critère de qualité finale du produit, tandis que trois paramètres (ordre de dépôt, puissance de la source de chaleur et temps de chauffage) représentent le procédé complexe de fabrication additive. Avec quelques outils de régression, nous essayons d'obtenir la relation phénoménologique qui estime quantitativement l'influence de ces trois paramètres sur la contrainte résiduelle.

.....

## Chapitre 5

L'évolution de la température dans un champ thermique de FA est simulée pour démontrer la faisabilité de la simulation d'une boucle de rétroaction dans la fabrication additive. Comme une alternative à l'expérience coûteuse sur la machine de FA, la simulation de FA nous offre une possibilité de configurer plus facilement le régulateur dans les systèmes de FA au lieu de le configurer directement dans le dispositif embarqué de la machine de FA.

Pour les chercheurs académiques de la fabrication additive, les nouveaux matériaux peuvent être testés sans l'authentification de la société qui fabrique la machine de FA. Dans ce cas, il est souvent nécessaire de reconfigurer de nouveaux paramètres du procédé sur la machine de FA.

Parmi les paramètres du procédé de la fabrication additive, la puissance de la source de chaleur et le temps de chauffage sont deux des facteurs ajustables dans la pratique industrielle. Dans notre étude, nous nous concentrons sur la simulation du procédé de FA pour le contrôle en boucle fermée de puissance, ce qui sera utile pour mieux comprendre le comportement de la boucle de contrôle avant la fabrication réelle sur les machines de FA. Notre travail est un exemple qui montre l'intérêt de la simulation de procédé de FA à l'échelle macroscopique en raison de son potentiel de réduction des dépenses dans l'expérience réelle de FA. Nous simulons le procédé de construction d'une piste simple en zigzag dans une couche, où chaque dépôt de matériau est composé de plusieurs éléments.

Parmi les différents régulateurs, le régulateur PID (proportionnel-intégral-dérivé) est le plus utilisé dans l'industrie. Nous prenons le régulateur PID comme un exemple. Le régulateur PID et son auto-réglage des paramètres sont étudiés par itérations de calcul et de post-processing. Un code de Bash Shell, qui combine toutes les manipulations ci-dessus, est réalisé dans nos travaux. Pour la source de chaleur, la régulation de la puissance est effectuée afin de contrôler la température maximale d'une pièce. Un contrôleur PID est intégré à la simulation de FA dans laquelle l'échantillonnage de la température est effectué par un travail de post-processing.

L'ajustement manuel n'est pas la méthode unique qui permet de créer une boucle stable de PID. Le réglage peut être automatiquement effectué avec moins d'expérimentation. Il y a déjà quelques brevets spécifiques et logiciels commerciaux pour le réglage de PID dans l'industrie, mais les algorithmes accessibles sont plus faciles pour les chercheurs académiques.

La méthode Ziegler-Nichols et la méthode de relais sont adoptées dans ce chapitre, visant à améliorer l'efficacité de l'auto-réglage du régulateur PID. La méthode Ziegler-Nichols est empirique pour déterminer les trois coefficients de PID. Dans la méthode de relais, le contrôleur « tout ou rien » est échangé temporairement au contrôleur PID. L'étalonnage du contrôleur « tout ou rien » est facilement affecté par la présence du bruit ou de la perturbation de température. Cette sensibilité au bruit peut être minimisée en modifiant le filtre de Heaviside par un filtre d'hystérésis.

\*\*\*\*\*

## **Conclusion**

Dans cette thèse, nous avons étudié quelques problèmes de simulation numérique en fabrication additive. Les procédures pour surmonter ces problèmes illustrent les étapes de la simulation de FA à l'échelle macroscopique. La qualité d'une pièce métallique fabriquée par la technologie de FA n'est pas toujours satisfaisante pour de nombreuses applications industrielles. Afin de mieux comprendre le procédé de fabrication additive, les simulations numériques utilisant la méthode FEM sont utilisées dans notre étude. Quelques conclusions intéressantes peuvent être obtenues de cette thèse, qui seront probablement utiles pour les chercheurs dans ce domaine:

### **1. Nouveau moyen potentiel pour la réduction de la contrainte résiduelle**

Au lieu de tests avec une géométrie relativement simple, notre étude se concerne sur des objets 3D avec géométrie complexe, qui sont générés à partir d'un logiciel de tranchage ou « slicer » de FA. Grâce à la simplification du regroupement des couches minces voisines en une couche plus épaisse, nous pouvons simuler au chapitre 3 les champs thermo-métallurgiques-mécaniques d'une aube torsadée. La contrainte résiduelle d'une géométrie tellement complexe est normalement difficile pour les simulations précédentes.

D'après les résultats de la simulation, nous concluons que la contrainte résiduelle existe à la fois en surface et à l'intérieur de la pièce construite par le système de FA. L'histogramme de contrainte résiduelle dans une pièce obéit approximativement à la distribution de Burr XII. Tandis que l'énergie d'entrée totale est maintenue constante à celle du cas de référence, nous pouvons réduire la contrainte résiduelle avec une température de préchauffage inférieure. Dans cette technique potentielle, la puissance d'entrée est diminuée pour chaque couche et le temps de chauffage est allongé de manière correspondante. Cet ajustement du procédé peut permettre à la chaleur de se transférer de manière plus homogène. Cet ajustement des paramètres d'entrée de procédé indique un nouveau moyen pour réduction de la contrainte résiduelle à une température de préchauffage plus basse, plutôt qu'une grande température de préchauffage qui présente des inconvénients en termes de la limite de matière et de la consommation d'énergie. Comme les fabricants de la machine de FA s'approchent de la température de préchauffage de plus en plus, le rôle du contrôle du procédé de FA deviendra important en tant que nouvelle direction technique.

### **2. Méthodologie pour les problèmes spéciaux de pré-processing de la simulation de FA**

Certains cas de simulation FA ont été réalisés dans cette thèse pour démontrer la faisabilité du pré-processing. Au chapitre 3, la méthodologie de pré-processing est étudiée à deux niveaux: le niveau de la couche et le niveau de la pièce. Dans la simulation au niveau des couches, deux algorithmes sont proposés. Il est prouvé que le calcul inverse offsetting-clipping des polygones peut servir d'outil pour

extraire les informations de chemin de balayage dans la FA à partir du G-code. Entre le système B-Rep de CAO et le générateur de maillage, l'incompatibilité des ensembles d'élément 3D peut être résolue grâce à une technique de base de données. Dans cette base de données, la transformation des coordonnées locales et globales est effectuée. Cette méthode peut être étendue à des problèmes similaires dans la simulation de FA. Dans la simulation à l'échelle de la pièce, la méthode de voxélisation est adoptée dans notre travail. Différente des procédures ordinaires de génération de maillage, la voxélisation apparaît comme un outil utile et pratique pour la simulation de FA à l'échelle macroscopique. Grâce à ces méthodologies et à ces outils pratiques que nous avons mentionnés ci-dessus, les chercheurs académiques sont capables de simuler moins laborieusement le procédé complexe de FA pour un objet avec une géométrie complexe.

### **3. Mise en œuvre pour l'optimisation des paramètres de contrainte résiduelle**

Pour découvrir la relation entre les paramètres de procédé de FA et la contrainte résiduelle finale d'une pièce à la température de l'environnement, l'analyse par régression est mise en œuvre. Elle est associée à la simulation macroscopique d'une ligne de trajectoire en zigzag dans FA. Au chapitre 4, nous utilisons quelques codes de régression pour analyser les données générées par la simulation de FA. Notre travail est simplifié en supposant que la contrainte résiduelle maximale d'une pièce  $\sigma_{\max}$  est influencée par trois paramètres du procédé (ordre de dépôt  $i$ , puissance de la source de chaleur  $P_i$  et temps de chauffage  $\Delta t_i$ ). Sans formules empiriques pour une certaine pièce, nous essayons de prédire statistiquement cette relation. Le rôle de la simulation de FA dans le chapitre 4 est de générer virtuellement des pièces en tant que données initiales pour la régression au lieu de la fabrication réelle sur une machine de FA. Les différences de performance entre le réseau neuronal artificiel et les autres algorithmes de régression sont également observées dans notre étude. Ces différences indiquent l'importance du choix de l'algorithme avant l'application de régression. Notre méthodologie pour les contraintes résiduelles dans ce travail sera l'étape essentielle pour des études ultérieures à l'aide d'un outil phénoménologique basé sur la régression.

### **4. Intégration de la boucle de contrôle dans la simulation de FA**

Avant d'optimiser les paramètres de procédé FA pour la réduction de la contrainte résiduelle, le système FA doit être équipé d'une boucle de régulation. Le contrôle de la température en un point est une préparation fondamentale pour la réalisation de réduction de contrainte résiduelle par le nouveau moyen décrit dans le chapitre 3. La réponse fluctuante dans la simulation en boucle ouverte révèle la complexité du système FA. Le système FA est non-LTI (invariant et linéaire dans le temps). Cette propriété nous empêche d'appliquer directement la plupart des outils mathématiques de l'automatique, si le système FA n'est pas encore simplifié de manière appropriée. Au chapitre 5, nous intégrons un régulateur PID à la simulation FA et essayons d'obtenir une température stable en régulant la puissance d'entrée. Au lieu de manipuler sur une machine de FA, l'auto-réglage de PID est réalisé dans la simulation numérique

FA avec la méthode de Ziegler-Nichols et la méthode du relais. Les performances différentes de nombreux types de régulateurs (Tous sont dans la famille de PID) sont comparées. La méthode de Ziegler-Nichols est seulement une des méthodes approximatives pour l'auto-réglage. Si le régulateur doit encore être optimisé, un réglage plus fin doit être exécuté. Le choix d'un régulateur approprié dépend des exigences du système de FA. Dans cette thèse, nous avons proposé la boucle basique de contrôle combinant avec la simulation FA. Nous pouvons intuitivement percevoir l'avantage de simuler le procédé de fabrication d'une pièce, par exemple la prévention du risque de dépassement de puissance ou de température.

.....







## FOLIO ADMINISTRATIF

### THESE DE L'UNIVERSITE DE LYON OPEREE AU SEIN DE L'INSA LYON

NOM : CHEN

DATE de SOUTENANCE : 5 juillet 2019

Prénoms: Shuai

TITRE : Investigation of FEM numerical simulation for the process of metal additive manufacturing in macro scale

NATURE : Doctorat

Numéro d'ordre : 2019LYSEI048

Ecole doctorale : Mécanique, Énergétique, Génie Civil, Acoustique (ED 162 MEGA)

Spécialité : GÉNIE MÉCANIQUE

#### RESUME :

Additive manufacturing (AM) has become a new option for the fabrication of metallic parts in industry. However, there are still some limitations for this application, especially the unfavourable final shape and undesired macroscopic properties of metallic parts built in AM systems. The distortion or crack due to the residual stress of these parts leads usually to severe problems for some kinds of metal AM technology. In an AM system, the final quality of a metallic part depends on many process parameters, which are normally optimized by a series of experiments on AM machines. In order to reduce the considerable time consumption and financial expense of AM experiments, the numerical simulation dedicated to AM process is a prospective alternative for metallic part fabricated by additive manufacturing. Because of the multi-scale character in AM process and the complex geometrical structures of parts, most of academic researches in AM simulation concentrated on the microscopic melting pool. Consequently, the macroscopic simulation for the AM process of a metallic part becomes a current focus in this domain.

In this thesis, we first study the pre-processing of AM simulation on Finite Element Method (FEM). The process of additive manufacturing is a multi-physics problem of coupled fields (thermal, mechanical, and metallurgical fields). The macroscopic simulation is conducted in two different levels with some special pre-processing work. For the layer level, the reconstruction of 3D model is conducted from the scan path file of AM machine, based on the inverse manipulation of offsetting-clipping algorithm. For the part level, the 3D model from CAD is reconstructed into a voxel-based mesh, which is convenient for a part with complex geometry. The residual stress of a part is analysed under different preheat temperatures and different process parameters. These simulations imply the potential technique of reducing residual stress by the optimisation of process parameters, instead of traditional way by increasing preheat temperature.

Based on the FEM simulation platform above, two simulations at line level are also studied in this thesis, aiming at the relation between AM process and part's final quality. These examples demonstrate the feasibility of using macroscopic simulations to improve the quality control during AM process. In the first task, dataset of heating parameters and residual stress are generated by AM simulation. The correlation between them is studied by using some regression algorithm, such as artificial neural network. In the second task, a PID controller for power-temperature feedback loop is integrated in AM process simulation and the PID auto-tuning is numerically investigated instead of using AM machine. Both of the two tasks show the important role of AM macroscopic process simulation, which may replace or combine with the numerous trial and error of experiments in metal additive manufacturing.

MOTS-CLÉS : Additive manufacturing, Numerical simulation, Finite element method, Multiphysics, Residual stress, Voxelization, PID controller, Regression, Artificial neural network

Laboratoire (s) de recherche : Laboratoire de Mécanique des Contacts et des Structures, UMR CNRS 5259 – INSA de Lyon

Directeur de thèse: Fabrice MORESTIN

Président de jury: Jean-Michel BERGHEAU

Composition du jury : Jean-Michel BERGHEAU, Michel CORET, Fabrice MORESTIN,  
Pierre VACHER, Laurent VAN BELLE, Hélène WALTER-LE BERRE

